GENETIC DISSECTION OF GLYCAN FUNCTIONS AT THE SYNAPSE

By

Neil Chandrakant Dani

Dissertation

Submitted to the Faculty of the

Graduate School of Vanderbilt University

in partial fulfillment of the requirements

for the degree of

DOCTOR OF PHILOSOPY

In

Biological Sciences

December, 2014

Nashville, Tennessee

Approved

Todd Graham, Ph.D.

Kendal Broadie, Ph.D.

David Miller, Ph.D.

Douglas McMahon, Ph.D.

Billy Hudson, Ph.D.

Michael Tiemeyer, Ph.D.

To my family,

Chandrakant, Poonam and Neha

For standing by me through everything

ACKNOWLEDGEMENTS

A number of individuals deserve my most sincere gratitude for contributing to my training and growth as a scientist. Foremost is Dr. Kendal Broadie, who has served as an outstanding research advisor and mentor. While giving me the freedom to pursue my research interests, he has been steadfast in his guidance at every stage of my training, thereby edifying me with an exceptional learning experience. For their input on my dissertation research, I am very grateful to my committee members Dr. Todd Graham, Dr. David Miller, Dr. Douglas McMahon, Dr. Billy Hudson, and Dr. Michael Tiemeyer. I am particularly grateful to my external committee member, Dr. Tiemeyer, who on numerous occasions has lent his expertise in glycobiology and for welcoming me to the glycobiology community.

Over the years, several Broadie lab members have contributed significantly to my training as an experimentalist. I am indebted to Dr. Jeffrey Rohrbough and Emma Rushton for training in electrophysiology, imaging, and genetics, all of which became the essential tools that allowed me to complete my dissertation research. I am also thankful to other lab members Dr. Cheryl Gatto, Dr. Charles Tessier, Dr. Lane Coffee, and Dr. Caleb Doll, for their constructive criticism and for providing invaluable career advice. I am likewise appreciative of the many educators and administrators at Vanderbilt University, who have profoundly shaped my academic experience and guided me through the completion of this degree. In no specific order they are Dr. John Wikswo, Dr. James Patton, Dr. Kathy Friedman, and Leslie Maxwell. Through these years, I

have also been fortunate to be surrounded by exceptional peers and friends who have challenged and helped me grow as an individual. They include Dr. Dawit Jowhar, Ari Stillman and Mary Lynn Dear.

Importantly, I thank my parents, Chandrakant and Poonam Dani, for their unending love and support though all my academic ventures. To my sister Neha, I thank you for always being there for me and for being my champion through graduate school. Ultimately, these acknowledgements are incomplete without expressing my sincerest gratitude towards my grandmother, Asha Bhide, for believing in me and instrumentally influencing my academic trajectory.

TABLE OF CONTENTS

Page

LIST OF FIGURES

LIST OF TABLES

LIST OF ABBREVIATIONS

GPI	glycosyl phosphatidylinositol
CDG	congenital disorders of glycosylation
NMJ	neuromuscular junction
PSA	polysialic acid
NCAM	neural cell adhesion molecule
ECM	extracellular matrix
SynCAM	synaptic cell adhesion molecule
CAM	cell adhesion molecule
GAG	glycosaminoglycan
OB	olfactory bulb
TRP	transient receptor potential
NMDAR	N-methyl-D-aspartate receptor
ERAD	ER specific stress response
AMPAR	α-amino-3-hydroxy-5-methyl-4-isoxazolepropionic acid receptor
LTD	long term depression
LTP	long term potentiation
NET	norepinephrine transporter
SERT	serotonin transporter
SNP	single nucleotide polymorphism
DA	dopamine
DAT	dopamine transporter
PD	Parkinson’s disease
GLYT2	glycine transporter

GAT1	gamma-aminobutyric acid transporter 1
NKCC1	Na(+)-K(+)-2Cl(-) cotransporter-1
NGF	nerve growth factor
AMP	adenosine monophosphate
CREB	cyclic AMP response element binding protein
IRS-1	insulin receptor
ALS	Amyotrophic Lateral Sclerosis
NF	neurofilament
AD	Alzheimer's disease
PHF	paired helical filament
GSK-3β	glycogen synthase kinase 3β
AGE	advanced glycation end products
ADCC	antibody-dependent cellular cytotoxicity
PCD	para-neoplastic cerebellar degeneration
HL	Hodgkin lymphoma
DNER	Delta/Notch-like epidermal growth factor related receptor
GB	granzyme B
HSPG	heparan sulfate proteoglycan
SSR	sub-synaptic reticulum
AZ	active zone
BM	basement membrane
GalNAc	N-acetyl galactosamine
HRP	horse radish peroxidase
DGC	dystroglycan
LGMD	limb-girdle muscular dystrophy

CT	carbohydrate antigen
HS	heparan sulfate
WNT	wingless-type MMTV integration site family
TGF	transforming growth factor
BMP	bone morphogenic protein
UDPG	uridyl-diphosphate-6-glucose dehydrogenase
Ttv	*tout velu*
DLG	discs large
PSD	postsynaptic density
PS	position specific
JNK	jun N-terminal kinase
PIX	PAK-interacting exchange factor
GIT1	G protein couple receptor kinase interacting target
Tkv	thick veins
Jeb	jelly belly
Gbb	glass bottom boat
GluR	glutamate receptor
Wit	wishful thinking
Sax	saxophone
Alk	anaplastic lymphoma kinase
Mad	mothers against decapentaplegic
Erk	extracellular signal-regulated kinases
CamKII	calcium calmodulin kinase
Fz2	frizzled receptor 2

MTG	mind the gap
RNA	ribonucleic acid
GAG	glycosaminoglycan
VDRC	Vienna drosophila RNAi center
TEVC	two electrode voltage clamp
KEGG	Kyoto encyclopedia of genes and genomes
EJC	evoked junctional current
GFP	green fluorescence protein
Sdc	syndecan
FGF	fibroblast growth factor
P-mad	phosphorylated mothers against decapentaplegic
FasII	fasciclin
PI	propidium iodide
VNC	ventral nerve cord
RGD	arginine glycine aspartate
PSP	postsynaptic pocket
SV	synaptic vesicles
PTP	post tetanic potentiation
VVA	*Vicia villosa* agglutinin
HPL	*Helix pomatia* lectin
CHIEF	channelrhodopsin IEF variant
RAD	arginine alanine aspartate peptide
RGD	arginine glycine aspartate peptide

Brp	bruchpilot
ER	endoplasmic reticulum
MOGS	mannosyl-oligosaccharide glucosidase
GWAS	genome-wide association studies
CRISPR	clustered regulatory interspaced short palindromic repeat
TALEN	transcription activator-like effector nucleases
WGA	wheat germ agglutinin
DBA	*Dolichos biflorus* agglutinin
FMRP	fragile X mental retardation protein
FAK	focal adhesion kinase

Chapter I

INTRODUCTION

Glycans in the nervous system: A primer for the glyco-skeptic

Glycans (carbohydrates or oligosaccharides) are sugar modifications on glycoproteins and glycolipids that richly populate all nerve cell membranes (Figure 1). Glycans are known to play important, non-exclusive roles as ligands, modulators and co-receptors, but nevertheless remain enormously understudied in the context of neurobiology (Matani et al., 2007; Dityatev et al., 2010b; Soleman et al., 2013). This oversight has inhibited dissection of the fascinating glycan-mediated mechanisms that regulate neural development and synapse biology, including synaptic adhesion, neurotransmission and plasticity. The need to explore glycan mechanisms is underscored by the growing list of human 'glycanopathies', with a new disorder reported every 17 days on average (Freeze et al., 2014). Indeed, well over a 100 heritable genetic disorders result from mutations in genes encoding products that catalyze and regulate glycans, including O-fucosylation, O-GalNAcylation, O-GlcNAcylation, N- glycosylation, glycosaminoglycans, GPI-Anchors and dystroglycans (Figure 2). Surprisingly, there is a clear predominance of neural defects in congenital disorders of glycosylation (CDG) disease states (Freeze et al., 2014). Here I illustrate, glycan-mediated regulation of the nervous system, from molecules to behavior.

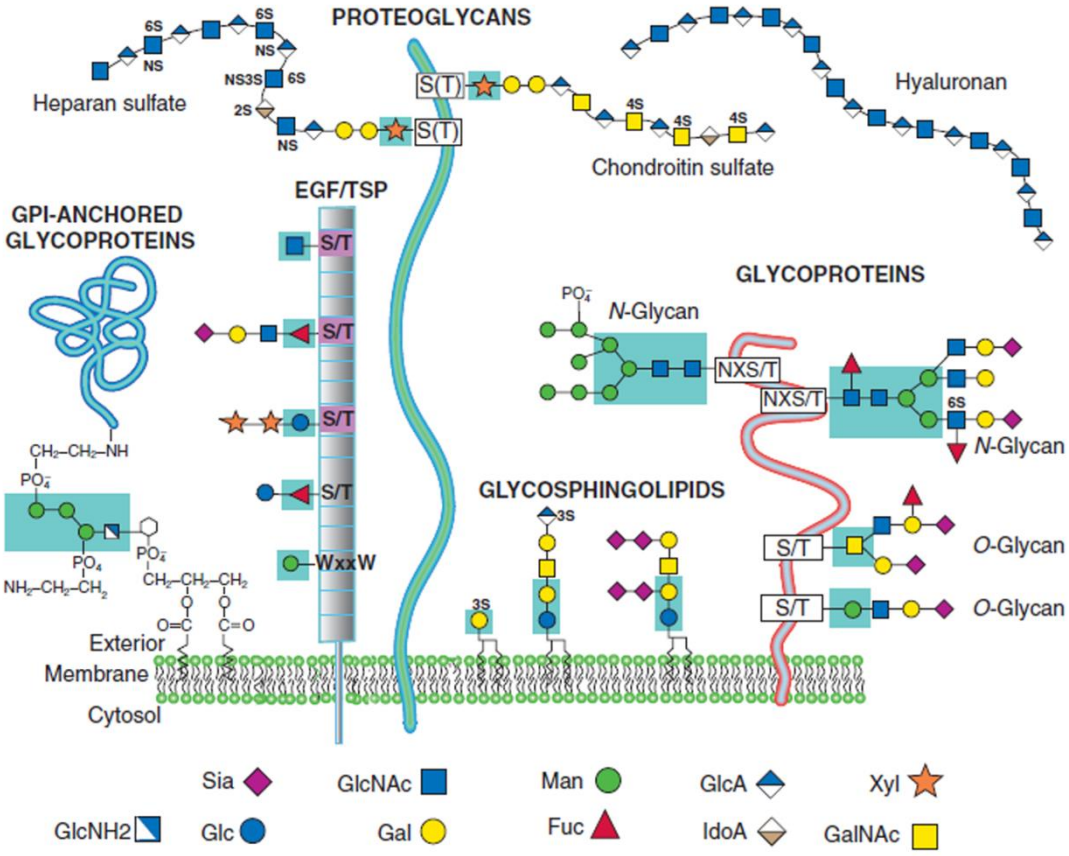

Figure 1. Glycocalyx of the cell membrane. Sugars boxed in teal are added in the endoplasmic reticulum. Other sugars are added during passage through the golgi. Abbreviations: mannose (Man), galactose (Gal), glucose (Glc), N-acetylglucosamine (GlcNAc), glucosamine ($GlcNH_2$), glucuronic acid (GlcA), iduronic acid (IdoA), N-acetylgalactosamine (GalNAc), xylose (Xyl), fucose (Fuc), sialic acid (Sia), 3-O-sulfated (3S), 6-O-sulfated (6S) and phosphate (PO_4^-). (Modified from Stanley, 2011)

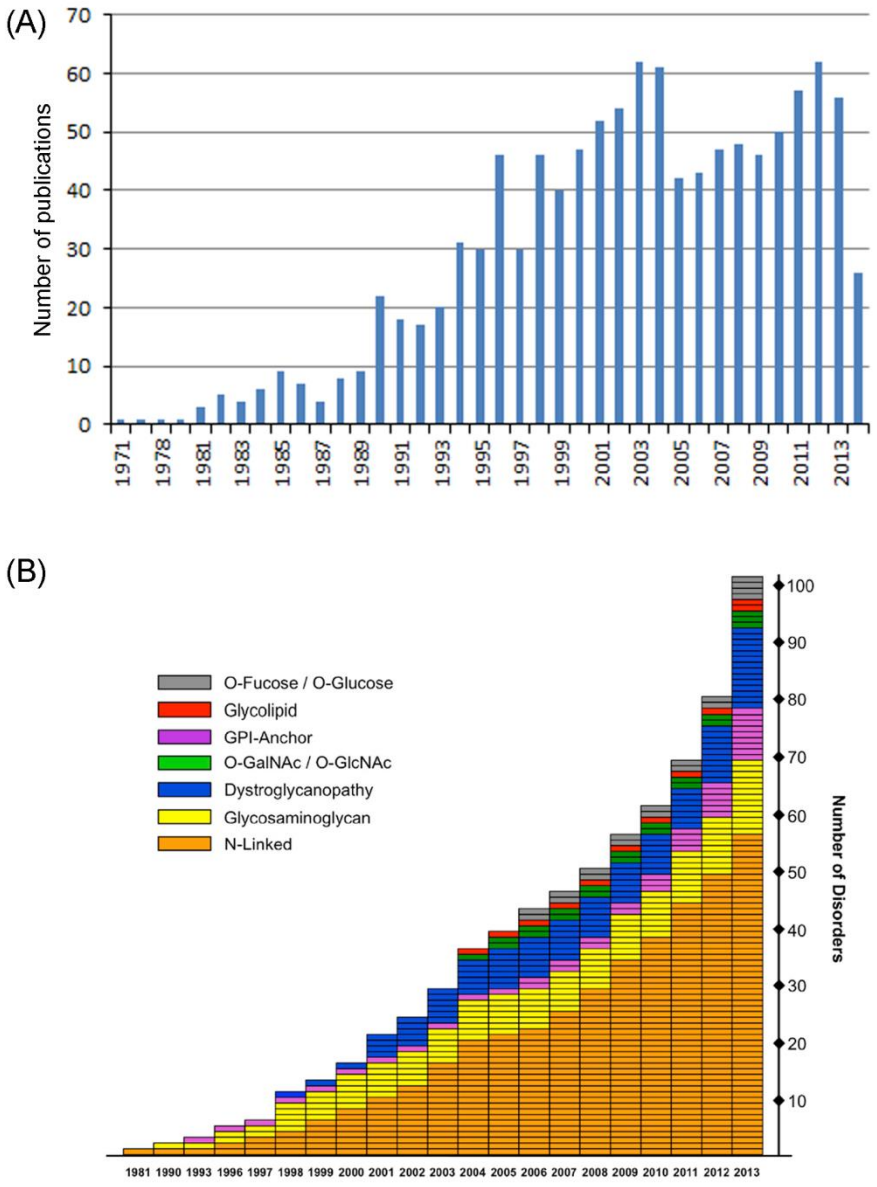

Figure 2. Neuroglycobiology publications and glycanopathies. (A) Number of papers with the search terms 'glycosylation' and 'neuron' in PubMed from 1971 to 2013. **(B)** Distribution shows the rate of identified dystroglycanopathies per year. (Adapted from Freeze et al. 2014)

It is my hope that these illustrated glycan roles will convince the glyco-skeptic, and illuminate the bounty that awaits explorers in the nascent field of neuroglycobiology. A PubMed search including the terms 'glycosylation' and 'neuron' yields a little over thousand articles from 1973 till present, clearly highlighting the infancy of this field (Figure 2). Here, I review with specific examples, some of the relatively well understood glycan-mediated effects on neural cell adhesion, neurotransmission and mechanisms underlying neural disease. This general overview (Chapter 1) is followed by a much more focused discussion of glycan functions at peripheral neuromuscular synapses in vertebrate and invertebrate systems (Chapter 2). The latter topic has been my focus during characterization of glycogene effects on synapse structure, function and plasticity at the *Drosophila* neuromuscular junction (NMJ) model synapse.

Glycosylation spatiotemporally regulates neural cell adhesion

Glycans form a dense glycocalyx layer on all cell surfaces (Varki et al., 1999). Given their location, one would predict glycan macromolecules to be obvious key regulators of cellular adhesion. One prime example of this function is polysialic acid (PSA), a post-synthetic N-linked modification found on neural cell adhesion molecule (NCAM), which decreases homophilic binding to attenuate intercellular adhesion (Rutishauser, 1998). *In vivo* experiments show that complete loss of PSA modification, by simultaneous deletion of two polysialyltransferase genes (St8sia-II and St8sia-IV), produces severe brain wiring defects, progressive hydrocephalus, postnatal growth retardation and

death. When NCAM was simultaneously deleted in this St8sia null background, all observed phenotypes were restored to normal, identifying for the first time a glycan to be more important than the glycoconjugate (glycan modified protein) as a whole (Weinhold et al., 2005). Another example where glycans play a key role in mediating adhesion is found on laminin, a major component of the extracellular matrix (ECM) (Chen et al., 2003). Non-glycosylated laminins support cell attachment but do not promote neural spreading or outgrowth, while glycosylated laminins increase cell spreading is a dose dependent manner. Further, proteolytic digestion of glycosylated laminin restores cell-spreading, suggesting that the laminin carbohydrates provide the essential information (Chandrasekaran et al., 1991). Glycans also control the activity of ECM receptor integrins, which bind laminins. Expression of O-mannosyltransferases, protein O-linked mannose N-acetylglucosaminyl-transferase 1 (PomGnT1) and N-acetylglucosaminyltransferase-VB (GnT-Vb) all enhance β1-integrin dependent neurite outgrowth on laminin (Abbott et al., 2006; Lee et al., 2006). Thus, glycosylation of both ECM and ECM receptors can regulate neural adhesion, spreading/migration and neurite outgrowth

Importantly, cell adhesion molecules (CAMs) can be multiply glycosylated for specific roles. For example, synaptic cell adhesion molecules (SynCAMs) mediating *trans*-synaptic adhesion come in multiple isoforms (SynCAM1, SynCAM2, SynCAM3 and SynCAM4) that can form homophilic and heterophilic complexes (Biederer, 2006). With expression of all 4 isoforms, removal of a single N-glycosylation site (N290) in SynCAM3 increases adhesion (Gao et al.,

2008), while mutation of another N-glycosylation residue (Asn60) in SynCAM2 reduces adhesion (Fogel et al., 2010). Thus, N-glycans at specific positions have differential effects on SynCAMs in regulating *trans*-synaptic adhesion. Likewise, enzymatic removal of a single N-glycosylation at Asn303 in the extracellular domain of postsynaptic Neuroligin-1 increases association with presynaptic Neurexin-1β (Comoletti et al., 2003), showing a similar mechanism in other *trans*-synaptic adhesion molecules. Moreover, modulation of glycosylation states of secreted synaptic cleft resident proteins, such as acetylcholinesterase (AChE), demonstrate an N-glycosylation requirement for interaction with Neurexin-1β. Conversely, excessive glycosylation can competitively disrupt neurexin/neuroligin adhesion to impair synapse adhesion (Xiang et al., 2014). Thus, glycans can specifically and singularly regulate neural cell adhesion by influencing the function of *trans*-synaptic, synaptic cleft resident or extracellular matrix glycoproteins.

Glycans can mediate the malleability of cell adhesion during physiological morphology changes associated with neural migration, axonal path finding and plasticity. For example, the levels of sialylated PSA isoforms are temporally regulated through development, with highly sialylated forms predominating in the developing brain that are gradually replaced by adult isoforms with lower silaic acid levels (Edelman, 1984). Consistently, hippocampal brain regions that maintain morphological plasticity during learning activity, as well as regenerating neurons, retain high density sialic acid modified NCAMs (Kiss and Rougon, 1997). Conversely, some glycans are progressively lost through development.

For example, in rat fetal neural cells, the N-linked glycosylated, polysialylated and sulfated D2 CAM progressively loses sulfated forms in postnatal stages (Lyles et al., 1984). Another example is Neuroglycan C, a brain specific proteoglycan involved in adhesion, that loses chondroitin sulfate glycosaminoglycan (GAG) chains during cerebellum and retinal development (Aono et al., 2000; Oohira et al., 2004).

Glycan modifications may also be transiently present during development. Levels of dolichyl phosphate mannose synthases that catalyzes formation of Dol-P-P-GlnCNAc2Man9Glc3, a major substrate of N-glycosylation, are higher at day 36 than day 15 in postnatal mouse development, with a peak coincident with synapse formation in the cerebral cortex (Idoyaga-Vargas and Carminatti, 1982). Similarly, the ECM glycoprotein Tenascin-R associated with Purkinje neuron cell bodies and dendrites in the molecular layer of cerebellum carries N-linked oligosaccharides that terminate with β1,4-linked GalNAc-4-SO(4) that are temporally regulated, increasing through cerebellar development between postnatal days 14 and 21, corresponding to a period of Purkinje cell dendrite extension and synaptogenesis (Woodworth et al., 2002). In mouse olfactory epithelium sensory neurons that extend into the olfactory bulb (OB), mutants deficient in glycosyltransferase β1,3 N-acetyl glucosaminyl transferase 1 (β3GnT1), a key enzyme in lactosamine glycan synthesis, exhibit disorganized OB innervation and postnatal smell perception deficit (Henion et al., 2005). However, at two weeks of age, lactosamine is unexpectedly re-expressed in sensory neurons of mutant mice through a secondary pathway, accompanied by

regrowth of axons in to the OB glomerular layer and a return of smell perception (Henion et al., 2005). Thus, glycans can spatiotemporally regulate neural cell adhesion with increases, decreases or transient peaks of specific glycan expression during brain development, particularly during synaptogenesis.

Glycosylation effects on neurotransmission

In addition to regulating neural development, glycans directly modulate neurotransmission strength. For example, synaptic vesicle associated proteins Synapsin I and II contain terminal N-acetylglucosamine (GlcNAc), and Synapsin I is also modified by O-GlcNAc addition (Lüthi et al., 1991). When the single O-GlcNAc site Thr-87 is mutated to alanine in primary hippocampal neurons, Synapsin I increasingly localizes to synapses, which increases synaptic vesicle clustering and vesicle reserve pool size (Skorobogatko et al., 2014). Similarly, the Ca^{2+} sensor Synaptotagmin1 bears both N and O-linked glycosylation, and mutational analysis reveals that the O-linked glycosylation partially targets the protein to dense core vesicles (Kanno and Fukuda, 2008). Mutation of the N-terminal N-glycosylation site re-directs Synaptotagmin 1 from vesicles to plasma membrane, while transplanting this same site onto Synaptotagmin 7 re-directs from plasma membrane to secretory vesicles (Han et al., 2004). In contrast, a more recent analysis showed clear requirements for N-glycosylation of integral synaptic vesicle protein SV2 in synaptic vesicle sorting, but no effects of glycosylation on Synaptotagmin1 (Kwon and Chapman, 2012). Thus, amino acid

residue specific glycans can instruct cellular localization and trafficking of synaptic vesicle proteins.

Glycans can also regulate the activity of channels to potently modulate synaptic transmission. Sialylation of β1 subunit of voltage-gated Na^+ channels induces a uniform hyperpolarizing shift of steady state membrane potential and kinetic gating of two alpha subunits, and reducing sialylation and N-glycosylation impairs β1-induced gating effects (Johnson et al., 2004). Sialylation also controls K^+ channel function, as Kv1.1 sialylation causes abnormal macroscopic activation and C-type inactivation kinetics producing a depolarized shift and shallower voltage slope (Sutachan et al., 2005). Removal of N-glycosylated chains from Kv12.2 in the mouse brain also causes a depolarizing shift in steady state activation, and unglycosylated Kv12.2 is not trafficked to the cell surface (Noma et al., 2009). Removal of glycosylation by site-directed mutagenesis of Asn220 and Asn229 N-glycan sites on yet another K^+ channel, Kv3.1, causes differential channel distribution and the generation of outward ionic currents with slower activation and deactivation rates than the glycosylated form (Hall et al., 2011).

Glycans have also been increasingly identified to regulate ion channels involved in sensory function. Insights into residue-specific effects of glycan loss on channel function is seen in the N-glycosylated Transient Receptor Potential Vanilloid 1 (TRPV1), which is the major determinant of capsaicin-evoked sensory responses (Veldhuis et al., 2012). Specific de-glycosylation or site-directed mutagenesis at residue N604 leads to rapid de-sensitization and loss of ion

selectivity of the TRPV1 channel (Veldhuis et al., 2012). Similarly, channel properties are also affected in conditions of specific loss of glycosylation in Transient Receptor Potential Melastatin 8 (TRPM8) channels (N934Q), leading to a shift in the threshold of temperature activation and reduced response to menthol/cold stimuli (Pertusa et al., 2012). Glycosylation also affects the trafficking of sensory receptors. For example, in human bitter taste receptors (TAS2R), non-glycosylated forms lacking N-glycosylation show substantially lower cell surface localization, potentially due to reduced association with chaperone calnexin (Reichling et al., 2008). Interestingly, site-specific glycosylation can also differentially regulate activity-dependent function. In the acid-sensing ion channel-1a (AISC1a), N-linked glycosylation at Asn393 and Asn366 residues produce differential effects: Asn393 mutations increase cell surface/dendrite trafficking, pH sensitivity and current density, and increase dendritic targeting in N366Q mutants under conditions of acidosis-induced spine loss, whereas N393Q mutants display the opposite effect (Jing et al., 2012). Thus, TRP channels that respond to numerous sensory modalities are subject to site-specific glycan-mediated control of their properties leading to perturbed neural responses.

The Ca^{2+} influx fundamental to neurotransmission and plasticity is also subject to glycan-mediated modulation(Frank, 2014). For example, voltage-gated Ca^{2+} channels are modulated by alpha-2 delta subunits in which N-glycan removal by N glycosidase F affects the current amplitude (Gurnett et al., 1996). Intracellular Ca^{2+} release is also subject to glycan-mediated regulation by inositol

1,4,5 triphosphate (InsP3) receptor type I, which is modified by O-GlcNAc glycosylation. Altering O-GlcNAc levels via oligosaccharyl transferase or loading with UDP-GlcNac decreases Ca^{2+} channel activity, which is reversed by sugar removal (Rengifo et al., 2007). N-glycosylation of Ca(V)3.2 T-type voltage-gated Ca^{2+} channels affects function by accelerating current kinetics, increasing current density and augmenting channel membrane expression, while de-glycosylating this channel inhibits T-currents and reverses hyperalgesia in diabetic ob/ob mice (Orestes et al., 2013). Thus, glycan-mediated effects on Ca^{2+} channel function play critical functions across a range of channel families.

Neurotransmitter-gated channels are also modulated by glycosylation. The cell surface expression of glutamatergic N-methyl-D-aspartate receptor (NMDAR) can be repressed by tunicamycin treatment through regulation of NR1 but not NR2A subunit synthesis. The inhibition of N-glycosylation activates Endoplasmic-reticulum-associated protein degradation(ERAD), which degrades non-glycosylated NR1 via ubiquitination and proteasome delivery (Gascón et al., 2007). The NMDAR GluN2 subunit is also subject to glycan-mediated regulation for synaptic targeting of the receptor, with GluN2B recruited in an activity-dependent manner requiring N-linked glycosylation (Storey et al., 2011). The α-amino-3-hydroxy-5-methyl-4-isoxazolepropionic acid receptor (AMPAR), another ionotropic glutamate receptor class, is similarly regulated by O-linked GlcNAc modification of the GluA2 subunit to modulate hippocampal long term depression (LTD) (Taylor et al., 2014). Further, acute inhibition of N-glycosylation depresses both NMDA and AMPA receptor currents by 30% in cultured hippocampal

neurons, and similar enzyme treatments in hippocampal slices reduces the amplitude of population spikes and long term potentiation (LTP) (Maruo et al., 2003). Mechanistically, N-glycan removal shifts the agonist concentration response curve of both receptor classes, causing a decrease in single channel opening probability and a depression of whole cell currents (Maruo et al., 2006). Thus, the critical flux of ions across cellular membranes can be modulated by glycosylation of voltage and neurotransmitter gated channels to modulate neural transmission, plasticity and behavior.

Neurotransmitter transporters are also modulated by glycosylation. For example, both norepinephrine and serotonin transporters (NET and SERTs) require N-glycosylation for assembly and surface expression, although not for antagonist binding affinity (Blakely et al., 1994). The human SERT extracellular loop has two sites for N-linked glycosylation that are critical for functional transporter expression. Curiously, a non-synonymous single nucleotide polymorphism (SNP) that introduces a third N-inked glycosylation site could substitute for either one or the two original glycosylation sites (Rasmussen et al., 2009). Further, dopamine (DA) transporter (DAT) activity depends on its glycosylation status, with DA transport more efficient in glycosylated forms compared to the non-glycosylated forms, which are less stable at the cell surface (Li et al., 2004). The glycan-dependent regulation of DAT may also have pathological ramifications, as glycosylated DAT was significantly higher in terminals of nigrostriatal neurons than the mesolimbic neurons. The former are progressively lost in Parkinson's Disease (PD), suggesting that glycosylation may

dictate differential vulnerability of midbrain dopaminergic cells in this neurodegenerative disease (Afonso-Oramas et al., 2009). Disruption of the N-glycosylation sites on the Glycine transporter (GLYT2), that removes glycine from the inhibitory synaptic cleft, reduces activity by 35-40% (Martínez-Maza et al., 2001). Likewise, mutations of two of the three N-glycosylation sites in the extracellular loop of gamma-aminobutyric acid transporter 1 (GAT1) at inhibitory synapses reduces transporter turnover (Liu et al., 1998). Inhibiting N-linked glycosylation of the Na(+)-K(+)-2Cl(-) cotransporter-1 (NKCC1), normalizes GABA reversal potentiation and restores GABA inhibition of presympathetic neurons in spontaneously hypertensive rats (SHRs), and restores GABAergic inhibition by maintaining chloride homeostasis (Ye et al., 2012). Thus, neurotransmitter transporters represent another class of synaptic proteins sensitive to specific glycosylation states, largely by affecting trafficking and cell surface expression.

Interestingly, for some synaptic proteins, glycan modifications can suppress function. For example, in neurotrophic factors responsible for neural growth, survival and plasticity (Thoenen, 1995), the nerve growth factor (NGF) Tyrosine Kinase Receptor 1 (TrkA) contains four N-glycosylation sites necessary to prevent ligand independent activation and correctly localize TrkA to the cell surface. Non-glycosylated forms are trapped intracellularly and are unable to activate the Ras/MAP kinase signaling pathway (Watson et al., 1999). Moreover, downstream signaling factors such as cyclic AMP response element binding protein (CREB) known to contribute to synapse development and plasticity, also

exhibit glycan-mediated regulation. In response to neuronal activity, CREB is dynamically modified by O-linked N-acetyl glucosamine and this glycosylation represses CREB-dependent transcription (Rexach et al., 2012). Thus, glycan modification can affect neurotransmission by positively or negatively influencing a wide range of synaptic targets including synaptic vesicle proteins, voltage-gated ion channels, ligand-gated ion channels, neurotransmitter transporters, neurotrophic factors and associated downstream signaling pathways. This modulation may arise from defects in protein folding, trafficking or expression of the glycan-modified targets.

Novel mechanisms revealed by studying glycan related diseases

While a complete description of diseases arising from aberrant glycosylation is beyond the scope of this overview, I will briefly discuss novel modes of glycan-mediated regulation that are aberrant in specific disease conditions. One such mechanism is observed in proteins where glycan modification can affect subsequent post-translational modifications (Seet et al., 2006). This interaction is best understood for cytosolic O-GlcNAc modifications and phosphorylation at serine/threonine residues. The mechanism of cross-talk can include alternative/competitive occupancy of the same residue, alternative and reciprocal occupancy at different sites, simultaneous occupancy at different sites, or site-dependent reciprocal (O-glycosylation or phosphorylation) or simultaneous (O-glycosylation and phosphorylation) occupancy (Zeidan and Hart, 2010). These mechanisms regulate neural transcription factor C/EBPβ,

insulin receptor IRS-1 and calcium-dependent kinase CaMKIV, affecting DNA-binding capacity, turnover and enzymatic activity, respectively (Yang et al., 2008; Dias et al., 2009; Li et al., 2009). Similar cross-regulation also occurs in Amyotrophic Lateral Sclerosis (ALS) disease models, where neurofilament (NF) proteins form intermediate filaments that are modified and regulated by competing post-translational modifications. On a single NF subunit, O-GlcNAc levels on the tail domain decrease with reciprocal increases in phosphorylation, suggesting that synchronous regulation of glycosylation and hyperphosphorylation may underlie the pathophysiological contribution (Lüdemann et al., 2005).

Cross-talk between glycosylation and phosphorylation also appears in Alzheimer's disease (AD) models, in neurofibrillary plaques composed of post-translationally modified microtubule associated Tau protein. Tau is known to form abnormal bundles of straight filaments under conditions of hyperphosphorylation and de- glycosylation (Arnold et al., 1996). However, restoration of normal microtubule polymerization activity occurs only when Tau is both dephosphorylated and de-glycosylated. Hence, hyper-phosphorylation appears to promote aggregation of Tau and inhibit assembly of microtubules, while glycosylation appears to stabilize the abnormal Tau paired helical filament (PHF) structure (Wang et al., 1996). Increased non-enzymatic glycosylation of PHFs decreases ability to bind tubules and leading to the pathological aggregations. Further evidence of cross talk comes from *in vitro* studies where de-glycosylation of aberrantly glycosylated tau decreases subsequent phosphorylation of Tau at

Ser214, Ser262 and Ser356 by protein kinase A. Interestingly, this de-glycosylation of Tau positively modulates further de-phosphorylation by protein phosphatase 2A and protein phosphatase 5 at another set of residues Ser198, Ser199 and Ser202 (Ledesma et al., 1994). Tau protein can also be regulated by kinase pair Cdk2/GSK-3β, such that phosphorylation of neighboring residues S396 and S404 significantly decreases S400 O-GlcNAcylation. Reciprocally, S400 O-GlcNacylation reduces S404 phosphorylation by Cdk2/Cyclin A3 kinase and interrupts GSK3-β mediated sequential phosphorylation (Smet-Nocca et al., 2011). Additionally, Tau can also be non-enzymatically glycosylated, which is characterized by reducing sugars condensing with free amino groups of proteins, leading to rearrangement and dehydration to forming unsaturated pigments and cross-linked products called advanced glycation end products (AGEs) (Monnier and Cerami, 1981; Vlassara et al., 1983; Peppa et al., 2003). AGEs are routinely found in neurodegenerative diseases including Alzheimer's (Smith et al., 1994), Parkinson's (Castellani et al., 1996), Pick's (Kimura et al., 1996) diseases, ALS (Kato et al., 2000) and diabetic conditions (Garlick et al., 1984), but it remains to be identified if cross-regulatory mechanisms are also involved in these conditions. Taken together, these studies show that glycosylation modifications at specific residues can lead to a number of compounding effects.

Glycans can also be important for the detection of neural disorders, and used as biomarkers for diagnosis. For example, in ALS high levels of sialylated glycans, low levels of core fucosylated glycans and the expression of specific glycan A2BG2 is observed in patient sera. These glycan changes increase the

affinity of IgG type antibodies to CD16 of effector cells leading to Antibody-Dependent Cellular Cytotoxicity (ADCC) in brain and spinal cord tissue (Edri-Brami et al., 2012). In this way, glycan changes correlated with ALS can serve as an effective biomarker. Similarly, diagnostic glycan patterns in the brain occur in para-neoplastic cerebellar degeneration (PCD) combined with Hodgkin lymphoma (HL). In this neurological condition, anti-Tr antibodies are generated against the Delta/Notch-like epidermal growth factor related receptor (DNER), with the antibodies recognizing a N-glycosylation epitope (de Graaff et al., 2012). A similar situation also arises in Rasmussen's encephalitis, a severe form of pediatric epilepsy, in which granzyme B(GB) serine protease is released by activated immune cells generating the GluR3B autoantigenic peptide, as long as no N-linked glycosylation is present within GluR3-GB recognition site (Gahring et al., 2001). This change may serve as a prime candidate for the development of antibodies against the N-linked glycosylation, allowing us to exploit the activation of the particular glycan modification as a biomarker for diagnosis.

In summary, these few examples illustrate that glycans can widely regulate neural properties at molecular, synaptic, circuit, developmental and behavioral levels. Through these examples, we can make some general conclusions about glycan-mediated neural effects. First, the neural proteins that mediate these effects can be modulated either by virtue of their own glycan modifications or by glycan-mediated regulation of their interacting partners. Second, the same classes of glycan modification can have positive or negative regulatory effects when attached to protein A, while being completely

dispensable for the function of protein B, indicating molecule-specific effects of glycosylation. Third, multiply glycosylated proteins show position-specific effects of loss or gain of glycan modifications, which can also influence other post-translational modifications. Fourth, glycan modifications are spatiotemporally regulated during normal development and in neuropathological conditions. Moving forward, studying neuroglycobiology, particularly in genetically tractable models, will allow for novel mechanistic characterization of these critically important non-template driven macromolecules.

Chapter II

Glycosylated Synaptomatrix Regulation of Trans-Synaptic Signaling

This paper has been published under the same title in *Developmental Neurobiology*, 2012

Neil Dani and Kendal Broadie

Departments of Biological Sciences, and Cell and Developmental Biology,

Kennedy Center for Research on Human Development,

Vanderbilt University, Nashville, TN 37232 USA

Abstract

Synapse formation is driven by precisely orchestrated intercellular communication between the presynaptic and the postsynaptic cell, involving a cascade of anterograde and retrograde signals. At the neuromuscular junction (NMJ), both neuron and muscle secrete signals into the heavily glycosylated synaptic cleft matrix sandwiched between the two synapsing cells. These signals must necessarily traverse and interact with the extracellular environment, for the ligand-receptor interactions mediating communication to occur. This complex synaptomatrix, rich in glycoproteins and proteoglycans, comprises heterogeneous, compartmentalized domains where specialized glycans modulate *trans*-synaptic signaling during synaptogenesis and subsequent synapse modulation. The general importance of glycans during development, homeostasis and disease is well established, but this important molecular class has received less study in the nervous system. Glycan modifications are now understood to play functional and modulatory roles as ligands and co-receptors in numerous tissues, however roles at the synapse are relatively unexplored. We highlight here properties of synaptomatrix glycans and glycan-interacting proteins with key roles in synaptogenesis, with a particular focus on recent advances made in the *Drosophila* NMJ genetic system. We discuss open questions and interesting new findings driving the current investigation of the complex, diverse and largely understudied glycan mechanisms at the synapse.

Introduction

Electrically excitable cells (neurons and muscles) are precisely connected via chemical synapses to form functional networks. Study of the neuromuscular junction (NMJ) synapse between motor neuron and muscle cell has been particularly instrumental in elucidating molecular mechanisms that drive synaptogenesis, both in vertebrate and invertebrate models (Sanes and Lichtman, 2001; Marques, 2005; Kummer et al., 2006; Collins and DiAntonio, 2007; Korkut and Budnik, 2009). Secreted glycoproteins (GPs) and proteoglycans (PGs) interface with presynaptic and postsynaptic cell surfaces within the NMJ synaptic cleft and in adjacent perisynaptic domains. These highly compartmentalized extracellular environments harbor heavily glycosylated extracellular matrix (ECM) proteins as well as glycosylated transmembrane receptors and outer-leaflet glycolipids, which together form the 'synaptomatrix' (Dityatev et al., 2010c; Vautrin, 2010). All of these sugar-coated molecules potentially interact with the multiple bidirectional *trans*-synaptic signals, themselves highly glycosylated, which must necessarily traverse this extracellular landscape to induce and modulate synaptic development, homeostasis, plasticity and disease (Akins and Biederer, 2006; Margeta and Shen, 2010; Shen and Cowan, 2010; Wu et al., 2010). Recent studies have begun to reveal the importance of glycans in enabling and directing intercellular signaling in a wide variety of cellular contexts (Hynes, 2009; Dityatev et al., 2010c). An appreciation of the extracellular glycan environment, including knowledge of the many glycan

classes and their biochemical properties, is becoming essential for the understanding of many areas of developmental neurobiology (Varki et al., 1999).

To date, the function of glycosylated ECM components has primarily been studied in non-neuronal cells (Kalluri, 2003; Nelson and Bissell, 2006; Hynes, 2009; Sorokin, 2010); however, a range of glycan functions are increasingly being appreciated at both vertebrate and invertebrate synapses (Dityatev et al., 2010a, 2010c). We have known that the synaptomatrix is rich in glycan modifications (Vautrin, 2010), but are only now beginning to more fully understand the function of glycans during synaptogenesis and synaptic modulation. Glycan modifications such as glycosaminoglycans (GAGs) have well established roles in differentiation, tissue morphogenesis and organogenesis (Kramer, 2010). Genetic studies in mice, *Drosophila* and *C. elegans* have also revealed developmental requirements for numerous specific monosaccharide and polysaccharide sugar modifications including O-fucose, O-mannose (Man), mucin-type O-glycans and N-glycans (Haltiwanger and Lowe, 2004). A true testament to the importance of glycans arises from the growing list of human diseases attributed to mutations in glycan biosynthetic genes (Jaeken and Matthijs, 2007; Jaeken et al., 2009), homologs of which are actively being studied in genetic model organisms (Altmann et al., 2001; Hewitt, 2009). For example, N-glycan biosynthesis defects induce disease states collectively categorized as congenital diseases of glycosylation (CDGs), with common disorders such as metabolic syndrome and autoimmunity also tied to this glycan class (Dennis et al., 2009). Similarly, O-linked glycosylation defects give rise to numerous

diseases that include the muscular dystrophy class of neuromuscular disorders (Wopereis et al., 2006). Mechanistically, glycan modifications feature prominently in intercellular signaling, with cell surface organization and receptor clustering dependent on specific glycans being recognized and organized by glycan-binding lectin proteins (Martin, 2002; Yamaguchi, 2002; Kleene and Schachner, 2004; Patnaik et al., 2006). These precedents warrant scrutiny of these same molecular classes during physiological processes of synaptogenesis and synaptic modulation, as well as in synaptic disease states, which are all highly dependent on intercellular signaling.

One way forward in the exploration of glycans and glycan-mediated mechanisms at the synapse is to exploit the genetically-tractable *Drosophila* NMJ, a reduced genetic redundancy for the inherently complex glycan modification pathways (Hagen et al., 2009). Mammalian glycan modifications including hybrid and sialylated N-glycans are found in *Drosophila*, albeit at lower concentrations, with the majority of modifications being high- or paucimannosidic glycans (Koles et al., 2007). Further, *Drosophila* and mammalian glycan biosynthetic galactosaminyltransferases enzymes show similar substrate preferences and share preferred sites of O-linked N-acetylgalactosamine (GalNAc) sugar modifications on target proteins (Ten Hagen et al., 2003a). Unbiased forward genetic *Drosophila* screens have already contributed to understanding of heparan sulfate proteoglycan (HSPG) biosynthetic pathways, which have subsequently been shown to be important for cell-signaling, morphogenesis, metabolism and tissue repair in mammals (Bishop et al., 2007).

Based on the confidence of conserved glycan pathways, investigations using the *Drosophila* NMJ are now poised to make significant contributions to the systematic *in vivo* study of glycan functions involved in synapse formation and modulation. The aim of this review article is to highlight synaptomatrix glycans, glycan-interacting proteins, glycosylated ligands and their receptors, focusing on their recently discovered roles in synapse assembly at the *Drosophila* NMJ. Such studies should be of interest not only to synapse biologists, but also within other fields of neuroscience and developmental biology, as insights derived from glycan roles in synaptogenesis are likely to be directly relevant to other arenas of intercellular communication in the nervous system and during global development.

The glycosylated synaptomatrix at the neuromuscular junction

Architecture of the NMJ synaptomatrix

At the vertebrate NMJ, the primary (1°) synaptic cleft is the space between the motor neuron and the muscle that is continuous with secondary (2°) synaptic clefts formed by muscle cell membrane invaginations that lie apposed to the innervating motor neuron (Patton, 2003). The *Drosophila* NMJ cleft has a similar architecture, however the postsynaptic muscle folds form the sub-synaptic reticulum (SSR) that opens into the synaptic junctional cleft adjacent to presynaptic active zones (AZ) (Prokop, 2006). The vertebrate cholinergic NMJ 1° cleft is generally 40-50 nm wide and contains a clearly-defined synaptic basal lamina, or basement membrane (BM), that also occupies the 2° clefts and is

continuous with the ensheathing muscle lamina (Patton, 2003). In comparison, the *Drosophila* glutamatergic NMJ 1° cleft is only 15-20 nm wide, and in place of a synaptic lamina there is an electron-dense specialization found only between the apposing presynaptic AZ and postsynaptic density (Prokop, 2006). In cross-section, this synaptic cleft domain contains periodic densities, and in freeze-fracture displays a highly-ordered honeycomb pattern (Prokop, 1999). At the vertebrate NMJ, the synaptic basal lamina provides mechanical support, harbors signaling factors and serves as a substratum during synaptogenesis (Patton, 2003). At the *Drosophila* NMJ, loss of the cleft synaptomatrix causes catastrophic failure of postsynaptic assembly and a near complete silencing of functional synapses during embryonic synaptogenesis (Rohrbough et al., 2007). These animals are consequentially paralyzed and die as mature embryos unable to escape the eggcase.

Synaptomatrix contains glycosylated ECM protein isoforms

Glycosylation at the vertebrate NMJ has long been studied using fluorescently-conjugated lectins (Ribera et al., 1987; Scott et al., 1988; Crnefinderle and Sketelj, 1993), which bind specific carbohydrates, and to a lesser extent, with anti-carbohydrate monoclonal antibodies that detect specific carbohydrates such as β-linked GalNAc (Martin et al., 1999b) and cytotoxic T cell (CT) carbohydrate antigens (Lefrancois and Bevan, 1985). Both approaches reveal restriction of synaptic carbohydrate modifications to different presynaptic (e.g. CT1) and postsynaptic (e.g. CT2) compartments, suggesting localized requirements for specific glycan modifications (Martin et al., 1999b). Likewise,

anti–heparan sulfate antibodies that recognize HSPG glycosaminoglycan modifications show clearly distinguishable synaptic and extrasynaptic (on the muscle, but away from the synapse) glycan environments(Jenniskens et al., 2000). Plant and fungal lectins have been especially useful for revealing localized sugar modifications at the vertebrate NMJ. For example, Wheat Germ Agglutinin (WGA), Soy bean agglutinin (SBA), Concanavilin A (ConA), *Griffonia simplicifolia* 1 isolectin B-4 (GS-1), *Limax flavus* agglutinin (LFA), Peanut agglutinin (PNA) and *Dolichos biflorus* agglutinin (DBA) lectins all show strong labeling of NMJ synaptic regions compared to low labeling of extrasynaptic regions (Iglesias et al., 1992). In addition to highlighting spatially localized glycan modifications, these studies provide insight into specialization of the ECM associated with the NMJ (Lis and Sharon, 1986; Iglesias et al., 1992).

Similar localized carbohydrate distributions are also seen in *Drosophil*a. Studies show that embryonic neuronal somata bind ConA and *Limulus polyphemus* agglutinin (LPA); central and peripheral neuronal processes bind WGA, PNA, *Ulex Europeus* agglutinin 1 (UEA-1) and *Bauhina purpura* agglutinin (BPA) lectins; while SBA labeling is completely excluded from the nervous

system (Fredieu and Mahowald, 1994; Damico and Jacobs, 1995). At the *Drosophila* NMJ, WGA and *Vicia villosa* agglutinin (VVA) lectins show clearly enriched synaptic labeling (Fig. 3) (Haines and Stewart, 2007; Rushton et al., 2009). WGA labels clearly defined extracellular punctae that are widely distributed over the muscle surface, but is much more intense, densely-spaced and organized immediately adjacent to presynaptic boutons (Fig. 3A). These

WGA domains clearly indicate that the extracellular space is compartmentalized into glycan-specialized regions. VVA labeling is almost wholly restricted to the NMJ, with little or no labeling in extrasynaptic domains (Fig. 3B). In clear contrast to WGA, VVA labels a more contiguous synaptomatrix domain closely associated with NMJ boutons. Importantly, the NMJ synaptomatrix is defined as much by the absence of carbohydrates as their presence. PNA (Fig. 3C) and DBA (Fig. 3D) lectins clearly and intensely label non-synaptic areas but are effectively excluded from the NMJ. This is in contrast to vertebrate NMJ lectin labeling, where DBA exclusively labels rat synaptic domains (Iglesias et al., 1992), indicating some species-specific differences. DBA recognizes trisaccharide-linked GalNAc, and does label other *Drosophila* neuronal tissues such as the omatidia in the developing eye (Yano et al., 2009). The lack of DBA labeling at the *Drosophila* NMJ indicates the presence of a regulated and controlled synaptic environment that expresses specific arrangement of sugars. These studies indicate conservation of glycan modifications, as well as the fact that differences exist in glycan expression between vertebrate and invertebrate NMJs.

Besides charting the NMJ glycan landscape, lectins have been used to directly identify glycan modifications on synaptic proteins. *In vit*ro studies show that purified synaptic laminin (s-laminin) binds WGA, ConA, *Maackia amurensis* agglutinin (MAA), *Ricinus communis* agglutinin (RCA120), *Datura stramonium* agglutinin (DSA) and *Aleuria aurantia* agglutinin (AAA) (α(1-6)-fucose) lectins, without binding PNA (Chiu et al., 1992). These findings illustrate the specific but heterogeneous nature of glycan modifications present on just a single

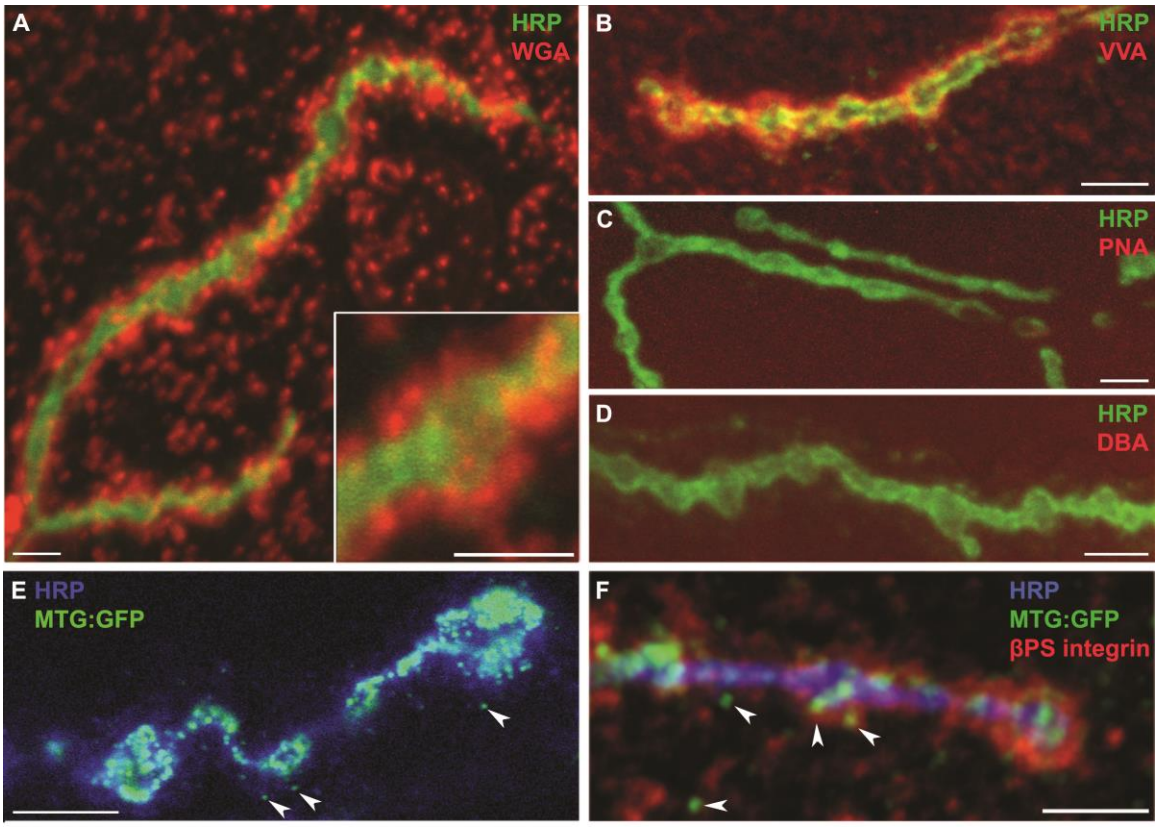

Figure 3. Glycan and glycan-interacting lectin expression domains at the *Drosophila* NMJ.

The *Drosophila* wandering third instar NMJ probed with a range of lectins and antibodies in detergent-free conditions to maintain synaptomatrix integrity. **A**) NMJ probed with WGA lectin (red) and anti-HRP (green), which recognizes glycans associated exclusively with the presynaptic neuronal membrane. The inset shows WGA domains in the synaptomatrix surrounding a single NMJ bouton. **B**) VVA lectin (red) and HRP (green). The VVA labeling occupies a different domain than WGA labeling, and is very highly enriched in the NMJ synaptomatrix. **C**) PNA lectin (red); HRP (green). **D**) DBA lectin (red); HRP (green). Note that both PNA and DBA lectins do not detectably label the NMJ synaptomatrix, although strong labeling is present in adjacent tissues (not shown). **E**) The MTG:GFP fusion protein (green) co-labeled with anti-HRP (blue). The MTG lectin localizes to synaptomatrix punctae (arrows) surround NMJ synaptic boutons. **F**) Triple labeling of MTG:GFP (green), βPS integrins (red) and HRP (blue). Note the three overlapping domains in the synaptomatrix. Scale bars = 5 μm.

synaptomatrix molecule required for NMJ development (Table IA) (Maselli et al., 2009). Lectin staining also has helped to visualize sugar modifications on dystroglycan, an ECM receptor found both at vertebrate and *Drosophila* NMJs. At the *Drosophila* synapse, VVA lectin co-localizes with dystroglycan (Haines and Stewart, 2007). More recently, lectins such as *Galanthus rivalis* agglutinin (GNA), *Nicotiana tabacum* (Nictaba) and *Rhizoctoni solani* agglutinin (RSA) have been utilized in lectin-affinity chromatography coupled to mass spectrometric analysis to elucidate N- and O- linked glycosylation of a large number of *Drosophila* synaptomatrix components such as lamininB2, LamininA, *terribly reduced optic lobes* (*trol*; homolog of vertebrate perlecan) and the HSPG *division abnormally delayed* (*dally*) (Vandenborre et al., 2010). Lectins are a powerful tool for glycan investigation with enormous scope for increased use in future *Drosophila* NMJ studies.

In addition to the above mentioned glycan distributions, the specialization of NMJ synaptomatrix stems from the presence of specific isoforms of otherwise ubiquitous ECM glycoproteins and proteoglycans, including laminin, collagen (IV) and perlecan. At the vertebrate NMJ, global basal lamina glycoproteins such as lamininα2/γ1, entactin, fibronectin and perlecan are present, along with synaptically-specialized isoforms such as laminin α4/α5/β2, collagen α3(IV)/α4(IV)/α5(IV), neuregulin α2, synaptic entactin (s-entactin), perlecan and agrin (Table IA). Synaptic cleft specific proteins like laminin α4, β2 and α5 are N-glycosylated, and recent proteomic studies have established two galactosyltransferases involved in core glycosylation of s-collagen (Chen et al.,

2009c; Schegg et al., 2009). GalNAc sugar modifications found exclusively in synaptic basal lamina further indicate the importance of glycosylation of NMJ synaptomatrix proteins (Scott et al., 1988; Hall and Sanes, 1993; Patton, 2003). In contrast, the molecular composition of the cleft material in the *Drosophila* NMJ is only poorly characterized (Table IB). Indirect evidence for vertebrate-like NMJ specialization comes from the a number of orthologous proteins to laminin B2 (Montell and Goodman, 1989), collagen IV (Borchiellini et al., 1996), dystroglycan (Bogdanik et al., 2008) and perlecan (Voigt et al., 2002) which have been identified at the *Drosophila* NMJ. However, clear roles in *Drosophila* synaptogenesis have only been tested for laminin A (Prokop et al., 1998); mutations cause a decrease in the extent of interaction between the motor neuron and muscle (Table 1B). Clearly, there is enormous scope for further studies using the *Drosophila* genetic model.

Synaptomatrix bounding cell membranes bear glycosylated proteins

In addition to secreted ECM protein glycosylation, most of the transmembrane proteins involved in cell adhesion and signaling during synaptogenesis carry extensive carbohydrate modifications. For example, *Drosophila* cell adhesion molecules (CAMs), such as fasciclins I-III (e.g. fasII homolog of vertebrate neural cell adhesion molecule (NCAM)) and neuroglian (homolog of vertebrate L1), are developmentally-regulated glycoproteins involved in homophilic recognition, adhesion and maintenance functions during synaptogenesis (Table IB) (Bastiani et al., 1987; Patel et al., 1987; Harrelson and Goodman, 1988; Bieber et al., 1989; Elkins et al., 1990; Halpern et al., 1991).

NCAM and L1 are decorated with specific L2/HNK-1 carbohydrate moieties (Kruse et al., 1984), and their *Drosophila* homologs are similarly modified and recognized by an antibody against the horse radish peroxidase (HRP) epitope, a fucosylated N-glycan (Fig. 3) (Jan and Jan, 1982). Interestingly, fasciclins expressed outside developing neural tissue are not bound by HRP antibodies, indicating these are neural-specific glycosylation pathways (Snow et al., 1987). NCAM is also modified by polysialic acid (PSA) addition, which inhibits cell adhesive activities (Sadoul et al., 1983). Indeed, sialic acid modifications are particularly important in modulating the activities of membrane proteins involved in vertebrate intercellular signaling (Rutishauser, 2008), and similarly during *Drosophila* development (Roth et al., 1992). In vertebrate synapses, sialylated glycans are present in the synaptic cleft extracellular space, where they are involved in cell adhesion and intercellular communication (Varki and Varki, 2007; Rutishauser, 2008; Muhlenhoff et al., 2009), although the function of synaptic sialylation remains poorly characterized.

Conserved *Drosophila* sialylation biosynthetic pathways include sialic acid phosphate synthase (Kim et al., 2002), CMP-sialic acid synthetase (Viswanathan et al., 2006) and *Drosophila* sialyltransferase (DSiaT) with homology to mammalian ST6Gal sialyltransferases (Koles et al., 2004). At the *Drosophila* NMJ, DSiaT plays roles in synaptogenesis that affect the manifestation of locomotory behavior (Repnikova et al., 2010). One aspect of this requirement is that DSiaT modulates voltage-gated sodium channels. In vertebrates, similar regulation involves negative charge due to polysialylation, but in *Drosophila* the

mechanism appears dependent on monosialylation (Koles et al., 2004). Sialic acid modifications also modulate synaptogenesis independently through regulation of CAM homophilic interactions. For example, addition of polysialic acid to NCAM attenuates adhesion and also interferes with other CAMs, such as L1 (Rutishauser, 1998). Recently, a screen for synaptic mutants in *Drosophila* uncovered *fuseless* (*fusl*), the putative homologue of the mammalian Sialin 8-pass transmembrane sialic acid transporter (Long et al., 2008). In vertebrates, the monosaccharide sialic acid cleaved from sialoglycoconjugates is exported across membranes by the Sialin transporter (Morin et al., 2004; Wreden et al., 2005) and two inherited cognitive dysfunction diseases occur in humans when the sialin gene is mutant (Verheijen et al., 1999). At the *Drosophila* NMJ, *fusl* mutants display >75% reduction in evoked synaptic transmission due to a presynaptic requirement in localizing Cacophony Ca^{2+} channels (Kawasaki et al., 2000; Xing et al., 2005). The homologous vertebrate Ca^{2+} channel (α-1 subunit) binds ECM laminins, to facilitate organization of presynaptic active zones (Table IA) (Nishimune et al., 2004). At the *Drosophila* NMJ, the Bruchpilot protein stabilizes active zone formation by integrating Cacophony Ca^{2+} channels with intracellular components and, just like *fusl* mutants (Long et al., 2008), *bruchpilot* mutants show reduced Ca^{2+} channel clustering and impaired vesicular release (Kittel et al., 2006; Wagh et al., 2006). Since sialic acid modifications are typically added as the terminal residue of cell surface oligosaccharides, one attractive model is that such a carbohydrate addition to the extracellular domain of the

presynaptic Ca^{2+} channel provides a critical link to the synaptic cleft ECM, driving active zone assembly during synaptogenesis.

Another important synaptomatrix component that is required to tether the muscle to the ECM is dystroglycan (Dg), part of the dystrophin associated glycoprotein complex (DGC) (Pilgram et al., 2010). In addition to binding the intracellular cytoskeleton, the α-dystroglycan in the DGC binds multiple extracellular synaptomatrix components such as secreted agrin (Sugiyama et al., 1994) and perlecan (Talts et al., 1999), and transmembrane neurexin (Sugita et al., 2001). At the *Drosophila* NMJ, dystroglycan facilitates the organization of glutamate receptor (GluR) clusters in the postsynaptic domain (Table IB), and plays roles in the organization of muscle costameres and attachment sites to the epidermal tendon cells (Bogdanik et al., 2008). In vertebrates, mutations in at least three glycan biosynthetic genes (POMT1 (de Bernabe et al., 2002), POMT2 (van Reeuwijk et al., 2005) and POMGnT1 (Yoshida et al., 2001)), produce hypo-glycosylation of α-dystroglycan. Dysfunctional glycosyltransferases give rise to a range of diseases termed dystroglycanopathies that give rise to congenital muscular dystrophies (CGDs) and limb-girdle muscular dystrophy (LGMD) (Martin, 2007). In vertebrates, dystroglycan serine/threonine residues are modified by glycans Neu5Ac(α2-3)Gal(β1-4)GlcNAc(β1-2)Man(α1-O-S/T) and a core 1 O-linked structure Gal(β1-3)GalNAc(α1-O-S/T) (Endo, 1999). Other sugar modifications include CT carbohydrate antigen (Hoyte et al., 2002), HNK-1 antigen (Smalheiser and Kim, 1995) and Lewis-X antigen (Martin, 2003a). At the *Drosophila* NMJ, mutation of the two mannosyltransferase enzymes that target

dystroglycan for glycosylation, *tw* (POMT1) and *rt* (POMT2) (Nakamura et al., 2010), recapitulate synaptic phenotypes of reduced *Dg* function (Table IB) (Haines et al., 2007; Shcherbata et al., 2007; Wairkar et al., 2008). These studies highlight the utility of the *Drosophila* NMJ model for further study of the glycobiology at the synapse, and as a model system for human neuromuscular diseases arising from defects in glycan biosynthesis.

Glycosylated synaptomatrix interaction with *trans*-synaptic signals

The immediately obvious signal that traverses the glycosylated synaptomatrix is the neurotransmitter itself: acetylcholine (ACh) at the vertebrate NMJ and glutamate at the *Drosophila* NMJ. It was first shown in *Drosophila* that neurotransmitter release from the presynaptic terminal suppresses the surface presentation and localized clustering of its postsynaptic receptors, so that the neurotransmitter inhibits its own receptor during synapse formation and modulation (Featherstone et al., 2000, 2002; Augustin et al., 2007). ACh at the vertebrate NMJ has the same effect, acting as a negative regulator of acetylcholine receptor (AChR) surface maintenance and clustering (Misgeld et al., 2002; Brandon et al., 2003). Recent evidence suggests that glycans like polysialic acid can interact directly with such neurotransmitters, indicating a putative modulatory role for these glycans with this classical *trans*-synaptic signaling (Sato et al., 2010). At the vertebrate NMJ, negative ACh function is counteracted by the action of the secreted signal agrin (Bezakova and Ruegg,

2003; Misgeld et al., 2005), a key player in synaptogenesis and the founding example of secreted *trans*-synaptic signaling ligands.

HSPG trans-synaptic signaling

The HSPG Agrin secreted by the motor neuron is 50% sugar by weight due to glycan modifications that include heparan sulfate chains (Tsen et al., 1995), O-linked glycans (Parkhomovskiy et al., 2000) and N-linked glycans (Rupp et al., 1991). Agrin induces phosphorylation of the muscle-specific kinase (MuSK) receptor that can be inhibited by glycans Gal(β1,4)GlcNAc and Gal(β1,3)GalNAc (Parkhomovskiy et al., 2000). MuSK also binds Gal(β1,4)GlcNAc, which suggests that this glycan modification is required for agrin mediated AChR stabilization during synaptogenesis (Table IA) (Parkhomovskiy et al., 2000; Kummer et al., 2006). Other glycans such as heparin, heparan sulfate and sialic acid show inhibitory effects that perturb agrin-mediated AChR stabilization (Wallace, 1990; Grow and Gordon, 2000). Treatment with enzymes that cleave sugars, such as neuraminidase (exposes glycans Gal(β1,4)GlcNAc or Gal(β1,3)GalNAc) (Martin and Sanes, 1995) or α-galactosidase (removes α-galactose sugars to expose lactosamines or N-acetyllactosamines) (Parkhomovskiy and Martin, 2000), causes agrin-independent MuSK activation and AChR stabilization (Grow et al., 1999). Besides regulation of synaptogenesis and associated signal transduction, other glycans attached to synaptomatrix components such as laminin-1 and -2 can bind to agrin by both heparan-sulfate glycan-dependent and -independent mechanisms (Table IA) (Hall et al., 1997). Further, agrin not only presents glycan

chains, but also binds to carbohydrates of other glycoconjugates through its lectin domain, extending its capacity to form an inter-connected compartmentalized meshwork at the synapse (Kleene and Schachner, 2004). Agrin is not identifiable in the *Drosophila* genome. However, other secreted HSPGs such as syndecan, as well as the GPI-anchored HSPG *dally-like protein* (*dlp*), have been identified at the *Drosophila* NMJ (Table IB) (Johnson et al., 2006; Ren et al., 2009) where they mediate axon guidance and synapse formation (Yamaguchi, 2001; Lee and Chien, 2004; Holt and Dickson, 2005; Van Vactor et al., 2006). The basic structure shared by HSPGs is a protein core to which heparan sulfate glycosaminoglycan (HS) chains are attached (Bernfield et al., 1999). GAG chains are attached to serine/threonine residues on proteins via a linker (GlcA-Gal-Gal-Xyl) by alternate addition of glucuronic acid (GlcA) and N-acetylglucosamine (GlcNAc) via 1,4- linkages (Lind et al., 1993). HS saccharides are further modified by addition of sulfate groups to diversify GAG chains that direct HSPG functions. These modifications are catalyzed by N-deacetylase/N-sulfotransferase (*Ndst*), which replaces the N-acetyl group of GlcNAc with a sulfate group (Aikawa and Esko, 1999), and then by substrate-specific iduronosyl 2-O-sulfotransferase (*hs2st*), glucosaminyl 6-O-sulfotransferase (*hs6st*) and glucosaminyl 3-O-sulfotransferase (*hs3st*) (Rosenberg et al., 1997; Habuchi et al., 2000). Along the HS chains, sulfate modifications can be concentrated into highly sulfated domains (S domains) of 6-10 disaccharides that resemble heparin (Maccarana et al., 1996). Only 10% of the disaccharide units are S domains, indicating a possible spatial encoding of information by the sulfate positions on

A. Vertebrate NMJ

	Glycomatrix component	Functions	Sample References
ECM	Laminins		
	β2	presynaptic active zone formation, synaptic vesicle organization, postsynaptic fold formation, NMJ α(7B) integrin expression, clustering of voltage gated Ca^{2+} channels	(Noakes et al., 1995; Nishimune et al., 2004)
	α2	postsynaptic fold formation, NMJ α(7A) integrin receptor expression	(Martin et al., 1996)
	α4	apposition of presynaptic active zones and postsynaptic junctional folds	(Patton et al., 2001)
	Collagen		
	α2(IV), α3(IV), α6(IV)	synaptic vesicle clustering, prevention of excessive neural outgrowth	(Fox et al., 2007)
	Col XIII	neuron and muscle apposition, active zone formation, postsynaptic AChR clustering	(Latvanlehto et al., 2010)
ECM Receptors	Dystroglycan	postsynaptic clustering and anchoring of AChRs, cytoskeletal link to ECM	(Bewick et al., 1996)
	Integrins		
	α7	postsynaptic AChR clustering	(Burkin et al., 2000)
	β1	postsynaptic AChR clustering; directing presynaptic axon growth and arborization	(Schwander et al., 2004)
Secreted signals	Agrin	postsynaptic AChR stabilization	(Kummer et al., 2006)
	Perlecan	localization of acetylcholinesterase	(Peng et al., 1998; Arikawa-Hirasawa et al., 2002)
	s-entactin	maintenance of NMJ morphology	(Fox et al., 2008)
	WNT (3a)	postsynaptic AChR clustering	(Henriquez et al., 2008)
	TGF-β2	amplification of postsynaptic spontaneous transmission, decrease in number of presynaptic vesicles used per stimulation	(Fong et al., 2010)

	acetylcholine	neurotransmission, negative regulator of postsynaptic AChR clustering	(Misgeld et al., 2002; Brandon et al., 2003)

B. *Drosophila* NMJ

	Glycomatrix component	Functions	Sample References
ECM	Laminin A	formation of appropriate contact area between neuron and muscle	(Prokop et al., 1998)
ECM Receptors	Dystroglycan	regulation of postsynaptic GluR subunit composition, decrease in presynaptic release of glutamate neurotransmitter, postsynaptic protein assembly	(Bogdanik et al., 2008)
	Integrins		
	βPS	synaptic bouton formation, NMJ synapse specification, localization of postsynaptic proteins, postsynaptic assembly	(Beumer et al., 1999, 2002)
	αPS1, αPS2	formation of appropriate contact sites between nerve and muscle	(Prokop et al., 1998)
	αPS3	NMJ synapse specification, synaptic bouton formation, regulation of neurotransmission strength and activity-dependent modulation	(Rohrbough et al., 2000)
	Fasciclins		
	Fas I	presynaptic arborization control, neurotransmission strength	(Zhong and Shanley, 1995)
	Fas II	synaptic patterning, specificity, growth, stabilization, presynaptic functional plasticity	(Davis et al., 1996; Schuster et al., 1996)
	Fas III	homophilic synaptic target recognition	(Kose et al., 1997)
	Syndecan	presynaptic terminal growth regulation	(Johnson et al., 2006)
	Dally-like protein (dlp)	presynaptic active zone morphology, synaptic transmission strength	(Johnson et al., 2006)
Secreted	Mind-the-Gap (Mtg)	organization of synaptic cleft matrix, postsynaptic GluR localization, integrin localization, Jeb/Alk signaling regulation	(Rohrbough et al., 2007; Rushton et al., 2009; Rohrbough K. et al., 2010)

	Jelly-belly (Jeb)	regulation of cell adhesion proteins, BMP signaling pathway interaction	(Englund et al., 2003; Rohrbough K. et al., 2010)
	Wingless (Wg)	presynaptic active zone formation, postsynaptic GluR distribution, activity dependent synaptic bouton formation, regulation of spontaneous release function	(Packard et al., 2002; Mathew et al., 2005; Ataman et al., 2008; Korkut and Budnik, 2009)
	Glass Bottom Boat (Gbb)	localization of presynaptic active zones, regulation of cell adhesion molecules, regulation of spontaneous release function and neurotransmission strength	(Aberle et al., 2002; Haghighi et al., 2003; McCabe et al., 2003; Nahm et al., 2010)
	Glutamate	neurotransmission, negative regulator of postsynaptic GluR clustering	(Jan and Jan, 1976; Featherstone et al., 2000, 2002; Augustin et al., 2007; Chen et al., 2009a)

Table I: Neuromuscular junction synaptomatrix components

A) The vertebrate NMJ. The table summarizes only the major synaptomatrix components discussed in this review. **B) The Drosophila NMJ.** Synaptomatrix components are listed in the same order as for the vertebrate NMJ; including ECM, ECM receptors and secreted *trans*-synaptic signals.

the HS (Nakato and Kimata, 2002).

Once added, the sulfate groups can be cleaved by sulfatases (e.g. *sulf1*), which selectively removes sulfates attached to particular disaccharide units (Lamanna et al., 2007). The resultant HS sulfation profiles dictate HSPG co-receptor functions that modulate ligand-receptor interactions (Dreyfuss et al., 2009). For example, Fibroblast growth factor (FGF) ligand dimerization occurs on characteristically sulfated HS sequences of 10-14 sugars (Walker et al., 1994), and interaction of the dimerized ligand with its receptor (FGFR) is dependent on sulfated HS (Springer et al., 1994). Structural studies confirm HS mediated stabilization in a 2:2 tetrameric assembly between the FGF1 and FGFR2 dimers associated with HS chains (Schlessinger et al., 2000). The role of such modifications in directing HSPG functions during synaptic development and modulation is a critical area for future investigation.

WNT-Wingless signaling

Numerous morphogens that are required during many phases of development are also found to play important roles at synapses, including the WNTs (Hall et al., 2000; Packard et al., 2002; Salinas, 2005; Henriquez et al., 2008), fibroblast growth factors (FGFs) (Umemori et al., 2004), and Transforming growth factor/Bone morphogenic proteins (TGF-β/BMPs) (Packard et al., 2003; Salinas, 2003). Glycan modifications have an intimate relationship with such classical morphogens, and there is great potential for HS modifications regulating *trans*-synaptic signaling. *Drosophila* forward genetic screens of WNT signaling

pathways have identified genetic interactions with heparan sulfate (HS) biosynthetic enzymes (Hacker et al., 2005). For example, screens for mutants phenocopying the founding WNT *wingless* (*Wg*) mutant identified *sugarless* (*sgl*), a uridyl-diphosphate-6-glucose dehydrogenase (UDPG) that synthesizes glucuronic acid building blocks of HS chains, and *tout-velu* (*ttv*), a polymerase that extends these chains (Bellaiche et al., 1998). These findings indicate a link between HS sulfation and WNT-wingless signaling. At the *Drosophila* NMJ, *trans*-synaptic Wg plays an important role in synaptogenesis (Fig. 4), where it has recently been shown to mediate anterograde signaling via an unusual exosome delivery mechanism (Korkut et al., 2009). Phenotypes of loss-of-function mutations in this pathway include reduced number of synaptic boutons, disrupted organization of the postsynaptic scaffold protein Discs Large (DLG), a postsynaptic density 95 kDa (PSD-95) homolog, and glutamate receptor (GluR) mislocalization (Fig. 4) (Ataman et al., 2008). Likewise, WNT signaling in *C. elegans* regulates GluR-1 abundance in the ventral nerve cord (Juo and Kaplan, 2004). WNT signaling similarly operates at mammalian synapses, where *Wnt7a* enhances synapsin I clustering and branching in cultured granule cells and cerebellar synapses (Table IA) (Lucas and Salinas, 1997). The cognate receptor for WNT-Wg is Frizzled 2 (Fz2), which is endocytosed upon ligand binding and then transported to the nuclear region where its cleaved C-terminal region translocates into the nucleus to induce transcription (Fig. 4) (Mathew et al., 2005). WNT-Wg can also function as a retrograde signal by modulating *futsch* (*Drosophila* microtubule associated protein 1B) via inhibition of Shaggy

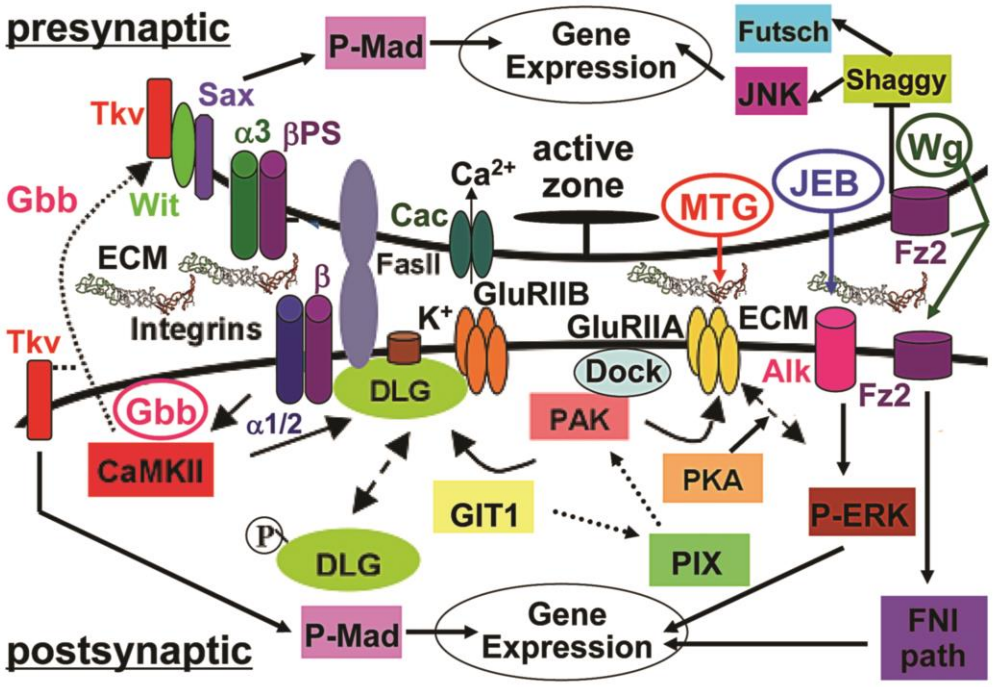

Figure 4. Diagram of *trans*-synaptic signaling pathways at the *Drosophila* NMJ. Presynaptic: The active zone (AZ) is indicated by a T-bar. Cell membrane components include PS integrins (α3 and βPS subunits), homophilic CAM Fasciclin II (FasII) and Cacophony calcium channels (Cac). Cytoplasmic proteins include kinases JNK and Shaggy, and the MAP1B Futsch. **Postsynaptic**: The glutamate receptor (GluR) domain includes two GluR classes (GluRIIA and B) and potassium channels (K^+). Cell membrane components include PS integrins (α1/2 and βPS) and FasII. Membrane associated and cytoplasmic proteins include scaffolding proteins Discs large (DLG) and Dock, kinase PAK and regulators PIX and GIT1, and calmodulin kinase II (CamKII). **Trans-synaptic pathways:** Secreted signals Wingless (Wg), Glass bottom boat (Gbb) and Jelly belly (Jeb), and their respective membrane cognate receptors Frizzled 2 (Fz2), Thickveins (Tkv)/Wishful Thinking (Wit)/Saxophone (Sax) and Anaplastic lymphoma kinase (Alk). The Frizzled nuclear import pathway is indicated as FNI. The known downstream transcription factor for Gbb is Mothers against decapentaplegic (Mad; P-Mad indicating phosphorylated form), and for Jeb is ERK (P-ERK indicating phosphorylated form). Extracellular synaptomatrix components are indicated as ECM between the presynaptic neuron and postsynaptic muscle cells.

(*Drosophila* homolog of GSK3β), hence affecting microtubule function that modulates NMJ formation (Franco et al., 2004; Franciscovich et al., 2008)

WNT-Wg signaling also prevents ectopic synapse formation on non-target muscle cells hence directing appropriate synaptogenesis (Table IB) (Inaki et al., 2007). The potential role of glycans in mediating such signaling stems from studies in *Drosophila* wing disc showing that WNT-Wg localization, as well as activation of the downstream signaling pathway, is dependent on the precise extent of HS sulfation (Reichsman et al., 1996). For example, *sulf1* mutants that cannot cleave sulfate modifications show increased Wg expression along the dorso-ventral axis of the wing disc, supporting a role for sulfated HS chains in regulating Wg signaling (Kleinschmit et al., 2010). By extension, HS at the *Drosophila* NMJ could sequester Wg and other *trans*-synaptic signals, or present them as co-receptors to their transmembrane receptors to initiate downstream signaling processes driving synaptogenesis and subsequent synapse maturation (Fig. 4). In support of this hypothesis, quail sulfatase (Qsulf1) can positively influence the ability of WNT ligand to associate with its cognate receptor Frizzled (Ai et al., 2003). A high priority is to assay for similar glycan mechanisms regulating *trans*-synaptic signaling.

TGFβ/BMP signaling

TGFβ/BMP signaling is also modulated by heparan sulfate glycan modifications (Chen et al., 2006). In mammals, BMP proteins have roles in neural crest formation (Kishimoto et al., 1997; Dick et al., 2000; Nguyen et al., 2000)

and migration (Graham et al., 1994; Shah et al., 1996; Marazzi et al., 1997; Sela-Donenfeld and Kalcheim, 2000), axon guidance (Augsburger et al., 1999; Butler and Dodd, 2003), neurite outgrowth and synaptogenesis (Meng et al., 2002; Endo et al., 2003). At the *Drosophila* NMJ, the retrograde BMP signal Glass Bottom Boat (Gbb) is similarly required for synapse stabilization (Fig. 4) (Eaton and Davis, 2005). Null *gbb* mutants, as well as mutations in its BMP receptors (type I receptors Thickveins (Tkv) and Saxophone (Sax), type II receptor Wishful thinking (Wit)) and BMP pathway regulators (e.g. the Cdc42 selective GAP Rich), produce gross synaptic defects that include distorted pre- and postsynaptic membranes, mislocalized presynaptic T-bars, reduced active zone number, and decreased synaptic transmission at the NMJ (Fig. 4) (Marques et al., 2002; McCabe et al., 2003, 2004; Rawson et al., 2003; Nahm et al., 2010). As above, *sulf1* activity has an activating effect on BMP signaling, suggesting that HS modifications may have a role in this *trans*-synaptic signaling pathway as well. For example, *sulf1* regulates release of the BMP antagonist noggin, allowing BMP to interact with its cognate receptor in cell culture (Viviano et al., 2004). It should be noted that glycan regulation of these signaling pathways are based mostly on *in vitro* data and are highly context specific; hence directly predicting stimulatory and/or inhibitor roles of glycan modifications at the synapse is not straightforward. In addition to binding, presenting and/or sequestering WNT-wingless and BMP molecules bound to HS, these signaling molecules can be released by the enzymatic activity of matrix metalloproteinases (MMPs) that shed ecto-domains of HSPGs (Kainulainen et al., 1998). Other glycosylated synaptic

ECM components can similarly bind and present signaling factors. Thus, glycans in the synaptomatrix could potentially serve as a repository for *trans*-synaptic signaling molecules, and likely modulate known WNT and BMP signaling pathways by sequestering away or presenting signals to cognate receptors.

Glycan-binding lectins regulate *trans*-synaptic signaling

Mind-the-gap: secreted lectin that organizes cell surface receptors

An exciting idea that has arisen in recent years is that endogenous lectins (glycan-binding proteins) play critical roles in development, immunity and intercellular signaling (Drickamer and Taylor, 1993; Marth and Grewal, 2008; Dam and Brewer, 2010). At the *Drosophila* NMJ, a prime example is the N-acetylglucosamine (GlcNAc)-binding lectin encoded by *mind-the-gap (mtg)* (Rohrbough et al., 2007; Rushton et al., 2009; Rohrbough K. et al., 2010). The MTG protein is secreted from the presynaptic terminal to reside within the synaptic cleft, and in perisynaptic extracellular domains, where it co-localizes with WGA (Fig. 3E,F). Consistently, both proteins share binding affinity for GlcNAc sugar residues. Transgenic MTG-GFP is trafficked to synapses, where the secreted protein remains near the cell surface (Fig. 3E). Ultrastructural immunogold labeling shows secreted MTG adjacent to active zones in the presynaptic terminal, and in the extracellular lumen of the postsynaptic SSR (Rohrbough et al., 2007). During embryonic development, the dynamic *mtg* expression pattern correlates closely with key periods of NMJ synaptogenesis, with the expression peak coinciding with the presynaptic induction of

postsynaptic GluR domain assembly (Broadie and Bate, 1993a, 1993b, 1993c). Null *mtg* mutants exhibit severe abrogation of the glycosylated synaptomatrix between the presynaptic active zone and postsynaptic GluR domains, and greatly reduced GluR localization with a corresponding loss of GluR function (Table IB) (Rohrbough et al., 2007). Moreover, all known postsynaptic signaling/scaffold proteins functioning upstream of GluR localization are grossly reduced or severely mislocalized in *mtg* mutants, including the dPix–dPak–Dock cascade (Parnas et al., 2001; Ang et al., 2003) and the DLG/PSD-95 scaffold (Fig. 4) (Thomas et al., 2000; Ataman et al., 2006b; Gorczyca et al., 2007). Neuronally-targeted *mtg* RNA-interference (RNAi) likewise reduces postsynaptic assembly, whereas postsynaptically-targeted RNAi has no effect (Rohrbough et al., 2007). Similarly, neuronally-targeted wildtype *mtg* in the null mutant rescues the postsynaptic assembly loss. These data conclusively indicate that presynaptic MTG is required for the induction of the postsynaptic pathways driving GluR domain formation; hence it serves as an anterograde *trans*-synaptic signal.

It was recently shown that direct loss of GalNAc transferase alters *Drosophila* NMJ structure and function, as well as locomotory behavior (Haines and Stewart, 2007). This work independently demonstrates that GlcNAc-mediated interactions have key roles in synaptic maturation. Thus, together this recent work indicates that both the GlcNAc sugar itself and GlcNAc-binding lectins modulate synaptogenesis. Since GlcNAc is a repeating sugar unit of HS, it seems probable that MTG regulates localization of HS-carrying proteins and

thereby any *trans*-synaptic signaling proteins bound to this lattice. With this mechanism, MTG could coordinately regulate multiple *trans*-synaptic pathways via binding GlcNAc moieties on both HSPGs and receptors such as integrins (Fig. 3F). The fact that null *mtg* mutants exhibit a gross reduction or complete absence of electron-dense synaptic matrix (Rohrbough et al., 2007) certainly suggests disorganization/loss of multiple synaptic ECM components and ECM-binding proteins. Consistent with this prediction, targeted presynaptic *mtg* knockdown strongly decreases the level of position specific (PS) integrin synaptic expression, present in both pre- and postsynaptic membranes (Fig. 4; Table IB) (Beumer et al., 1999; Rohrbough et al., 2000), causing a loss of NMJ localization of this ECM binding receptor (Rushton et al., 2009). Thus, interaction between synaptic membranes and the ECM are weakened in the absence of MTG. Moreover, since PS integrin receptors exist in a physical complex with the DLG scaffold and control calcium/calmodulin dependent kinase II (CaMKII) activation (Beumer et al., 2002), this MTG-dependent pathway also provides a mechanism to regulate localization of postsynaptic proteins in the GluR domain during synaptogenesis (Fig. 4). Similarly in mammals, endogenous galactose binding lectins (galectins) bind lactosamine residues (Hirabayashi et al., 2002), such as those found in the extracellular domain of β1 integrin chains, to organize lattice signaling microdomains at the cell surface (Perillo et al., 1995; Chung et al., 2000; Brewer et al., 2002; Braccia et al., 2003). Although this mechanism has not been studied at the vertebrate NMJ, it supports the possibility of a conserved glycan-dependent organizing event.

Mind-the-gap: modulator of trans-synaptic signaling

Integrins are just one component of MTG-regulated *trans*-synaptic signaling. The working hypothesis is that secreted MTG organizes a GlcNAc glycomatrix that coordinately regulates the multiple bidirectional signals that traverse the synaptic cleft between neuron and muscle (Fig. 4). For example, it was just recently shown that MTG strongly modulates the secreted signaling ligand Jelly Belly (Jeb) and its receptor tyrosine kinase Anaplastic Lymphoma Kinase (Alk), an anterograde signaling pathway from neuron to muscle (Bazigou et al., 2007; Palmer et al., 2009; Rohrbough K. et al., 2010). In the *Drosophila* nervous system, this Jeb-Alk signaling activates transcription of downstream genes, including cell adhesion proteins and the TGFβ/BMP signal Dpp (Loren et al., 2001; Englund et al., 2003; Lee et al., 2003; Shirinian et al., 2007). At the *Drosophila* NMJ, Jeb is presynaptically secreted to reside in punctate domains closely associated with presynaptic boutons, while its Alk receptor exhibits a more uniform expression in the postsynaptic domain (Fig. 4) (Rohrbough K. et al., 2010). This signaling array is set up during embryonic synaptogenesis and maintained throughout postembryonic development. In *mtg* null synapses, the Jeb signal is grossly over-expressed, with elevated levels, increased size of extracellular domains and an increased number of these domains throughout the synaptomatrix (Rohrbough K. et al., 2010). Conversely, the postsynaptic Alk receptor expression is decreased, albeit to a lesser degree, potentially a reflection of the general postsynaptic disorganization (Table IB). Although direct mutation of the Jeb-Alk pathway has not, as yet, been demonstrated to cause

overt synaptogenesis defects, it is predicted that this pathway must regulate transcription modulating synapse formation and/or maintenance. Consistent with this hypothesis, Alk receptor signaling regulates TGFβ/BMP-dependent transcription in *C. elegans* (Reiner et al., 2008). By extension, at the *Drosophila* NMJ Jeb-Alk signaling could potentially regulate the TGFβ/BMP Gbb retrograde pathway involved in synaptic modulation (Aberle et al., 2002; Haghighi et al., 2003; McCabe et al., 2003, 2004). Of course, such a mechanism would be in addition to the prediction that MTG directly regulates WNT-Wg and Gbb *trans*-synaptic signals as they navigate the synaptomatrix. Putative interactions with these signaling pathways have yet to be tested.

Unanswered Questions and Future Directions

The extracellular synaptomatrix is densely packed with glycoproteins and proteoglycans in highly compartmentalized domains (Figs. 4 and 5). There are numerous unanswered questions about the development and organization of this environment. What is the origin of these different molecules? They could be expressed locally (e.g. neuron, muscle and associated glia) or trapped from distant sources (e.g. haemocytes and fat body). How are these molecules packed into such a constrained space, and spatially organized? Synaptomatrix-resident molecules seem prohibitively large for the narrow cleft, and show clear regional domain distributions. What dictates selective posttranslational modification of glycans on particular synaptomatrix proteins? Possibly the three dimensional structure of proteins effectively masks potential glycosylation sites, allowing only certain exposed domains to be modified. Is the glycosylation status

of synaptomatrix proteins locally regulated within the synaptic cleft? If so, what is the nature of these modifications, and what mechanisms control such dynamic shifts? Such mechanisms could lead to differential glycosylation of identical isoforms of synaptomatrix proteins in a spatial and/or temporal manner. It must also be remembered that protein glycosylation is likely only part of the story, as lipids are also heavily glycosylated. For example, two *Drosophila* genes, *egghead* (*egh)* and *braniac* (*brn)* (Goode et al., 1996), encode enzymes responsible for glycosphingolipid biosynthesis, and mutation of both genes causes clear behavioral phenotypes (Chen et al., 2007). Together, all of these glycosylation mechanisms could affect *trans*-synaptic signaling.

At the *Drosophila* NMJ, multiple *trans*-synaptic signals, including WNT (Wg) and TGF-β/BMP (Gbb), navigate through the heavily glycosylated synaptomatrix to bind their respective receptors (Fig. 4). We propose here that the glycan-rich environment in the synaptomatrix likely directly modulates these *trans*-synaptic pathways during synaptogenesis, as has been clearly demonstrated in other arenas of development. For example, the HSPG Dlp that binds WNT-wingless to regulate its extracellular distribution in the developing *Drosophila* wing disc (Han et al., 2005). Dlp is enriched at the NMJ, along with the HSPG syndecan, where they control NMJ growth and presynaptic active zone assembly (Table I) (Johnson et al., 2006). Thus, HSPGs through their glycan modifications are here hypothesized to modulate WNT signals, likely jointly with TGF-β/BMP signals (Rider, 2006), suggesting significant intersection between these pathways within the synaptomatrix. In this scenario, glycan

structures could bind and modulate multiple *trans*-synaptic signals simultaneously to coordinately regulate interactions with their cognate receptors. These signals could individually be stimulatory or inhibitory to the process of synaptogenesis, and therefore extracellular glycans may serve as platforms for signal integration that allow only the net effect of bound signaling molecules to determine synapse formation and subsequent modulation.

If *trans*-synaptic signals are modulated by glycans, then what modulates the glycans? We propose here that endogenous lectins are enormously important in shaping glycan distribution within the synaptomatrix environment. *Mind-the-gap* is one such lectin secreted into the *Drosophila* NMJ synaptomatrix, where it binds GlcNAc moieties (Rohrbough et al., 2007; Rushton et al., 2009). Interestingly, HS glycan modifications are abundant in GlcNAc residues, as this monosaccharide is repeated several times to form the final HS glycan chains (Lamanna et al., 2007). HS chains are also be modified by sulfate groups, with periodic highly sulfated regions (S-domains) interspersed by regions with almost no sulfation. We propose here that sulfation could provide an additional level of information processing to regulate *trans*-synaptic signaling (Lamanna et al., 2007). By binding GlcNAc-rich HS chains, MTG is hypothesized to organize secreted and/or membrane-bound HSPGs in the synaptomatrix, to regulate synapse formation. Does MTG interact directly with WNT and/or TGF-β/BMP *trans*-synaptic pathways through such a mechanism? Although this has not yet been tested, these pathway's binding site preferences may be similar to other signaling molecules such as FGFs (Wu et al., 2003) and Antithrombin III

(Kuberan et al., 2002), which bind sulfate rich domains. This leaves the GlcNAc moieties in non-sulfated regions open for recognition by MTG, which could then drive organization of HS glycans carrying HSPGs. We have just recently shown that Mtg strongly modulates the newly defined Jeb/Alk *trans*-synaptic signaling pathway (Rohrbough K. et al., 2010), in direct support of our core hypothesis. Clearly, the Jeb/Alk pathway could be regulated by similar glycan-dependent mechanisms, perhaps in a combinatorial manner with other *trans*-synaptic pathways. The combinatorial regulation hypothesis warrants direct investigation.

It should be abundantly clear from the above discussion that glycan modification of the synaptomatrix plays critical roles in the formation of new synapses and the subsequent modulation of synaptic properties. This densely-packed extracellular compartment provides an interface environment where glycan-glycan and glycan-protein interactions occur in a restricted space, providing exciting scope for crosstalk between different *trans*-synaptic signaling pathways. The molecular mechanisms that govern synaptogenesis may very well intimately depend on the cumulative effects of integrated and intersecting pathways within the synaptic glycomatrix, where glycosylation determines ligand life-time and either facilitates or thwarts the presentation of ligand to receptor. Further studies of the synaptic glycomatrix in the context of synaptogenesis are expected to reveal mechanisms of cross-talk between established signaling pathways, and to yield insights into novel signaling mechanisms that direct synapse formation.

Acknowledgements

We thank Jeffrey Rohrbough and Emma Rushton for Figure 3 contributions and help with figure construction, and for critical input on the manuscript. This work was supported by NIH R01 grant

Chapter III

A Targeted Glycan-Related Gene Screen Reveals Heparan Sulfate Proteoglycan Sulfation Regulates WNT and BMP Trans-Synaptic Signaling

This paper has been published under the same title in *PLoS Genetics*, 2012

Neil Dani[†], Minyeop Nahm[¥], Seungbok Lee[¥] and Kendal Broadie[†]

[†]Departments of Biological Sciences, Cell and Developmental Biology, Kennedy Center for Research on Human Development, Vanderbilt University, Nashville, TN 37232, USA

[¥]Department of Cell and Developmental Biology, Seoul National University, Seoul 110-740, Republic of Korea

Shortened Title: HSPG regulated *trans*-synaptic signaling

Keywords: *Drosophila*, glycobiology, transgenic RNAi, synaptogenesis, transcription

Abstract

A *Drosophila* transgenic RNAi screen targeting the glycan genome, including all N/O/GAG-glycan biosynthesis/modification enzymes and glycan-binding lectins, was conducted to discover novel glycan functions in synaptogenesis. As proof-of-product, we characterized functionally-paired heparan sulfate (HS) 6-O-sulfotransferase (*hs6st*) and sulfatase (*sulf1*), which bidirectionally control HS proteoglycan (HSPG) sulfation. RNAi knockdown of *hs6st* and *sulf1* causes opposite effects on functional synapse development, with decreased (*hs6st*) and increased (*sulf1*) neurotransmission strength confirmed in null mutants. HSPG co-receptors for WNT and BMP intercellular signaling, Dally-like Protein and Syndecan, are differentially misregulated in the synaptomatrix of these mutants. Consistently, *hs6st* and *sulf1* nulls differentially elevate both WNT (Wingless; Wg) and BMP (Glass Bottom Boat; Gbb) ligand abundance in the synaptomatrix. Anterograde Wg signaling via Wg receptor dFrizzled2 C-terminus nuclear import, and retrograde Gbb signaling via synaptic MAD phosphorylation and nuclear import, are differentially activated in *hs6st* and *sulf1* mutants. Consequently, transcriptional control of presynaptic glutamate release machinery and postsynaptic glutamate receptors is bidirectionally altered in *hs6st* and *sulf1* mutants, explaining the bidirectional change in synaptic functional strength. Genetic correction of the altered WNT/BMP signaling restores normal synaptic development in both mutant conditions, proving that altered *trans*-synaptic signaling causes functional differentiation defects.

Author summary

Glycans are sugar additions to proteins. Surrounding all eukaryotic cells, secreted and membrane glycans form a glycocalyx that regulates cell-cell signaling. However, the mechanisms controlling glycan-dependent intercellular communication are largely unknown. In the nervous system, glycans play important roles in the development and regulation of synapses mediating intercellular communication. The *Drosophila* neuromuscular junction serves as a genetically tractable synapse in which expression of glycan-related genes can be systematically knocked down to investigate effects on synaptic morphology and function. This study employs a transgenic RNAi screen to characterize the synaptic requirements of 130 glycan-related genes. From this screen, two functionally paired genes (*hs6st* and *sulf1*) that add or remove a sulfate at the 6-O position on heparan sulfate proteoglycans (HSPGs) were identified as being critically important for synaptic functional development. Removal of each gene produces an opposite effect on neurotransmission strength, weakening and strengthening communication, respectively. This mechanism controls the synaptic expression of two HSPGs, which act as co-receptors to control the abundance of anterograde WNT and retrograde BMP signals, which drive intracellular signal transduction pathways regulating gene transcription to control synaptic functional development. This screen serves as a platform for systematic investigation of glycan mechanisms regulating synaptic development.

Introduction

Glycans coat cell surfaces, and glycosylation decorates secreted molecules of the pericellular space and extracellular matrix (ECM) (Iozzo, 1998; Varki, 2011). It is well known that glycan modifications mediate critical functions of intercellular signaling and regulate interactions of numerous growth factors with the ECM (Kleene and Schachner, 2004; Dityatev and Schachner, 2006). The synthesis, modification and degradation of glycoconjugates, including O/N-linked glycoproteins, glycosaminoglycan (GAG) proteoglycans and glycan-binding lectins, is controlled by a dedicated cadre of genes (Varki et al., 1999; Hagen et al., 2009). In the nervous system, these glycan-related genes play key roles in development, including neuron fate specification, migration, formation of axon tracts and synapse maturation (Barros et al., 2011). At synapses, glycosylated ECM molecules, membrane receptors and outer-leaflet glycolipids together form the highly specialized synaptomatrix interface (Dityatev and Schachner, 2006; Vautrin, 2010), which interacts with *trans*-synaptic signals to modulate synaptogenesis (Dani and Broadie, 2012).

A prime example is the classic Agrin proteoglycan, which bears heparan sulfate (HS) chains, O/N-linked glycans and also a glycan-binding lectin domain that binds other glycoconjugates (Rupp et al., 1991; Tsim et al., 1992; Tsen et al., 1995). Reduction of GAG sulfation perturbs the Agrin signaling that drives postsynaptic acetylcholine receptor (AChR) cluster maintenance at the neuromuscular synapse (McDonnell and Grow, 2004). Likewise, Galbeta1,4GlcNAc and Galbeta1,3GalNAc glycans inhibit Agrin signaling by

suppressing muscle specific kinase (MuSK) autophosphorylation, a key step during synaptogenesis (Parkhomovskiy et al., 2000). Analogous glycan-dependent mechanisms at the *Drosophila* neuromuscular synapse involve the secreted Mind-the-Gap (Mtg) lectin, which assembles the glycosylated synaptomatrix between presynaptic active zone and postsynaptic glutamate receptor (GluR) domains (Rohrbough et al., 2007). This glycan mechanism induces GluR clustering, synaptic localization of integrin ECM receptors, and shapes *trans*-synaptic signaling by controlling ligand/receptor abundance (Rushton et al., 2009, 2012; Rohrbough K. et al., 2010). Thus, many long-term studies in vertebrate and invertebrate genetic models suggest that glycan mechanisms are a core foundation of synapse development.

In the current study, we conducted a broad transgenic RNA interference (RNAi) screen of synaptic glycan function, assaying requirements in both structural and functional development of the *Drosophila* neuromuscular junction (NMJ). We tested 130 genes from 8 functional categories: N-glycan, O-glycan and GAG biosynthesis; glycosyltransferases and glycan modifying/degrading enzymes; glycoprotein and proteoglycan core proteins; sugar transporters and glycan-binding lectins. We found that RNAi-knockdown of genes in all eight categories affects synaptic morphological development, with gene-specific effects on branching, bouton differentiation and synapse area. Likewise, all eight categories regulate synaptic functional development, with gene-specific effects both weakening and strengthening neurotransmission. Interestingly, only a few genes affect both structure and function, suggesting separable roles for glycans

in regulating these synaptogenic pathways. The results of this genomic transgenic screen are presented as a platform from which to pursue systematic investigation of glycan mechanisms in synaptic development.

Two genes were selected for screen validation and mechanistic characterization; functionally-paired HS 6-O-endosulfatase (*sulf1*) and HS 6-O-sulfotransferase (*hs6st*). RNAi knockdown and null mutants identically alter synaptic functional development in a bidirectional manner; loss of *sulf1* elevates neurotransmission strength, whereas loss of *hs6st* weakens it. Heparan sulfate proteoglycan (HSPG) targets Dally-like Protein (Dlp) and Syndecan (Sdc) (Carey, 1997; Dejima et al., 2011) are mislocalized in *sulf1* and *hs6st* null synapses. In other developmental contexts, the sulfation state of these HSPG co-receptors strongly regulates WNT and BMP intercellular signaling (Yan and Lin, 2009; Kleinschmit et al., 2010; Dejima et al., 2011). At *Drosophila* synapses, WNT (Wg) is a key anterograde (Packard et al., 2002; Korkut and Budnik, 2009) and BMP (Gbb) a key retrograde (McCabe et al., 2003; Keshishian and Kim, 2004) *trans*-synaptic signal. Consistently, loss of *sulf1* and *hs6st* differentially changes synaptomatrix levels of Wg and Gbb, and downstream signaling into muscle and motor neuron nuclei, respectively. Glutamate release and receptor machinery is thereby bidirectionally altered in the two nulls. Genetic restoration of Wg/Gbb signaling to control levels restores the bidirectional changes in synaptic functional strength and pre-/post- synaptic differentiation in both *sulf1* and *hs6st* nulls. We conclude that extracellular HSPG sulfation state in the synaptomatrix is a point of intersection between WNT/BMP *trans*-synaptic signaling pathways that drive

functional development of the neuromuscular synapse.

Results

RNAi screen of glycan-related genes identifies multiple synaptogenesis defects

Synaptic glycans play important roles as ligands, modulators and co-receptors regulating cell-matrix and intercellular communication (Kleene and Schachner, 2004; Holt and Dickson, 2005; Matani et al., 2007). Differential glycan distribution on pre- and postsynaptic surfaces, and in the cleft, of numerous protein classes, strongly suggests that glycan mechanisms mediate synaptic structural and functional development (Martin, 2002, 2003b; Yamaguchi, 2002). To test the genomic scope of this requirement, we used confocal imaging and electrophysiological recording at the well-characterized *Drosophila* glutamatergic neuromuscular junction (NMJ) (Keshishian et al., 1996; Gramates and Budnik, 1999; Ruiz-Canada and Budnik, 2006) to screen the Vienna *Drosophila* RNAi Center (VDRC) library of glycan-related genes (Dietzl et al., 2007). We induced UAS-RNAi knockdown using the ubiquitous UH1-GAL4 driver (Wodarz et al., 1995; Rohrbough et al., 2007) . We assayed morphological defects by co-labeling for pre- and postsynaptic markers, and assayed functional defects with two-electrode voltage clamp (TEVC) recording of neurotransmission strength. A summary of the screen results is shown in Figure 5. Full numerical results of the screen are shown in Table II.

Candidate glycan-related genes were identified and classified into eight functional categories using the Kyoto Encyclopedia of Genes and Genomes (KEGG) database (Kanehisa and Goto, 2000) [37] (Fig. 5). Additional genes were added to the screen based on ortholog identification using the Information Hyperlinked over Proteins (iHOP) database (Hoffmann and Valencia, 2004). The candidate gene list was expanded and verified using Flybase (Tweedie et al., 2009). From this list, genes were cross-referenced with available VDRC UAS-RNAi transgenic lines to generate a final candidate list containing 130 genes within eight functionally-defined categories (Fig. 5): N-glycan, O-glycan and glycosaminoglycan (GAG) biosynthesis; glycan core proteins (HSPG core proteins/glycoproteins); sugar transporters; glycosyltransferases; glycan modification genes (modification and degradation of glycans); and glycan-binding lectins. On genetic knockdown, 103 lines were viable until the wandering 3rd instar, whereas 27 lines showed developmental lethality at embryonic and early larval stages of development. From the 103 genetic lines characterized by confocal microscopy and TEVC electrophysiology in the 3rd instar (Fig. 5), 21 exhibited pupal stage developmental lethality. Interestingly, >50% of pupal lethal lines displayed statistically significant defects in NMJ synaptic morphology and function. For all 103 larval-viable lines, synapse morphology and function was quantified at the wandering 3rd instar NMJ (Fig. 5; Table II). Each UAS-RNAi line driven by UH1-GAL4 in the w^{1118} background was compared to the genetic control of w^{1118} crossed to UH1-GAL4 (UH1-GAL4 x w^{1118}) (Dietzl et al., 2007).

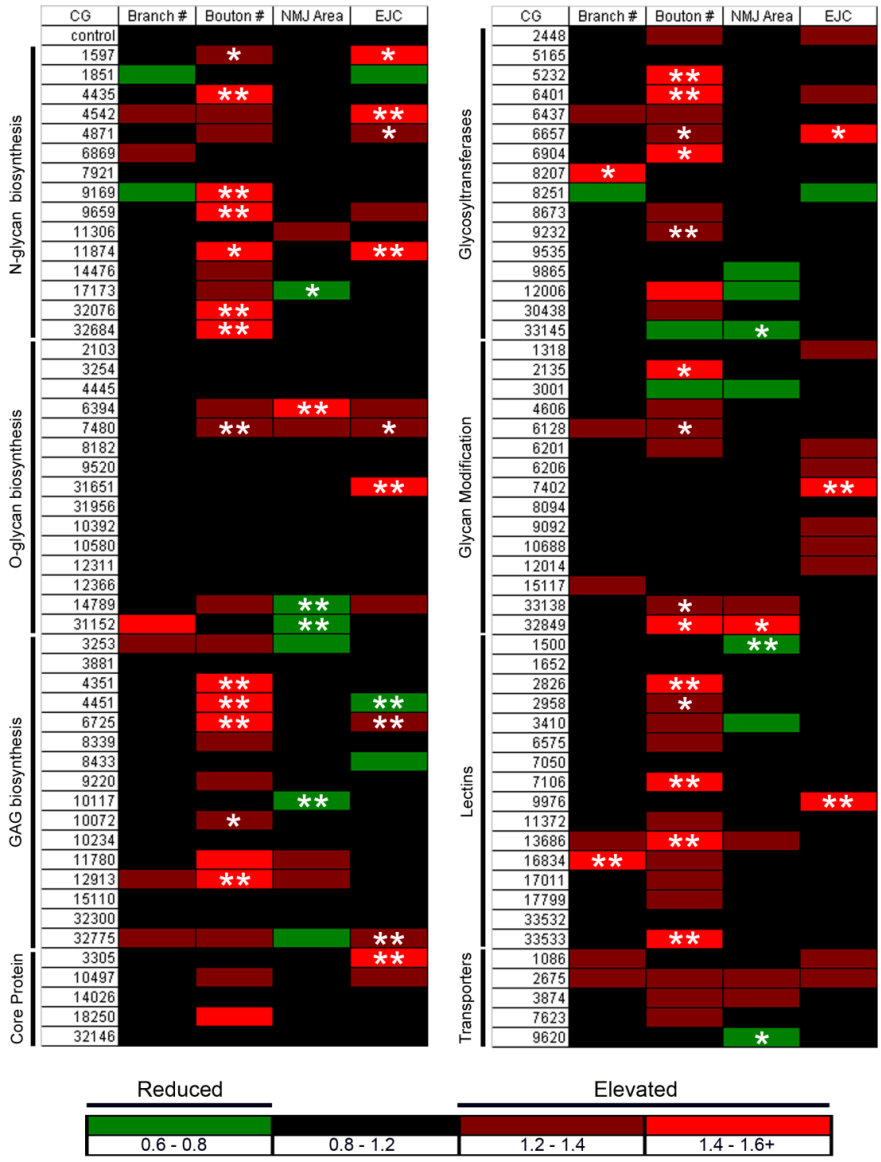

Figure 5. Glycan-related gene RNAi screen for synapse structure/function defects. Transgenic RNAi screen interrogating effects of glycan-related gene knockdown on the morphology and function of the *Drosophila* neuromuscular junction (NMJ) synapse. All VDRC UAS-RNAi lines were crossed to the UH1-GAL4 driver line. Target genes are indicated by *Drosophila* genome CG annotation number and categorized by function. Confocal imaging of co-labeled pre- and postsynaptic markers was used to quantify NMJ architecture, including branch number, bouton number and synaptic area. TEVC electrophysiology was used to quantify evoked excitatory junctional current (EJC) amplitudes. The magnitude of fold changes compared to control (w^{1118}×UH1-GAL4) is shown on a color scale (see legend below the two columns). Statistical significance was calculated using one-way ANOVA analysis, and displayed as $p<0.05$ (*), $p<0.01$ (**).

			Bouton Mean		Branch		NMJ area		EJC	
Human gene	Drosophila gene	CG	Mean	SD	Mean	SD	Mean	SD	Mean	SD
		control	22.103	4.828	3.185	0.933	190.67	57.291	279.391	53.344
MOGS	n/d	1597	30	6.066	3.333	0.516	169.205	48.809	400.270	26.083
n/d	Ady43A	1851	18	5.196	2.333	0.577	148.064	8.454	189.310	28.793
FUT10	FucTB	4435	35.667	1.527	3	1.155	186.213	23.67	321.383	68.022
ALG8	n/d	4542	27	4.583	4	0.633	159.583	43.879	444.660	36.252
ST6GAL1	ST6Gal	4871	28.833	7.305	3.333	0.985	213.39	67.511	365.230	119.690
FUT5	FucTA	6869	26.333	4.633	3.8	1.304	147.817	36.392	305.748	117.470
MGAT2	Mgat2	7921	22	3.742	3.5	0.837	189.773	22.672	246.187	3.809
n/d	FucTD	9169	37	4	2.25	0.500	194.396	25.843	272.132	64.077
n/d	egghead	9659	39	6.244	3.5	1.000	195.263	19.213	355.295	17.430
ALG11	n/d	11306	25.333	3.512	3.333	0.577	230.813	29.049	225.406	125.710
MAN1B1	n/d	11874	34	10.52	3.167	0.408	181.955	74.303	395.570	102.630
GANAB	n/d	14476	28.667	33.966	3.667	0.577	216.678	33.966	223.710	22.690
n/d	n/d	17173	28.5	6.807	3.6	0.548	124.356	46.355	307.180	57.973
ALG10	Alg10	32076	31	4.561	3.667	0.516	197.429	17.163	279.570	46.372
MAN1A2	α-Man-I	32684	34	4.582	2.75	0.500	169.013	33.821	333.670	66.085
GALNT10	pgant6	2103	21.5	3.834	2.833	0.577	194.424	25.064	287.176	71.023
GALNT2	pgant2	3254	24.167	7.408	3.222	0.943	204.517	16.806	329.211	74.372
n/d	pgant3	4445	22.363	6.253	3.583	0.900	204.088	46.144	283.633	71.781
GALNT7	GalNAc-T2	6394	26.667	7.202	3.333	0.985	267.491	28.555	346.103	70.061
GALNT11	Pgant35A	7480	30.75	5.514	3.4	0.548	225.928	54.736	384.920	113.470
n/d	GalNAc-T1	8182	26	2.898	2.833	1.169	204.585	27.409	262.726	36.814
C1GALT1	C1GalTA	9520	25.5	5.671	3.083	0.830	190.985	47.339	287.106	47.779
GALNT1	pgant5	31651	22.833	1.835	2.833	1.169	193.122	15.031	463.473	114.000
n/d	pgant4	31956	21.167	4.355	3.667	1.211	216.217	3.565	241.505	58.796
OGT	sxc	10392	19.833	3.43	3	0.707	193.308	44.025	241.217	7.358
RFNG	fng	10580	22.167	6.853	3.333	0.516	191.667	38.482	312.147	21.118
POMT2	tw	12311	22.867	3.623	3.33	1.033	192.855	42.817	253.687	51.372
POFUT1	O-fut1	12366	23.667	0.577	3	0.817	147.801	41.089	258.148	58.650
POFUT2	O-fut2	14789	27	5.329	2.75	0.957	136.323	30.379	341.320	41.460
POGLUT1	rumi	31152	23	2.708	4.333	1.506	128.274	29.862	295.523	22.455
B3GNT1	n/d	3253	27.333	7.257	4.167	0.983	140.891	52.097	285.230	72.183
n/d	GlcAT-S	3881	25.5	6.654	3.364	0.809	193.28	20.529	326.828	97.482
CHPF	n/d	4351	32.333	9.688	3	0.603	206.671	40.309	292.107	47.009
HS6ST3	Hs6st	4451	32.3	6.195	3.182	0.982	160.382	51.968	221.445	76.016
SULF1	Sulf1	6725	31.614	5.335	3.1667	0.753	182.304	41.794	390.791	77.178
NDST2	sfl	8339	27.667	7.371	2.5	0.548	151.417	13.814	233.830	28.840
EXT2	Ext2	8433	24	4.328	3.25	1.422	173.777	36.755	222.140	47.690
CHSY1	n/d	9220	27.833	4.956	3.5	0.548	183.432	23.112	295.953	103.380
EXT1	ttv	10117	24.167	6.145	3.333	0.817	133.221	29.341	321.280	73.667
UGDH	sgl	10072	29.5	4.68	2.5	0.548	173.36	58.236	284.297	16.373
HS2ST1	Hs2st	10234	18.5	3.391	2.5	0.837	158.557	30.162	256.106	42.834
B4GALT7	β4GalT7	11780	31	3.464	2.667	0.817	241.78	33.859	280.748	80.240
CSGALNACT1	n/d	12913	47.333	4.367	3.833	0.983	237.477	12.936	255.450	15.958
EXTL3	botv	15110	25.667	2.887	3.667	0.577	208.774	20.338	237.780	54.332
XYLT1	oxt	32300	22	5.586	3.333	0.516	178.204	47.231	271.733	28.785

B3GAT3	GlcAT-I	32775	26.833	5.913	3.8333	0.753	138.585	27.628	357.973	57.666
n/d	Lamp1	3305	21.8	9.418	2.833	0.753	162.125	86.057	415.217	93.494
n/d	Sdc	10497	28.2	5.404	3.2	1.095	175.03	43.881	369.440	23.913
BMPR1A	tkv	14026	23.4	4.722	3.6	1.140	153.965	44.908	318.610	41.332
DAG1	Dg	18250	32.333	2.887	3	0.894	179.973	25.716	247.725	32.376
GPC4	dlp	32146	23.167	4.579	2.667	0.516	178.265	44.432	320.060	27.625
FUT8	FucT6	2448	27.5	8.167	3.6	0.548	154.319	61.493	339.230	58.474
PGM1	Pgm	5165	21.833	3.71	2.916	0.515	206.119	39.981	252.970	50.370
NANS	Sas	5232	31.333	9.873	3.3	0.823	153.102	35.941	294.317	44.404
PIGA	n/d	6401	42	8.509	2.667	0.516	206.846	46.72	344.273	52.533
UGCG	GlcT-I	6437	26.667	8.083	4	1.000	216.773	16.353	233.829	79.773
n/d	veg	6657	30.167	7.25	3.167	1.169	205.144	27.966	398.740	35.558
GYS1	n/d	6904	32.333	10.504	3	0.000	207.118	57.579	269.623	30.786
GMPPA	n/d	8207	24.833	2.787	4.333	1.211	177.999	27.549	268.644	41.288
GPI	Pgi	8251	24.333	1.528	2.333	0.577	194.383	19.923	201.820	19.608
B3GALT5	n/d	8673	27.5	3.017	3	1.095	146.754	41.517	303.453	82.266
GALT	Galt	9232	30.667	3.011	3.2	0.837	153.632	28.734	293.016	25.469
UAP1	mmy	9535	25.167	2.483	2.667	0.985	182.304	28.075	315.563	82.648
PIGM	n/d	9865	22.5	5.244	3.5	1.049	144.827	59.411	242.390	26.816
PIGB	n/d	12006	31.167	5.115	3.667	1.211	134.796	28.835	291.793	58.065
UGT8	n/d	30438	27.5	5.822	2.833	0.753	181.873	30.45	306.521	101.000
n/d	n/d	33145	17.167	4.622	2.833	0.753	128.98	32.529	319.993	113.290
n/d	Hexo1	1318	25.333	2.16	3.667	0.516	215.715	25.786	364.250	31.756
n/d	n/d	2135	31	3.578	3.5	1.225	167.263	53.965	320.120	63.546
HK2	Hex-A	3001	16	5.586	3.5	1.643	140.193	63.045	332.046	53.046
n/d	α-Man-IIb	4606	30	5.727	3.2	0.447	190.397	34.896	250.280	38.711
FUCA2	Fuca	6128	27.333	5.033	3.75	0.500	171.796	31.487	289.288	38.343
IDUA	n/d	6201	27.667	3.445	3.25	0.754	201.597	14.957	376.125	59.557
n/d	n/d	6206	23.4	2.074	3.333	1.211	214.18	20.927	380.517	17.713
ARSB	n/d	7402	25.166	3.189	3.333	1.506	212.965	24.657	467.046	64.949
GCK	Hex-C	8094	24.4	2.51	3.667	1.033	180.536	20.949	267.080	86.281
GLB1	Gal	9092	19.25	3.304	3.636	1.027	177.423	49.938	337.420	26.981
PMM2	n/d	10688	19.33	9.416	3.167	0.753	182.76	73.797	341.740	52.213
IDS	n/d	12014	21.167	4.07	2.8733	0.753	166.262	44.156	376.323	51.119
GUSB	n/d	15117	22.167	4.75	3.833	1.169	147.51	35.494	295.890	43.041
GBE1	n/d	33138	30.667	7.371	3	1.000	220.125	18.167	249.926	20.682
HK1	Hex-t2	32849	31	5.568	3.333	0.577	278.224	36.517	306.070	41.116
n/d	fw	1500	21.857	5.551	2.5	0.548	127.544	25.087	308.248	92.674
n/d	lectin-46Cb	1652	23.333	0.5744	3	0.000	190.972	23.371	248.513	21.387
n/d	lectin-21Ca	2826	31.583	6.142	3.667	1.303	180.812	30.264	246.890	12.486
n/d	lectin-24Db	2958	30.333	2.733	3.167	0.753	195.685	35.978	296.626	45.587
n/d	lectin-24A	3410	28.167	3.71	3.167	0.753	144.841	13.427	254.893	36.372
n/d	glec	6575	28	1	2.5	0.577	161.402	48.768	237.911	40.374
n/d	Nrx-1	7050	19.5	5.958	3.167	0.753	173.703	50.319	230.490	40.784
n/d	lectin-28C	7106	33.833	5.492	3.167	0.983	166.873	46.092	319.500	26.068
n/d	Lectin-galC1	9976	24.667	9.866	3.333	0.577	192.248	75.2809	460.623	52.526
LGALS9B	galectin	11372	29.667	3.011	2.5	0.548	177.635	39.298	239.073	33.651
n/d	lectin-21Cb	13686	38.167	8.377	4	0.894	248.003	106.58	300.010	38.486

n/d	lectin-33A	16834	28	3.536	4.8	1.483	168.059	37.381	303.560	38.403
n/d	lectin-30A	17011	27.667	7.767	3.333	0.577	187.305	61.135	298.137	62.090
n/d	lectin-29Ca	17799	29.667	3.386	3.667	1.862	207.744	31.663	327.926	88.079
n/d	lectin-37Da	33532	25.5	4.506	3.167	0.753	154.475	27.428	287.150	33.351
n/d	lectin-37Db	33533	35.667	5.428	3.167	0.408	210.426	34.634	268.326	60.086
SLC2A1	Glut1	1086	25.5	3.873	3.833	0.718	181.751	30.84	358.287	24.932
SLC35A2	Csat	2675	26.5	5.648	4.167	1.169	226.021	30.701	373.160	21.740
SLC35D1	frc	3874	27.833	2.563	3.5	1.314	219.609	40.526	299.290	43.799
SLC35B2	sll	7623	27.333	3.502	3.667	0.516	195.407	35.123	277.510	10.289
SLC35C1	Gfr	9620	19.167	3.764	2.667	0.817	142.467	26.185	225.942	25.866

Table II. Primary screen results. Raw number values of the RNAi screen indicated by human ortholog name, *Drosophila* gene name and CG number. Mean value and standard deviation (SD) included for NMJ morphology parameters of bouton number, branch number and synaptic area, and for NMJ functional parameter of evoked excitatory junctional current (EJC) amplitude. Sample sizes ≥6 NMJs and ≥3 animals for morphology and function measurements.

All morphological and functional assays were done blind to genotype, with values reported as fold-change compared to genetic control, as well as statistical significance calculated using one-way ANOVA analyses (see color scheme; $P<0.05$ (*), $P<0.01$ (**); Fig. 5). The data represents $\geq$6 NMJs from $\geq$3 animals from every genotype. Synapse morphology was imaged by co-labeling with presynaptic marker anti-horse radish peroxidase (HRP) and postsynaptic marker anti-Discs Large (DLG). A synaptic bouton was defined as a varicosity of $\geq$2 µm in minimum diameter labeled by both HRP and DLG, and a synaptic branch was defined as a process containing at least two boutons (Gatto and Broadie, 2008). NMJ branch number was the least affected morphological parameter, with only 2 of 103 genes showing a statistically significant change (Fig. 5). Many more genes were involved in bouton development. All 27 genes showing a statistically significant change compared to genetic control exhibited elevated bouton numbers (Fig. 5), suggesting that glycan mechanisms primarily limit morphological growth. Synapse area was determined by outlining the terminal area labeled by DLG using the thresholding function in ImageJ. The majority of gene knockdown conditions showed a decrease in NMJ area compared to control (Fig. 5). 7 RNAi lines exhibited a statistically significant decrease in area, whereas only 2 lines exhibited a statistically significant increase in synaptic area. All raw values of measured morphological parameters are included in Table I.

To assay functional differentiation, the motor nerve was stimulated with a suction electrode while the evoked excitatory junctional current (EJC) was recorded in the muscle (Fig. 5) (Beumer et al., 1999). Nerve stimulation was

applied at 4V for 0.5 ms at a frequency of 0.2 Hz, with the muscle clamped at -60 mV. EJC amplitudes were calculated from recorded traces in the ubiquitously-driven RNAi lines (w^{1118} background) compared to the w^{1118}; UH1-GAL4/+ control. Recordings were obtained from $\geq$3 independent trials for each RNAi knockdown condition. All electrophysiological screening was done blind to genotype, with values reported as fold-change and statistical significance calculated by one-way ANOVA analyses (see color scheme; $P<0.05$ (*), $P<0.01$ (**); Fig. 5). Genes from all eight glycan classes were identified to produce changes in neurotransmission strength upon genetic knockdown. For the 103 larval-viable lines tested, 26 lines showed a trend towards increased transmission strength, and 12 were statistically elevated compared to genetic control (Fig. 5). 4 gene knockdowns showed a trend towards decreased transmission strength, of which only 1 line reached statistical significance. 73 of the 103 lines tested showed no change in functional strength (Fig. 5). Interestingly, only 6 RNAi lines showed statistically significant effects on both NMJ morphology parameters and EJC amplitude: CG1597, CG6657, CG7480, CG4451, CG6725 and CG11874 (Fig. 5). This suggests that glycan effects on synapse morphological and functional development are largely separable. All raw values of EJC measurements are included in Table II.

To validate results, a secondary screen was conducted using independent RNAi lines obtained from the VDRC and Harvard TRiP collections (Table III). Of the 44 genes that showed morphological and functional defects in the primary screen, 33 were retested using independent RNAi lines, with the others lacking

available secondary lines from any source. Using the same screen of morphological and functional characterization, we determined that ~80% of retested secondary lines showed the reported structural (bouton number) and functional (EJC) phenotypes consistent with primary screen (Table II). These primary and secondary RNAi screen results now represent a resource for the systematic characterization of glycan mechanisms underlying synaptic structural and functional development. Screen results were further studied by comparing synaptogenesis phenotypes of RNAi knockdown with defined genetic nulls for two genes, CG6725 and CG4451, from the glycosaminoglycan biosynthesis class (Fig. 5). The RNAi screen of functional strength as measured by EJC amplitudes indicated opposite effects for these two lines, with CG6725 (RNAi-*sulf1*) knockdown exhibiting an increase in transmission strength and CG4451 (RNAi-*hs6st*) knockdown producing a decrease (Fig. 5). Along with our goal to identify interesting glycan-related genes involved in synapse development, we show here characterization of null alleles of two genes obtained from screen results and define the associated mechanisms driving the bidirectional regulation of synaptic functional development.

Synaptogenesis is bidirectionally regulated by paired *sulf1* and *hs6st* genes

The RNAi screen identified two functionally-paired genes, *sulf1* (CG6725) and *hs6st* (CG4451), with similar effects on morphological development but opposite effects on synaptic functional differentiation (Fig. 5). Our goal was to use these

Secondary Screen - Morphology (Bouton number)							
Human Gene	Drosophila Gene	CG	ID	Fold	ID	Fold	Confirmed
		control		1		1	
FUT10	FucTB	4435	GD40519	1.613	GD40520	1.162	N
n/d	FucTD	9169	CG27008	1.673	CG27009	1.301	Y
n/d	egghead	9659	GD10137	1.764	GD405160	1.567	Y
MAN1B1	n/d	11874	GD101661	1.538	GD4919	1.553	Y
MAN1A2	α-Man-I	32684	GD39572	1.538	GD5528	1.447	Y
PIGA	n/d	6401	KK107714	1.900	GD39552	1.294	N
GYS1	n/d	6904	GD35136	1.462	GD35137	1.693	Y
GALT	Galt	9232	KK100025	1.387	GD29087	1.494	Y
n/d	n/d	2135	KK103338	1.402	GD16628	1.241	N
n/d	α-Man-IIb	4606	GD42652	1.357	KK108043	1.338	Y
HK1	Hex-t2	32849	KK100218	1.402	GD47331	1.640	Y
n/d	lectin-24Db	2958	KK105118	1.372	GD45294	1.4403	Y
n/d	lectin-21Cb	13686	KK106450	1.726	GD32507	1.513	Y
n/d	lectin-37Db	33533	KK107567	1.613	GD51100	1.617	Y
Secondary Screen - EJC							
Human Gene	Drosophila Gene	CG	ID	Fold	ID	Fold	Confirmed
		control		1		1	
ALG8	n/d	4542	KK104870	1.782	GD7132	1.333	Y
ST6GAL1	ST6Gal	4871	KK100284	1.464	GD47955	0.978	N
MAN1B1	n/d	11874	KK101661	1.586	GD4419	1.214	Y
GALNT1	pgant5	31651	GD2629	1.858	KK110647	1.090	N
HS6ST3	hs6st	4451	KK101636	0.796	GD42658	0.658	Y
SULF1	sulf1	6725	GD37362	1.389	GD37361	1.326	Y
B3GAT3	GlcAT-I	32775	KK107840	1.435	TRiP.HMS00289	1.280	Y
n/d	Lamp1	3305	GD7309	1.664	TRiP.GLV21040	1.404	Y
n/d	Lectin-galC1	9976	GD38002	1.846	KK100935	1.680	Y

Table III. Secondary screen results. Raw number values for the secondary screen results indicated by human ortholog name, *Drosophila* gene name and CG number. The two independent IDs for RNAi lines are shown. For all retested lines, morphological quantification for NMJ bouton number (top) and evoked excitatory junctional current (EJC) amplitude (bottom). All results are shown as fold-changes compared to genetic control. Sample sizes are ≥6 individual animals per genotype. Replication of primary screen result is indicated in the final column as Y. and failure to replicate indicated as N.

genes as a test case from the completed glycan screen, by assaying phenotypes in recently characterized null mutants of both genes (Kamimura et al., 2001; You et al., 2011). The gene products Sulfated (Sulf1), an HS 6-endosulfatase, and Hs6st, an HS 6-O-sulfotransferase, drive opposing changes in sulfation state of the same C_6 carbon of the repeated glucosamine unit in GAG modified heparan sulfate proteoglycans (Kamimura et al., 2001; Ai et al., 2003). Viable null mutants are available for both genes, e.g. *sulf1* (*sulf1*$^{\Delta 1}$) and *hs6st* (*hs6st*^{d770}) (Kamimura et al., 2001; You et al., 2011), but requirements have never been assayed in the nervous system or neuromusculature. We therefore first compared phenotypes of RNAi knockdown and null alleles at the NMJ synapse by confocal imaging of synaptic morphogenesis and TEVC recording of synaptic functional neurotransmission.

Using double-labeling for HRP (presynaptic) and DLG (postsynaptic), NMJ structural parameters including bouton number, branch number and synaptic area were quantified in *sulf1* and *hs6st* null alleles. The mutant results closely recapitulated the RNAi knockdown findings from the screen (Table II, III). To consistently compare RNAi and null mutant conditions, both animal groups were simultaneously reared and processed to visualize the NMJ (Fig. 6). Structural quantification showed an increased bouton number with RNAi-mediated *sulf1* knockdown (*sulf1*-RNAi x UH1-GAL4; 36.4±1.6, n=10) and *hs6st* knockdown (*hs6st*-RNAi x UH1-GAL4; 35.1±1.96, n=10) compared to the transgenic control (*w*^{1118} x UH1-GAL4; 21.9±1.84, n=10 $p<0.001$, n=10; Fig. 6A,B). Consistently, increased bouton number was observed in both *sulf1* (31.9 ± 1.37, n=10) and

hs6st (36.25 ± 2.58, n=8) null mutants compared to genetic control (w^{1118}*, 19.3* ± 1.69, p<0.001, n=10; Fig. 6C,D). In contrast, no significant change in branch number was exhibited with *sulf1* knockdown (3.22 ± 0.28, p>0.05, n=9) or *hs6st* knockdown (3.22 ± 0.22, p>0.05, n=9) compared to control (w^{1118} x UH1-GAL4; 2.64 ± 0.06, n=11). Similarly, no significant change was observed in the synaptic branch number in *sulf1* (2.8 ± 0.33, p=0.27, n=10,) and *hs6st* (3.63 ± 0.38, p=0.115, n=10) nulls compared to control (w^{1118}; 3.4 ± 0.46, n=8). Further, there was no significant difference in synaptic area in *sulf1* (138.16 ± 5.82, p>0.05, n=10,) and *hs6st* (138.48 ± 13.38, p>0.05, n=8,) mutants compared to the control (w^{1118} ; 118.04 ± 8,38, n=10), however a slight increase in synaptic area was observed in *sulf1* knockdown (178.68 ± 10.64, p<0.05, n=9), while no change was observed for *hs6st* knockdown (164 ± 8.47, p>0.05, n=10) as compared to control (w^{1118} x UH1-GAL4; 134.57 ± 11.95, n=10). Based on these imaging studies, we conclude morphological differences in synaptic architecture observed in both *sulf1* and *hs6st* null allele conditions is consistent with both RNAi knockdown conditions.

Functional development was next tested with electrophysiological recording to compare RNAi and null mutant phenotypes (Fig. 7). Representative TEVC records are shown as an average of 10 consecutive nerve stimulus responses in 1.0 mM extracellular Ca^{2+} for each transgenic genotype in Figure 7A; *sulf1* knockdown (UH1-GAL4 x *sulf1*-RNAi), *hs6st* knockdown (UH1-GAL4 x *hs6st*-RNAi) and genetic control (UH1-GAL4 x w^{1118}). There was a striking ~80% difference in EJC amplitude between *sulf1* and *hs6st* knockdown conditions, with

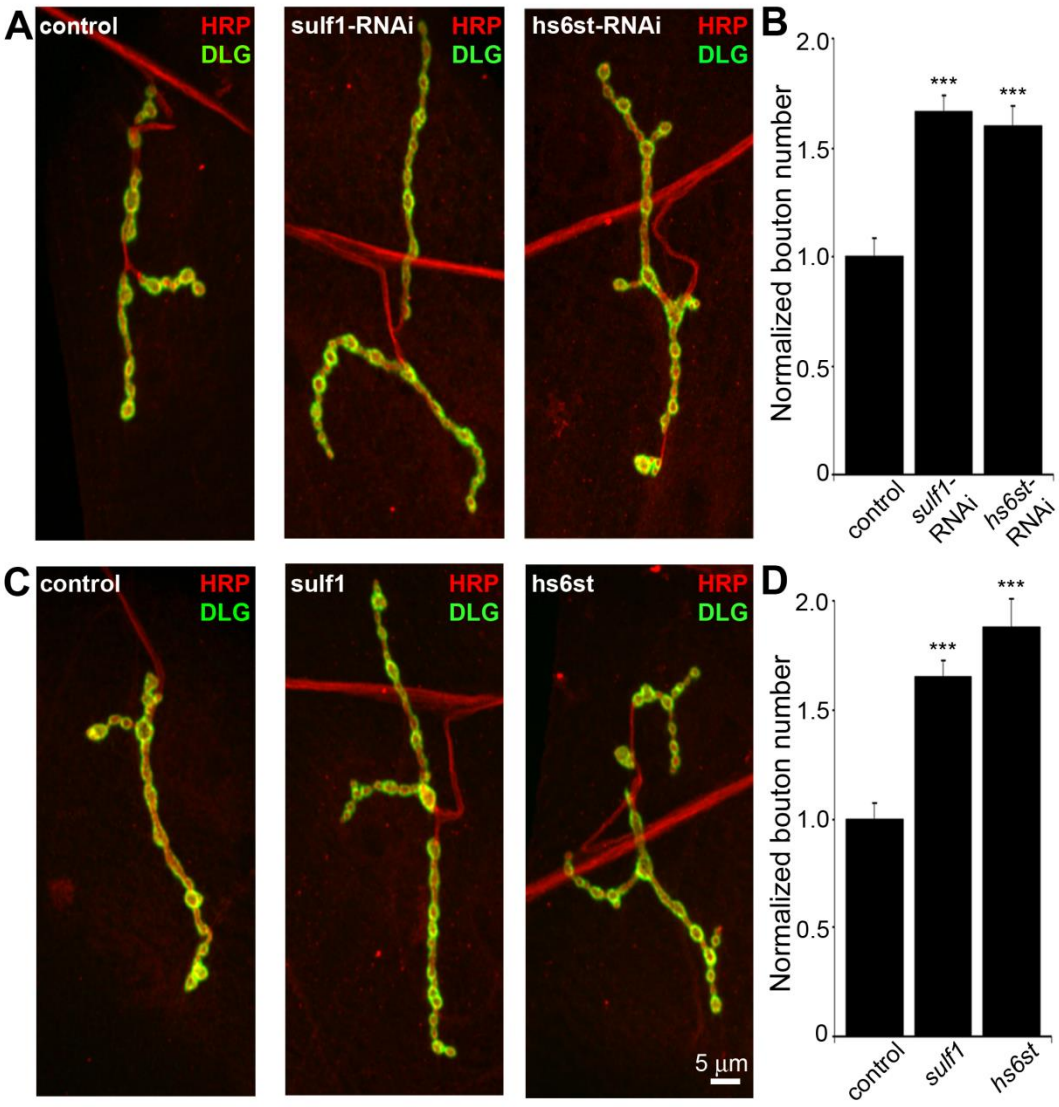

Figure 6 NMJ synaptic bouton number in *sulf1* **and** *hs6st* **mutants.** (A) Representative NMJ images from muscle 4 in segment A3 showing anti-horseradish peroxidase (HRP; red) and anti-Discs Large (DLG; green) in control (w^{1118}×UH1-GAL4), *sulf1* RNAi (UH1-GAL4×UAS-CG6725) and *hs6st* RNAi (UH1-GAL4×UAS-CG4451). (B) Quantification of synaptic bouton number in RNAi-knockdown conditions for *sulf1* and *hs6st*, normalized to genetic control (w^{1118}×UH1-GAL4). Sample sizes are ≥10 animals per indicated genotypes. (C) Representative NMJ images of anti-HRP (red) and anti-DLG (green) in w^{1118} control, *sulf1* and *hs6st* null mutants. (D) Quantification of synaptic bouton number in mutant conditions normalized to genetic control. Sample sizes are ≥8 animals per indicated genotype. Statistically significant differences were calculated using student's t-test and indicated as ***p<0.001. Error bars indicate S.E.M.

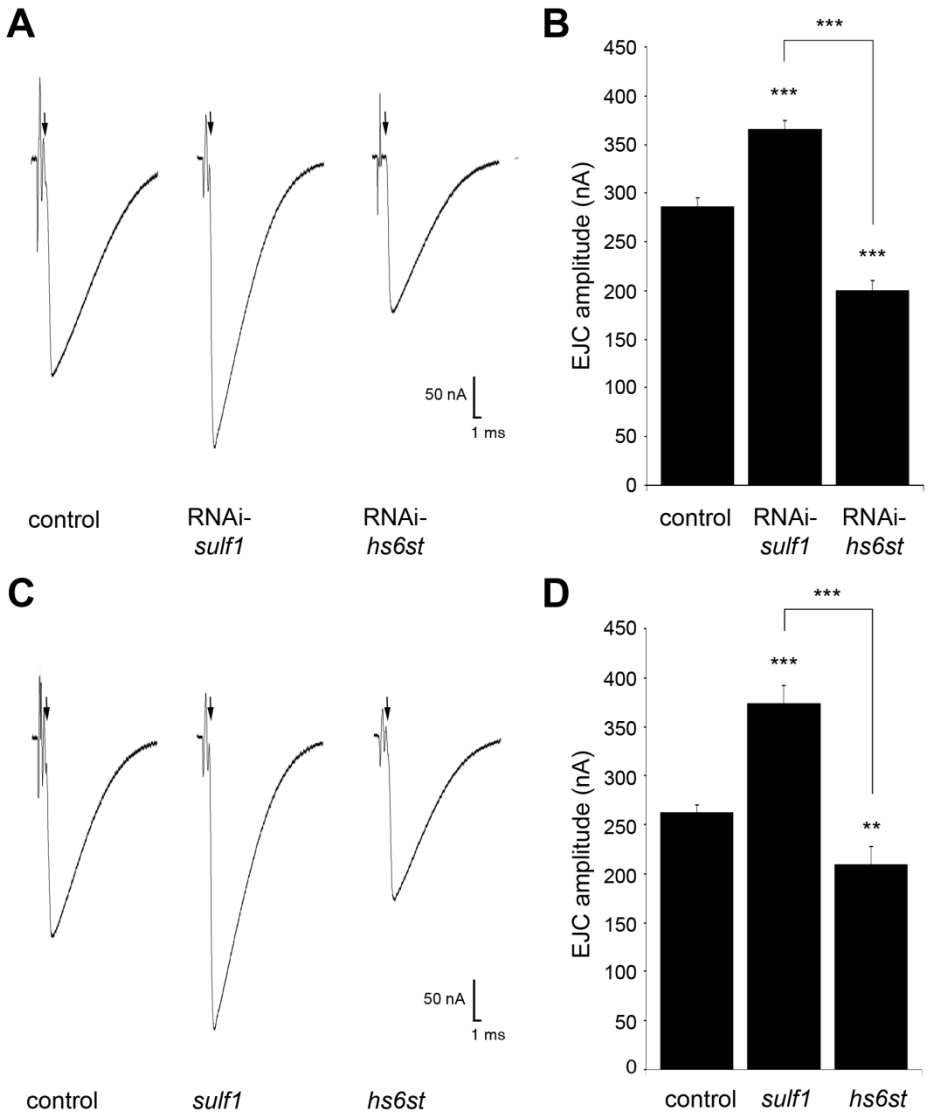

Figure 7. Loss of *sulf1*/*hs6st* causes opposite effects on transmission strength. (A) Representative excitatory junctional current (EJC) traces from control (w^{1118}×UH1-GAL4), *sulf1* RNAi (UH1-GAL4×UAS-CG6725) and *hs6st* RNAi (UH1-GAL4×UAS-CG4451). The nerve was stimulated (arrows) in 1.0 mM external Ca^{2+}, with TEVC records (−60 mV holding potential) from muscle 6 in segment A3. Each trace averaged from 10 consecutive recordings. (B) Quantified mean EJC amplitudes (nA) for the three genotypes shown in panel A. (C) Representative traces from control (w^{1118}), $sulf1^{\Delta 1}$ and $hs6st^{d770}$ null alleles under the same conditions described in panel A. (D) Quantified mean EJC amplitudes (nA) for the three genotypes shown in panel C. Sample sizes are at least 11 animals per indicated genotype. Statistically significant differences calculated using student's t-test, ** p<0.01, *** p<0.001. Error bars indicate S.E.M.

sulf1 elevated by ~30% and *hs6st* reduced by ~30% compared to control.

Quantification of EJC amplitudes showed both knockdown conditions to be highly significantly different from control and each other (control, 286.22 ± 8.56 nA; *sulf1*-RNAi, 365.01 ± 9.502 nA, p<0.001; *hs6st*-RNAi, 199.19 ± 11.84 nA, p<0.001; *sulf1*-RNAi vs. *hs6st*-RNAi, p<0.001; Fig. 7B). These opposite effects on neurotransmission strength were confirmed in characterized null alleles for both genes [42,43]. Representative traces from $sulf1^{\Delta 1}$ and $hs6st^{d770}$ null mutants compared to w^{1118} control are shown in Figure 7C. Quantification of EJC amplitudes showed null mutants to be highly significantly different from control and each other (w^{1118}, 256.14 ± 7.38 nA; $sulf1^{\Delta 1}$, 372.86 ± 18.49 nA, n=11, p<0.001; *hs6st*, 209.66 ± 13.44 nA, n=14, p<0.01; $sulf1^{\Delta 1}$ vs. *hs6st*, p<0.001; Fig. 7D). These results were confirmed in an independent *sulf1* null allele ($sulf1^{\Delta P1}$), which shows comparable elevation compared to control (w^{1118}, 244.91 ± 9.04 nA; $sulf1^{\Delta P1}$, 282.28 ± 13.59, p<0.05, n=22), as well as the *hs6st* null ($hs6st^{d770}$) over deficiency (Df(3R)ED6027), which shows comparable depression compared to control (w^{1118}, 256.14 ± 7.38 nA; *hs6st*/Df(3R)ED6027, 224.06 ± 7.65 nA, p<0.05, n=18). These results reveal a critical role for *sulf1* and *hs6st* genes in synaptic functional development.

Given the functionally-paired nature of *sulf1* and *hs6st* activities on 6-O-S modification, and the epistatic function of *hs6st* to *sulf1*, we predicted that knocking both genes down would produce a phenotype similar to knockdown of *hs6st* alone. Consistently, *hs6st* and *sulf1* double knockdown produced EJC amplitudes significantly lower than control (w^{1118} x *hs6st*-RNAi; *sulf1*-RNAi

(control), 225.17 ± 6.28 nA, n=12; *hs6st*-RNAi, *sulf1*-RNAi x UH1-GAL4, 198.22 ± 9.77 nA, n=15, $p<0.05$; Fig. 8). Cell-specific knockdown in neural (*elav*-GAL4), muscle (24B-GAL4) and glia (*repo*-GAL4) also support the observed opposite effects in neurotransmission strength. With *sulf1* knockdown in muscle, EJC amplitude was significantly elevated compared to control (w^{1118} x *sulf1*-RNAi (control), 199.97 ± 21.86 nA; 24B-GAL4 x *sulf1*-RNAi (knockdown), 222.88 ± 25.78 nA, $p<0.01$, n=10), but no change occurred with neural knockdown (*elav*-GAL4 x *sulf1*-RNAi, 196.09 ± 25.08 nA, p=0.72, n=10) or glial knockdown (*repo*-GAL4 x *sulf1*-RNAi, 208.40 ± 32.45 nA, p=0.53, n=7). Moreover, only neural knockdown of *hs6st* caused a decrease in EJC amplitude (w^{1118} x *hs6st*-RNAi (control), 211.496 ± 22.142 nA, *elav*-GAL4 x *hs6st*-RNAi (knockdown), 184.68 ± 28.97 nA, $p<0.05$, n=16), while no change occurred with muscle knockdown (24B-GAL4 x *hs6st*-RNAi, 209.92 ± 24.74 nA, p=0.88, n=9) or glial knockdown (*repo*-GAL4 x *hs6st*-RNAi, 216.38 ± 37.80 nA, p=0.32, n=7). We conclude that HSPG sulfation state strongly modulates NMJ functional development, with contributions from both motor neuron and muscle, but not glia. The clear next step was to test for differences in the localization and abundance of synaptic HSPG targets known to regulate NMJ synaptogenesis.

HSPG abundance at the synaptic interface is dependent on *sulf1* and *hs6st*.

Both GPI-anchored HSPG glypican Dally-like (Dlp) and transmembrane HSPG Syndecan (Sdc) are clearly expressed at the *Drosophila* NMJ (Fig. 9), where they are known to regulate synaptogenesis (Johnson et al., 2006). We detect no enrichment of the secreted HSPG perlecan (Trol) at the NMJ, although

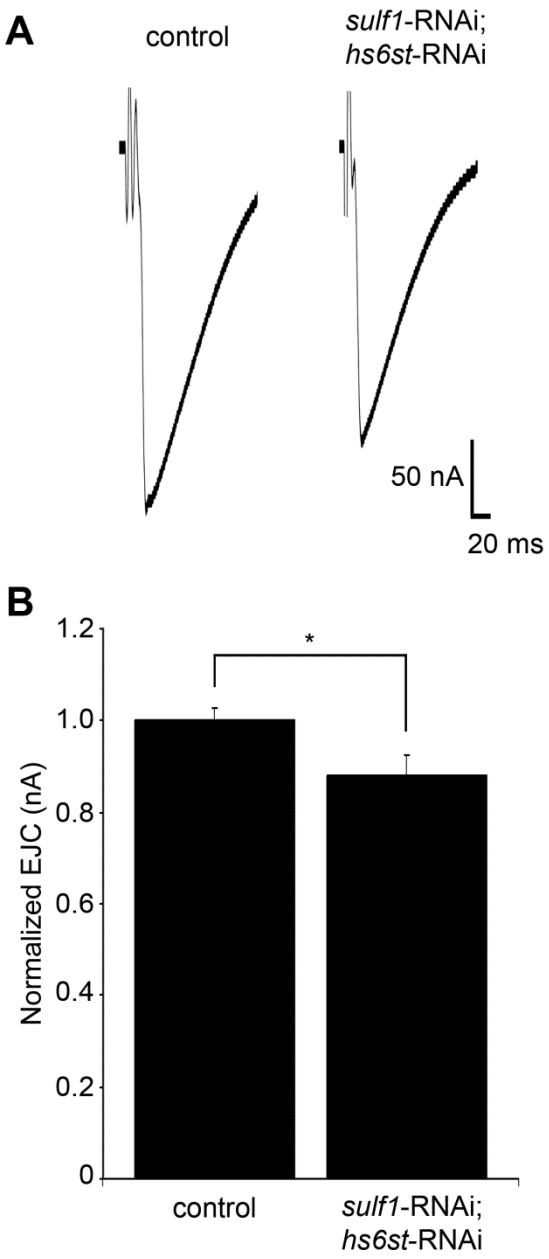

Figure 8. Double knockdown of *sulf1* **and** *hs6st* **measure of EJC amplitude**. (A) Representative evoked excitatory junctional current (EJC) traces from control (w^{1118}×UH1-GAL-4) and double knockdown with both *sulf1* and *hs6st* RNAi transgenic lines (UH1-GAL4×UAS-*sulf1*-RNAi; UAS-*hs6st*-RNAi). (B) Quantified mean EJC amplitudes (nA) for the two genotypes shown in panel A normalized to control. Sample sizes are ≥12 animals per indicated genotype. Statistically significant differences calculated using student's t-test, * $p<0.05$, Error bars indicate S.E.M.

it is abundantly expressed in the motor nerve leading up to the synaptic terminal and present in lower levels throughout the muscle (Fig. 10). We therefore hypothesized that membrane-associated Dlp and Sdc HSPGs are targeted by *sulf1* and *hs6st* activity to regulate their synaptic distribution and/or function. To test this hypothesis, we assayed both Dlp and Sdc under non-permeabilized, detergent-free conditions to examine their cell surface expression at the NMJ synaptic interface of *sulf1* and *hs6st* null mutants compared to control. These data are summarized in Figure 11.

In the genetic background control (w^{1118}), Dlp shows a punctate expression pattern strongly concentrated in a halo-like array around the anti-HRP labeled presynaptic membrane (Fig. 9, Fig. 11, top). In *sulf1* mutants there was a clear and consistent increase in Dlp abundance, with more numerous and intense punctae at the synaptic interface surrounding NMJ boutons, while at *hs6st* mutant synapses there was an opposing decrease in Dlp abundance (Fig. 11). This bidirectional and differential effect on Dlp abundance was quantified as fluorescence intensity normalized to the internal HRP labeling control. There was a significant Dlp increase in *sulf1* compared to control (~40% elevated over control; $p<0.05$; $n=11$), and a significant Dlp decrease in the *hs6st* null synapse (~15% reduced compared to control; $p<0.05$; $n = 11$; Fig. 11B). Importantly, the difference between *sulf1* and *hs6st* nulls was very highly significant ($p<0.001$). In comparison, cell surface Sdc labeling also showed a dense halo-like localization around NMJ synaptic boutons labeled with cell adhesion marker Fasciclin II

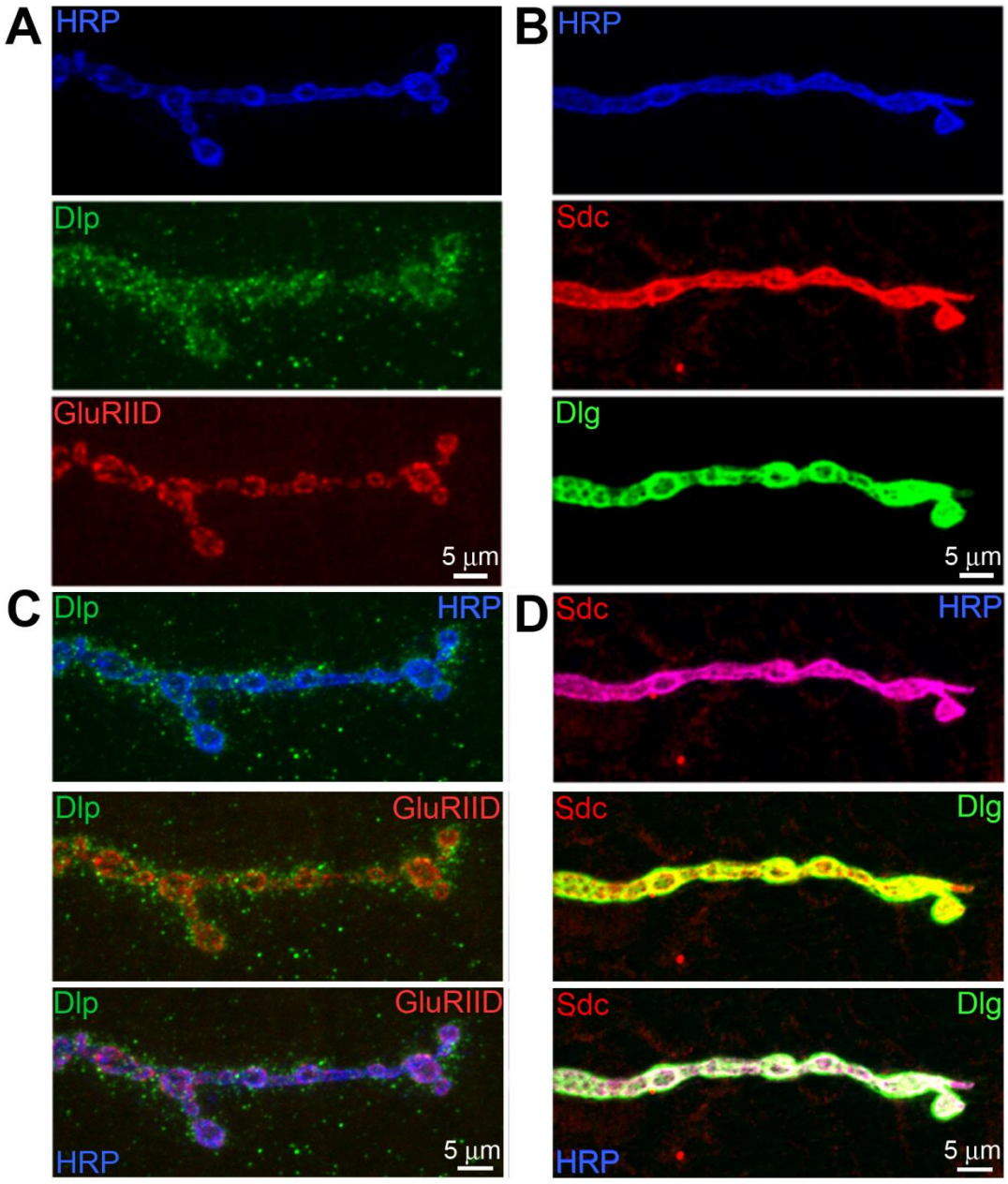

Figure 9. NMJ synaptic localization of Dally-like and Syndecan HSPGs. Representative confocal images showing HSPG synaptic localization at the larval NMJ. (A) Single channel images of presynaptic anti-horseradish peroxidase (anti-HRP, blue), Dally-like Protein (anti-Dlp, green) and postsynaptic glutamate receptor subunit IID (anti-GluRIID, red). (B) Single channel images showing presynaptic anti-horseradish peroxidase (anti-HRP, blue), syndecan (anti-Sdc, red) and postsynaptic Discs Large (anti-DLG, green). (C) Merged image showing Dlp localization with respect to presynaptic HRP, postsynaptic GluRIID and the triple-labeled terminal. (D) Merged image showing Sdc localization with respect to presynaptic HRP, postsynaptic DLG and the triple-labeled terminal.

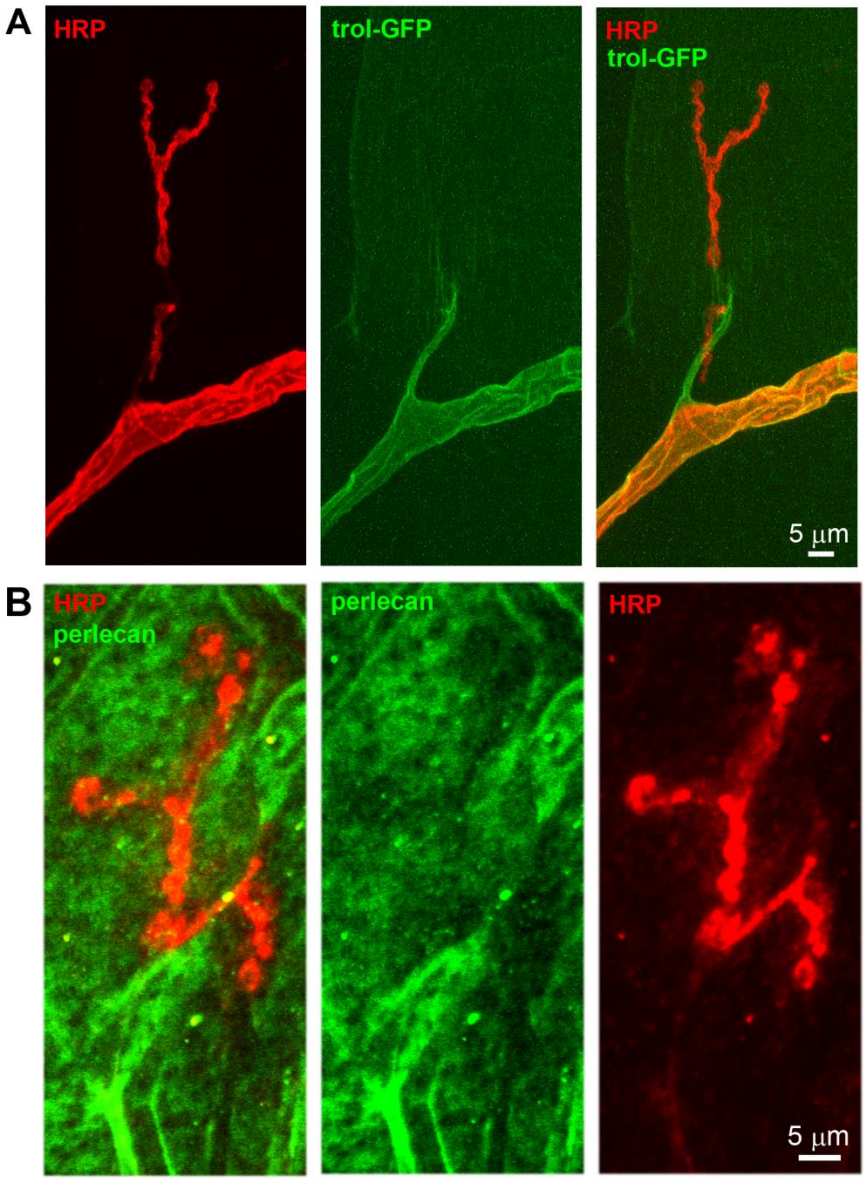

Figure 10. HSPG Perlecan (Trol) is absent from the NMJ synaptic terminal. (A) Representative confocal image showing Perlecan expression at the wandering third instar larval NMJ using the Trol-GFP Flytrap line ZCL1700 from the Flytrap GFP Resource. Single channel and merged images show presynaptic anti-horseradish peroxidase (anti-HRP, red) and Trol-GFP (green). (B) Representative confocal image showing Perlecan (anti-PcanV) antibody staining, shown at a much higher confocal gain than in A to emphasize muscle expression. Perlecan is strongly expressed in the motor nerve, and clearly present on the muscle surface, but is never detectably enriched at the NMJ terminal. In many cases, as in the example shown, Perlecan appears at lower levels in the perisynaptic region surrounding the NMJ than elsewhere on the muscle.

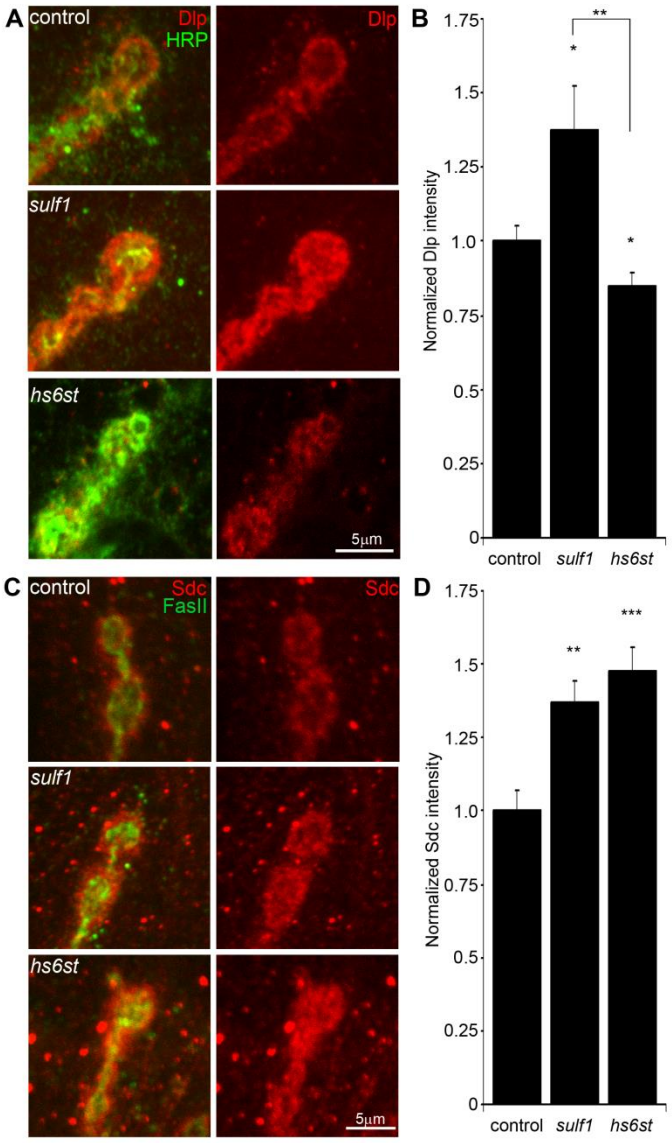

Figure 11. Synaptic HSPG co-receptor abundance is modified by 6-O-S sulfation. (A) Representative NMJ synaptic boutons imaged from control (w^{1118}), *sulf1* and *hs6st* nulls, probed with presynaptic neural marker anti-HRP (green) and Dally-like (Dlp; red). Right: Dlp distribution without the HRP signal is shown for clarity. (B) Quantification of mean fluorescent intensity levels of anti-Dlp labeling normalized to the HRP co-label at the muscle 6 NMJ, normalized to genetic control. (C) Boutons labeled with neural marker anti-Fasciclin II (FasII, green) and anti-Syndecan (Sdc, red). Right: Sdc distribution is shown alone for clarity. (D) Quantification of the mean fluorescent intensity levels of anti-Sdc labeling at the muscle 6 NMJ, normalized to genetic control. Sample sizes are at least 12 independent NMJs of at least 7 animals per indicated genotypes. Statistically significant differences calculated using student's t-test, * $p<0.01$, ** $p<0.01$, ***$p<0.001$. Error bars indicate S.E.M.

(FasII; Fig. 9, Fig. 11C). Synaptic Sdc labeling intensity was consistently greater in both *sulf1* and *hs6st* nulls compared to control (Fig. 11). Quantification of fluorescence intensity normalized to HRP revealed that Sdc abundance was greatly increased in *sulf1* null synapses compared to control (~35% elevated over control; $p<0.01$; $n=17$) and, to a greater degree, also in *hs6st* nulls (~50% elevated over control; $p<0.001$; $n=12$; Fig. 11D). Thus, both Dlp and Sdc HSPGs are strongly altered in *sulf1* and *hs6st* null NMJ synapses, with Dlp bidirectionally misregulated and Sdc differentially elevated in the two mutant conditions.

HSPGs act as co-receptors for WNT and BMP intercellular signaling ligands in many developmental contexts, acting to modulate extracellular ligand abundance and downstream signaling (Lin and Perrimon, 2000; Hacker et al., 2005). *Drosophila* WNT Wingless (Wg) distribution and signaling is known to be modulated by Dlp, which retains Wg at the cell surface in a mechanism that is enhanced by HS GAG chains (Yan et al., 2009). Specifically, Wg ligand abundance and signaling activity along the dorso-ventral axis of the developing *Drosophila* wing disc is elevated in *sulf1* mutants (Kleinschmit et al., 2010). Likewise, BMP ligands in other cellular contexts are closely regulated by HSPG co-receptors (Dejima et al., 2011). Specifically, Dlp has been suggested to similarly regulate *Drosophila* BMP Glass Bottom Boat (Gbb) (Dejima et al., 2011). We therefore hypothesized that altered HSPG co-receptors Dlp and/or Sdc in *sulf1* and *hs6st* null synapses regulate Wg and Gbb abundance to drive differentially altered *trans*-synaptic signaling across the synaptic cleft.

HSPG sulfation regulates abundance of WNT/BMP *trans*-synaptic ligands

Classical WNT and BMP morphogens act locally at synapses to fine tune synaptogenesis (Salinas, 2003; Marques, 2005). At the *Drosophila* NMJ, the WNT Wg is well-characterized as an anterograde *trans*-synaptic signal modulating synaptogenesis (Packard et al., 2002, 2003; Korkut and Budnik, 2009). Similarly, the BMP Gbb is well-characterized as a retrograde signal driving synaptic development (McCabe et al., 2003; Rawson et al., 2003; Keshishian and Kim, 2004). A third *trans*-synaptic signaling pathway, presynaptically-secreted Jelly Belly (Jeb) to postsynaptic Alk receptor (Rohrbough K. et al., 2010), has no known interaction with HSPGs and therefore would not be expected to be affected in *sulf1* and *hs6st* nulls, providing a comparison for specificity. To test the hypothesis that the observed alterations of HSPG co-receptor abundance will drive specific changes in WNT and BMP intercellular pathways, we labeled NMJ synapses with antibodies under non-permeablized conditions to reveal extracellular *trans*-synaptic signaling ligands (Fig. 12), and compared protein abundance and distribution in controls, *sulf1* and *hs6st* null mutants. The data are summarized in Figure 13.

NMJ synapses were first labeled with Wg antibody (green) together with anti-HRP (red) to label the presynaptic membrane (Fig. 13A). In control animals (w^{1118}), external Wg localized at large type Ib synaptic boutons in a dynamic pattern of punctuate distribution at the synaptic interface between motor neuron and muscle (Fig. 12, Fig. 13A, top). In *sulf1* and *hs6st* mutants, Wg was consistently elevated and concentrated uniformly in the extracellular domain

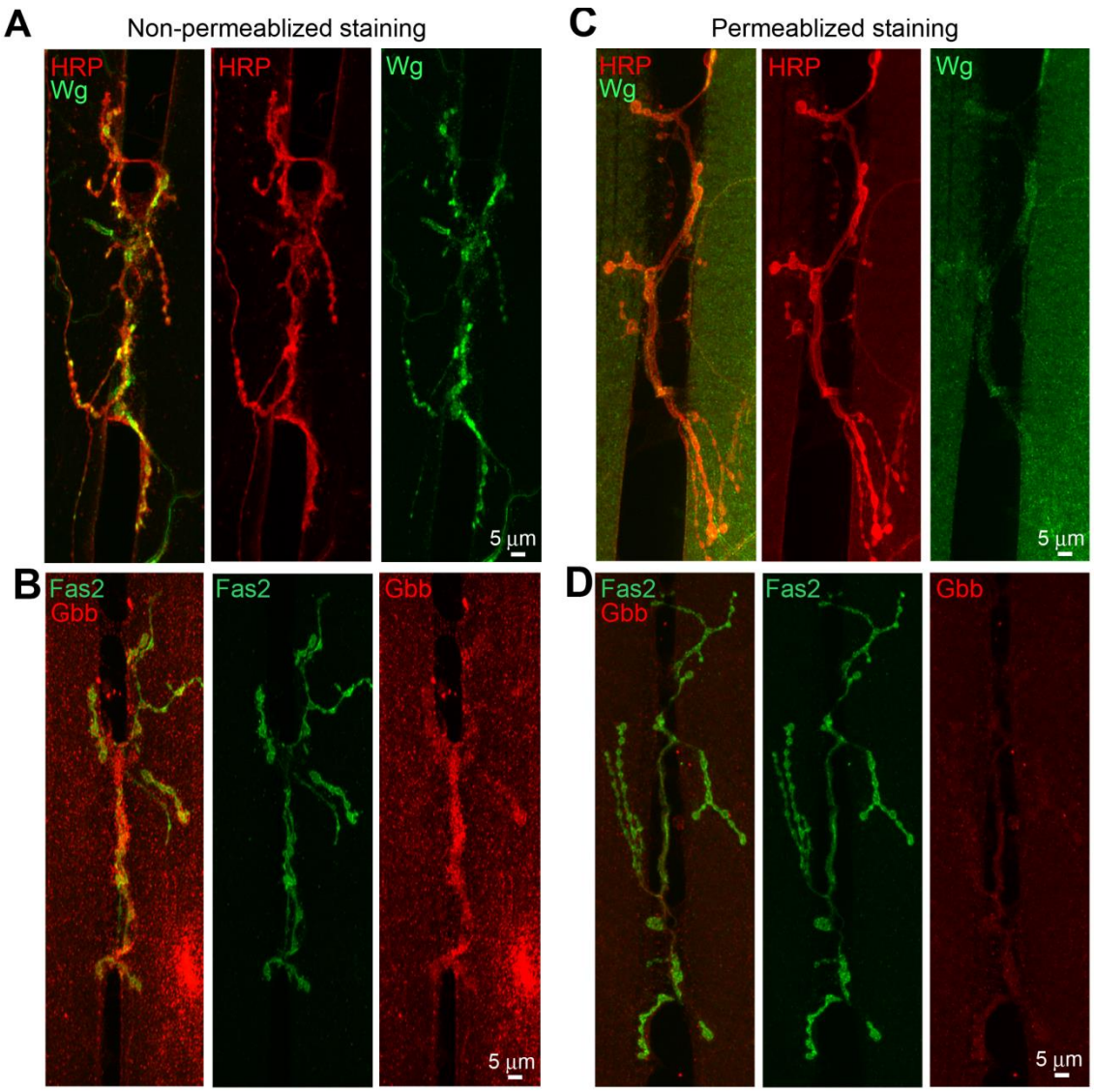

Figure 12. Permeablized versus non-permeabilized Wg and Gbb labeling. Representative NMJ images of muscle 6/7 in segment A3 from the wandering third instar. Merged and single channel images of (A) anti-horseradish peroxidase (HRP; red) and anti-Wingless (Wg; green), and (B) anti-Fasciclin II (FasII; green) and anti-glass bottom boat (Gbb; red), in non-permeablized labeling conditions in the absence of detergent. Note strong localization of both Wg and Gbb at the NMJ terminal. Merged and single channel images of (C) anti-HRP (red) and anti-Wg (green), and (D) anti-FasII (green) and anti-Gbb (red) in permeablized labeling conditions with 4% paraformaldehyde added to all antibody incubations. Note that most of the synaptic localization of Wg and Gbb is lost.

adjacent to, and overlapping with, the anti-HRP-labeled presynaptic membrane (Fig. 13A, middle and bottom). The elevated Wg levels in mutants were clearly observed at the level of individual synaptic boutons, as shown in the magnified insets in Figure 13A. To examine changes in Wg spatial distribution, cross-sectional planes were examined in single confocal line scans through the diameter of individual synaptic boutons (Fig. 13A, white lines). Representative distribution plots for membrane-marker HRP (red) and external Wg (green) are shown in Figure 13B. In all genotypes, extracellular Wg was closely associated with the HRP-labeled presynaptic membrane, but both *sulf1* and *hs6st* nulls displayed a consistent increase in Wg label intensity and broadening of the spatial domain occupied by the secreted Wg ligand (Fig. 13B, middle and bottom). To quantify changes in extracellular Wg abundance, the mean fluorescent signal intensity was normalized to the internal HRP co-label, and then normalized to analogous control intensity ratios. In $sulf1^{\Delta 1}$ nulls, there was very highly significant elevation of Wg compared to control (~90% increased; $p<0.001$; n=16; Fig. 13C). A similar increase was observed in the independent $sulf1^{\Delta P1}$ null ($p<0.001$; n=11). The *hs6st* null displayed a smaller significant increase in Wg abundance (~40% increased; $p<0.001$; n=15; Fig. 13C), which was again recapitulated in *hs6st* null over deficiency (Df(3R)ED6027) condition. Importantly, Wg abundance is differentially elevated in *sulf1* vs. *hs6st* mutants ($p<0.01$, Fig. 13C). To test whether the *sulf1/hs6st* mechanism might coordinately regulate multiple *trans*-synaptic signals, we next assayed the BMP Gbb, a muscle-derived retrograde signal. A barrier to previous Gbb analyses has been the absence

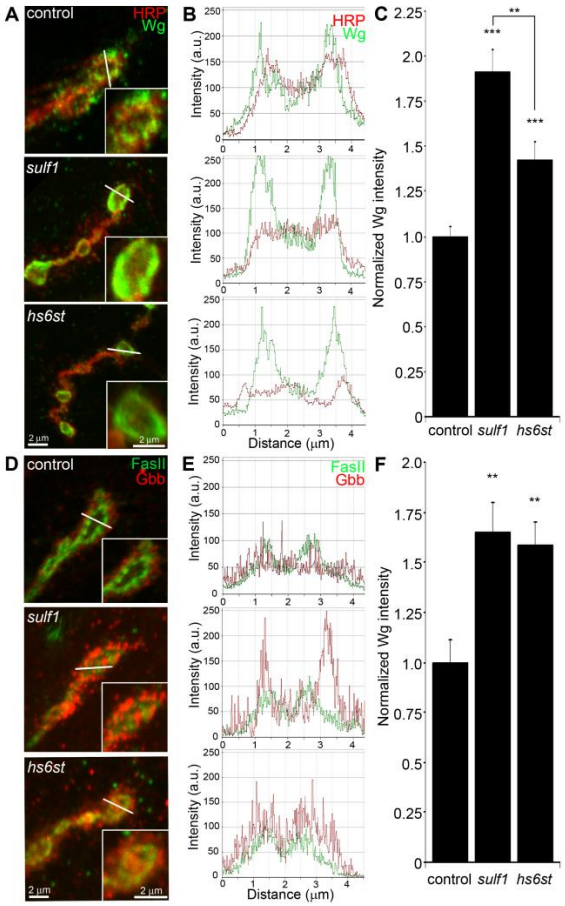

Figure 13. Synaptic WNT and BMP ligand abundance is modified by 6-O-S sulfation. Images show muscle 6 NMJ in segment A3 probed in non-detergent conditions, so that only extracellular protein distributions are detected. The white lines indicate cross-section planes for spatial measurements. Insets indicate single synaptic boutons at higher magnification. (A) Representative NMJ boutons from control (w^{1118}), *sulf1* and *hs6st* null genotypes, labeled for presynaptic anti-horseradish peroxidase (HRP, red) and anti-wingless (Wg, green). (B) Extracellular distribution of Wg across the diameter of a synaptic bouton. The Y-axis indicates intensity and the X-axis shows distance in microns. The HRP intensity profile is indicated in red; Wg intensity is shown in green. (C) Quantification of Wg mean intensity levels normalized to the HRP co-label, and to genetic control. Sample sizes are at least 15 animals per indicated genotypes. (D) Representative synaptic boutons labeled with presynaptic anti-Fasciclin II (FasII; green) and anti-Glass Bottom Boat (Gbb; red). (E) Gbb distribution across the diameter of a synaptic bouton. Y-axis indicates intensity and the X-axis shows distance in microns. FasII intensity profile is indicated in green; Gbb intensity is shown in red. (F) Quantification of Gbb mean intensity levels normalized to genetic control. Sample sizes are at least 11 independent NMJs of at least 7 animals per indicated genotypes. Statistically significant differences calculated using student's t-test and Mann-Whitney test for non-parametric data, ** $p<0.01$, *** $p<0.001$. Error bars indicate S.E.M.

of an anti-Gbb antibody. We therefore generated a specific anti-Gbb antibody for this study (see Methods). As above, labeling was done under non-permeabilized conditions to reveal only the extracellular Gbb, together with labeling for HRP or the cell adhesion molecule marker FasII to reveal the presynaptic membrane (Fig. 12). In the control (w^{1118}), extracellular Gbb concentrated in a ring of punctate domains around boutons (Fig. 13D, top). Gbb was similarly punctate in *sulf1* and *hs6st* nulls, but consistently more extensive and denser (Fig. 13D, middle and bottom; see magnified insets). To examine Gbb spatial distribution, cross-sectional planes of confocal line scans were made through individual synaptic boutons (Fig. 13D, white lines). Representative plots for FasII (green) and Gbb (red) show extracellular Gbb closely associated with the FasII-labeled presynaptic membrane in all genotypes (Fig. 13E). However, *sulf1* and *hs6st* nulls consistently displayed increased Gbb intensity and broadened expression compared to the control. Upon quantifying signal intensity of Gbb normalized to HRP co-label, $sulf1^{\Delta 1}$ exhibited a significantly higher Gbb abundance than control (65% increased; $p<0.01$; n=12; Fig. 13F). The independent $sulf1^{\Delta P1}$ null allele showed a similar increase ($p<0.001$; n=12). The *hs6st* null also showed Gbb elevation compared to control (59% increased; $p<0.01$; n=11; Fig. 13E), which was confirmed in *hs6st* null over deficiency (Df(3R)ED6027; $p<0.05$; n=23).

To test further whether extracellular Wg and Gbb abundance was sensitive to the sulfation state of GAGs, a biochemical approach was next used to determine effects on Wg and Gbb *trans*-synaptic signals (Fig. 14). Specifically, NMJs were acutely exposed to heparin, the most sulfated form of GAG, and then synaptic

Wg and Gbb abundance was measured by immunolabeling as above. We found that both *trans*-synaptic signals were rapidly altered by heparin incubation in a dose-dependent manner. Specifically, incubation with increasing concentrations of heparin caused a reciprocal decrease in Wg labeling intensity in the NMJ synaptic domain (Fig. 14A,C), with a significant decrease first detected with 0.315 mg/ml heparin incubation (~50% less than control, $p<0.01$, $n=4$). Interestingly, incubation with heparin caused the opposing loss of Gbb from the synaptic domain. In a dose-dependent manner, increasing heparin concentrations caused a parallel increase in Gbb abundance in the NMJ synaptic domain (Fig. 14B,C), with significant increases again first detected at 0.315 mg/ml heparin (~25% greater than control, $p<0.05$) and rising further at 0.625 mg/ml heparin (~40% greater than control, $p<0.001$). These results indicate that HSPG sulfation state does indeed affect *trans*-synaptic signal abundance, supporting the observed alterations in Wg and Gbb abundance in mutants of heparan sulfate modifying genes, *sulf1* and *hs6st.*

To examine effects on other *trans*-synaptic signaling pathways in the *sulf1* and *hs6st* mutant synapses, we also assayed for changes in Jeb and FGF signaling (Rohrbough K. et al., 2010). In both control and mutants, extracellular Jeb labeling was tightly associated with NMJ type Ib boutons and, like other *trans*- synaptic ligands, occupied an extracellular domain closely associated with the presynaptic membrane (Fig. 15). However, in stark contrast to Wg and Gbb ligands in the same extracellular synaptomatrix domain, no change was

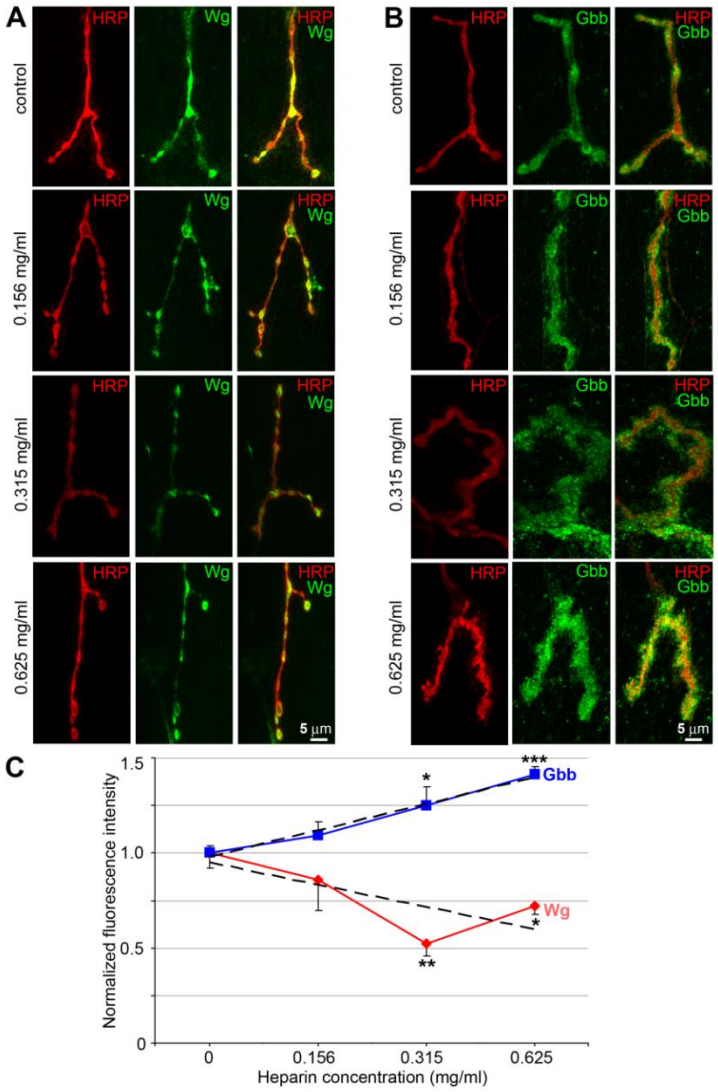

Figure 14. NMJ retention of Wg/Gbb altered by highly-sulfated heparin. Confocal imaging of Wg and Gbb *trans*-synaptic ligand abundance at the wandering third instar NMJ (muscle 4, segment A3) following acute incubation with highly-sulfated heparin. (A) Single channel and merged images of anti-horseradish peroxidase (HRP; red) and anti-Wingless (Wg; green) following control (no heparin), 0.156 mg/ml, 0.315 mg/ml and 0.625 mg/ml heparin treatments. (B) Single channel and merged images of anti-HRP (red) and anti-glass bottom boat (Gbb; green) following control, 0.156 mg/ml, 0.315 mg/ml and 0.625 mg/ml heparin treatments. (C) Quantification of fluorescence intensity of Wg and Gbb normalized to the internal HRP co-label for the control and indicated heparin concentrations. Individual data points are an average of ≥3 animals. Dotted line shows fitted linear trend lines. Statistically significant differences calculated using student's t-test and indicated as ***p<0.001, ** p<0.01, * p<0.05. Error bars indicate S.E.M.

observed in Jeb abundance or spatial distribution in *sulf1* null (p=0.99, n=10) or *hs6st* null (p=0.36, n=8) compared to control (w^{1118}) NMJ synapses (Fig. 15). FGF signaling is also well established to be affected by HSPGs (Shimokawa et al., 2011), and one pioneering study has investigated roles for FGF signaling at the *Drosophila* NMJ (Sen et al., 2011). The probe used in the previous study was an antibody against the FGF receptor Heartless (Htl) (Shishido et al., 1997). Using this antibody, we confirmed that the Htl receptor beautifully localizes to NMJ boutons to mediate FGF signaling (Fig. 16). However, Htl receptor synaptic abundance and distribution was very similar for the *sulf1* (p=0.89, n=9) and *hs6st* (p=0.69, n=7) mutants compared to control (w^{1118}) (Fig. 16B). Unfortunately, no antibody probes are available for *Drosophila* FGF ligands, so these signals have not yet been queried. Together, these results show that both WNT (Wg) and BMP (Gbb) ligand abundance is coordinately upregulated by the *sulf1* and *hs6st* mechanism at the NMJ synapse, but that a spatially overlapping signaling ligand (Jeb) and at least FGF receptor expression are unaffected. These results strongly predict that Wg and Gbb *trans*-synaptic signaling controlled by *sulf1* and *hs6st* activity regulates synaptic functional development.

Trans-synaptic WNT/BMP signaling is regulated by HSPG sulfation

Wg and Gbb serve as anterograde and retrograde *trans*-synaptic signals, respectively, activating cognate receptors to initiate downstream signaling cascades and nuclear import pathways in muscles and motor neurons, respectively (Keshishian & Kim, 2004; Marques, 2005; M Packard et al., 2003).

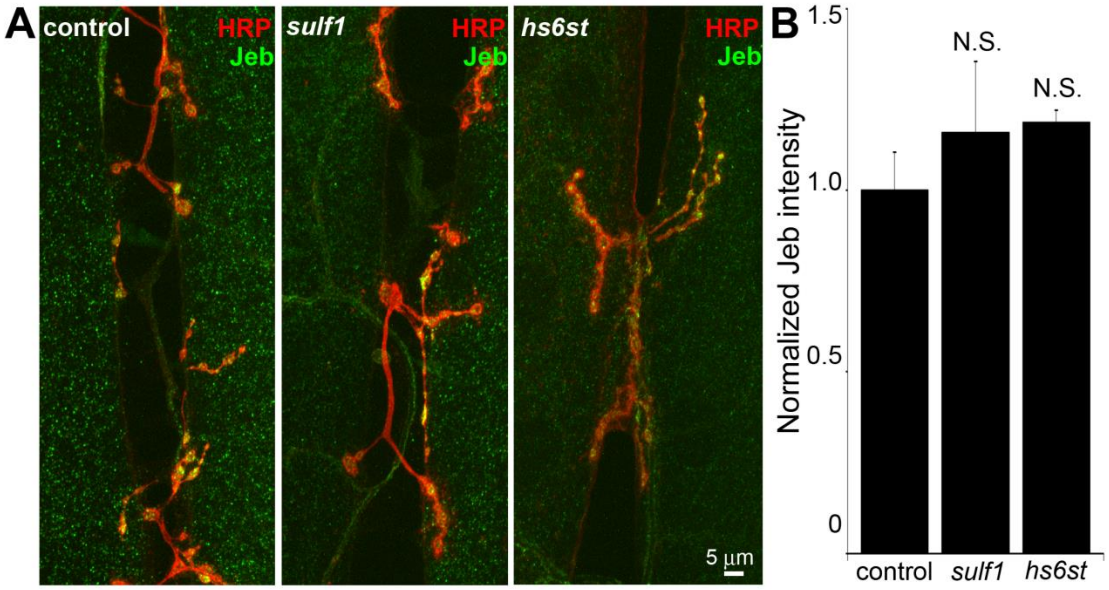

Figure 15. NMJ expression of Jeb ligand unchanged in *sulf1*/*hs6st* nulls. (A) Representative NMJ images at the wandering third instar NMJ on muscle 6 in segment A3 from control (w^{1118}), *sulf1* and *hs6st* nulls, labeled with neural marker anti-horseradish peroxidase (HRP; red) and anti-Jelly belly (Jeb; green). Merged images show Jeb tightly localized at synaptic boutons. (B) Quantification of anti-Jeb mean fluorescence intensity levels normalized to HRP co-label and the genetic control. Sample sizes are ≥8 animals per indicated genotypes. Statistically significant differences calculated using student's t-test. N.S. indicates no significant difference. Error bars indicate S.E.M.

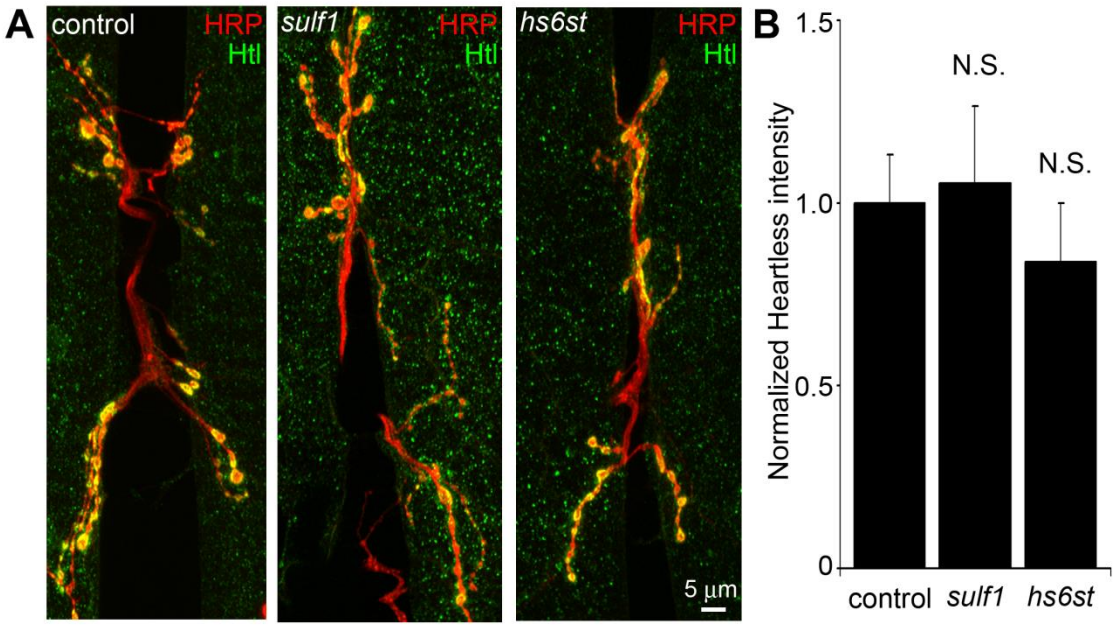

Figure 16. NMJ expression of FGF receptor unchanged in *sulf1/hs6st* nulls. (A) Representative NMJ images at the wandering third instar NMJ on muscle 6 in segment A3 from control (w^{1118}), *sulf1* and *hs6st* nulls, labeled with neural marker anti-horseradish peroxidase (HRP; red) and anti-Heartless (Htl; green). Merged images show the Htl FGF receptor tightly localized at synaptic boutons. (B) Quantification of Htl mean fluorescence intensity levels normalized to HRP co-label and the genetic control. Sample sizes are ≥7 animals per indicated genotypes. Statistically significant differences calculated using student's t-test. N.S. indicates no significant difference. Error bars indicate S.E.M.

The anterograde Wg signal drives dFrizzled-2 (dFz2) receptor internalization in the postsynaptic domain followed by cleavage of the receptor C-terminus, which then enters the muscle nuclei (Mathew et al., 2005). The muscle-derived retrograde Gbb signal activates presynaptic receptors to drive phosphorylation of the Mothers Against Decapentaplegic (Mad) transcription factor, and then P-Mad enters the motor neuron nuclei to regulate transcription (McCabe et al., 2003; Keshishian and Kim, 2004; Kim G., 2010). Given the differential change in both HSPG co-receptor and Wg/Gbb ligand abundance in *sulf1* vs. *hs6st* mutants, we hypothesized that these signaling pathways would be differentially affected during synaptogenesis. We therefore quantitatively assayed the paired muscle and motor neuron nuclear import pathways to determine whether and how *trans*-synaptic signaling may be modulated by *sulf1* and *hs6st* at the NMJ synapse.

Characterized antibodies specifically recognizing the N- and C-termini of the WgdFz2 receptor allow measurements of the receptor at the NMJ synapse (dFz2N; Fig. 17) and the cleaved fragment (dFz2C; Fig. 18) imported into muscle nuclei (Mathew et al., 2005; Mosca and Schwarz, 2010). We first assayed dFz2 receptor abundance at the NMJ with the N-terminal specific antibody. The dFz2 receptor is closely associated with the synaptic cell membrane marker FasII and occupies a domain that envelopes all type Ib boutons (Fig. 17). In *hs6st* nulls, the dFz2 receptor domain was spatially extended as compared to controls, however *sulf1* alleles showed no detectable change in the receptor. Likewise, fluorescence intensity measurements showed no significant difference between

control and *sulf1* nulls, but *hs6st* null synapses displayed a ~25% increase in dFz2 receptor abundance, a very significant elevation ($p<0.01$, n=12; Suppl. Fig. 17B) in synaptic dFz2 abundance. Thus, importantly (see Discussion), significantly more dFz2 receptors occur in the *hs6st* null compared to *sulf1* null synapse.

To assay downstream signal transduction, the cleaved Fz2C fragment imported into muscle nuclei was quantified using the established method of counting dFz2C-positive punctae in nuclei proximal to the NMJ (Fig. 18) (Mosca and Schwarz, 2010) [59]. In genetic control (w^{1118}), most muscle nuclei contained a small number (1-3) of detectable dFz2C punctae, but some nuclei contained more and others were devoid of detectable dFz2C (Fig. 18A, top). More than 100 muscle nuclei were quantified in >7 different animals to determine the control level of dFz2C nuclear import. In *sulf1* and *hs6st* mutants, there was a clear and consistent bidirectional difference in the number and size of dFz2C punctae in muscle nuclei (Fig. 18A, middle and bottom). Null *sulf1* nuclei showed a highly significant decrease in number of dFz2C punctae per nuclei (>50% decreased; $p<0.01$; n=163; Fig. 18B). In contrast, *hs6st* nulls had an opposing highly significant increase in dFz2C punctae per nuclei (>60% increased; $p<0.01$; n=163; Fig. 18B). The difference between *sulf1* and *hs6st* null mutants was very highly significant ($p<0.001$), with a differential change in signaling paralleling the bidirectional change in synaptic functional differentiation (Fig. 7). A characterized antibody specifically recognizing phosphorylated Mad (P-Mad) allowed independent measurements of Gbb signaling in the presynaptic terminal and

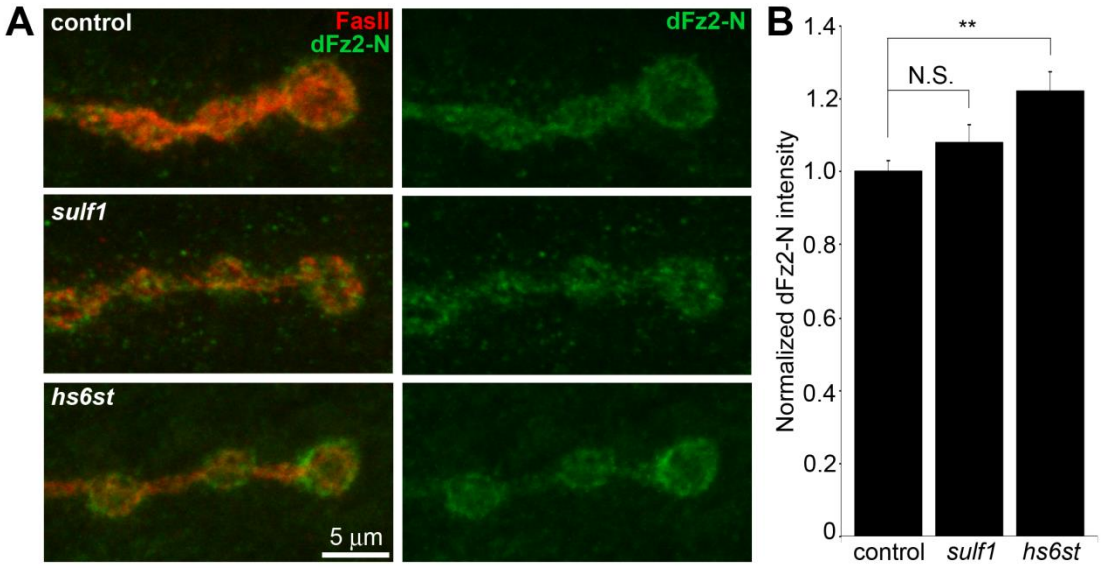

Figure 17. Synaptic Frizzled-2 receptor levels in *sulf1* and *hs6st* nulls. Frizzled-2 receptor N-terminus (dFz2-N) specific antibody shows localized expression surrounding synaptic boutons at the NMJ. (A) Representative wandering third instar NMJ images from muscle 6 in segment A3 for control (w^{1118}), *sulf1* and *hs6st* null mutants, double-labeled with presynaptic neural marker anti-Fasciclin II (FasII, red) and dFz2-N (green). Right: dFz2-N shown alone for clarity. (B) Quantification of dFz2-N mean fluorescence intensity for the indicated genotypes, normalized to the genetic control. Sample sizes are ≥12 animals per genotype. Statistically significant differences calculated using student's t-test, ** $p<0.01$. Error bars indicate S.E.M.

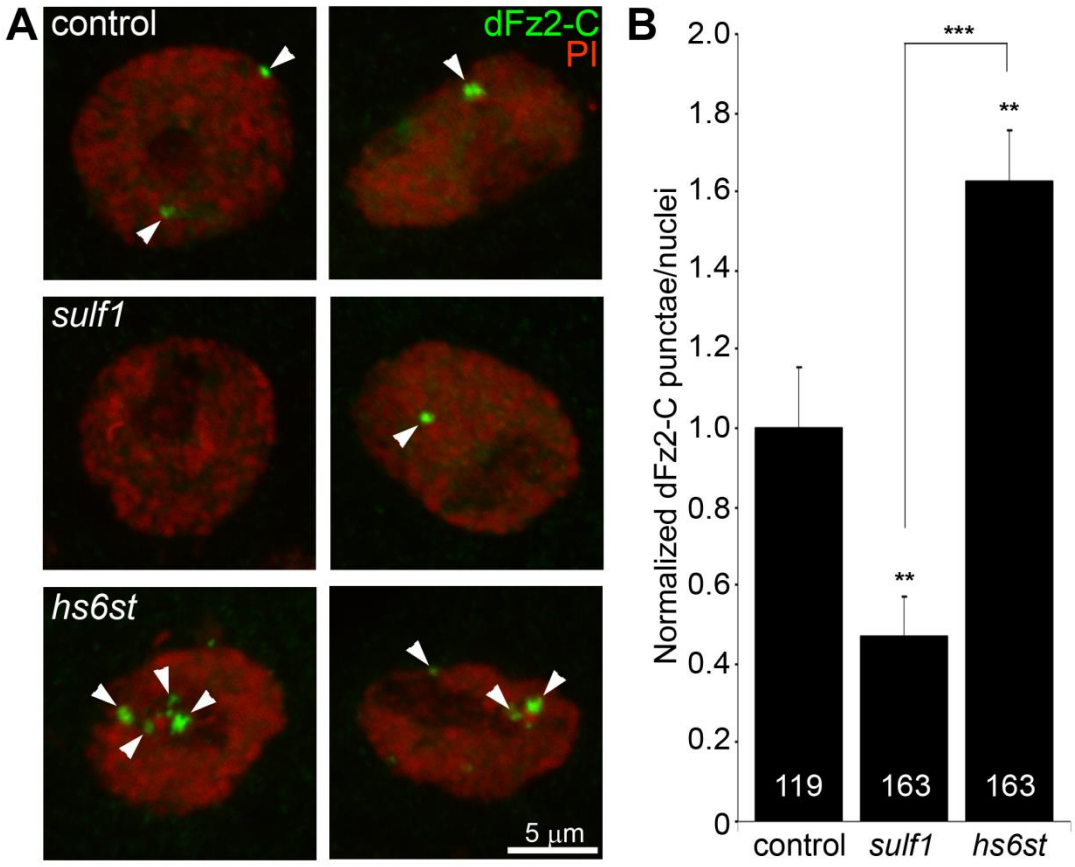

Figure 18. Loss of *sulf1* and *hs6st* causes opposite effects on WNT signaling. (A) Representative images of muscle nuclei from control (w^{1118}), *sulf1* and *hs6st* nulls, labeled with nuclear marker propidium iodide (PI, red) and for the C-terminus of the Wingless receptor Frizzled 2 (dFz2-C, green). Arrows indicate punctate dFz2-C nuclear labeling. Nuclei shown from muscle 6 in segment A3. (B) Quantification of the number of dFz2-C punctae per nuclei, normalized to genetic control. The total number of nuclei analyzed is indicated in each column; 119 for control (w^{1118}) and 163 nuclei each for *sulf1* and *hs6st* null mutants. Sample sizes are ≥9 animals per indicated genotypes. Statistically significant differences calculated using student's t-test; ** $p<0.01$ *** $p<0.001$. Error bars indicate S.E.M.

P-Mad import into the motor neuron nuclei as a transcriptional regulator (Fig. 19) (Persson et al., 1998; McCabe et al., 2003). To assay this transduction pathway, P-Mad fluorescent intensity normalized to FasII was first assayed in presynaptic boutons (Higashi-Kovtun et al., 2010; Nahm et al., 2010). In the genetic control (w^{1118}), P-Mad labeling was bounded by the synaptic cell adhesion molecule marker FasII, with P-Mad localized in numerous punctate domains (Fig. 19A, arrows). In *sulf1* and *hs6st* nulls, both the intensity and size of P-Mad positive punctae were obviously and consistently greater than in controls (Fig. 19A, middle and bottom). In fluorescence intensity quantification, *sulf1* null synapses displayed a significant increase in synaptic P-Mad (45% increased; $p<0.05$; n=10; Fig. 19C). An increase in P-Mad was also observed in the *hs6st* null boutons (42% greater than control; $p<0.01$; n=15; Fig. 19C). The motor neuron nuclei at the ventral nerve cord (VNC) midline accumulate P-Mad transcription factor downstream of Gbb signaling at the NMJ (McCabe et al., 2003; Higashi-Kovtun et al., 2010; Nahm et al., 2010). In genetic control (w^{1118}), P-Mad nuclear labeling was consistently detected in these motor neuron nuclei (Fig. 19B, arrows). A similar P-Mad distribution was observed in motor neuron nuclei of *sulf1* and *hs6st* nulls, but the intensity of P-mad expression was clearly and consistently elevated in both mutants compared to control (Fig. 19B, middle and bottom). In fluorescence intensity quantification, *sulf1* null neuronal nuclei displayed a very significant increase in P-Mad accumulation (15% increased; $p<0.01$; n=14; Fig. 19D), paralleling increased P-Mad signaling at the NMJ (Fig. 19C). Likewise, *hs6st* null motoneuron nuclei

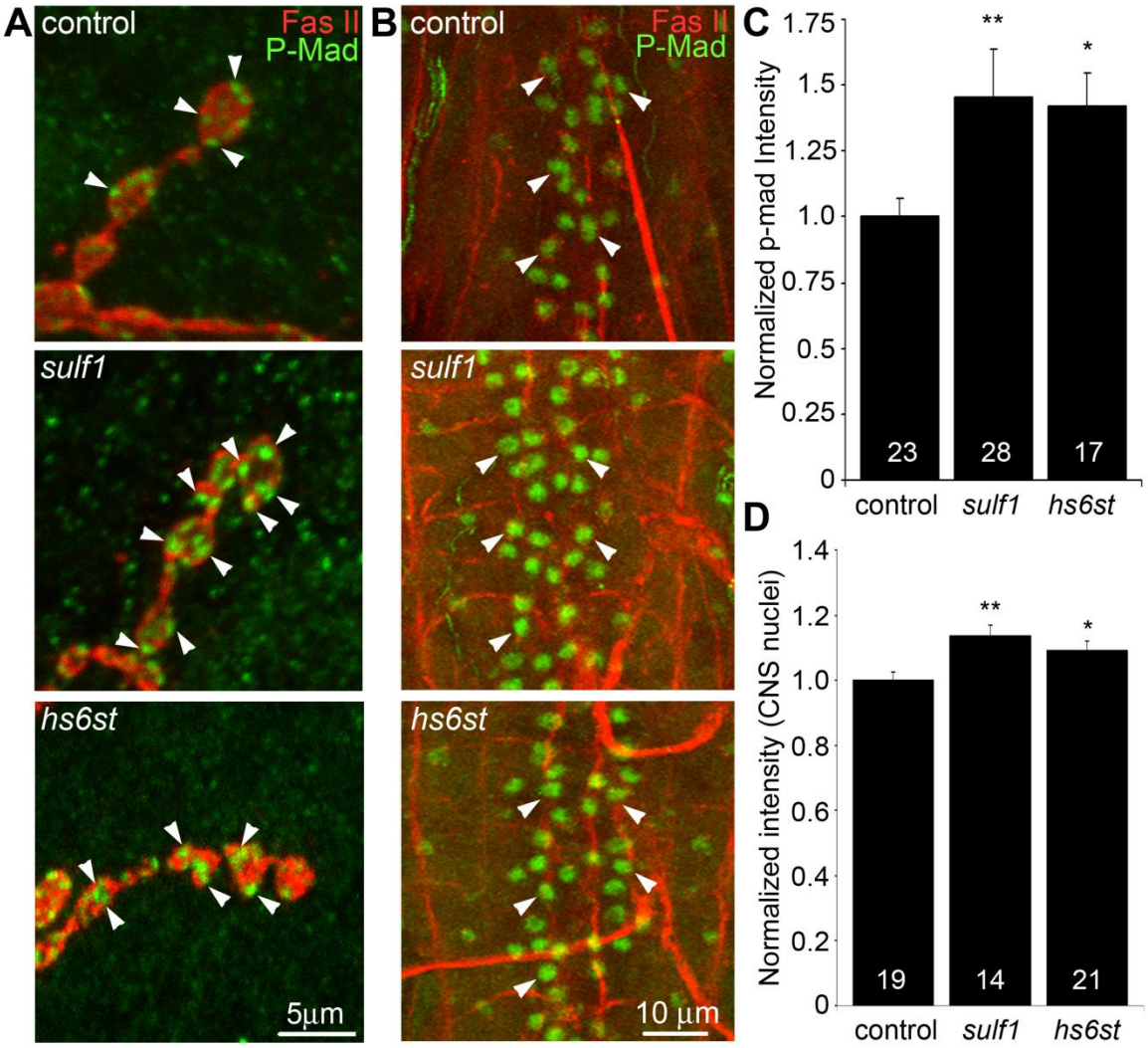

Figure 19. Loss of *sulf1* and *hs6st* causes differential effects on BMP signaling. (A) Representative NMJ synaptic boutons on muscle 6 in segment A3 from control (w^{1118}), *sulf1* and *hs6st* nulls, labeled with neural marker anti-Fasciclin II (FasII, red) and for phosphorylated Mothers against decapentaplegic (P-Mad; green) activated downstream of Gbb signaling. Arrows indicate representative P-Mad punctae in the indicated genotypes. (B) Representative ventral nerve cord (VNC) midlines from the same 3 genotypes, labeled with anti-FasII (red) and P-Mad (green). Labeled motor neuron nuclei are indicated by arrows. Quantification of the mean fluorescent intensity level of P-Mad labeling normalized to FasII co-label at the NMJ synapse (C) and in motor neuron nuclei (D), normalized to genetic control. Sample sizes are ≥14 animals per indicated genotypes. Statistically significant differences calculated using the Mann-Whitney test for non-parametric data, * $p<0.05$, ** $p<0.01$. Error bars indicate S.E.M.

exhibited a smaller but still significant elevation in P-Mad accumulation (9% elevated over control; $p<0.05$; n=21; Fig. 19D), again paralleling the observed P-Mad signaling change at the NMJ (Fig. 19C). We conclude that both anterograde WNT (Wg) and retrograde BMP (Gbb) *trans*-synaptic signaling in muscle and motor neuron nuclei, respectively, is differentially regulated by the *sulf1* and *hs6st* HSPG sulfation mechanism.

Trans-synaptic WNT/BMP signals genetically interact with *sulf1* and *hs6st* nulls

In the *sulf1* and *hs6st* nulls we identified a bi-directional change in synaptic functional differentiation, measured as evoked junction current amplitudes increased in *sulf1* and decreased in *hs6st* null synapses (Fig. 7). We therefore hypothesized that these functional changes are driven by the differential Wg and Gbb *trans*-synaptic signaling defects characterized above in *sulf1* and *hs6st* mutants (Figs. 12, 14, 19). We reasoned that correcting Wg and Gbb levels in *sulf1* and *hs6st* nulls should restore neurotransmission to control levels. To test this hypothesis, we crossed heterozygous *wg*/+ and *gbb*/+ mutants into both *sulf1* and *hs6st* homozygous null backgrounds, both singly and in combination, and compared them to both positive and negative controls. The resulting 9 genotypes were all assayed with TEVC electrophysiology to compare EJC transmission strength. A summary of these data is given in Figure 20. Representative transmission records are shown as an average of 10 consecutive EJC responses (1.0 mM extracellular Ca^{2+}) for the genotypes in Figure 20A, with quantification of mean peak amplitudes in all genotypes shown in Figure 20B.

First testing *sulf1* nulls, we examined the consequences of heterozygous genetic reduction of Wg and Gbb, alone and in combination. Compared to the elevated EJC amplitude of the *sulf1* null condition (381.28 ±1 62.24 nA, $p<0.01$, n=9; Fig. 20B), genetic reduction of Wg (*wg/+; sulf1/sulf1*) caused very significantly reduced transmission, similar to genetic reduction of Gbb (*gbb/+; sulf1/sulf1*) with a comparable effect, restoring EJC amplitude to control levels (267.16 ± 16.33, $p<0.01$, n=9; Fig. 20B). Combinatorial genetic reduction of both Wg and Gbb in the *sulf1* null (*wg/gbb;sulf1/sulf1*) similarly returned EJC amplitudes to control levels (278.78 ± 23.17, n=7; Fig. 20B). Secondly testing *hs6st* nulls, genetic reduction of either Wg or Gbb alone was not sufficient to significantly change the depressed synaptic function (Fig. 20B). In this case, combinatorial genetic reduction of both Wg and Gbb in the *hs6st* null (*wg/gbb;hs6st/hs6st*) was required to raise the depressed EJC amplitude, a very significant increase back to control levels (272.98 ± 18.58, $p<0.01$, n=8; Fig. 20B). Therefore, we conclude that combinatorial Wg and Gbb *trans*-synaptic signaling defects are causative for the observed bi-directional effects on synaptic functional differentiation in the *sulf1* and *hs6st* null mutant conditions.

The *sulf1* and *hs6st* mechanism regulates pre- and postsynaptic differentiation

The consequence of WNT (Wg) and BMP (Gbb) *trans*-synaptic signaling is nuclear import and transcriptional regulation in both synaptic partner cells (Packard et al., 2003; Salinas, 2003). We therefore hypothesized that *sulf1* and *hs6st* null mutants would show bidirectional changes in pre- and postsynaptic

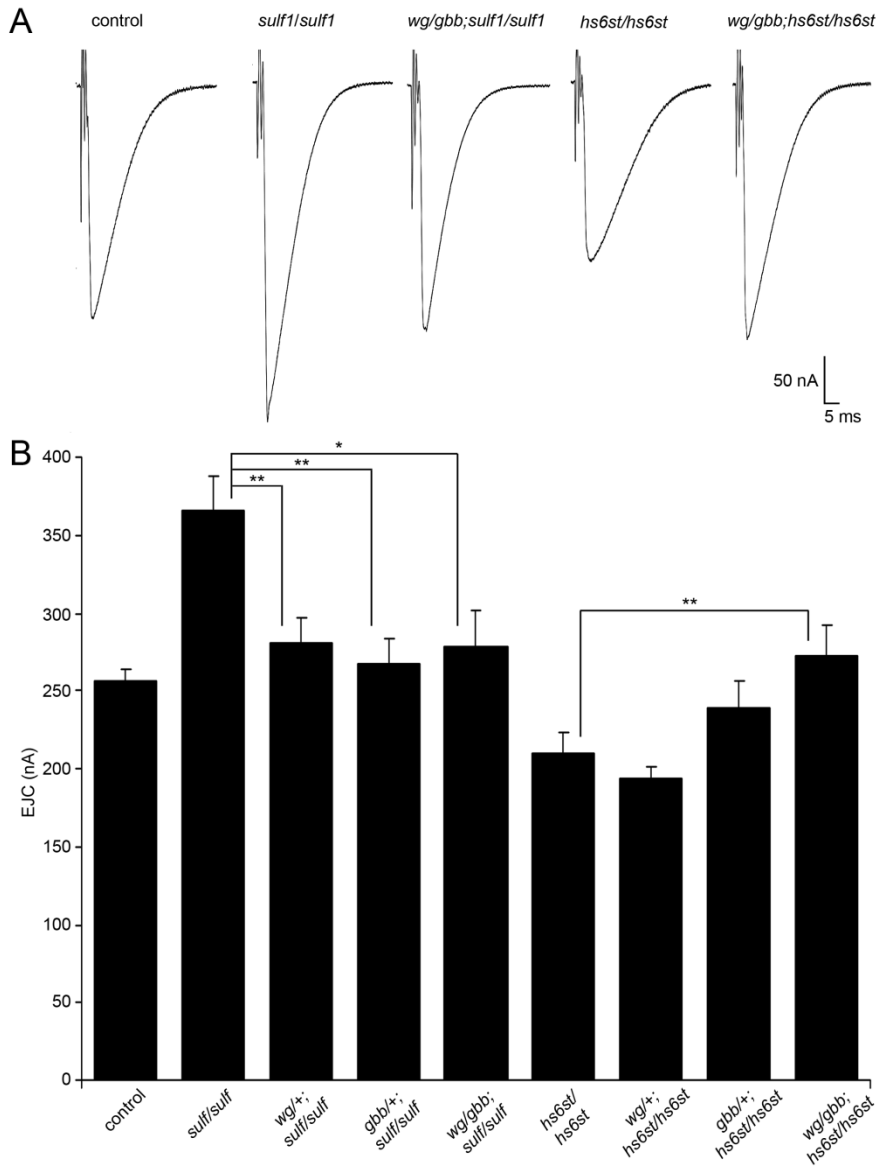

Figure 20. WNT and BMP signals genetically interact with *sulf1* **and** *hs6st* **nulls.** Genetic reduction of Wg and Gbb levels in *sulf1* and *hs6st* homozygous conditions restore EJC amplitudes to control levels. (A) Representative excitatory junctional current (EJC) traces from control (w^{1118}), homozygous $sulf1^{\Delta 1}$ null, heterozygous *wg*/+ and *gbb*/+ in *sulf1* null background ($wg^{l\text{-}12}/gbb^{2}$; $sulf1^{\Delta 1}/sulf1^{\Delta 1}$), homozygous $hs6st^{d770}$ null and heterozygous *wg*/+ and *gbb*/+ in *hs6st* null background ($wg^{l\text{-}12}/gbb^{2}$; $hs6st^{d770}/hs6st^{d770}$). The nerve was stimulated (arrows) in 1.0 mM external Ca^{2+}, and TEVC records (−60 mV holding potential) made from muscle 6 in segment A3. Each trace was averaged from 10 consecutive evoked EJC recordings. (B) Quantified mean EJC amplitudes (nA) for the nine genotypes shown. Sample sizes are ≥7 animals per indicated genotype. Statistically significant differences calculated using student's t-test, * $p<0.05$, ** $p<0.01$. Error bars indicate S.E.M.

molecular components that would explain the bidirectional change in synaptic functional differentiation (Figs. 8 and 21). To test this hypothesis, we examined a key component of the presynaptic active zone (Bruchpilot; Brp) (Wagh et al., 2006), and an essential subunit of the postsynaptic glutamate receptor (Bad Reception (Brec); GluRIID) (Featherstone et al., 2005). In parallel, we also performed a miniature EJC (mEJC) analysis to compare functional presynaptic vesicle release probability and postsynaptic response amplitude. A summary of these data is shown in Figure 21.

First, NMJ synapses were double-labeled for GluRIID recognized with anti-Brec (green) and Brp recognized with anti-nc82 (red) to compare genetic control (w^{1118}) with *sulf1* and *hs6st* nulls (Fig. 21A). We found that GluRIID was very significantly elevated at *sulf1* synapses compared to control (~30% increased; $p<0.01$, n=20; Fig. 21B). In the opposing direction, *hs6st* null synapses showed a significant decrease in GluRIID abundance (~15% reduced; $p<0.05$, n=21; Fig. 21B). The GluRIID field area per bouton and number of GluRIID punctae normalized to field area per synaptic bouton were also bidirectionally altered in the *sulf1* and *hs6st* nulls (Fig. 21C,D). GluRIID receptor field area was increased in *sulf1* (~30% greater; $p<0.01$, n=47) but decreased in *hs6st* (~25% reduced; $p<0.01$, n=51). Conversely, measurements of GluRIID puncta normalized to field area per synaptic bouton were decreased in *sulf1* (~15% lower; $p<0.05$, n=47), but increased in *hs6st* nulls (~40% greater; $p<0.01$, n=51, Fig. 21D). The bi-directional differences between *sulf1* and *hs6st* were very highly significant ($p<0.001$). The active zone protein Brp also showed opposite

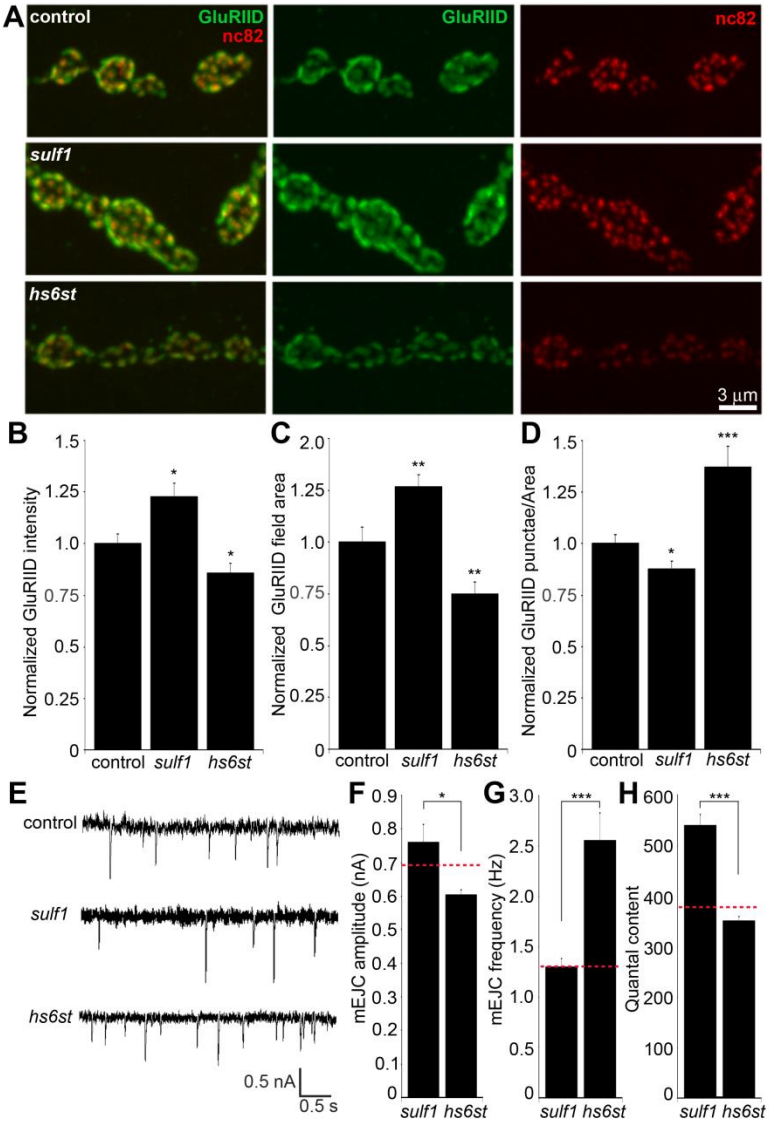

Figure 21. Bi-directional effects of *sulf1* and *hs6st* nulls on synaptic assembly. (A) Representative NMJ boutons from control (w^{1118}), *sulf1* and *hs6st* null genotypes, labeled for postsynaptic Bad Reception (Brec) glutamate receptor IID subunit (GluRIID, green) and presynaptic active zone Bruchpilot (anti-nc82, red). Quantification of GluRIID mean fluorescent intensity (≥18 animals per indicated genotype) (B), GluRIID field area (≥40 boutons from ≥9 animals per indicated genotype) (C), and GluRIID punctae number per synaptic bouton (≥40 boutons from ≥9 animals per indicated genotype) (D), all normalized to genetic control. (E) Representative mEJC traces from control (w^{1118}), $sulf1^{\Delta 1}$ and $hs6st^{d770}$ null alleles. Quantified mean mEJC amplitude (nA) (F), mean mEJC frequency (Hz) (G) and mean quantal content (H), with genetic control levels indicated as a dotted red line in each case. Sample sizes ≥15 recordings per indicated genotype. Statistically significant differences calculated using student's t-test or Mann-Whitney test for non-parametric data and indicated as, * p<0.05, ** p<0.01, *** p<0.001. Error bars indicate S.E.M.

effects (Fig. 21A). Although the difference between *sulf1* null and control was not quite significant ($p>0.05$, n=20), *hs6st* null synapses showed a very significant decrease in Brp compared to control (~20% reduced; $p<0.01$, n=21; Fig. 21A).

Based on these results, we next tested pre- (Brp) and postsynaptic (Brec/GluRIID) changes in *sulf1* and *hs6st* mutants with genetic reduction of Wg and Gbb (*wg/ gbb;sulf1/sulf1* and *wg/gbb;hs6st/hs6st*), as in Figure 21. Distribution changes of both pre- and postsynaptic components were assayed as measurements of glutamate receptor field and active zone areas (Fig. 22). To measure glutamate receptor distribution comparing *wg/gbb;sulf1/sulf1* to matched control, we counted the number of GluRIID punctae per bouton ($p=0.73$, n=48; Fig. 22B) and GluRIID area ($p=0.92$, n=48; Fig. 22C), and found both corrected back to control levels. Likewise, for *wg/gbb;hs6st/hs6st* compared to control, GluRIID puncta number ($p=0.88$, n=48) and area ($p=0.41$, n=58) were both corrected to control levels. To measure Brp-positive presynaptic active zones comparing *wg/gbb;sulf1/sulf1* to matched control, we counted the number of Brp punctae per bouton ($p=0.43$, n=48; Suppl. Fig. 22D) and Brp area ($p=0.39$, n=48; Suppl. Fig. 22E), and found both corrected back to control levels. Likewise, for *wg/gbb;hs6st/hs6st* compared to control, Brp number ($p=0.54$, n=58) and area($p=0.19$, n=58) were also corrected back to control levels. These results provide strong genetic evidence that Wg and Gbb *trans*-synaptic signaling changes are causative for the pre- and postsynaptic molecular differentiation defects in the *sulf1* and *hs6st* null mutants. These bidirectional pre- and postsynaptic molecular changes parallel functional transmission changes in *sulf1*

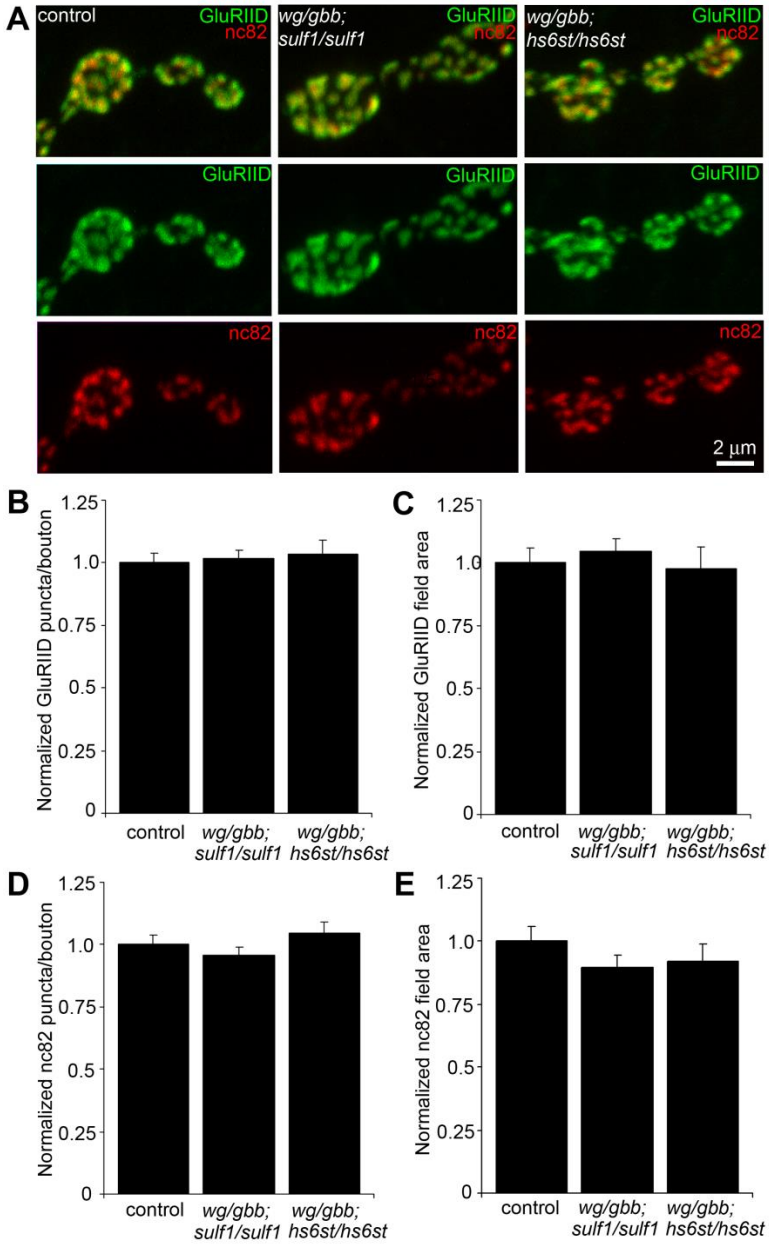

Figure 22. Wg and Gbb signals genetically interact with *sulf1* and *hs6st* nulls. Genetic reduction of Wg and Gbb levels in *sulf1* and *hs6st* homozygous conditions restores molecular synaptic assembly to control levels. (A) Representative NMJ boutons from control (w^{1118}), heterozygous *wg*/+ and *gbb*/+ in *sulf1* null background ($wg^{l\text{-}12}/gbb^{2}$; $sulf1^{\Delta 1}/sulf1^{\Delta 1}$) and *hs6st* null background ($wg^{l\text{-}12}/gbb^{2}$; $hs6st^{d770}/hs6st^{d770}$) labeled for postsynaptic Bad Reception (Brec) glutamate receptor IID subunit (GluRIID, green) and presynaptic active zone Bruchpilot (anti-nc82, red). Quantification of GluRIID punctae/bouton (B), total GluRIID area (C), Brp punctae/bouton (D) and total Brp area (E), all normalized to the genetic control. All multiply mutant conditions are restored to control levels for all parameters, with no significant differences remaining.

and *hs6st* mutants (Fig. 21). To assay function at the single synapse level, we finally assayed spontaneous synaptic vesicle fusion events. Representative mEJC traces for control compared to *sulf1* and *hs6st* nulls are shown in Figure 21E. Consistent with observed bidirectional changes in evoked transmission, mEJC amplitudes in *hs6st* were ~25% lower than in *sulf1* nulls (*hs6st,* 0.60 ± 0.02 nA vs. *sulf1*, 0.76 ± 0.05 nA; $p<0.5$, n=34; Fig. 21F). Moreover, *hs6st* nulls had a ~100% elevated mEJC frequency compared to *sulf1* nulls (*hs6st*, 2.56 ± 0.27 vs. *sulf1,* 1.30 ± 0.09; $p<0.001$, n=34; Fig. 21G). Based on these mEJC measurements, there was a highly significant bidirectional change in quantal content between the two mutant conditions, with *sulf1* quantal content ~50% greater than *hs6st* (*sulf1,* 539.98 ± 22.02 vs. *hs6st*, 350.69 ± 8.92; $p<0.001$, n=34; Fig. 21H). Taken together, these results show a bi-directional change in presynaptic glutamate release machinery and vesicle fusion probability, as well as postsynaptic glutamate receptor levels and functional responsiveness. We conclude that these changes underlie the bi-directional switch in neurotransmission strength characterizing *sulf1* and *hs6st* mutants.

Discussion

It is well known that synaptic interfaces harbor heavily-glycosylated membrane proteins, glycolipids and ECM molecules, but understanding of glycan-mediated mechanisms within this synaptomatrix is limited (Dani and Broadie, 2012). Our genomic screen aimed to systematically interrogate glycan roles in both structural and functional development in the genetically-tractable *Drosophila* NMJ synapse. 130 candidate genes were screened, classified into 8 functional

families: N-glycan biosynthesis, O-glycan biosynthesis, GAG biosynthesis, glycoprotein/proteoglycan core proteins, glycan modifying/degrading enzymes, glycosyltransferases, sugar transporters and glycan-binding lectins. From this screen, 103 RNAi knockdown conditions were larval viable, whereas 27 others produced early developmental lethality. 35 genes had statistically significant effects on different measures of morphological development: 27 RNAi-mediated knockdowns increased synaptic bouton number, 9 affected synapse area (2 increased, 7 decreased) and 2 genes increased synaptic branch number. These data suggest that overall glycan mechanisms predominantly serve to limit synaptic morphogenesis. 13 genes had significant effects on the functional differentiation of the synapse, with 12 increasing transmission strength and only 1 decreasing function upon RNAi knockdown. Thus, glycan-mediated mechanisms also predominantly limit synaptic functional development. A very small fraction of tested genes (CG1597; *pgant35A*, CG7480; *veg*, CG6657; *hs6st*, CG4451; *sulf1,* CG6725 and CG11874) had effects on both morphology and function. A large percentage of genes (~30%) showed morphological defects with no corresponding effect on function, while only 7% of genes showed functional alterations without morphological defects, and <5% of all genes affect both. These results suggest that glycans have clearly separable roles in modulating morphological and functional development of the NMJ synapse.

A growing list of neurological disorders linked to the synapse are attributed to dysfunctional glycan mechanisms, including muscular dystrophies, cognitive impairment and autism spectrum disorders (Inlow and Restifo, 2004; Muntoni et

al., 2008; Schachter, 2009). *Drosophila* homologs of glycosylation genes implicated in neural disease states include *ALG3* (CG4084), *ALG6* (CG5091), *DPM1* (CG10166), *FUCT1* (CG9620), *GCS1* (CG1597), *MGAT2* (CG7921), *MPDU1* (CG3792), *PMI* (CG33718) and *PPM2* (CG12151) (Inlow and Restifo, 2004). Two of these genes, *Gfr* (CG9620) and CG1597, showed synaptic morphology phenotypes in our RNAi screen. Given that connectivity defects are clearly implicated in cognitive impairment and autism spectrum disorders (Belmonte et al., 2004; Gatto and Broadie, 2011), it would be of interest to explore the glycan mechanism affecting synapse morphology in *Drosophila* models of these disease states. Glycans are well known to modulate extracellular signaling, including ligands of integrin receptors, to regulate intercellular communication (Zhang et al., 2008, 2010). In our genetic screen, several O-glycosyltransferases mediating this mechanism were identified to show morphological (*GalNAc-T2*, CG6394; *pgant35A,* CG7480, *O-fut2,* CG14789; *rumi,* CG31152) and functional (*pgant5,* CG31651; *pgant35A,* CG7480) synaptic defects upon RNAi knockdown. These findings suggest that known integrin-mediated signaling pathways controlling NMJ synaptic structural and functional development (Beumer et al., 1999, 2002; Rohrbough et al., 2000; Rushton et al., 2009) are modulated by glycan mechanisms. Our screen showed CG6657 RNAi knockdown affects functional differentiation, consistent with reports that this gene regulates peripheral nervous system development (Prokopenko et al., 2000). The corroboration of our screen results with published reports underscores the utility of RNAi-mediated screening to identify glycan mechanisms, and supports use of

our screen results for bioinformatic/meta-analysis to link observed phenotypes to neurophysiological/pathological disease states and to direct future glycan mechanism studies at the synapse.

From our screen, the two functionally-paired genes *sulf1* and *hs6st* were selected for further characterization. As in the RNAi screen, null alleles of these two genes had opposite effects on synaptic functional differentiation but similar effects on synapse morphogenesis, validating the corresponding screen results. The two gene products have functionally-paired roles; Hs6st is a heparan sulfate (HS) 6-O-sulfotransferase (Kamimura et al., 2001), and Sulf1 is a HS 6-O-endosulfatase (Dhoot et al., 2001). These activities control sulfation of the same C_6 on the repeated glucosamine moiety in HS GAG chains found on heparan sulfate proteoglycans (HSPGs). At the *Drosophila* NMJ, two HSPGs are known to regulate synapse assembly; the GPI-anchored glypican Dally-like protein (Dlp), and the transmembrane Syndecan (Sdc) (Johnson et al., 2006). In contrast, the secreted HSPG Perlecan (Trol) is not detectably enriched at the NMJ (Morin et al., 2001), and indeed appears to be selectively excluded from the perisynaptic domain. In other developmental contexts, the membrane HSPGs Dlp and Sdc are known to act as co-receptors for WNT and BMP ligands, regulating ligand abundance, presentation to cognate receptors and therefore signaling (Yan et al., 2009; Dejima et al., 2011). Importantly, the regulation of HSPG co-receptor abundance has been shown to be dependent on sulfation state mediated by extracellular sulfatases (Lai et al., 2008). Consistently, we observed upregulation of Dlp and Sdc in *sulf1* null synapses, whereas Dlp was

reduced in *hs6st* null synapses. In the developing *Drosophila* wing disc, HSPG co-receptors increase levels of the Wg ligand due to extracellular stabilization (Han et al., 2005), and the primary function of Dlp in this developmental context is to retain Wg at the cell surface (Yan and Lin, 2009). Likewise, in developing *Drosophila* embryos, a significant fraction of Wg ligand is retained on the cell surfaces in a HSPG-dependent manner (Pfeiffer et al., 2002), with the HSPG acting as an extracellular co-receptor. Syndecan also modulates ligand-dependent activation of cell-surface receptors by acting as a co-receptor (Carey, 1997; Dejima et al., 2011). At the NMJ, regulation of both these HSPG co-receptors occurs in the closely juxtaposed region between presynaptic bouton and muscle subsynaptic reticulum, in the exact same extracellular space traversed by the secreted *trans*-synaptic Wg and Gbb signals (Johnson et al., 2006). We therefore proposed that altered Dlp and Sdc HSPG co-receptors in *sulf1* and *hs6st* mutants differentially trap/stabilize Wg and Gbb *trans*-synaptic signals at the interface between motor neuron and muscle, to modulate the extent and efficacy of intercellular signaling driving synaptic development.

HS sulfation modification is linked to modulating the intercellular signaling driving neuronal differentiation (Gorsi and Stringer, 2007). In particular, WNT and BMP ligands are both regulated via HS sulfation of their extracellular co-receptors, and both signals have multiple functions directing neuronal differentiation, including synaptogenesis (Packard et al., 2003; Salinas, 2003; Marques, 2005). In the *Drosophila* wing disc, extracellular WNT (Wg) ligand abundance and distribution was recently shown to be strongly elevated in *sulf1*

null mutants (Kleinschmit et al., 2010). Moreover, *sulf1* has also recently been shown to modulate BMP signaling in other cellular contexts (Otsuki et al., 2010). Consistently, we have shown here increased WNT Wg and the BMP Gbb abundance and distribution in *sulf1* null NMJ synapses. The *hs6st* null also exhibits elevated Wg and Gbb at the synaptic interface, albeit the increase is lower and results in differential signaling consequences. In support of this contrasting effect, extracellular signaling ligands are known to bind HSPG HS chains differentially dependent on specific sulfation patterns (Baeg and Perrimon, 2000; Baeg et al., 2001; Mohammadi et al., 2005). It is important to note that the *sulf1* and *hs6st* modulation of *trans*-synaptic signals is not universal, as Jelly Belly (Jeb) ligand abundance and distribution was not altered in the *sulf1* and *hs6st* null conditions (Rohrbough K. et al., 2010). This indicates that discrete classes of secreted *trans*-synaptic molecules are modulated by distinct glycan mechanisms to control NMJ structure and function.

At the *Drosophila* NMJ, Wg is very well characterized as an anterograde *trans*-synaptic signal (Packard et al., 2002; Ataman et al., 2006a; Korkut and Budnik, 2009) and Gbb is very well characterized as a retrograde *trans*-synaptic signal (Marques et al., 2002; McCabe et al., 2003; Keshishian and Kim, 2004; Marques, 2005). In Wg signaling, the dFz2 receptor is internalized upon Wg binding and then cleaved so that the dFz2-C fragment is imported into muscle nuclei (Mathew et al., 2005; Ataman et al., 2006a; Mosca and Schwarz, 2010). In *hs6st* nulls, increased Wg ligand abundance at the synaptic terminal corresponds to an increase in dFz2C punctae in muscle nuclei as expected. In contrast, the

increase in Wg at the *sulf1* null synapse did not correspond to an increase in the dFz2C-terminus nuclear internalization, but rather a significant decrease. One explanation for this apparent discrepancy is the 'exchange factor' model based on the biphasic ability of the HSPG co-receptor Dlp to modulate Wg signaling (Yan et al., 2009). In the *Drosophila* wing disc, this model suggests that the transition of Dlp co-receptor from an activator to repressor of signaling depends on Wg cognate receptor dFz2 levels, such that a low ratio of Dlp:dFz2 potentiates Wg-dFz2 interaction, whereas a high ratio of Dlp:dFz2 prevents dFz2 from capturing Wg (Yan et al., 2009). In *sulf1* null synapses, we observe a very great increase in Dlp abundance (~40% elevated) with no significant change in the dFz2 receptor. In contrast, at *hs6st* null synapses there is a decrease in Dlp abundance (15% decreased) together with a significant increase in dFz2 receptor abundance (~25% elevated). Thus, the higher Dlp:dFz2 ratio in *sulf1* nulls could explain the decrease in Wg signal activation, evidenced by decreased dFz2-C terminus import into the muscle nucleus. In contrast, the Dlp:Fz2 ratio in *hs6st* is much lower, supporting activation of the dFz2-C terminus nuclear internalization pathway. This previously proposed competitive binding mechanism dependent on Dlp co-receptor and dFz2 receptor ratios predicts the observed synaptic Wg signaling pathway modulation in *sulf1* and *hs6st* dependent manner (Yan et al., 2009).

At the *Drosophila* NMJ, Gbb is very well characterized as a retrograde *trans*-synaptic signal, with muscle-derived Gbb causing the receptor complex Wishful thinking (Wit), Thickveins (Tkv) and Saxophone (Sax) to induce

phosphorylation of the transcription factor mothers against Mothers against decapentaplegic (P-Mad) (Wharton et al., 1999; McCabe et al., 2003; Keshishian and Kim, 2004). Mutation of Gbb ligand, receptors or regulators of this pathway have shown that Gbb-mediated retrograde signaling is required for proper synaptic differentiation and functional development (Marques et al., 2002; McCabe et al., 2003, 2004; Rawson et al., 2003). Further, loss of Gbb signaling results in significantly decreased levels of P-Mad in the motor neurons (McCabe et al., 2003). We show here that accumulation of Gbb in *sulf1* and *hs6st* null synapses causes elevated P-Mad signaling at the synapse and P-Mad accumulation in motor neuron nuclei. Importantly, *sulf1* null synapses show a significantly higher level of P-Mad signaling compared to *hs6st* null synapses, and this same change is proportionally found in P-Mad accumulation within the motor neuron nuclei. These findings indicate differential activation of Gbb *trans*-synaptic signaling dependent on the HS sulfation state controlled by the *sulf1* and *hs6st* mechanism, similar to the differential effect observed on Wg *trans*-synaptic signaling. Our genetic interaction studies show that these differential effects on *trans*-synaptic signaling have functional consequences, and exert a causative action on the observed bi-directional functional differentiation phenotypes in *sulf1* and *hs6st* nulls. Genetic correction of Wg and Gbb defects in the *sulf1* null background restores elevated transmission back to control levels. Similarly, genetic correction of Wg and Gbb in *hs6st* nulls restores the decreased transmission strength back to control levels. These results demonstrate that the

Wg and Gbb *trans*-synaptic signaling pathways are differentially regulated and, in combination, induce opposite effects on synaptic differentiation.

Both *Wg* and *Gbb* pathway mutants display disorganized and mislocalized presynaptic components at the active zone (e.g. Bruchpilot; Brp) and postsynaptic components including glutamate receptors (e.g. Bad reception; Brec/GluRIID) (Aberle et al., 2002; Marques et al., 2002; Packard et al., 2002). Consistently, the bi-directional effects on neurotransmission strength in *sulf1* and *hs6st* mutants are paralleled by dysregulation of these same synaptic components. Changes in presynaptic Brp and postsynaptic GluR abundance/distribution causally explain the bi-directional effects on synaptic functional strength between *sulf1* and *hs6st* null mutant states. Alterations in active zone Brp and postsynaptic GluRs also agree with assessment of spontaneous synaptic activity. Null *sulf1* and *hs6st* synapses showed opposite effects on miniature evoked junctional current (mEJC) frequency (presynaptic component) and amplitude (postsynaptic component). Further, quantal content measurements also support the observation of bidirectional synaptic function in the two functionally paired nulls. Genetic correction of Wg and Gbb defects in both *sulf1* and *hs6st* nulls restores the molecular composition of the pre- and postsynaptic compartments back to wildtype levels. When both *trans*-synaptic signaling pathways are considered together, these data suggest that HSPG sulfate modification under the control of functionally-paired *sulf1* and *hs6st* jointly regulates both WNT and BMP *trans*-synaptic signaling pathways in a differential manner to modulate synaptic functional development on both sides of the cleft.

We present here the first systematic investigation of glycan roles in the modulation of synaptic structural and functional development. We have identified a host of glycan-related genes that are important for modulating neuromuscular synaptogenesis, and these genes are now available for future investigations, to determine mechanistic requirements at the synapse, and to explore links to neurological disorders. As proof for the utilization of these screen results, this study has identified extracellular heparan sulfate modification as a critical platform of the intersection for two secreted *trans*-synaptic signals, and differential control of their downstream signaling pathways that drive synaptic development. Other *trans*-synaptic signaling pathways are independent and unaffected by this mechanism, although it is of course possible that a larger assortment of signals could be modulated by this or similar mechanisms. This study supports the core hypothesis that the extracellular space of the synaptic interface, the heavily-glycosylated synaptomatrix, forms a domain where glycans coordinately mediate regulation of *trans*-synaptic pathways to modulate synaptogenesis and subsequent functional maturation.

Materials and Methods

Drosophila stocks and genetics

The glycan-related gene collection was generated using the KEGG glycan databases and Flybase annotation. The 163 UAS-RNAi lines tested were obtained from the Vienna *Drosophila* RNAi Center (VDRC) and Harvard TRiP collection. Transgenic UAS-RNAi males were crossed to GAL4 driver females,

with progeny raised at 25°C on standard food, controlling for density (3 ♀ crossed to 2 ♂). The UH1-GAL4 driver was used for ubiquitous knockdown of target gene expression (Rohrbough et al., 2007). Neural specific *elav*-GAL4 (Lin and Goodman, 1994a), muscle specific 24B-GAL4 (Brand and Perrimon, 1993) and glia specific *repo*-GAL4 lines (Sepp et al., 2001) from Bloomington stock center were used to assay cell-targeted knockdown. The two *sulf1* null alleles used were $sulf1^{\Delta 1}$ (You et al., 2011) and $sulf1^{\Delta P1}$ (Kamimura et al., 2001). The two *hs6st* null alleles used were $hs6st^{d770}$ and the deficiency Df(3R)ED6027 (Kamimura et al., 2006). The *wg* allele wg^{l-12} (Marie et al., 2010) and *gbb* alleles gbb^{1} and gbb^{2} were used (Wharton et al., 1999; McCabe et al., 2003). Multiply mutant animals were made using standard genetic crosses. The trol-GFP line was obtained from Flytrap (Morin et al., 2001).

Antibody production

We generated a rabbit polyclonal anti-Gbb antibody using a 1:1 combination of two Gbb-specific peptides (SHHRSKRSASHP, NDENVNLKKYRNMIVKSC) corresponding to amino acids 319-330 and 435-452 of Gbb (Young-In Frontier, Seoul, Korea). The antibody was purified by Protein A affinity chromatography, and antibody specificity demonstrated by examining immunoreactivity in the wandering third instar neuromusculature with *gbb* mutants and by expressing $UAS\text{-}gbb^{9.1}$ under the control of the muscle driver *BG57-GAL4* (Figure 23). Immunoreactivity in the wandering third instar neuromusculature was severely reduced in a strong hypomorphic *gbb* allele (gbb^{1}/gbb^{2}, $UAS\text{-}gbb^{9.9}$), which has leaky expression of $UAS\text{-}gbb^{9.9}$ in a null allelic combination [25,87,95]. In sharp

contrast, the anti-Gbb signal was strongly elevated in *BG57-GAL4/UAS-gbb*$^{9.1}$ relative to wildtype larvae.

Immunocytochemistry

Wandering third instars were dissected in Ca^{2+}-free saline and then immediately fixed in either 4% paraformaldehyde for 10 minutes (all labels except anti-Dlp) or Bouin's fixative for 30 mins (anti-Dlp). Preparations were then washed in permeabilizing PBST (PBS + 0.1% Triton-X) or detergent-free PBS for extracellular labeling only (Rushton et al., 2009) . The following primary antibodies were used: rabbit or goat anti-HRP (1:250; Jackson ImmunoResearch Laboratories); mouse anti-DLG (4F3; 1:250; Developmental Studies Hybridoma Bank (DSHB)); mouse anti–Fasciclin II (1D4; 1:5; DSHB); mouse anti-Dlp (13G8, 1:5; DSHB) and rabbit anti-Syndecan (1:200) (Spring et al., 1994); mouse anti-Wg (4D4; 1:2 DSHB) and rabbit anti-Gbb (1:100); rabbit anti-PcanV (1:1000) (Friedrich et al., 2000) guinea pig anti-Jeb (1:100) (Rohrbough K. et al., 2010); rabbit anti-dFz2-C (1:500) and rabbit anti-dFz2-N (1:100) (Mathew et al., 2005); rabbit anti-Htl (1:100) (Shishido et al., 1997); rabbit anti-P-Mad (PS1; 1:1000) (Persson et al., 1998); rabbit anti-GluRIID (1:500) (Featherstone et al., 2005) and mouse anti-BRP (1:100; DSHB). Primary antibodies were incubated at 4°C overnight. Alexa-conjugated secondary antibodies (Jackson ImmunoResearch Laboratories) were used at 1:250 dilutions for 2 hours at room temperature. Staining with propidium iodide (Sigma Aldrich) to visualize cell nuclei was done at 1:100 dilution of 1 mg/ml propidium iodide incubated for 30 minutes at room temperature.

Imaging quantification

Images were taken with on an upright Zeiss LSM 510 META laser-scanning confocal using a Plan Apo 63X oil objective. For structural quantification, including NMJ synapse branch number, bouton number and area, preparations were double-labeled with anti-HRP and anti-DLG, with counts made at muscle 4 in segment A3. For nuclear import studies, nuclei were identified by propidium iodide staining with fluorescent punctae counted and intensity quantified [59]. For synaptic functional protein quantitation, glutamate receptor and Brp punctae were quantified for muscle 4, segment 3. Glutamate receptor number and field area was quantified in consecutive boutons of >3µm diameter. All preparations were fixed, stained and processed simultaneously to allow for intensity comparisons. All analyses were done with ImageJ software (National Institutes of Health) using the threshold function to outline areas and Z-stacks made using the maximum projection function. Statistics were done with one-way ANOVA analysis followed by Dunnett's post-test. All analyses were done blind to genotypes during all stages of experimentation and analysis. All figure images were projected in LSM Image Examiner (Zeiss) and exported to Adobe photoshop.

Heparin treatment

Stock solution of heparin (Sigma, H3393) in 1XPBS was prepared and serially diluted to obtain concentrations (e.g. 0.625, 0.315 and 0.156 mg/ml). Dissected wandering third instar larvae were incubated with these heparin concentrations for 5 minutes at RT, followed by a 1 minute wash with 1XPBS and then 10

minute fix with 4% paraformaldehyde in 1XPBS. After fixation, anti-Wg or anti-Gbb antibodies were used as above with appropriate secondary antibodies. Processed animals were analyzed for changes in intensity measurements as above in the image quantification section. All fluorescence intensity measurements were compared to preparations treated identically with only 1XPBS and no heparin, and the processed simultaneously for immunolabeling, microscopy and quantification.

Electrophysiology

Two-electrode voltage-clamp (TEVC) records were made from the wandering third instar NMJ as previously described (Beumer et al., 1999). In brief, staged control, mutant and transgenic RNAi animals were secured on sylgard-coated coverslips with surgical glue (liquid suture), dissected longitudinally along the dorsal midline, and glued flat. The segmental nerves were cut near the base of the ventral nerve cord. Recording was performed in 128 mM NaCl, 2 mM KCl, 4 mM $MgCl_2$, 1.0 mM $CaCl_2$, 70 mM sucrose, and 5 mM Hepes. Recording electrodes (1-mm outer diameter capillaries; World Precision Instruments) were filled with 3 M KCl and had resistances of >15 MΩ. Spontaneous mEJCs were collected using continuous (gap-free) recording and evoked EJC recordings were made from the voltage-clamped (V_{hold} = −60 mV) muscle 6 in segment A3 with a TEVC amplifier (Axoclamp 200B; MDS Analytical Technologies). The cut segmental nerve was stimulated with a glass suction electrode at a suprathreshold voltage level (50% above baseline threshold value) for a duration of 0.5 ms. Records were made with 0.2 Hz nerve stimulation in episodic

acquisition setting and analyzed with Clampex software (version 7.0; Axon Instruments). Each *n*=1 represents a recording from a different animal. Statistical comparisons were performed using student's t-test or the Mann-Whitney test for non-parametric data.

Acknowledgments

We are particularly grateful to Hiroshi Nakato (*sulf1*$^{\Delta P1}$ and *hs6st*^{d770}), Xinhua Lin (*sulf1*$^{\Delta 1}$), Kristy Wharton (*gbb*^{1}/*gbb*^{2}, UAS-*gbb*$^{9.9}$ and UAS-*gbb*$^{9.1}$), the Vienna *Drosophila* RNAi Center (VDRC), the Harvard TriP Collection and the Bloomington *Drosophila* Stock Center for providing essential *Drosophila* stocks. We also particularly thank Joachim Schulz (Sdc), Peter ten Dijke (P-Mad), Vivian Budnik (dFz2-C and dFz2-N), Stefan Baumgartner (PcanV) and the Iowa Hybridoma Bank for essential antibodies. We thank Samuel Friedman for providing a representative image of anti-Perlecan antibody staining at the NMJ. We thank William Parkinson, Emma Rushton, Lane Coffee and Sean Schaffer for technical assistance.

Chapter IV

Two *pgant* O-GalNAc transferases regulate synaptic plasticity by activity-dependent regulation of integrin signaling

This paper has been published under the same title in *Journal of Neuroscience*, 2014

Neil Dani, He Zhu and Kendal Broadie

Departments of Biological Sciences, Cell & Developmental Biology and Pharmacology, and The Vanderbilt Kennedy Center for Research on Human Development, Vanderbilt University, Nashville, TN 37232, USA

Abstract

Using a *Drosophila* whole-genome transgenic RNAi screen for glycogenes regulating synapse function, we have identified two protein α-N-acetylgalactosaminyltransferases (*pgant3* and *pgant35A*) that regulate synaptic O-linked glycosylation (GalNAcα1-O-S/T). Loss of either *pgant* alone elevates pre-/postsynaptic molecular assembly and evoked neurotransmission strength, but synapses appear restored to normal in double mutants. Likewise, activity-dependent facilitation, augmentation and post-tetanic potentiation are all suppressively impaired in *pgant* mutants. In non-neuronal contexts, *pgant* function regulates integrin signaling, and we show here that the synaptic αPS2 integrin receptor and transmembrane tenascin ligand (ten-m) are both suppressively down-regulated in *pgant* mutants. Channelrhodopsin-driven activity rapidly (<1 minute) drives integrin signaling in wildtype synapses, but is suppressively abolished in *pgant* mutants. Optogenetic stimulation in *pgant* mutants alters presynaptic vesicle trafficking and postsynaptic pocket size during the perturbed integrin signaling underlying synaptic plasticity defects. Critically, acute blockade of integrin signaling acts synergistically with *pgant* mutants to eliminate all activity-dependent synaptic plasticity.

Introduction

The heavily glycosylated transmembrane and extracellular synaptomatrix at the synaptic interface plays pivotal roles in synaptogenesis, neurotransmission and synaptic plasticity (Dityatev and Schachner, 2003; Broadie et al., 2011; Dani and Broadie, 2012). Neurological disease states arising from aberrant glycosylation occur in numerous congenital disorders of glycosylation (CDGs) and dystroglycanopathies (Freeze, 2006). However, the mechanisms by which synaptomatrix glycan modifications regulate normal synapse function and dysfunction in heritable disease states remain poorly understood (Ohtsubo and Marth, 2006). *Drosophila* is a powerful genetic model to pursue these synaptic glycan mechanisms, given the conservation of glycan pathways, reduced glycogene genomic redundancy in this system, and host of techniques available at the well-characterized glutamatergic neuromuscular synapse (Keshishian et al., 1996; Gagneux and Varki, 1999). Using this model, we have recently shown that endogenous glycan-binding lectin (*mind the gap*; Rushton et al., 2009), heparan sulfate proteoglycan (HSPG) modifiers (*sulf1/hs6st*; Dani et al., 2012) and N-linked glycosylation (*mgat1*; Parkinson et al., 2013) glycan mechanisms all act as potent regulators of *trans*-synaptic integrin, WNT and BMP signaling.

To systematically pursue synaptic glycan mechanisms, we undertook a *Drosophila* whole-genome screen of glycogenes using RNAi-mediated knockdown of all N-/O-/glycosaminoglycan-linked enzymes, glycosaminoglycans, glycosyltransferases and glycan-binding lectins, characterizing effects on NMJ structure and function using confocal microscopy and two-electrode voltage-

clamp electrophysiology, respectively (Dani et al., 2012). This screen identified two α-N-acetylgalactosaminyltransferases, *pgant3* and *pgant35A*, which catalyze transfer of GalNAc monosaccharides onto serine/threonine residues (GalNAcα1-O-S/T) to form Tn antigens, as found within mucin-like O-linked glycans (Ten Hagen et al., 2003a). This most complexly regulated glycosylation is orchestrated by multiple GalNAc-transferases (12 *pgants* in *Drosophila*) with distinct and overlapping peptide specificities (Yoshida et al., 2008; Tran and Ten Hagen, 2013). Pursuing our screen results with well-characterized *pgant3* and *pgant35A* loss-of-function mutants (see Methods), we found elevated synaptic O-linked glycosylation, pre-/postsynaptic molecular assembly, pre-/postsynaptic ultrastructural elaborations and neurotransmission strength, which are all corrected in double mutants that show none of these synaptic defects, identifying a novel suppressive genetic interaction.

In non-neuronal tissues, *Drosophila* pgants regulate integrin signaling and intercellular adhesion (Zhang and Ten Hagen, 2011). Importantly, we have shown position specific (PS) integrins, localized both pre- and postsynaptically, regulate NMJ morphogenesis (Beumer et al., 1999), synaptic scaffold/synaptomatrix adhesion molecules (Beumer et al., 2002), functional differentiation (Rohrbough et al., 2007) and activity-dependent plasticity (Rohrbough et al., 2000). We therefore hypothesized that pgants regulate integrin signaling at the synapse, and consistently find suppressive down-regulation of αPS2-containing integrin receptors (Beumer et al., 1999), RGD-containing tenascin (ten-m) ligand (Mosca et al., 2012), and postsynaptic

membrane adhesion defects in *pgant* mutants. Furthermore, we find integrin- and activity-dependent functional synaptic plasticity is suppressively (reciprocal suppression) regulated in *pgant* mutants. Importantly, we find that channelrhodopsin activity stimulation (Wang et al., 2011) disrupts downstream integrin association with talin and pFAK signaling, and elevates postsynaptic membrane adhesion defects. RGD peptide blockade of integrin function synergistically abolishes all activity-dependent synaptic plasticity in *pgant* mutants. These data show two pgants suppressively regulate synaptic O-GalNAc glycosylation, synapse molecular assembly, neurotransmission strength and activity-dependent plasticity via *trans*-synaptic integrin-tenascin signaling.

Materials and Methods

Drosophila genetics

All stocks were maintained at 25°C on standard food. Two independent mutant alleles isolated by EMS mutagenesis were employed for *pgant3*; 1) $pgant3^{m1}$, a C>T transition changing conserved arginine to cysteine at amino acid 130 resulting in failure to glycosylate substrates in enzymatic activity tests, and 2) $pgant3^{m2}$, a G>A transition that creates a stop codon at amino acid 609, thereby deleting the C-terminal 59 amino acids and resulting in an unstable protein (Zhang et al., 2010). Similarly, the *pgant35A* mutations used were 1) $pgant35A^{HG8}$, a C>T transition at nucleotide 265 resulting in a glutamine to stop codon change at amino acid 89, and 2) $pgant35A^{3775}$, a T>A transversion at nucleotide 584 resulting in a premature stop codon at amino acid 195, both fully

eliminating the catalytic domain (Ten Hagen and Tran, 2002). All mutants were placed in the w^{1118} genetic background, and w^{1118} was therefore used as the wildtype control. Rescue and overexpression experiments were performed with *UAS-pgant3* and *UAS-pgant35A* (Zhang et al., 2008) wildtype transgenes driven by neural (*elav-gal4)* (Lin and Goodman, 1994a), muscle (*24B-gal4*) (Brand and Perrimon, 1993) and ubiquitous (*UH1-gal4*) (Wodarz et al., 1995) drivers. Standard genetic techniques were used to generate recombinant and multiply mutant animals. Optogenetic studies were performed with the UAS-ChIEF-tdTomato channelrhodopsin transgene (Wang et al., 2011) driven by the neural-specific *elav-gal4* driver in animals raised on 0.25 mM ATR (all-trans retinal; Sigma) supplemented food. Animals used for experimentation were of either sex.

Immunocytochemistry

Wandering third instars were dissected in Ca^{2+}-free saline and then fixed in 4% paraformaldehyde for 10 mins. Preparations were then washed in either permeabilizing PBST (PBS+0.1% Triton-X) or detergent-free PBS for extracellular labeling (Rushton et al., 2009). O-GalNAc glycans were visualized with TRITC-conjugated VVA (1:250; EY Laboratories) and HPL (1:250; Invitrogen) lectins (Chia et al., 2014) . Mouse antibodies obtained from the Developmental Studies Hybridoma Bank (DSHB) included: anti-βPS (1:500), anti-αPS1 (1:200), anti-αPS2 (1:500), anti-*scab* (1:200), anti-talin (1:10) and anti-DLG (4F3; 1:250). Other sourced primary antibodies included: mouse anti-Ten-m (1:3000) (Levine et al., 1994), mouse anti-Tig (1:200) (Fogerty et al., 1994), guinea pig anti-LanA (1:200) (Inoue and Hayashi, 2007), rat anti-Tsp (1:200)

(Subramanian et al., 2007), rabbit Wb-N (1:500) (Martin et al., 1999a), rabbit anti-βv (1:300) (Yee and Hynes, 1993) and rabbit anti-pFAK (pY397; 1:50; Invitrogen). All antibodies were incubated at 4°C overnight. Alexa-conjugated Fluor 647-goat anti-HRP and secondary antibodies (Jackson ImmunoResearch Laboratories) were incubated at 1:250 for 2 hours at RT.

Image quantification

Control and mutant preparations for antibody and lectin studies were processed simultaneously for all intensity comparisons (Dani et al., 2012). To allow for direct comparisons of signal intensity levels, all genotypes were dissected, fixed, labeled and imaged in parallel at the same time, with identical confocal settings and intensity measurements also made at the same time for all compared genotypes. Imaging was done on an upright Zeiss LSM 510 META laser-scanning confocal using a Plan Apo 63x oil objective. NMJ structural quantification was done with anti-HRP imaging at muscle 6/7 in segment A3. All intensity analyses were done with ImageJ software (NIH) using the threshold function to outline Z-stack areas with the maximum projection function. All statistical comparisons were performed with one-way ANOVA analysis followed by Dunnett's or Dunn's post-test for non-parametric data using Instat Graphpad software. All data are presented as mean ± SEM. All images were projected in LSM Image Examiner (Zeiss) and exported to Adobe Photoshop.

Electrophysiology

Two-electrode voltage-clamp (TEVC) records were made from NMJs of paired control and mutant wandering third instars as reported previously (Beumer et al.,

1999). Briefly, recordings were performed in 128 mM NaCl, 2 mM KCl, 4 mM $MgCl_2$, 1.0 mM $CaCl_2$, 70 mM sucrose, and 5 mM Hepes saline (PH 7.1). Recording electrodes (1-mm outer diameter capillaries; World Precision Instruments) filled with 3M KCl had resistances of >15 MΩ. Evoked excitatory junction currents (EJCs) were recorded at 18^{o}C using episodic recording from voltage-clamped (V_{hold}: −60 mV) muscle 6 in segment A3 with a TEVC amplifier (Axoclamp 2B; Axon). Excitatory junctional potentials (EJPs) were also recorded in parallel. Segmental nerves were stimulated with a glass suction electrode at a suprathreshold voltage (50% above threshold) for 0.5 ms duration at 0.5 Hz. For synaptic plasticity studies, the nerve was stimulated at 10 Hz for 60 seconds in 0.2 mM $CaCl_2$ saline (Rohrbough et al., 2000). EJCs were acquired via Clampex (Axon) and analyzed using Clampfit 9.0 by averaging 10 (during initial/PTP) to 20 (during tetanus) consecutive responses. Gly-Arg-Gly-Asp-Ser-Pro (G<u>RGD</u>SP) integrin inhibition and Gly-Arg-Ala-Asp-Ser-Pro (G<u>RAD</u>SP) control peptides (Sigma) were used at 0.2 mM, incubated for 1 hour at 18^{o}C. Statistical comparisons were done using one-way ANOVA analysis followed by Dunnett's post-test with Instat Graphpad software. Each N=1 represents a recording from a different animal. All data are presented as mean ± SEM.

Electron microscopy

Ultrastructural analyses were performed as reported previously

(Beumer et al., 1999). Briefly, staged third instar preparations were fixed in 1.6% paraformaldehyde/2% glutaraldehyde (20 mins), washed in 1XPBS (10 mins) and transferred to 2.5% glutaraldehyde in cacodylate buffer (12 hrs) with washes

in the same buffer (30 mins). Preparations were postfixed in 1% OsO_4 in cacodylate buffer (2 hrs) and then dehydrated in an ethanol series followed by propylene oxide (30 mins). Segment A3 muscle 6/7 was dissected free of the preparations and separately embedded in araldite resin. Ultrathin (40 nm) sections were cut using a Leica ultracut UCT 54 ultramicrotome and then transferred to formvar-coated slot grids. Sections were imaged using a Phillips CM10 transmission Electron Microscopy at 80 kV, with images collected on a 4 megapixel CCD camera. Sample sizes are $\geq$10 independent NMJs, with the statistical analyses calculated using unpaired t-tests. Images acquired from AMT Image Capture Software were exported to Adobe Photoshop. All data are presented as mean ± SEM.

Optogenetics

Wandering third instars were dissected in 0.2 mM Ca^{2+} saline on Sylgard-coated plates with the nervous system kept intact. An LEDD1B LED driver, M470L2 mounted LED at 470nm affixed with LA1951-A lens was used to stimulate channelrhodopsin activity (Gruntman and Turner, 2013). Preparations were subjected to a 60 sec train of light stimulation at 10 Hz, with a pulse duration of 60 ms, followed by immediate fixation and processing during continual stimulation, using the methods described above. $\geq$8 independent NMJs were analyzed for each genotype and condition, with statistical tests for activity-dependent changes in fluorescence intensity and ultrastructure performed as described above in the immunocytochemistry and electron microscopy sections.

Results

Pgants regulate synapse composition and transmission strength

An unbiased genetic screen of glycogenes identified synaptic function defects using inducible RNAi-mediated down regulation of two *pgants* (*pgant3* and *pgant35A*). This screen tested 130 glycan-related genes defined in 8 function categories: N-glycan, O-glycan and glycosaminoglycan biosynthesis; glycosyltransferases, glycan degrading/ modifying enzymes; glycoprotein and proteoglycan core proteins; sugar transporters and glycan-binding lectins. Using a combination of confocal microscopy and two-electrode voltage-clamp (TEVC) electropyhysiology, NMJ morphology and functional transmission defects were tested in *Drosophila* wandering third instar larvae following ubiquitous (*UH1-gal4*) RNAi knockdown. From this screen, 31 genes affected synapse structure (27 increased bouton number, 2 increased branching and 2 increased NMJ area) and 13 affected synapse function (12 increased and 1 decreased). Only 6 gene knockdowns affected both structure and function. To investigate mucin-type O-linked glycosylation, 9 available RNAi lines were used to test 6 *pgant* genes (*pgant2*, *pgant3*, *pgant4*, *pgant5*, *pgant6* and *pgant35A*) and 3 additional GalNAc transferases (GalNAcT-1, GalNAcT-2 and C1GalTA). Of these, 3 *pgant* genes (*pgant3, pgant5* and *pgant35A*) were identified to have increased neurotransmission strength upon knockdown, and GalNAc-T2 showed increased NMJ area. The other 5 gene knockdowns caused no detectable NMJ phenotypes. Well-characterized mutants are available for only *pgant3* and *pgant35A* (see Methods), which have been extensively studied in heteroallelic

null combinations (Ten Hagen and Tran, 2002; Zhang et al., 2010). In this study, we pursued a full characterization of these two *pgant* genes using the same conditions.

To characterize synaptic mechanisms in *pgant3* and *pgant35A* null single and double mutant larvae, we performed nerve-evoked excitatory junction current (EJC) recordings in the TEVC paradigm (Dani et al., 2012). Sample traces of 10 consecutive, superimposed responses are shown for 4 genotypes; the genetic background control (w^{1118}), *pgant3* ($pgant3^{m1}/pgant3^{m2}$) and *pgant35A* ($pgant35A^{HG8}/pgant35A^{3775}$) single mutants in w^{1118} background, and the double null mutant ($pgant3^{m1}$,$pgant35A^{HG8}$/ $pgant3^{m2}$,$pgant35A^{3775}$). Neurotransmission is clearly and consistently elevated in both *pgant* mutants, increased 25-40% compared to controls (Fig. 23A). Quantification of mean EJC amplitudes shows that synapse strength is very significantly elevated in both *pgant3* (255.46±8.12nA, n=26, $p<0.001$) and *pgant35A* (277.62±11.88nA, n=22, $p<0.001$) single mutants compared to control (198.73±7.77nA, n=17; Fig.24A, right). Surprisingly, however, neurotransmission in the recombinant double null mutant is not significantly elevated compared to control (231.64±7.24nA, n=21, $p>0.05$; Fig.24A. right), which behaves like the control. Thus, a similar phenotype occurs in the two *pgant* single mutants, which is absent in the double mutant. We use the term ‘suppression’ throughout this study, as the simplest genetic term describing the observed interaction. Importantly, there is a synaptic function defect only, with no differences in NMJ morphology in either of the *pgant* mutants. In quantifying synaptic branching, neither *pgant3* (5.00±0.28 decrease,

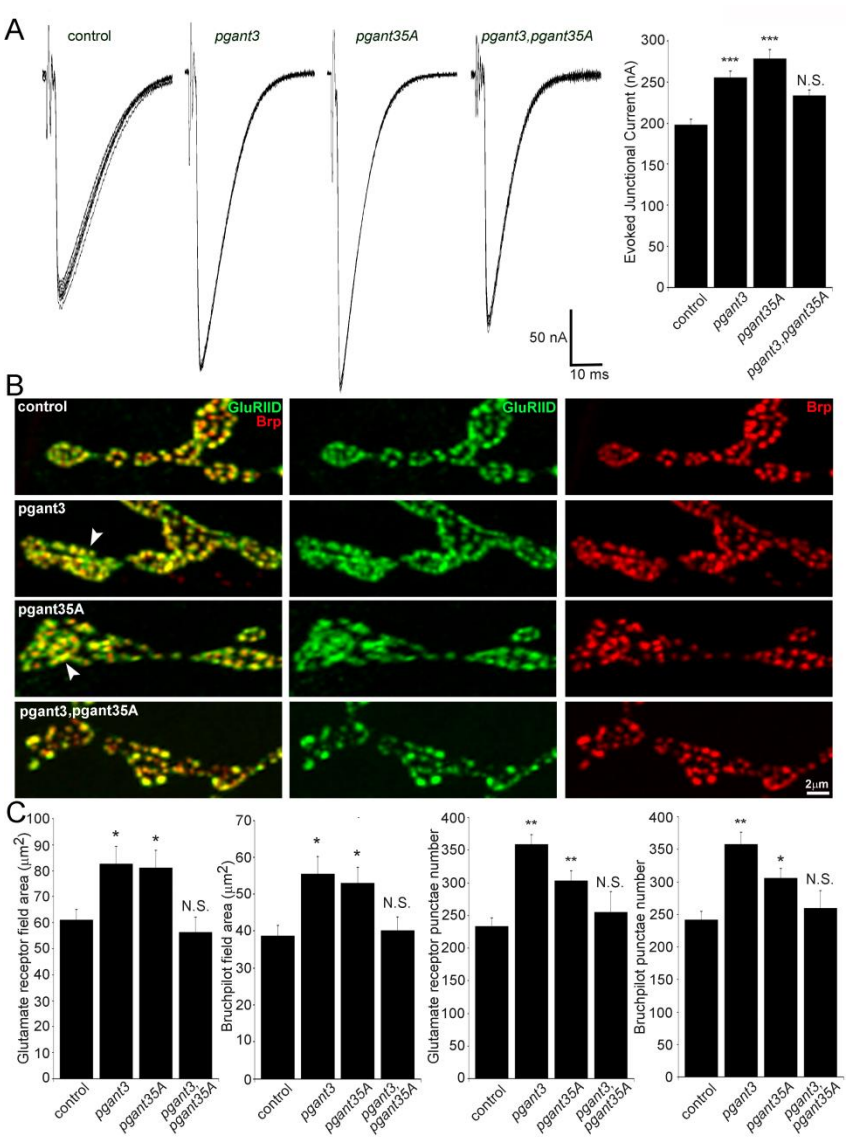

Figure 23. Null *pgant* mutants suppressively elevate neurotransmission strength. (A) Representative evoked excitatory junction current (EJC) records from genetic control (w^{1118}), *pgant3* ($pgant3^{m1}/pgant3^{m2}$) and *pgant35A* ($pgant35A^{HG8}/pgant35A^{3775}$) single mutants, and double mutants ($pgant3^{m1},pgant35A^{HG8}/pgant3^{m2},pgant35A^{3775}$). Ten consecutive EJCs traces shown at 0.2 Hz stimulation from the muscle 6 NMJ in segment A3. Scale bar indicates EJC amplitude (50nA, Y-axis) and time (10ms, X-axis). Right: Histogram of mean EJC amplitudes, with sample sizes $\geq$17 for each genotype. **(B)** Representative NMJ boutons for the above four genotypes labeled for postsynaptic glutamate receptors (GluRIID, green) and presynaptic active zone Bruchpilot (Brp, red), with split channels shown for clarity. White arrows indicate GluRIID/Brp paired punctae in single mutants. Scale bar: 2µm. **(C)** Quantification of GluRIID/Brp areas and punctae number per NMJ terminal. Statistical differences are calculated using one-way ANOVA with Dunnett's post-test; *p<0.05, **p<0.01, ***p<0.001, N.S. indicates no significance.

n=28) or *pgant35A* (5.79±0.26 n=24) single mutants, or the double mutants (6.26±0.41, n=23) showed any significant difference from controls (5.58±0.22, n=26). Likewise, NMJ bouton number is also not significantly affected in *pgant3* (90.89±4.25, n=28) or *pgant35A* (92.29±5.78, n=24) single mutants or double mutants (77.46±4.18, n=24) compared to controls (85.96±4.18, n=28). This finding was the first discovery of the suppressive action of *pgant* genes on synapse function.

To begin to determine how *pgant* co-repressive regulation arises at the synapse, we labeled NMJs for presynaptic active zones with Bruchpilot (Brp), and postsynaptic glutamate receptors (GluRIID), marking the two sides of each individual synapse (Fig.24B). There is a clear and consistent increase in Brp/GluRIID punctae in both *pgant3* and *pgant35A* single mutants, indicating a co-operative change on both pre- and postsynaptic sides of the synapse. Importantly, however, the double null mutant does not show any detectable increase in either synaptic marker (Fig. 23B). Quantification reveals significantly increased glutamate receptor field area and punctae number in *pgant3* (82.59±6.77μm^2 ($p<0.05$) and 358.0±16.20 ($p<0.01$); n=14) and *pgant35A* (81.02±6.95μm^2 and 302.73±15.61; n=15, $p<0.05$) single mutants, but with no differences in the double mutants in either parameter compared to controls (61.03±3.99μm^2 and 233.25±12.33, n=16; Fig.24C). Likewise, presynaptic Brp active zone area and punctae number are increased at *pgant3* (54.80±4.80μm^2 and 357.46±18.89; n=13, $p<0.05$) and *pgant35A* (52.96±4.30μm^2 and 305.4±14.86; n=15, $p<0.05$) single mutants, with no differences in

pgant3,pgant35A double mutants compared to controls (38.56±3.03μm^2 and 242±31.22; n=16; Fig. 23C). Both *pgant* mutants show no significant change in spontaneous miniature EJC (mEJC) frequencies (*pgant3*, 2.29±0.17Hz, n=10; *pgant35A*, 2.06±0.11Hz, n=9) compared to control (1.93±0.13Hz, n=10), but do show small, significant decreases in mEJC amplitudes (*pgant3*, 0.68±0.03nA, n=10, $p<0.05$; *pgant35A*, 0.69±0.03nA, n=9; $p<0.05$) compared to control (0.80±0.02nA, n=10). These results show that *pgant3* and *pgant35A* both up-regulate neurotransmission strength through elevated pre- and postsynaptic assembly via a mutually suppressive mechanism that predominantly impacts evoked function.

Pgants regulate presynaptic vesicles and postsynaptic pocket size

The synaptic ultrastructure of the *Drosophila* NMJ has been well characterized by transmission electron microscopy (TEM), categorizing multiple synaptic vesicle (SV) pools in the presynaptic bouton and the complex architecture of the expansive sub-synaptic reticulum (SSR) of the postsynaptic membrane (Rohrbough et al., 2007). As no gross morphology differences were associated with observed neurotransmission elevations in *pgant* mutants, we next investigated synapse ultrastructure. On the presynaptic side, we measured bouton area, active zone architecture, overall SV density and SV distribution in concentric rings (e.g. 250 nm, 500 nm) extending from each active zone (Fig. 24A,B; white arrows). On the postsynaptic side, we assayed SSR area, thickness on major and minor axes, density (folds/unit length) and postsynaptic pocket

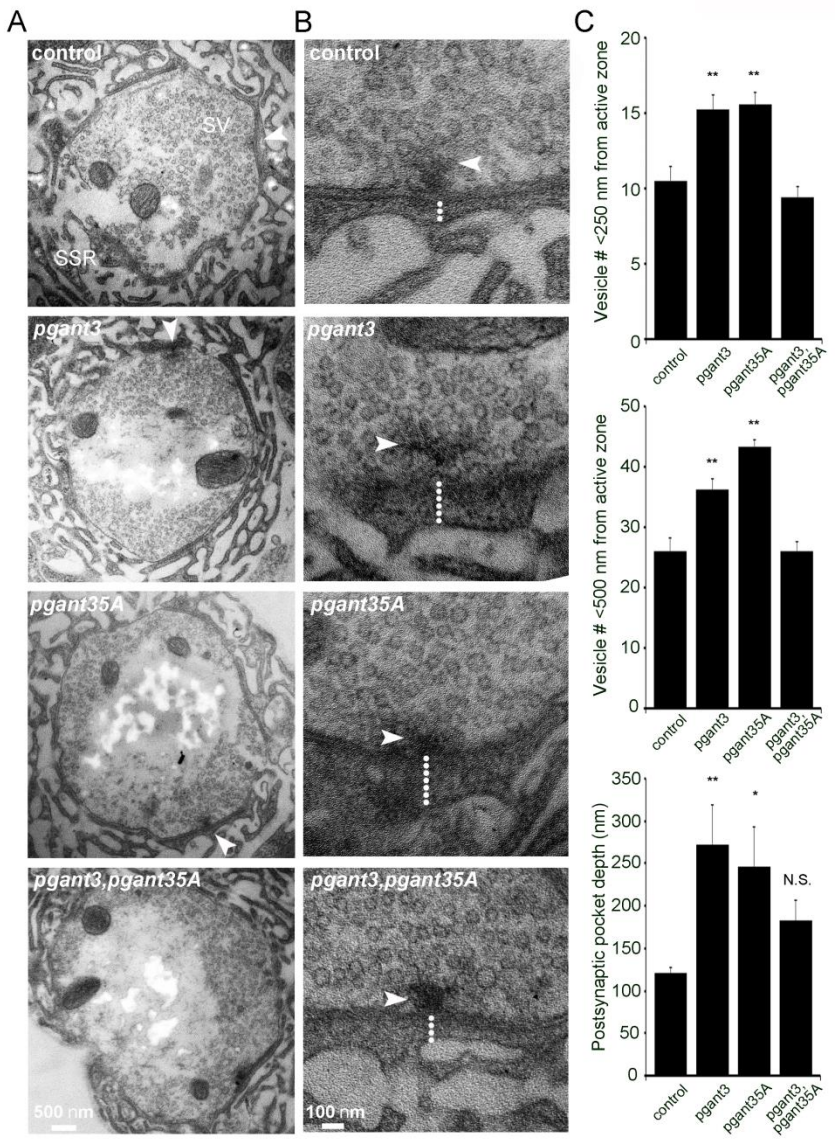

Figure 24. Null *pgant* mutants suppressively alter pre/postsynaptic ultrastructure. (A) Representative transmission electron microscopy (TEM) images of synaptic boutons from muscle 6 NMJ in segment A3 of genetic control (w^{1118}, top), *pgant3* ($pgant3^{m1}/pgant3^{m2}$) and *pgant35A* ($pgant35A^{HG8}/pgant35A^{3775}$) single mutants (middle), and double mutants ($pgant3^{m1},pgant35A^{HG8/3775}/pgant3^{m2},pgant35A^{3775}$, bottom). Labels indicate synaptic vesicle (SV) pools in presynaptic bouton, subsynaptic reticulum (SSR) of muscle membrane, and presynaptic active zones (arrowheads). Scale: 500nm. **(B)** High magnification images of single active zone synapses in all four genotypes. Labels indicate presynaptic t-bars (arrowheads) and postsynaptic pockets (white dotted lines). Scale: 100nm. **(C)** Quantification of SV pools (<250 nm (top), <500 nm (middle) from active zone t-bar) and postsynaptic pocket depth (bottom). Sample size $\geq$10 boutons for each of the four genotypes. Statistical differences calculated using one-way ANOVA with Dunnett's post-test; *p<0.05, **p<0.01, N.S. indicates no significance.

(PSP) size by measuring the distance from presynaptic active zone to the first SSR membrane layer (Fig. 24A,B; dotted white lines). Expansion of the postsynaptic pocket is a hallmark of mutants defective in synaptomatrix resident, *trans*-synaptic signaling ligands (Packard et al., 2002) and heparan sulfate proteoglycan (HSPG) extracellular regulators of *trans*-synaptic signaling (Kamimura et al., 2013).

Presynaptic bouton appearance (Fig. 24A) and area in both *pgant* mutants (*pgant3*, 7.53±0.85 μm^2, n=10 *pgant35A*, 7.76±0.80 μm^2, n=12,) are not significantly different from the genetic control (w^{1118}, 9.51±1.78 μm^2, n=7), although there is a trend towards smaller boutons. Likewise, active zone architecture and t-bar dimensions are not measurably affected by loss of *pgant* activity (Fig. 24B). In contrast, the density and distribution of SV pools is clearly aberrant in both *pgant* single mutants, although the double null mutant is not detectably different from the control (Fig. 24A,B). Immediately adjacent to active zone t-bars (Fig. 24B, arrows), SV clustering is increased in both *pgant* single mutants, but not in the double mutant combination. Quantifying SV number within 250 nm of the t-bar shows a consistent density in controls (10.5±0.91), which is significantly increased in both *pgant3* (15.22±0.99, $p<0.01$) and *pgant35A* (15.53±0.78, $p<0.01$) single mutants, but back at control level in double null mutants (9.4±0.67; n=15; Fig. 24C, top). Likewise, at a distance of 500 nm from the active zone t-bar, SV number increases in *pgant3* (36.3±1.66, $p<0.01$) and *pgant35A* (43.31±1.21, $p<0.01$) single mutants, but not in double mutants (26.06±1.44, n=15) compared to controls (26±2.18; Fig. 24C, middle). Thus,

presynaptic vesicle pool distribution is suppressively regulated by *pgant3* and *pgant35A*, in line with changes in synaptic function.

Postsynaptic SSR appearance, area, thickness and density are normal in all *pgant* mutants (Fig. 24A). Quantification of SSR area (*pgant3,* 1.26±0.16; *pgant35A,* 1.13±0.17; *pgant3,pgant35A,* 1.09±0.17), thickness (*pgant3,* 1.12±0.10; *pgant35A,* 0.84±0.08; *pgant3,pgant35A,* 0.80±0.07) and density (*pgant3,* 0.83±0.05; *pgant35A,*1.10±0.08; *pgant3,pgant35A,* 1.11±0.08) all show no significant changes normalized to controls (Fig. 24A). In contrast, however, there is a striking expansion in both *pgant* mutants of the postsynaptic pocket (PSP) (Packard et al., 2002; Kamimura et al., 2013). This compartment has been defined as "a postsynaptic area immediately apposed to an active zone containing amorphous material" (Packard et al., 2002), which is spatially localized between postsynaptic membrane and SSR (Ren et al., 2009). The PSP compartment has been shown to be expanded in *trans*-synaptic signaling disrupted mutants including WNT *wingless* (*wg*), BMP *glass bottom boat* (*gbb*), HSPG perlecan (*trol*) and HSPG sulfateless (*sfl*) mutants (Packard et al., 2002; Tian and Ten Hagen, 2007; Ren et al., 2009; Nahm et al., 2010; Kamimura et al., 2013). Both *pgant3* and *pgant35A* single mutants similarly display an enlarged PSP compartment, although the double null mutant is not detectably different from the control (Fig. 24B; dotted white lines). As a quantifiable PSP parameter, pocket depth from presynaptic active zone to the next adjacent postsynaptic SSR membrane was measured in all four genotypes. Compared to controls (mean PSP depth 121.17±4.95nm, n=10), both *pgant* single mutants display a >2-fold

expanded PSP (*pgant3*, 254.7±35.25nm, p<0.01; *pgant35A*, 233.96±41.83nm, p<0.05) (Fig. 24B,C bottom). In sharp contrast, the double null mutants show no significant increase in PSP depth compared to controls (169.09±15.46nm; n=12; Fig. 24C, bottom). Thus, we observe suppressive regulation by *pgant* genes of SV pools in the presynaptic compartment as well as postsynaptic compartment expansion, paralleling the changes in neurotransmission strength.

Neuronal and muscle *pgant3* and *pgant35A* modulate neurotransmission

To determine cell-specific requirements of *pgant3* and *pgant35A,* we used the inducible Gal4-UAS binary system (Brand and Perrimon, 1993) to express *UAS-pgant3* or *UAS-pgant35A* wildtype transgenes in neurons (*elav-gal4*) or muscles (*24B-gal4*) in respective single mutant backgrounds, and assayed for phenotype rescue (Fig. 25). Sample EJC traces show an average of 10 consecutive nerve-evoked responses for both rescue conditions in both *pgant* nulls (Fig. 25A). We find that functional neurotransmission strength is restored to control levels when *pgant3* is expressed in either neurons (*pgant3*^{m1}*/pgant3*^{m2}; *UAS-pgant3/elav,* 181.61±11.85 nA, n=14) or muscles (*pgant3*^{m1}*/pgant3*^{m2}; *UAS-pgant3/24B*, 187.47±12.72 nA, n=11) in the otherwise *pgant3* null background, as compared to controls (*w*^{1118}*,* 193.34±8.69 nA, n=14; Fig. 25C, top panel). Similarly, *pgant35A* expression in neurons (*pgant35A*^{HG8}*/pgant35A*^{3775}; *UAS-pgant35A/elav*, 197.50±14.26 nA, n=9) or muscles (*pgant35A*^{HG8}*/pgant35A*^{3775}; *UAS-pgant35A/24B*, 211.42±17.06 nA, n=10) in the *pgant35A* mutant background likewise rescues neurotransmission strength to control level (Fig.

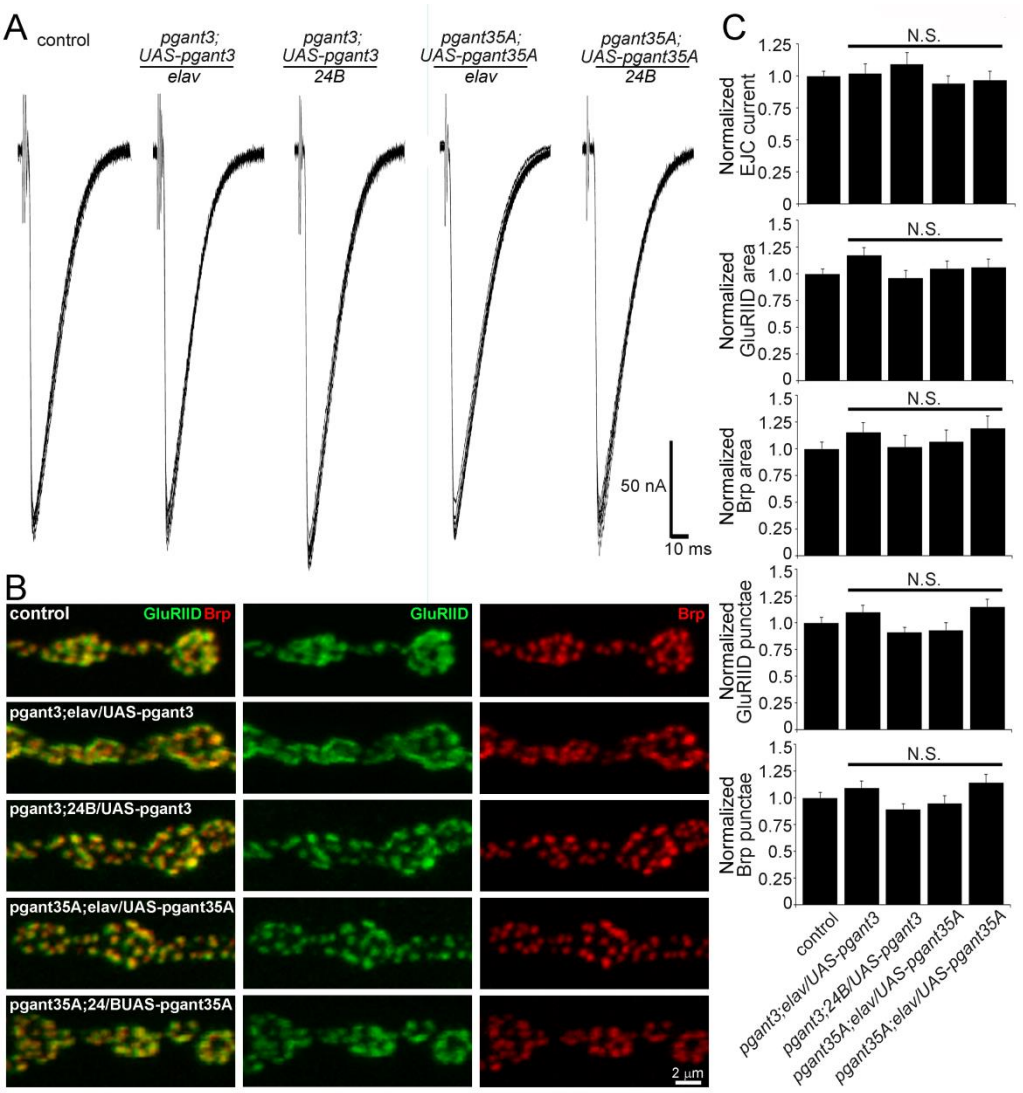

Figure 25. Pgants function in neurons and muscle to regulate neurotransmission. (A) Representative evoked junctional current (EJC) records from genetic control (w^{1118}), *pgant3* mutant with neuronal ($pgant3^{m1}/pgant3^{m2}$; *UAS-pgant3/elav*) and muscle ($pgant3^{m1}/pgant3^{m2}$; *UAS-pgant3/24B) pgant3* expression, *pgant35A* mutant with neuronal ($pgant35A^{HG8}/pgant35A^{3775}$; *UAS-pgant35A/elav*) and muscle ($pgant35A^{HG8}/pgant35A^{3775}$; *UAS-pgant35A/24B) pgant35A* expression. 10 consecutive EJC traces are shown at 0.2 Hz stimulation from the muscle 6 NMJ in segment A3. Scale bar indicates EJC amplitude (50 nA, Y-axis) and time (10 ms, X-axis). Sample size n≥8 animals for all conditions. **(B)** Representative NMJ boutons for the above five genotypes co-labeled for both postsynaptic glutamate receptors (GluRIID, green) and presynaptic active zone Bruchpilot (Brp, red), with split channels shown for clarity. Scale bar: 2µm. **(C)** Histograms show normalized EJC amplitude, punctae number and GluRIID/Brp area per NMJ terminal for the above five genotypes. Sample size n≥10 animals for all conditions. Statistical differences are calculated using one-way ANOVA with Dunnett's post-test. N.S. indicates no significance.

25C, top panel).

To test if this functional rescue correlates with corrected synaptic molecular assembly, NMJs were labeled for presynaptic Brp and postsynaptic GluRIID (Fig.26B). Brp punctae number in *pgant3* neuronal (392.56±22.86, n=9) or muscle (321.13±17.84, n=15) rescue conditions, as well as *pgant35A* neuronal (340±25.63, n=8) or muscle (409.58±27.71, n=12) rescue conditions, does not differ significantly from control (358.84±18, n=19; Fig. 25B,C). Similarly, GluRIID punctae number is also restored to control levels (360.73±19.16, n=19), with *pgant3* neuronal (395.89±23.95, n=9) or muscle (327.6±18.22, n=15) rescue, as well as *pgant35A* neuronal (336±24.71, n=8) or muscle (414.17±26.98, n=12) rescue. The same result is reflected in Brp area measurements, where *pgant3* neuronal (85.67±6.78, n=10) or muscle (75.66±7.99, n=15) rescue, as well as *pgant35A* neuronal (79.12±8.23 μm^2, n=10) or muscle (88.80±8.29 μm^2, n=12) rescue is similar to control values (74.35±4.69 μm^2, n=18; Fig. 25B,C). Similarly, postsynaptic GluRIID area measurements in *pgant3* neuronal (173.75±10.38 μm^2, n=10) or muscle (142.47±10.80 μm^2, n=15) rescue, as well as *pgant35A* neuronal (155.61±9.97 μm^2, n=10) or muscle (156.99±11.89 μm^2, n=12) rescue, are not significantly different from control (148.20±7.01 μm^2, n=18; Fig. 25C). These results show that both *pgant3* and *pgant35A* can function either pre- or postsynaptically to regulate synaptic assembly and neurotransmission strength.

Pre-/postsynaptic balance of *pgant3* and *pgant35A* regulate neurotransmission

Given the *pgant* suppressive mechanism and coupled pre/postsynaptic roles of

pgant3 and *pgant35A*, we next tested whether the balance of *pgant3* and *pgant35A* is required to properly regulate neurotransmission. We generated allelic combinations for *UAS-pgant3* wildtype transgene expression in neurons (*elav-gal4*), muscles (*24B-gal4*) or ubiquitously (*UH1-gal4*) in the *pgant3,pgant35A* double mutant background, and tested effects on neurotransmission strength. Representative EJC traces for each genotype are shown in Fig. 26A. Compared to the control mean EJC amplitude (*pgant3*^{m1},*pgant35A*^{HG8}/*pgant3*^{m2},*pgant35A*^{3775}*; UAS-pgant3*/+, 211.42±11.94 nA, n=8), neuronal (*pgant3*^{m1},*pgant35A*^{HG8}/*pgant3*^{m2},*pgant35A*^{3775}*; elav/UAS-pgant3,* 258.99±9.59 nA, n=9, p<0.05), muscle (*pgant3*^{m1},*pgant35A*^{HG8}/*pgant3*^{m2},*pgant35A*^{3775}*; 24B/UAS-pgant3*, 276.52±11.19 nA, n=9, p<0.05*)* as well as ubiquitous (*pgant3*^{m1},*pgant35A*^{HG8}/*pgant3*^{m2},*pgant35A*^{3775}*;* *UAS*-pgant3/*UH1*+, 254.47±13.59 nA, n=13, p<0.05) *pgant3* expression in the double mutant background, all significantly elevated neurotransmission strength (Fig. 26B). Thus, restoring *pgant3* to either neuron or muscle effectively reveals the *pgant35A* single mutant phenotype (Fig. 23A).

In parallel, we overexpressed both *pgant* genes alone to test the effect on neurotransmission strength. Representative EJC traces for each genotype are shown in Fig. 26C. As compared to control (*UAS-pgant3/*+, 205.55±8.77 nA, n=22), *pgant3* overexpression in neurons (*UAS-pgant3/elav*, 154.99±11.99 nA, n=11 p<0.01), muscles (*pgant3/24B*, 165.62±11.13 nA, n=10, p<0.05) or ubiquitous (*pgant3/UH1*, 164.80±9.79 nA, n=10, p<0.05) all similarly decreased

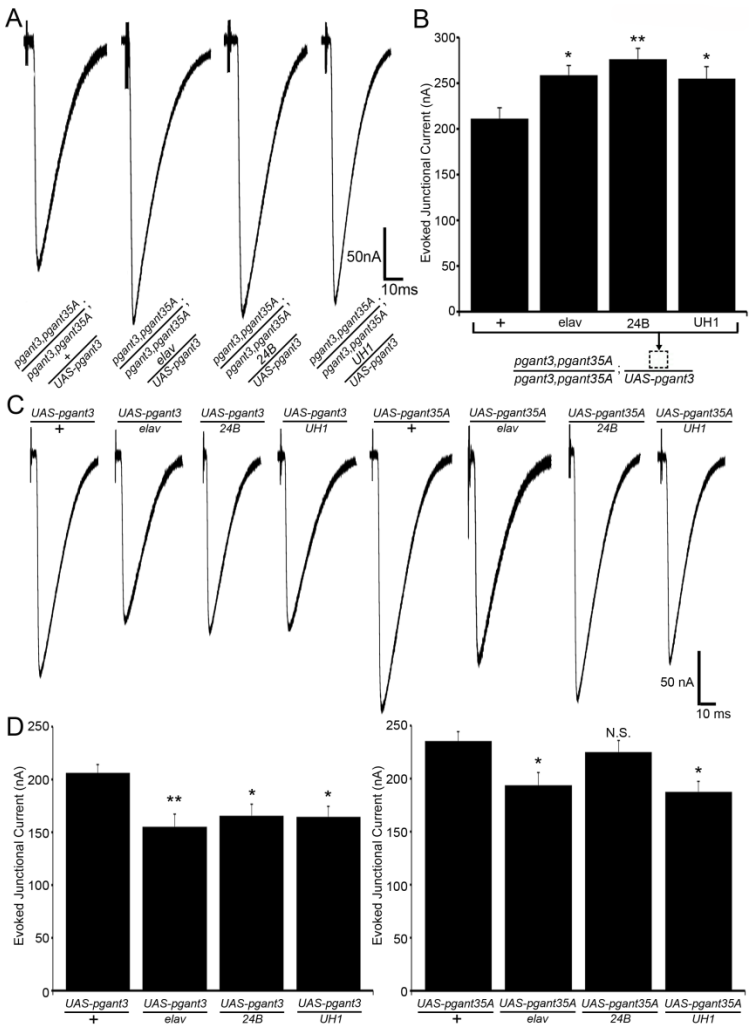

Figure 26. Pre/postsynaptic *pgant3/35A* balance regulates neurotransmission. Representative EJC records **(A)** and mean amplitudes **(B)** for *pgant3* expression in the double mutant background. The four genotypes include genetic control (*pgant3*^{m1},*pgant35A*^{HG8}/*pgant3*^{m2},*pgant35A*^{3775};+/*UAS-pgant3*), neuronal (*pgant3*^{m1}, *pgant35A*^{HG8}/*pgant3*^{m2},*pgant35A*^{3775};*elav/UAS-pgant3*), muscle (*pgant3*^{m1},*pgant35A*^{HG8}/ *pgant3*^{m2},*pgant35A*^{3775};*24B/UAS-pgant3)* and ubiquitous (*pgant3*^{m1},*pgant35A*^{HG8}/ *pgant3*^{m2},*pgant35A*^{3775};*UH1+/UAS*-pgant3) *pgant3* expression in the double mutant. Sample size n≥10 animals for all conditions. **(C)** Representative EJC records and **(D)** mean amplitudes for *pgant3* and *pgant35A* overexpression conditions. The eight genotypes include *pgant3* genetic control (*UAS-pgant3/*+), neuronal (*UAS-pgant3/elav*), muscle (*UAS-pgant3/24B*) and ubiquitous (*UAS-pgant3/UH1*) *pgant3* overexpression; and *pgant35A* genetic control (*UAS-pgant35A/*+), neuronal (*UAS-pgant35A/elav*), muscle (*UAS-pgant35A/24B*) and ubiquitous (*UAS-pgant35A/UH1*) *pgant35A* overexpression. Sample size ≥10 animals for each genotype. Statistical differences calculated using one-way ANOVA with Dunnett's post-test; *p<0.05, **p<0.01, N.S. indicates no significance.

mean EJC amplitudes (Fig 27D, left panel). Likewise, as compared to control (*UAS-pgant35A/+,* 235.15±10.77 nA, n=19), *pgant35A* overexpression in neurons (*UAS-pgant35A/elav,* 193.50±13.39 nA, n=18, $p<0.05$) and ubiquitous overexpression (*UAS-pgant35A/UH1*, 187.52±9.43 nA, n=10, $p<0.05$) both decrease neurotransmission transmission, although muscle overexpression alone has no significant effect (*UAS-pgant35A/24B*, 224.99±8.77 nA, n=20; Fig. 26D, right panel). Overall, *pgant* overexpression has the opposite consequence of *pgant* loss of function (Fig. 23A). Thus, the proper balance of *pgant3*/*pgant35A* in neurons and muscle bidirectionally regulates the strength of synaptic transmission.

Activity-dependent synaptic plasticity is impaired in *pgant* mutants

In the non-neuronal context of the *Drosophila* wing disc, *pgant* mutants specifically impair integrin signaling to cause intercellular de-adhesion (Zhang et al., 2010). Similarly, the above synaptic ultrastructure defects in *pgant* mutants recalls synaptic integrin signaling, which we have shown is required for activity-dependent synaptic plasticity (Rohrbough et al., 2000). We therefore next investigated the multiple phases of activity-dependent plasticity in *pgant* mutants, including immediate facilitation and maintained augmentation during a tetanic stimulus train (10 Hz, 60 seconds), and initiation and maintenance of post-tetanic potentiation (PTP) following return to basal stimulation. In this paradigm, EJCs are recorded initially at 0.5 Hz for 30 seconds, followed by the tetanic train, and then returned to basal 0.5 Hz for a total of 5 minutes recording (Rohrbough et al., 2000). Figure 27A shows representative traces for control (w^{1118}), single

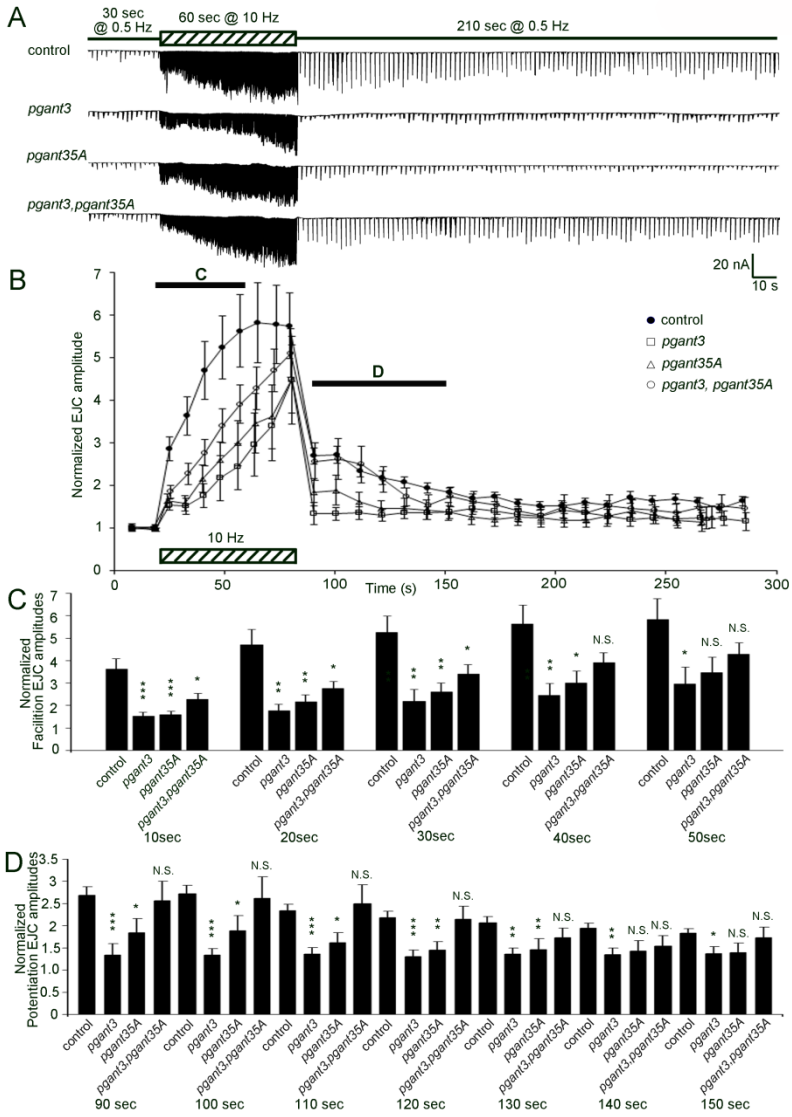

Figure 27. Impaired activity-dependent synaptic plasticity in *pgant* mutants. (A) Representative two-electrode voltage-clamp (TEVC) records from genetic control (w^{1118}, top), *pgant3* ($pgant3^{m1}/pgant3^{m2}$) and *pgant35A* ($pgant35A^{HG8}/pgant35A^{3775}$) single mutants (middle two traces), and double mutants ($pgant3^{m1}$, $pgant35A^{HG8}/pgant3^{m2}$,$pgant35A^{3775}$, bottom). The stimulation paradigm is 0.5 Hz for 30 seconds (solid bar), 10 Hz for 60 seconds (hatched bar), and then a return to 0.5 Hz (solid bar) for 5 minutes total recording time. Scale bars indicate 20nA (y-axis) and 10s (x-axis). **(B)** Mean EJC amplitudes over time normalized to initial mean EJC amplitude for control (solid circle), *pgant3* (hollow square) and *pgant35A* (hollow triangle) single mutants, and double mutant (hollow circle). Bars labeled "C" and "D" are expanded below, showing normalized EJC amplitudes during tetanic stimulation **(C)** and early post-tetanic stimulation periods **(D)**. Sample sizes $\geq$10 independent NMJs for each of the four genotypes. Statistical differences calculated using one-way ANOVA with Dunnett's post-test; *p<0.05, **p<0.01, ***p<0.001, N.S. indicates no significance.

(*pgant3*^{m1}/*pgant3*^{m2} and *pgant35A*^{HG8}/*pgant35A*^{3775}) and double mutants (*pgant3*^{m1},*pgant35A*^{HG8}/*pgant3*^{m2},*pgant35A*^{3775}).

For quantification, consecutive EJCs are averaged throughout the stimulation phases to display mean amplitudes normalized to the starting level (Fig. 27B). Controls show immediate, rapid facilitation leading to a 6-fold augmentation during tetanic stimulation, followed by 2-fold initial PTP phase, later maintained as a ~50% elevation for the duration of the recording (Fig. 27A,B). In contrast, both *pgant* single mutants show very significantly impaired initial facilitation and blunted 4-fold augmentation during tetanic stimulation (Fig. 27B, solid bar labeled C). For example, at 20 seconds into the tetanic train, EJC amplitudes show augmentation decreases of ≤65% in *pgant3* ($p<0.01$, $n=10$) and ≤55% in *pgant35A* ($p<0.01$, $n=11$) mutants. In contrast, the double null mutant is clearly less impaired than either single *pgant* mutant (Fig. 27A,B). At 20 seconds into the tetanic train, the double mutants exhibit a reduced impairment of ≤40% compared to controls ($p<0.05$, $n=11$; Fig. 27C). Following this initial facilitation phase, double mutants reach control levels of augmentation, whereas the single *pgant* mutants remain impaired (Fig, 28A,B), showing a suppressive interaction. Following the tetanic train, potentiation in double mutants is indistinguishable from controls, whereas both single mutants (*pgant3* and *pgant35A*) show strong loss of PTP initiation (Fig. 27B, solid bar labeled D). Quantification shows ≥50% decrease in *pgant3* ($p<0.001$, $n=10$) and ≥35% decrease in *pgant35A* ($p<0.05$, $n=11$) single mutants compared to controls, but no detectable decrease in the double null mutants (Fig. 27D). Thus, *pgant*

mechanisms regulate activity-dependent facilitation, augmentation and potentiation.

Pgants suppressively regulate integrin signaling

Synapses sandwich heavily-glycosylated transmembrane and extracellular proteins that regulate synaptic function and plasticity (Dani and Broadie, 2012). For example, we have previously shown that O-linked heparan sulfate glycosaminoglycans bidirectionally regulate WNT and BMP *trans*-synaptic signaling to modulate neurotransmission strength (Dani et al., 2012). To directly visualize changes in synaptic O-GalNAc glycosylation in *pgant* mutants, we used fluorescently-conjugated VVA-TRITC and HPL-488 lectins to label NMJ terminals (Fig. 28). Non-detergent conditions were used throughout to examine only the glycosylation state of the extracellular synaptomatrix (Dani et al., 2012). Representative images show the halo-like VVA (Fig. 28A, top left) and HPL (Fig. 28A, middle left) labeling surrounding the anti-HRP marked synaptic boutons. In comparison to controls, O-linked glycan expression is very significantly increased in both *pgant3* (31.65±5.61%, n=9, $p<0.01$) and *pgant35A* (58.50±4.39%, n=14, $p<0.01$) single mutants, however there is no significant change in the double mutants (13.54±5.04%, n=6, $p>0.05$) (Fig. 28B). Similarly, quantified HPL labeling is very significantly elevated in both *pgant3* (33.13±6.39%, n=21, $p<0.01$) and *pgant35A* (41.06±7.83%, n=18, $p<0.01$) single mutants, but no significant difference occurs in the double null mutants (7.49±6.85%, n=18, $p>0.05$) compared to controls (Fig. 28B). Thus, two independent approaches highlight the suppressive regulation of synaptic O-GalNAc modification by these

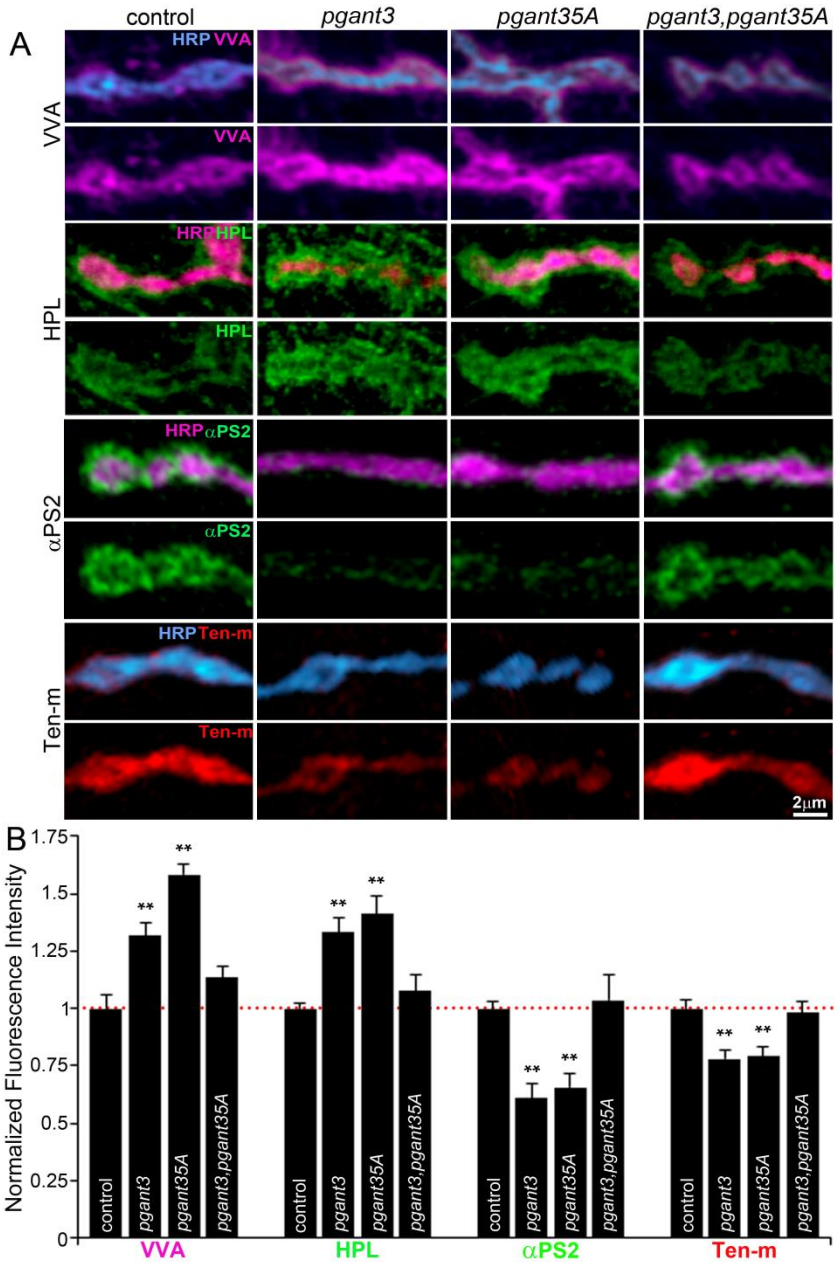

Figure 28. Synaptomatrix O-glycan and integrin signaling defects in *pgant* mutants. (A) NMJ synaptic boutons from control (w^{1118}, left column), *pgant3* ($pgant3^{m1}/pgant3^{m2}$) and *pgant35A* ($pgant35A^{HG8}/pgant35A^{3775}$) single mutants (middle two columns) and the double mutant ($pgant3^{m1},pgant35A^{HG8}/pgant3^{m2},pgant35A^{3775}$; right column) show co-labeling for synaptic O-linked glycosylation markers (VVA and HPL), integrin receptor (αPS2) and transmembrane integrin ligand (ten-m) relative to the presynaptic marker anti-HRP. Scale bar: 2 μm. **(B)** Histograms show fluorescence intensities for all four labels (VVA, HPL, αPS2 and ten-m) normalized to each genetic control (dotted red line). Sample size ≥10 independent NMJs for each label for all four genotypes. Statistical differences calculated using one-way ANOVA with Dunnett's post-test; **p<0.01.

two *pgant* genes.

Studies in non-neuronal tissues have shown that *pgant* mutants misregulate integrin signaling (Zhang et al., 2010). Consistently, we have previously identified pre-/postsynaptically localized Position Specific (PS) integrin receptors at the *Drosophila* NMJ, containing multiple different α and β subunits (Beumer et al., 1999, 2002; Rohrbough et al., 2000, 2007; Rushton et al., 2009). We therefore tested the multiple integrin receptor subunits, including αPS1 (*mew*), αPS2 (*if*), αPS3 (*scab/volado*), βPS (*mys*) (Brower et al., 1984) and β_v (Yee and Hynes, 1993). The two β subunits show an interesting *pgant*-specific change, with βPS increased in *pgant35A* (1.39±0.08, n=14, $p<0.01$) and β_v increased in *pgant3* (1.21±0.03, n=18, $p<0.05$) single mutants, but no significant change of either β subunit in the double mutant (βPS, 1.17±0.64, n=10, $p>0.05$; β_v, 0.91±0.06, n=10, $p>0.05$) normalized to control. Most of the α receptor subunits show no consistent changes in the *pgant* mutants, including αPS1 (*pgant3*, 1.27±0.07, n=18, *pgant35A*, 1.10±0.05, n=18) and αPS3 (*pgant3*, 1.05±0.02, n=8, *pgant35A*, 1.15±0.06, n=12; all $p>0.05$ with respect to control). The sole exception is αPS2, which sharply decreases in both *pgant3* (39.19±6.75%, n=10, $p<0.01$) and *pgant35A* (34.37±5.69%, n=11, $p<0.01$) single right). We next examined a host of characterized integrin ligands for changes in *pgant* single and double mutants (Zhang and Ten Hagen, 2011), including Tiggrin (Fogerty et al., 1994), laminin α subunits LanA (Inoue and Hayashi, 2007) and Wing-blister (Wb) (Martin et al., 1999a), Thrombospondin (Tsp) (Subramanian et al., 2007) and Tenascin (ten-m) (Levine et al., 1994). Most of

these ligands show no consistent changes in *pgant* single and double mutants as compared to control: Tiggrin (*pgant3*, 1.08±0.05, n=11, *pgant35A*, 1.03±0.05, n=14, *pgant3,pgant35A*, 1.07±0.03, n=8, as compared to control, p>0.05), LanA (*pgant3*, 1.25±0.07, n=11, p<0.05, *pgant35A*, 1.16±0.07, n=14, p>0.05, double mutant, 1.00±0.05, n=8, p>0.05), Wb-N terminus (*pgant3*, 1.00±0.05, n=10, *pgant35A*, 1.12±0.03, n=11, double mutant, 1.11±0.04, n=7, all p>0.05), and Tsp (*pgant3*, 1.02±0.07, n=9, *pgant35A*, 1.12±0.06, n=10, double mutant, 1.13±0.05, n=8, p>0.05), all normalized to control. The sole exception was the RGD domain-containing, transmembrane ten-m (Levine et al., 1994). Ten-m localizes in a halo-like ring around HRP-labeled synaptic boutons in controls, but is consistently reduced in both *pgant* single mutants (Fig. 28A, middle). Compared to controls, ten-m levels are very significantly decreased in *pgant3* (21.88±3.47%, n=15, p<0.01) and *pgant35A* (20.84±3.91%, n=16, p<0.01) single mutants, but show no change in double null mutants (Fig. 28A, right). Thus, the two *pgant* genes suppressively downregulate αPS2 integrin/ten-m ligand at the synapse.

Neuronal and muscle pgants regulate O-glycosylation and integrin signaling

To determine if changes in synaptic O–linked glycosylation and *trans*-synaptic ten-m/αPS2 integrin signaling are directed by pre- or postsynaptic *pgant* function, we next tested both *pgant3* and *pgant35A* rescue in neurons and muscle in their respective null mutant backgrounds (Fig. 29). Representative NMJs showing VVA lectin, αPS2 integrin and ten-m ligand labeling are shown for all genotype

conditions in Fig. 29A. Both *pgant3* neuronal (1.02±0.05, n=15) and muscle (1.05±0.05, n=15), as well as *pgant35A* neuronal (1.13±0.03, n=13) and muscle (1.01±0.03, n=22) expression restored VVA lectin labeling to control levels (1.00±0.03, n=18; Fig. 29B). Similarly, αPS2 integrin abundance is also rescued with *pgant3* neuronal (0.94±0.05, n=19) or muscle (0.99±0.06, n=20) expression, as well as *pgant35A* neuronal (0.90±0.04, n=21) or muscle (0.86±0.04, n=25) expression, as compared to control (1.00±0.03, n=20; Fig. 29B). Interestingly, only neuronal *pgant3* (0.99±0.04, n=10) and *pgant35A* (0.97±0.04, n=8) expression could restore synaptic ten-m levels to control levels (1.00±0.03, n=21), whereas muscle *pgant3* (0.88±0.04, n=17, $p<0.05$) and *pgant35A* (0.82±0.03, n=14, $p<0.01$) remained significantly decreased normalized to control (Fig. 29B, right panel). Thus, both pre- and postsynaptic *pgant3* and *pgant35A* are sufficient to properly regulate synaptic O-linked glycosylation and integrin levels, but regulation of the ten-m ligand requires *pgant* function in the presynaptic neuron.

Pgants regulate activity-dependent integrin signaling at the synapse

With striking activity-dependent effects on synaptic plasticity in *pgant* mutants, we next queried activity-dependent changes in integrin signaling (Fig. 30) presynaptic activity, followed by confocal microscopy examination for molecular changes at the NMJ synapse. The neuronal driver (*elav-gal4*) (Lin and Goodman, 1994b) was used to target UAS-CHiEF-tdTomato (Wang et al., 2011) in genetic control, single and double mutants. Channelrhodopsin targeting was confirmed by visualizing tdTomato expression (Fig. 30A) and eliciting evoked junctional

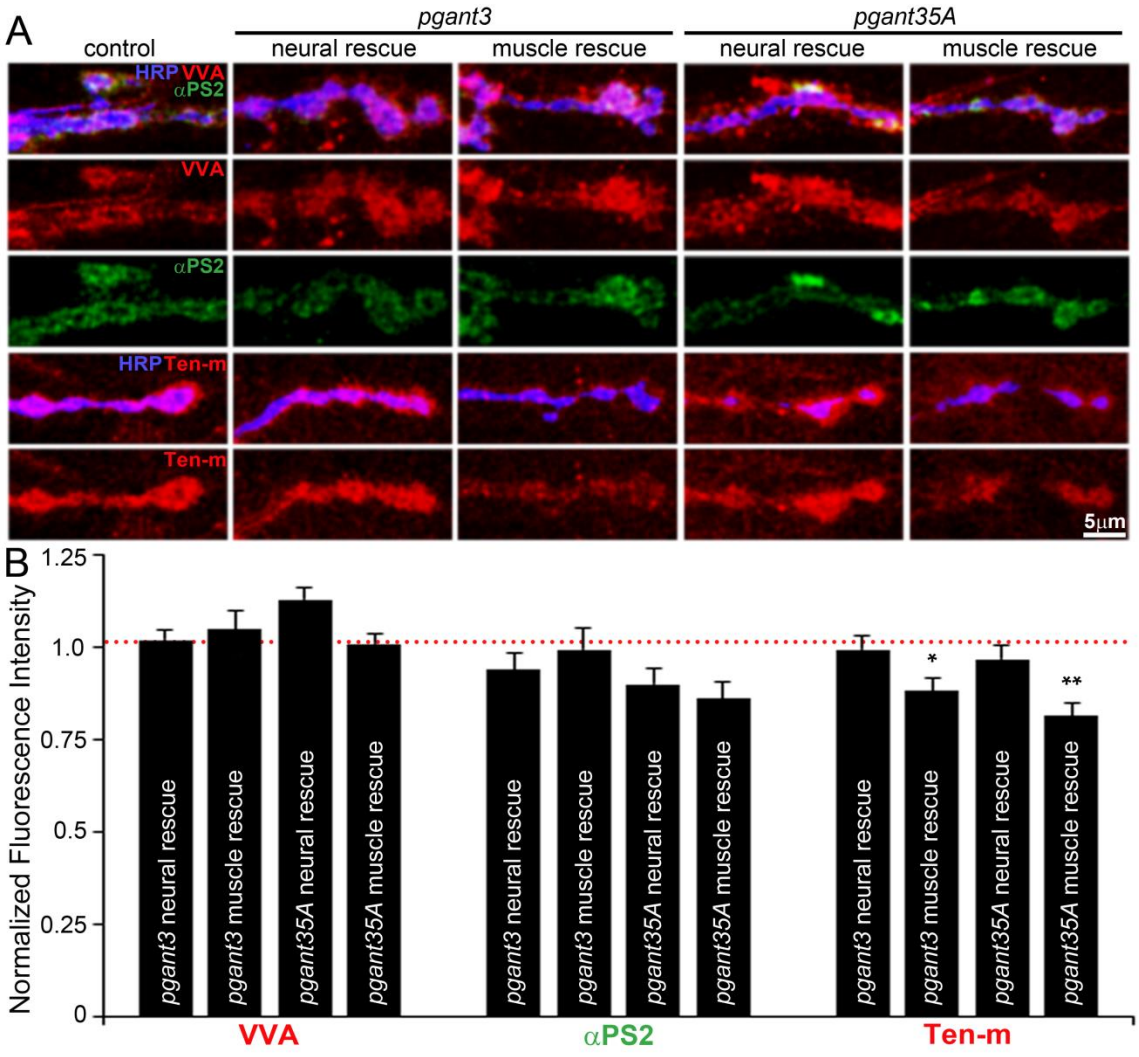

Figure 29. Pre/postsynaptic *pgant3/35A* regulate O-GalNAc and integrin signaling. (A) NMJ synaptic boutons co-labeled for synaptic O-linked glycosylation marker (VVA), integrin receptor (αPS2) (top three panels) and ten-m relative to the presynaptic marker anti-HRP (bottom two panels), with split channels shown for clarity. The five genotypes shown include genetic control (*w*^{1118}), neuronal (*pgant3*^{m1}/*pgant3*^{m2}; *UAS-pgant3/elav*) and muscle (*pgant3*^{m1}/*pgant3*^{m2}; *UAS-pgant3/24B) pgant3* expression, and neuronal (*pgant35A*^{HG8}/*pgant35A*^{3775}; *UAS-pgant35A/elav*) and muscle (*pgant35A*^{HG8}/*pgant35A*^{3775}; *UAS-pgant35A/24B) pgant35A* expression conditions. Scale bar: 2 μm. **(B)** Histograms showing the relative fluorescence intensities for all three labels (VVA, αPS2 and ten-m) normalized to each genetic control (dotted red line). Sample size ≥8 independent NMJs for each label for all five genotypes. Statistical differences calculated using one-way ANOVA with Dunnett's post-test; *p<0.05, **p<0.01.

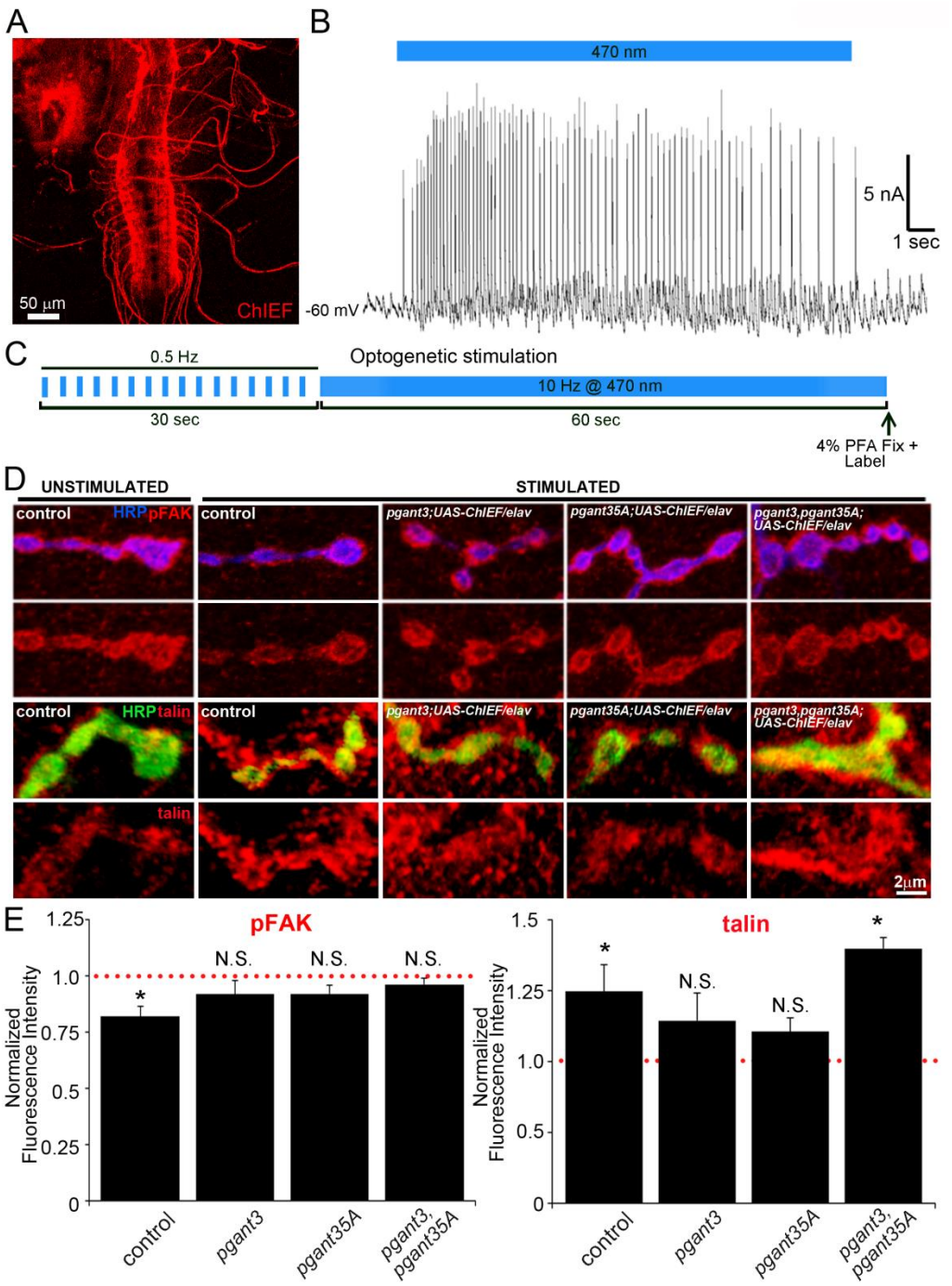

Figure 30. Activity-dependent integrin signaling changes in *pgant* mutants. **(A)** Representative image of neurally-targeted (*elav*-gal4) channelrhodopsin expression (ChIEF-tdTomato) in third instar ventral nerve cord. The native fluorescence of the tagged light-activated channel (red) is shown without amplification. Scale bar: 50 μm. **(B)** Representative evoked junctional potential (EJP) trace from the muscle 6 NMJ induced by blue light (470nm) stimulation of ChiEF-expressing neurons. **(C)** Schematic of the optogenetic stimulation paradigm used to assay changes in integrin signaling. Basal stimulation at 0.5 Hz

for 30 seconds to establish baseline, followed by 10 Hz blue light pulses for 60 seconds to induce-activity-dependent changes. Samples were then immediately fixed and labeled for analyses. **(D)** Representative images of pFAK (top) and talin (bottom) labeling, with HRP co-labeling, showing split channels to compare unstimulated control (left) and light-stimulated (10Hz, 60 seconds) synaptic boutons. The genotypes are ChIEF-expressing control (w^{1118}; *UAS-ChIEF/elav-gal4*, top), *pgant3* ($pgant3^{m1}/pgant3^{m2}$; *UAS-ChIEF/elav*) and *pgant35A* ($pgant35A^{HG8}/pgant35A^{3775}$; *UAS-ChIEF/elav-gal4*) single mutants (middle two rows), and the double mutant ($pgant3^{m1}$, $pgant35A^{HG8}/pgant3^{m2}$,$pgant35A^{3775}$; *UAS-ChIEF/elav-gal4* (far right). **(E)** Histograms show relative fluorescence intensities of pFAK (left) and talin (right) normalized to genetic control for all four genotypes. Sample size $\geq$8 independent NMJs for each label and condition for all genotypes. Statistics calculated using one-way ANOVA with Dunnett's post-test; *p<0.05.

potentiations (EJPs) with 5 Hz blue light (λ=460 nm, 60 ms duration) stimulation (Fig. 30B). Guided by the plasticity stimulation paradigm (Fig. 27), preparations were illuminated with 60 ms light pulses at 10 Hz for 60 seconds, then immediately fixed for imaging (Fig. 30C). VVA-TRITC O-GalNac labeling did not detectably change in unstimulated controls compared to optogenetically-stimulated preparations (*pgant3,* 1.09±0.04, *pgant35A,* 1.09±0.03, double mutant, 0.96±0.04 as normalized to controls, n≥13, all p>0.05). Similarly, we observe no change in levels of integrin ligand ten-m (*pgant3,* 1.00±0.04, *pgant35A*, 1.02±1.04, double mutant, 1.14±0.05, n≥17, all p>0.05) or integrin receptor αPS2 levels (*pgant3,* 0.94±0.04, *pgant35A,* 0.88±0.04, double mutant, 0.84±0.07 as normalized to controls, n≥8, all p>0.05). We therefore investigated integrin downstream signaling by assaying talin and pFAK abundance (Devenport et al., 2007; Tsai et al., 2012a).

To determine if activity-dependent integrin signal transduction is affected, we investigated channelrhodopsin-dependent changes in Talin recruitment and downstream pFAK production (Fig. 30D). Interestingly, when compared to respective unstimulated genotype controls, optogenetic stimulation drives a striking increase in Talin levels in both control (49.41±18.96%, n=8 p<0.05) and *pgant* double mutants (80.1±7.93%, n=13, p<0.05) compared to unstimulated conditions, whereas neither *pgant3* nor *pgant35A* single mutants showed any significant activity-dependent change in Talin recruitment to the synapse (Fig. 30D, bottom row; Fig. 30E, left panel). Moreover, we find an activity-dependent decrease pFAK levels in stimulated controls (*UAS-CHIEF/elav*, 17.85±4.23%,

n=49, p<0.05), with no change in stimulated *pgant3* (*pgant3^{m1}/pgant3^{m2}; UAS-CHIEF/elav* 8.15±6.28%, n=43, p>0.05), *pgant35A* (*pgant35A^{HG8}/pgant35A^{3775}; UAS-CHIEF/elav* 7.76±3.94%, n=61, p>0.05) and double mutant *pgant3,pgant35A* (*pgant3^{m1}*, *pgant35A^{HG8}/pgant3^{m2},pgant35A^{3775}; UAS-CHIEF/elav,* 3.61±2.61%, n =27, p>0.05) conditions (Fig. 30D top row; Fig. 27E, right). We conclude that both integrin recruitment of talin and downstream production of pFAK is activity-dependent and under *pgant*-dependent suppressive regulation.

Pgants regulate activity-dependent postsynaptic pocket size

Misregulated integrin signaling leads to intercellular de-adhesion and subsequent wing blistering in *pgant* mutant wing discs (Zhang et al., 2010). Moreover, mutants in *trans*-synaptic WNT/BMP and HSPG extracellular pathways manifest enlarged postsynaptic pockets at the NMJ (Packard et al., 2002; Kamimura et al., 2013). As we have shown that *pgant* mutants suppressively regulate basal and activity-dependent integrin signaling and postsynaptic pocket expansion, we next examined optogenetic activity-dependent synaptic ultrastructural changes, with a particular focus on the postsynaptic pocket. In the above channelrhodopsin-expressing mutants and controls, we adopted the same light stimulation paradigm, followed by fixation and transmission electron microscopy examination of synapse ultrastructure (Fig. 31).

In optogenetically-stimulated synaptic terminals, there is an obvious decrease in SV density in all four genotypes compared to unstimulated controls

(Fig. 31A). At <250 nm away from the active zone, quantification of SV number shows a ~30% decrease in controls, and a similar ~30% decrease in stimulated *pgant3* mutants (n=13, p<0.001 compared to unstimulated condition; Fig. 31B). Both the *pgant35A* single mutant (n=19) and the double null mutant (n=16) behave similarly. Further, there are no significant differences in suppressive regulation under basal conditions (Fig. 24) or unstimulated UAS-ChIEF carrying lines (Fig. 31) i.e. single mutants (*pgant3*^{m1}*/pgant3*^{m2}, 15.22±0.99 vesicles; *pgant35A*^{HG8}*/pgant35A*^{3775}, 15.54±0.78; p<0.05) are elevated compared to control (*w*^{1118}, 10.5±0.91) and the double mutant (*pgant3*^{m1},*pgant35A*^{HG8}*/ pgant3*^{m2},*pgant35A*^{37758}*,* 9.4±0.67). Similarly, in unstimulated single mutants carrying the channelrhodopsin transgene, synaptic vesicles are elevated (*pgant3*^{m1}*/pgant3*^{m2}*; UAS-CHIEF/elav*, 9.53±0.63;, p<0.01; *pgant35A*^{HG8}*/pgant35A*^{3775}*; UAS-CHIEF/elav*, 8.95±0.49, p<0.05) with respect to control (*UAS-CHIEF/elav*, 7.13±0.57) and double mutant (*pgant3*^{m1},*pgant35A*^{HG8}*/pgant3*^{m2},*pgant35A*^{3775}*; UAS-CHIEF/elav*, 7.68±0.39). Thus, activity drives SV cycling in all four genotypes comparably (Fig.32B). In contrast, optogenetically-stimulated control NMJ synapses show an activity-dependent increase in PSP depth that does not occur in either *pgant3* and *pgant35A* single mutant, although the double mutant is indistinguishable from control (Fig. 31A, dotted lines). Quantification of these differences reveal an activity-dependent PSP depth increase of >50% in control (p<0.05 compared to unstimulated condition) and ~35% increase in the double null mutants (n=14, p<0.05), but no significant change in either single *pgant* mutant (Fig. 31C).

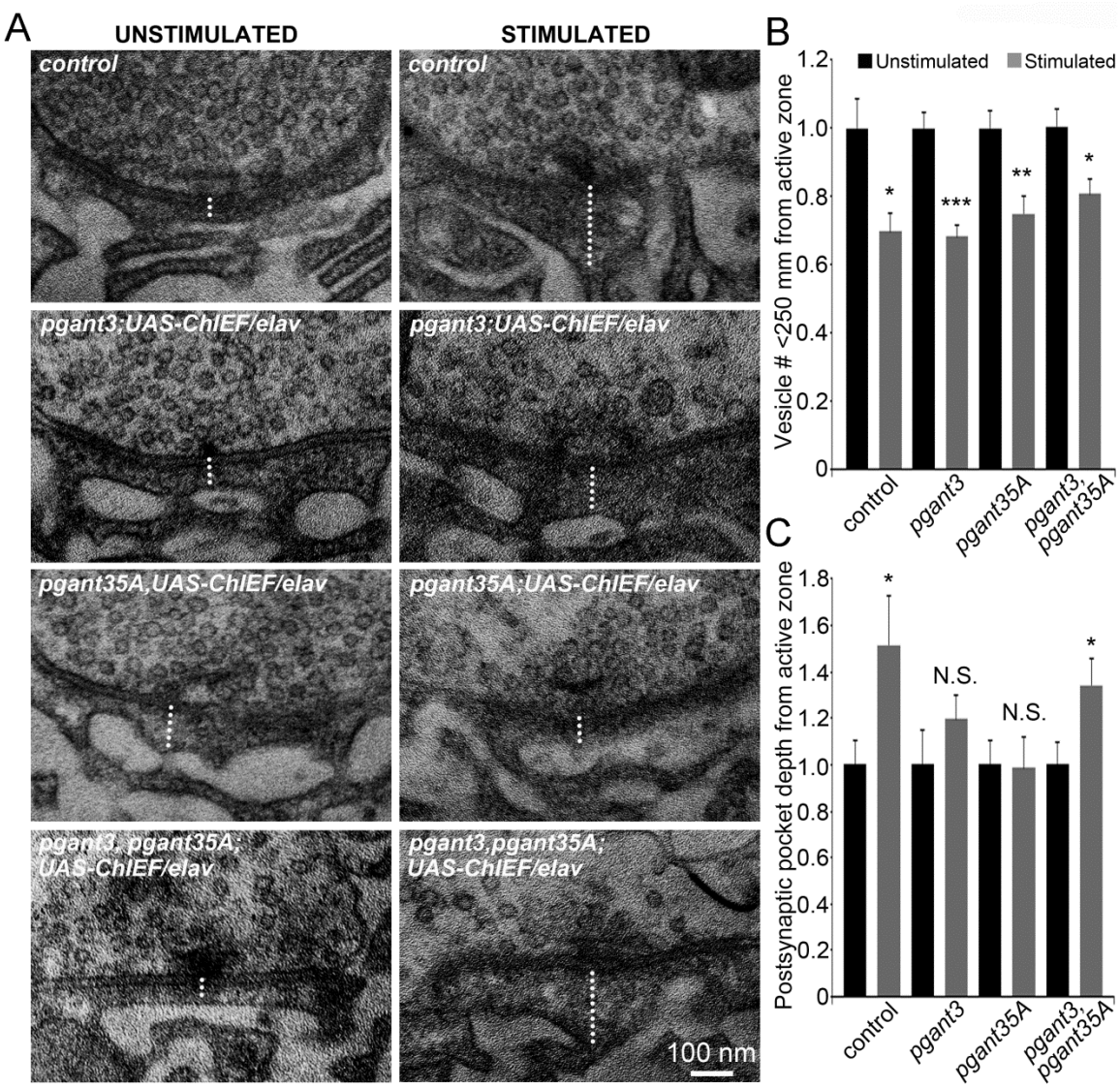

Figure 31. Activity-dependent changes in synapse ultrastructure in *pgant* mutants. (A) Representative active zone synapses of control (w^{1118}; *UAS-ChIEF/elav-gal4*, top), *pgant3* ($pgant3^{m1/m2}$; *UAS-ChIEF/elav*) and *pgant35A* ($pgant35A^{HG8/3775}$; *UAS-ChIEF/elav-gal4*) single mutants (middle two rows) and double mutant ($pgant3^{m1}$, $pgant35A^{HG8}$/$pgant3^{m2}$,$pgant35A^{3775}$; *UAS-ChIEF/elav-gal4*, bottom), comparing the unstimulated (left column) and light-stimulated (10Hz, 60 seconds; right column) conditions. Dotted white line indicates postsynaptic pocket (PSP) depth for each condition and genotype. Scale bar: 100 nm. **(B, C)** Histograms showing quantification of activity-dependent changes for normalized synaptic vesicle number **(B)** and PSP depth **(C)** for all four genotypes under stimulated (black bars) and unstimulated (gray bars) conditions. Sample size $\geq$15 independent boutons for each genotype and condition. Statistical differences calculated using one-way ANOVA with Dunnett's post-test; *p<0.05, **p<0.01, ***p<0.001, N.S. indicates no significance.

Further, comparing basal genotypes with unstimulated ChIEF carrying controls and mutants show no significant difference in PSP depth. For controls (w^{1118}, 120.47±7.46 nm, n=12 vs. unstimulated control, 147.41±15.69 nm, n=14, p>0.05), single mutants (*pgant3*, 272.36±45.83 nm, n=13 vs. unstimulated *pgant3*, 253.26±37.70 nm, n=14, p>0.05; *pgant35A*, 246.84±46.63 nm, n=12 vs. unstimulated *pgant35A*, 232.97±24.88 nm, n=15, p>0.05) and the double mutant *(pgant3,pgant35A*, 182.13±23.76 nm, n=14 vs. unstimulated *pgant3,pgant35A*, 227.31±18.56 nm, n=25, p>0.05). Thus, presynaptic vesicle number decreases in all genotypes with acute optogenetic stimulation, but *pgants* suppressively regulate activity-dependent postsynaptic pocket expansion, consistent with the dysregulated integrin-mediated signaling.

Integrin inhibition blocks activity-dependent synaptic plasticity in *pgant* mutants

We have previously shown that blocking integrin signaling with RGD peptides interferes with synaptic plasticity at the *Drosophila* NMJ, comparably to integrin mutations (Bahr et al., 1997; Rohrbough et al., 2000). Further, the ten-m integrin ligand that is found to be suppressively regulated by pgants, contains an RGD sequence. Hence, as a direct test of integrin signaling requirements in *pgant*-dependent facilitation, augmentation and potentiation phases of tetanic stimulus train induced synaptic plasticity, we utilized RGD integrin inhibitory peptides and scrambled RAD controls in the genetic background control, *pgant* single mutants and the double mutant (Rohrbough et al., 2000). Using our established protocols for peptide incubation (Rohrbough et al., 2000), we

recorded EJCs using the same stimulation paradigm employed above (Fig. 24). Recordings were normalized to the mean basal EJC amplitude in sham/RGD/RAD-treated controls (Fig. 32A), *pgant3* (Fig. 32B) and *pgant35A* (Fig. 32C) single mutants, and *pgant3,pgant35A* (Fig.33D) double mutants. Consecutive EJCs were averaged during the 0.5Hz and 10Hz stimulation phases, respectively, for data presentation and quantification.

In RGD compared to RAD-treated control (w^{1118}) synapses, a >50% elevation occurs in synaptic augmentation during the tetanic stimulus train, and >30% increase occurs in PTP following stimulation (Fig. 32A). In striking contrast, *pgant* single and double mutants show a synergistic interaction with integrin blockade to exhibit a loss of both phases of activity-dependent plasticity (Fig. 32B-D, left). Quantification of EJC amplitudes during the tetanic phase shows a significant increase in RGD-treated compared to RAD-treated control synapses ($p<0.05$, $n\geq9$; Fig. 32A, right). However, EJC amplitudes actually decrease ~60% in *pgant3* ($p<0.05$, $n\geq9$; Fig. 32B, right), *pgant35A* ($p<0.05$, $n\geq6$; Fig. 32C right) and *pgant3,pgant35A* ($p<0.05$, $n\geq4$; Fig. 32D) following RGD treatment. During PTP phases, RGD-treatment again causes a highly significant EJC amplitude increase compared to RAD-treated controls ($p<0.05$, $n\geq9$; Fig. 32A right). Remarkably, RGD-treatment instead causes >50% decreases in *pgant3* ($p<0.05$, $n\geq9$; Fig. 32B), *pgant35A* ($p<0.05$, $n\geq6$; Fig. 32C) and *pgant3, pgant35A* mutants ($p<0.05$, $n\geq4$; Fig. 32D), compared to RAD-treated synapses. Importantly there are no significant differences between RAD-treated synapses and sham controls(Fig. 32A-D). We conclude that integrin signaling blockade

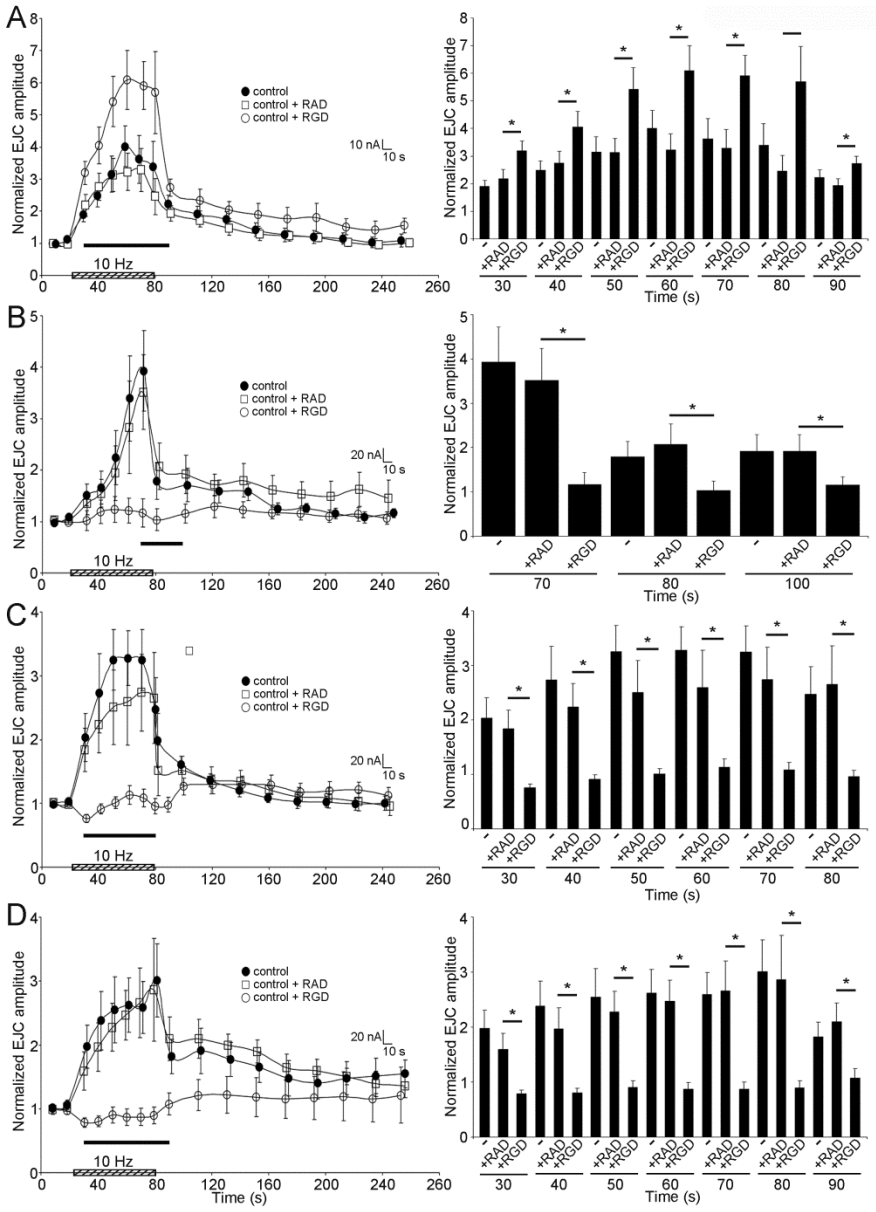

Figure 32. Integrin inhibition blocks all synaptic plasticity in *pgant* mutants. TEVC recordings from sham treated, RAD control and RGD integrin-blocking peptide applications in genetic control (w^{1118}, **A**), *pgant3* ($pgant3^{m1}/pgant3^{m2}$, **B**) and *pgant35A* ($pgant35A^{HG8}/pgant35A^{3775}$, **C**) single mutants, and the double mutant ($pgant3^{m1}$, $pgant35A^{HG8}/pgant3^{m2}$,$pgant35A^{3775}$, **D**). Left column: The stimulation paradigm is indicated on the X-axis with EJC amplitudes normalized to the basal EJC amplitude in each condition for sham control (solid circle), RAD control (hollow square) and integrin-blocking RGD (hollow circle) peptide applications. Right column: Histograms show normalized EJC amplitudes for sham/RAD/RGD peptide treatments for the indicated time-periods. Samples size: ≥5 independent NMJs for each genotype and treatment condition (>60 recordings total). Statistical differences calculated using one-way ANOVA with Dunnett's post-test; *p<0.05.

coupled to the loss of *pgant* function causes a complete loss of activity-dependent facilitation, augmentation and potentiation, consistent with a requirement of *pgant* activity in integrin-mediated functional synaptic plasticity.

Discussion

Across species, glycans are increasingly being recognized as key regulators of synaptic function and plasticity (Dani and Broadie, 2012; Scott and Panin, 2014). Classically, Gal(β1,4)GlcNAc, Gal(β1,3)GalNAc, CT carbohydrate antigen, heparin, heparan sulfate and sialic acid are all known to modulate the *trans*-synaptic agrin signal mediating postsynaptic acetylcholine receptor stabilization at mammalian NMJs (Wallace, 1990; Parkhomovskiy et al., 2000). Similarly, the *Drosophila* Mind-the-Gap (Mtg) glycan-binding lectin regulates the stabilization/organization of postsynaptic glutamate receptors and establishes the extracellular matrix-integrin interface at the NMJ (Rohrbough et al., 2007; Rushton et al., 2009). Other *Drosophila* glycan regulating genes including sialyltransferase (DSiaT), sialic acid transporter Fuseless (Fusl) and UDP-GlcNAc:α-3-D-mannoside-β1,2-N-acetylglucosaminyl-transferase I (Mgat1) also modulate ion channels, pre/postsynaptic organization and neurotransmission strength at the NMJ (Long et al., 2008; Repnikova et al., 2010). Our RNAi glycogene screen recently identified a pair of genes (*hs6st* and *sulf1*) that regulate HSPG sulfation state to modulate the bidirectional *trans*-synaptic WNT/BMP signaling driving pre/postsynaptic assembly and synapse function (Dani et al., 2012; Parkinson et al., 2013). Another gene pair, *pgant3* and *pgant35A*, catalyzing early steps of mucin O-glycan (GalNAcα1-O-S/T)

posttranslational modification as N-acetylgalactosaminyl transferases (Schwientek et al., 2002; Ten Hagen et al., 2003b), was identified to have neurotransmission effects in the same screen.

In *Drosophila*, *pgant3* is characterized to regulate integrin-ligand secretion and intercellular adhesion, and *pgant35A* for appropriate intercellular septate junction formation (Tian and Ten Hagen, 2007; Zhang et al., 2008). Microarray analyses have identified *pgant3* and *pgant35A* transcripts in the developing nervous system and musculature (Tian and Ten Hagen, 2006; Chintapalli et al., 2007), and our lectin analyses show NMJ O-GalNAc modifications dependent on both *pgant3* and *pgant35A*. Null mutants display increased presynaptic active zone *bruchpilot* (*brp*, ELKS/CAST) and postsynaptic glutamate receptor *bad reception* (*brec*, GluRIID) assembly (Featherstone et al., 2005; Wagh et al., 2006), and elevated evoked neurotransmission strength, and genetic rescue experiments show *pgant3* and *pgant35A* function both in neurons and muscle. All synaptic defects occurring in single *pgant* nulls are absent in double mutants, which are largely indistinguishable from controls. Similar observations have been described as ‘co-repression’ and ‘reciprocal suppression’ in the context of transcriptional regulation and physically interacting proteins, respectively. However, as the basis of the *pgant3*/*pgant35A* interaction is as yet unknown, we have opted here for the conservative ‘suppression’ genetic interaction definition. This suppressive regulation presumably arises from balanced *pgant3*/*pgant35A* function. Consistently, when a single wildtype transgene (*UAS-pgant3*) is expressed (pre- or postsynaptically) in the double mutant (*pgant3,pgant35A*), the

other mutant phenotype (*pgant35A*) re-emerges. Moreover, overexpression of either *pgant3* or *pgant35A* individually in neuron or muscle decreases neurotransmission strength, which is the opposite consequence of single loss-of-function. These results reveal a *pgant3/pgant35A* suppressive mechanism dependent on the balance between these two genes on both sides of the synapse.

The *pgant* suppressive mechanism regulates synaptic ultrastructural organization, including presynaptic vesicle pools and postsynaptic pocket size. Like other synaptic phenotypes, postsynaptic pocket size is elevated in single *pgant3/pgant35A* mutants, but normal in double mutants. Importantly, postsynaptic pocket compartments apposed to presynaptic active zones are expanded in *trans*-synaptic WNT/BMP signaling ligand mutants (Packard et al., 2002; Tian and Ten Hagen, 2007; Ren et al., 2009; Nahm et al., 2010; Kamimura et al., 2013) as well as mutants affecting extracellular HSPG regulators of *trans*-synaptic signaling (Packard et al., 2002; Tian and Ten Hagen, 2007; Ren et al., 2009; Nahm et al., 2010; Kamimura et al., 2013). Consistently, we identified the *trans*-synaptic ten-m/αPS2 integrin signaling pair (Mosca et al., 2012) to be suppressively regulated by the *pgant3*/*pgant35A* mechanism. Ten-m/αPS2 integrin interactions are known to drive intercellular adhesion (Graner et al., 1998), and *pgant3* is known to regulate integrin-ligand secretion and promote adhesion in the developing *Drosophila* wing (Zhang et al., 2010). At the *Drosophila* NMJ, both ten-m ligand and αPS2 integrin are localized pre- and postsynaptically (Mosca et al., 2012). Based on these extensive established

interactions, we interpret the enlarged PSP in *pgant3* and *pgant35A* single mutants to a consequence of impaired ten-m/integrin signaling. As the spacing between pre- and postsynaptic membranes is not affected, and normally apposed pre-/post-synaptic membranes occur with enlarged PSPs, we consider this to be a postsynaptic defect. This is not surprising as αPS2/ten-m are both transmembrane proteins, and integrin signaling is well known to bridge to the cytoskeleton (Delon and Brown, 2007). Thus, an enlarged PSP can manifest on the inside of the postsynaptic membrane due to impaired integrin signaling. The levels of ten-m and αPS2, as well as postsynaptic pocket size, are all suppressively regulated by the *pgant3*/*pgant35A* mechanism.

Synaptic O-GalNAc abundance is likewise suppressively regulated by *pgant3* and *pgant35A*, with levels elevated in single mutants and normal in double mutants. Like mammalian pgants (GalNAc-Ts or ppGalNAcTs), *Drosophila* pgants (12 total) are thought to function hierarchically, competing for naked or glycosylated substrates to regulate final O-GalNAc density (Ten Hagen et al., 2003a). The observed suppressive mechanism suggests *pgant3* and *pgant35A* may function at the same tier of glycosylation. Alternatively, with the imbalance induced by *pgant* mutations, other *pgant* family members may be dysregulated, leading to increased O-GalNAc synaptic glycosylation. Normally Golgi-resident *pgants* relocated to the ER are known to increase O-GalNAc glycosylation (Gill et al., 2010), dependent on Src activation downstream of integrin signaling (Mitra and Schlaepfer, 2006), which is misregulated in *pgant* mutants. In addition to well-described α/β-integrins functions at the mammalian

NMJ, α3 integrin affects hippocampal dendrite stability and function (Kerrisk et al., 2013), whereas β3 integrin associates with GluA2 AMPA receptors (Pozo et al., 2012). In *Drosophila*, we have shown that αPS1-3 and βPS regulate synapse assembly and neurotransmission strength (Beumer et al., 1999; Rohrbough et al., 2000), agreeing with *pgant* roles shown here in presynaptic vesicle pool and postsynaptic glutamate receptor regulation. In synaptic plasticity, α3/5/8 and β1 integrin knockdown all impair hippocampal long term potentiation (LTP) (Chan et al., 2003, 2006). Similarly, *Drosophila* αPS3 (*Volado*) and βPS mutants show impaired augmentation and post-tetanic potentiation (PTP) (Rohrbough et al., 2000), agreeing with *pgant* roles shown here in maintaining both plasticity phases. In addition to the joint ten-m/αPS2 downregulation in *pgant3* and *pgant35A,* each mutant also displays distinct misregulation of integrin signaling components (β_v and βPS, respectively), with roles in neurotransmission and synaptic plasticity (Rohrbough et al., 2000; Tsai et al., 2012a; Tran and Ten Hagen, 2013).

All phases of synaptic plasticity (facilitation, augmentation and potentiation) are suppressively regulated by *pgant3* and *pgant35A*. To investigate mechanisms of these activity-dependent changes, we employed optogenetic stimulation to test acute subcellular ultrastructure and integrin signaling effects (Fenno et al., 2011). Classical studies coupling traditional electrical nerve stimulation to ultrastructural analysis at frog NMJ revealed dynamic vesicle fusion after single stimuli (Heuser and Reese, 1981) and vesicle depletion after a prolonged train of 10 Hz stimulation (Ceccarelli et al., 1972). Recent studies

using channelrhodopsin (ChIEF) optogenetic stimulation identified an ultrafast endocytic mechanism at the *C. elegans* NMJ (Watanabe et al., 2013a), which was subsequently validated in hippocampal synapses (Watanabe et al., 2013b), but did not assay effects on vesicle pools. Utilizing the same ChIEF optogenetic tool in *Drosophila*, we find that a brief, high frequency light train (10Hz 60ms pulses for 60 seconds) drives a depression of vesicles in distinct pools around presynaptic active zones. We also find activity-dependent expansion of postsynaptic pockets in controls, which fails in both *pgant* single mutants but is restored in double mutants, again showing a suppressive mechanism. Consistently, we identify suppressive activity-dependent elevation of integrin downstream talin signaling in only control and double mutant conditions, supported by known roles of talin-mediated αPS2 integrin signaling (Devenport et al., 2007). Moreover, we find a lack of activity-dependent pFAK regulation, supported by previous studies showing activity-dependent decreases in pFAK signaling at the *Drosophila* NMJ (Tsai et al., 2012a). Importantly, RGD treatment perturbing integrin-signaling and synaptic plasticity, also alters synaptic pFAK levels (Staubli et al., 1998; Rohrbough et al., 2000; Russo et al., 2013). Consistent with this mechanism, RGD treatment acts synergistically with *pgant* mutations to prevent the manifestation of a synaptic plasticity.

In summary, this is the first investigation of synaptic *pgant* roles, which combines molecular, electrophysiological, electron microscopy and optogenetic approaches. We identify here a novel suppressive mechanism between two *pgant* family members (*pgant3* and *pgant35A*) regulating synaptomatrix O-

GalNAc glycosylation state, coupled presynaptic active zone and postsynaptic glutamate receptor assembly, transmission strength, integrin signaling and synaptic adhesion, and the appearance of activity-dependent plasticity. Future studies will seek to determine whether Ca^{2+} and/or CaMKII signaling mechanisms (Tsai et al., 2012a) are misregulated during *pgant* synaptic dysfunction, as the leading causal link between activity and observed synaptic changes. Based on recent reports that show O-GalNac levels regulate proteolytic cleavage and ligand secretion (Zhang et al., 2014), we will test whether the *pgant* suppressive mechanism may reflect interactions between pgants or within other enzymatic classes. A final priority will be investigation of *pgant*-mediated regulation of disease-related synaptic proteins, including Dystroglycan (Dg) (Henry et al., 2001) and Neurofimbrin (NF1) (Tsai et al., 2012b), to test hypotheses that heritable neurological and neuromuscular disorders are causally related to the *pgant* synaptic mechanisms.

Acknowledgements

We are particularly grateful to Kelly Ten Hagen for *pgant* mutant and transgenic lines (*pgant3*^{m1}, *pgant3*^{m2}, p*gant35A*^{HG8}, *pgant35A*^{3775}*, UAS-pgant3* and *UAS-pgant35A*), Zhuoren Wang for the optogenetic line (*UAS-ChIEF-tdTomato*) and the Bloomington *Drosophila* Stock Center for providing other essential stocks. We also particularly thank the following for essential antibodies; Ron Wides (Ten-m), John Fessler (Tig), Talila Volk (LanA, Tsp), Stephan Baumgartner (Wb-N), Richard Hynes (βv) and the Iowa Hybridoma Bank. This work was fully supported by NIMH grant MH096832 to K.B.

Chapter V

CONCLUSIONS AND FUTURE DIRECTIONS

The foundation of this work was a genome-level investigation of glycan related genes to identify mechanisms that regulate NMJ structure and function. By transgenic RNAi knockdown, I broadly investigated glycogenes involved in N/O/glycosaminoglycan biosynthesis; such as glycosyltransferases, glycosidases and glycan transporters; and encoding glycan-binding lectins and glycan targeted core-proteins (Fig 34). By validating the primary screen results with a secondary screen and the use of loss of function mutants, I have developed a resource that can guide targeted investigation of glycogenes in various synaptic contexts. Knockdown of 37 genes across the 8 tested groups showed statistically significant differences in morphological development, with 27 that increase synaptic bouton number and 2 that increase branch numbers (Fig 34). These findings suggest that glycans may generally serve as a mechanism to restrict NMJ growth. Knockdown of 13 genes had effects on functional differentiation, with 12 knockdowns showing an increase and only 1 showing a decrease in neurotransmission strength (Fig 34). These findings suggest that glycans generally limit synaptic transmission as well. A further key result is that glycogenes appear to regulate NMJ architecture and function in largely separable mechanisms. In only rare cases does the same glycogene affect both structure and function (Fig 34).

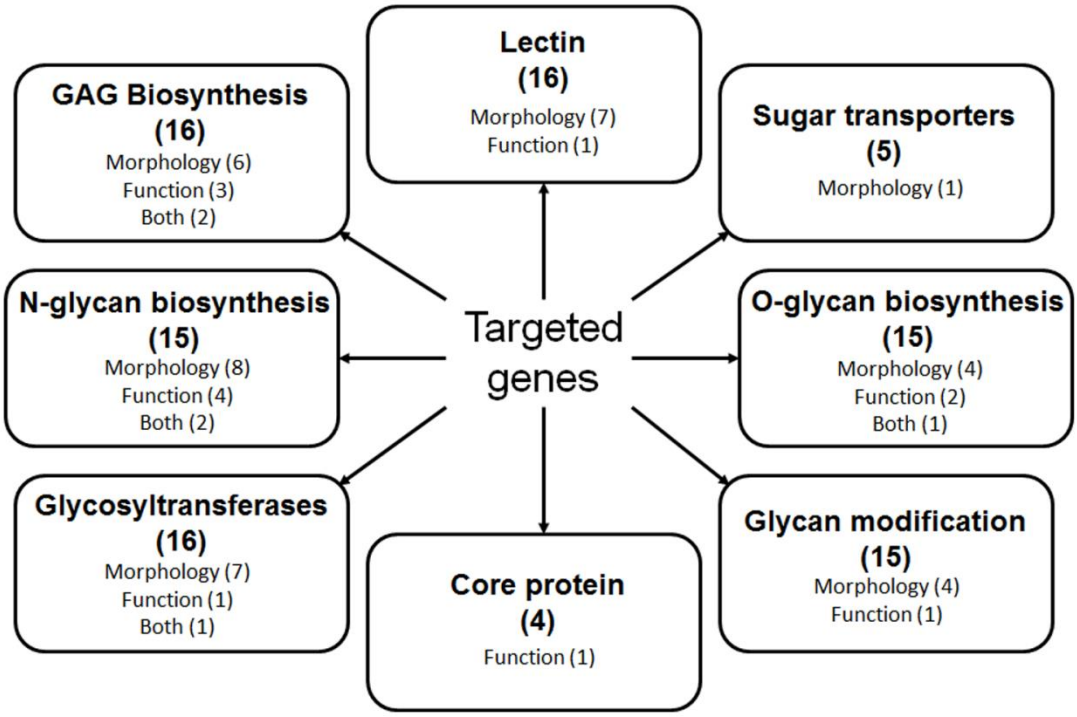

Figure 33. Glycogene screen results. Transgenic RNAi-mediated knockdown of glycogenes in the following gene families (clockwise from top): lectins, sugar transporters, O-glycan biosynthesis, glycan modification, core protein, glycosyltransferases, N-glycan biosynthesis and glycosaminoglycan (GAG) biosynthesis. The total number of genes tested in each glycan family listed in **bold** parentheses. The number of genes that affect NMJ morphology, function or both is indicated in regular parentheses.

All measured parameters of morphology and function are ensemble properties. For example, the comparator used to measure neurotransmission (evoked excitatory junction current; EJC) is a function of action potential propagation, Ca^{2+} influx/sensing, synaptic vesicle cycle, factors limiting neurotransmitter diffusion and postsynaptic responsiveness, among other factors. To pin-point the step specifically regulated by a targeted glycogene requires further analysis of spontaneous release measurements, ultrastructural analysis, FM1-43 dye labeling and measurements of postsynaptic receptor distribution and function, among other analyses. *Post hoc* analysis on collected EJC to assay rise/fall times might reveal altered kinetics. Likewise, morphological parameters quantitated from confocal microscopy can now be subject to further quantification, including subsynaptic reticulum (SSR) architecture, differences in number of mini-boutons to identify immature/newly developing boutons, or inter-bouton distance/clustering that may suggest pre/postsynaptic cytoskeletal defects. Coupling these studies with glycoproteomic, glycotranscriptomic and glycoanalytical approaches will be needed to define the underlying molecular regulation. These studies may also reveal any cross-talk or redundancy between glycogene products, giving us further insight into the emergent hypothesis that glycans largely limit synapse structure and function.

Also tested in the RNAi screen was the characterization of developmental defects caused by neural knockdown of glycogenes. Of the 120 glycan related genes tested, only 17 showed a developmental lethality phenotype (Table IV). Interestingly, the majority (13) showed post-embryonic

	Gene name	Gene function	CG	Vienna ID
Embryonic lethal	Tim8	P-P-bond-hydrolysis-driven protein transmembrane transporter activity	1728	2609
	N/A	alkaline sulfatase	8646	38092
		mitochondrial carrier protein	18022	20580
	vermiform	chitin deacetylase	8756	47128
		N-acetyllactosaminide beta-1,3-N-acetylglucosaminyltransferase activity	11149	7882
		alpha-1,3-mannosylglycoprotein 4-beta-N-acetylglucosaminyltransferase activity	9384	109285
		UDP-galactose:beta-N-acetylglucosamine beta-1,3-galactosyltransferase activity	8668	33156
		Oligosaccharide biosynthesis protein Alg14-like	6308	30273
	nervana	sodium:potassium-exchanging ATPase activity	8863	35904
	α-Man-Ib	mannosyl-oligosaccharide 1,2-alpha-mannosidase activity	11874	101661
	lectin-30A	C-type lectin	17011	107218
	comm3	-	32209	15466
1st instar lethal	Thor	4E-BP	8846	35439
	Mgat1	Alpha-1,3-mannosylltransferase	13431	103609
	myospheroid	BPS integrin	1560	103704
minute lethal/necrotic	Ost48	Oligosaccharyltransferase 48kD subunit	9022	105881
	lethal (2) k12914	dolichyl-diphosphooligosaccharide-protein glycotransferase activity	13393	33166
		Alpha-1,3/1,6-mannosyltransferase ALG2	1291	32116
	OstΔ	Oligosaccharide transferase Δ subunit	6370	107068
		lipase activity	10116	13731
		phospho-N-acetylmuramoyl-pentapeptide-transferase activity	5287	51882
	CG34238		8437	10641
		beta-1,4-mannosyltransferase activity	18012	20580
		alpha-1,2-mannosyltransferase activity	11306	104286
		voltage-gated chloride channel activity	5284	51882
2nd/3rd instar lethal		glycosyltransferase (hexosyl)	14512	108957
pupal lethal		mannosyl-oligosaccharide glucosidase activity	1597	108675
		alpha-1,3-mannosylglycoprotein 4-beta-N-acetylglucosaminyltransferase activity	17173	100347
	lectin-28C	C-type lectin	7106	104801
	Galt	Galactose-1-phosphate uridylyltransferase	9232	100025
		PIG-V	6657	10441

	Gene name	Gene function	CG	Vienna ID
pupal lethal		NADH:ubiquinone oxidoreductase-like, 20kDa subunit	2014	108457
	furrowed	C-type lectin	1500	106656
	Ext2 (sotv)	EXTL2, alpha-1,4-N-acetylhexosaminyltransferase	8433	109949
	GalNAc-T2	polypeptide N-acetylgalactosaminyltransferase activity	6394	105160
	trol	perlecan	33950	24259
	egghead	beta-1,4-mannosyltransferase activity	9659	45160
	meltrin	peptidase/ADAM	7649	102641
	medial glomeruli	UDP-galactose transmembrane transporter activity	5802	103753
	Cuticular protein 50Cb	cuticular protein	6305	30274
	tkv	TGF-beta receptor	14026	105834
		alpha-glucosidase activity	14476	48374
	botv	glucuronyl-galactosyl-proteoglycan 4-alpha-N-acetylglucosaminyltransferase activity	15110	108262
weak animals	lectin-33A	C-type lectin	16834	108412
disfigured non-inflated wings	Stubble	serine type endopeptidase	4316	108455
disfigured wings	Rac1	Small GTPase	2448	109432
hyperactive adults	AGBE	1,4-alpha-glucan branching enzyme activity	33138	108087
wings and eyes deformed		alpha-1,3-mannosylglycoprotein 4-beta-N-acetylglucosaminyltransferase activity	9384	109285
aggressive adult activity	trol	perlecan	33950	22642
extended proboscis	rumi	glucosyltransferase activity	31152	14480
hyperactive, spastic animals	Hex-t1	hexokinase	33102	46574

Table IV. Developmental phenotypes of neural glycogene knockdown

lethality in the 1st instar larval stage (11) or 2nd instar (2), compared to relatively rare embryonic lethality (4). Orthologs of a number of the screen hits are implicated in neurological diseases. For example, mannosyl-oligosaccharide glucosidase (MOGS) was recently identified in congential disorder of glycosylation type IIb (CDG-IIb), which presents with multiple neurological complications (Sadat et al., 2014). Interestingly, the *Drosophila* homolog (CG1597) identified in the screen produced increased NMJ architecture and very significantly elevated neurotransmission with RNAi knockdown. As new glycogene-associated diseases are rapidly being discovered, the screening results from this study may help identify and prioritize disease genes regulating synaptic properties (Table V). Alternatively, screen-derived glycogene targets may be cross-referenced to genome-wide association studies (GWAS) to generate new disease models in genetically malleable systems using newly identified gene disruption tools such as zinc-finger nucleases (ZFNs), clustered regulatory interspaced short palindromic repeat (CRISPR) and transcription activator-like effector nucleases (TALEN) tools (Gaj et al., 2013) .

Synaptic organization of glycans, glycoproteins and proteoglycans

This work has also revealed the spatial organization of a number of glycans/glycoproteins and proteoglycans in the *Drosophila* NMJ. Although this landscape is relatively well studied at vertebrate NMJs, this information is lacking in *Drosophila* (Martin et al., 1999b; Van Vactor et al., 2006; Ren et al., 2009; Parkinson et al., 2013). I have identified glycans, glycan modified

CG	Gene name	molecular dysfunction	Disease	Symptoms	Ref.
1597	-	mannosyl-oligosaccharide glucosidase needed for N-glycosylation	CDG-IIb	Multiple neurologic symptoms	Sadat et al., 2014
4542	xiantuan	dolichyl pyrophosphate Glc1Man9GlcNAc2 alpha-1,3-glucosyltransferase	CDG-Ih	reduced fetal movement	Schollen et al. 2004
11874	Mannosidase Ib	mannosyl-oligosaccharide 1,2-alpha-mannosidase activity	Mental retardation, Autosomal recessive 15	Multiple symptoms	Rafiq et al., 2011
32076	-	α-3 glucosyltransferase	Congenital long QT syndrome	ventricular arrhythmias	Jongbloed et al. 1999
32775	GlcAT-I	galactosylgalactosylxylosylprotein 3-beta-glucuronosyltransferase	TBD	developmental delay	von oettingen et al. 2014
6401	-	GPI-anchor synthesis	Multiple Congenital anomalies - hypotonia - seizures syndrome 2	epilepsy, developmental delay	Kato et al. 2014
6657	PIG-V	mannosyltransferase	Hyperphosphatasia with MRS 1	mental retardation	Krawitz et al. 2010
9232	Galactose-1-phosphate uridyltransferase	UDP-glucose:hexose-1-phosphate uridylyltransferase	Galactosemia	neurologic movement disorders	Lucioni et al. 2014
2135	-	beta glucuronidase	Mucopolysaccharidosis, Type VII	mental impairment	Shipley et al. 1993
6128	α-L-fucosidase	α-L-fucosidase	Fucosidosis	psychomotor retardation	Kousseff et al. 1976
7402	-	N-acetylgalactosamine-4-sulfatase activity	Mucopolysaccharidosis, Type VI	central nervous system defects	Giugliani et al. 2007
33138	1,4-α-Glucan Branching Enzyme	1,4-α-glucan branching enzyme activity	Polyglucosan body disease	CNS/PNS dysfunction	Lossos et al. 1998
32849	Hex-t2	Hexokinase	Charcot-Marie-Tooth disease, Type 4G	Motor/sensory neuropathy	Rogers et al. 2000
9620	neuronally altered carbohydrate	GDP-fucose transmembrane transporter	CDG-IIc	developmental delay	Dauber et al. 2014

Table V. Screen targets associated with neurological disease

glycoproteins/proteoglycans and secreted *trans*-synaptic glycoprotein signals spatially organized in discrete compartments on the extracellular surfaces of synapsing neuron and muscle. I have employed non-detergent conditions for labeling (immunohistochemistry) and visualization (confocal microscopy) of these signals (Chapter 3 and Chapter 4). Importantly, the routinely used anti-horseradish peroxidase (HRP) antibody that is used to mark presynaptic neurons, recognizes α(1,6) and α(1,3) fucose modifications on N-linked glycosylation and shows detergent sensitive spatial organization (Rendic et al., 2010). As routinely visualized under detergent conditions, anti-HRP closely labels the presynaptic bouton membranes. However, under non-detergent conditions I observe a diffuse and wispy anti-HRP pattern extending over a larger area of the muscle. These structures may form trans-synaptic connections, similar to cytoneme in developing wing disc (Roy et al., 2014). It would be of significant interest to determine if cytonemal markers localize to these structures, particularly because classic synaptic genes such as *neuroglian* that are shown to reduce cytoneme-mediated transport are also known to be recognized by anti-HRP (Desai et al., 1994). This approach may identify another mode of synaptic communication in addition to secreted/membrane-bound *trans*-synaptic signaling and neurotransmission.

I have also used fluorescently-labeled lectin proteins that recognize glycans to determine expression patterns at the neuromuscular junction. Many lectins reveal a halo-like domain bounding presynaptic boutons that envelopes presynaptic and postsynaptic regions and can extend well into the muscle,

depending on the particular lectin (for example: VVA, WGA (Fig. 3, Chapter 2). However, other lectin-defined glycans are completely absent from the NMJ synapse (for example: DBA (Fig. 3, Chapter 2), supporting the hypothesis that glycans are differentially expressed with cell-specific roles. Despite these interesting findings, it should be noted that this imaging approach is inherently limited. First, glycans are formed by monosaccharides linked together by glycosidic bonds, while lectin specificity is usually demonstrated by incubation with cognate monosaccharides (Simionescu et al., 1982). It is usually unknown if successively added glycans alter or mask the cognate monosaccharide recognition. Second, lectins are known to be sensitive to the density of the particular glycan, hence sparsely expressed glycans may not be identified at specific lectin concentrations (Godula and Bertozzi, 2012). It is also possible that endogenous lectins may compete with fluorescently tagged exogenous lectin labels. These caveats highlight the need for further investigation with novel tools and suggest guarded interpretation of lectin staining patterns upon glycogene manipulation at synapses and other tissues. These limitations may be partially circumvented by using metabolic labeling with chemically modified glycans, as applied in the zebrafish model system for *in vivo* imaging of membrane-associated glycans through development (Laughlin et al., 2008). However, my preliminary tests with these reagents provided mixed results. Optimizing metabolic labeling, including dosage and appropriate imaging techniques, may allow for better real-time investigation of glycan expression/turnover dynamics.

Overlapping with the extracellular glycan domain are *trans*-synaptic signaling glycoprotein ligands (e.g. WNT and BMP) that reside in a halo-like pattern around NMJ terminals (Fig 14, Chapter 3). Secreted Wg (*Drosophila* WNT- Wingless) is enriched at specific boutons, whereas Gbb (*Drosophila* BMP- glass bottom boat) shows relatively uniform expression pattern (Fig 14, Chapter 3). This differential pattern is not yet understood, but Wg-positive boutons may be sites of imminent morphological growth, or regions of suppressed neural activity as WNTs are actively endocytosed to mediate downstream signaling (Ataman et al., 2008). These differential patterns may also be regulated by heparan sulfate proteoglycan (HSPG) co-receptors, that are known to bind these signals via sulfate glycosaminoglycan side chains (Ren et al., 2009). My results in chapter 3 show that the relative abundance of Wg and Gbb is clearly sensitive to HSPG sulfation state regulated by heparan sulfate-6-sulfotransferases (*hs6st*) and heparan sulfate-6-endosulfatase (*sulf1*). As seen in Fig 35 the sulfation patterns of HSPG glycosaminoglycans (GAG) in the two mutants show an elevation of the GlcNS and the 2SGlcNS levels with complete loss of GlcNAc6S, GlcNS6S and 2SGlcNS6S. Null *sulf1* mutants have GlcNS and 2SGlcNS decreased while 2SGlcNS6s levels are increased, with no changes in GlcNAc6S and GlcNS6S compared to controls (Fig 35). While this may explain the magnitude of Wg and Gbb signal differences, it does not address observed differences in spatial distribution across the NMJ (Fig 13, Chapter 3). This could be addressed by using available HS sulfation-state specific phage display

A

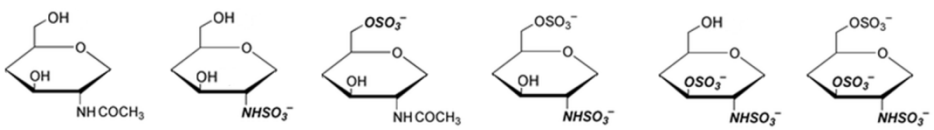

	UAS-GlcNAc	UA-GlcNS	UA-GlcNAc6S	UA-GlcNS6S	UA-2SGlcNS	UA-2SGlcNS6S
hs6st	-	↑	0	0	↑	0
sulf1	-	↓	-	-	↓	↑

B

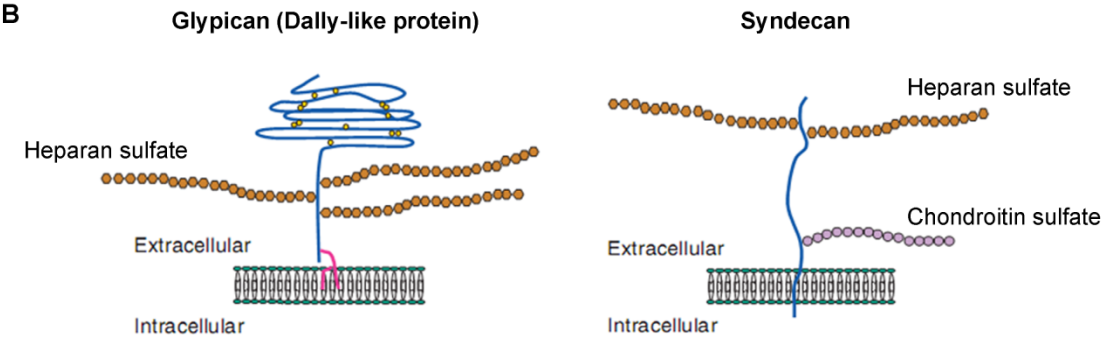

Figure 34. HSPG sulfation in *hs6st* and *sulf1* mutants.(A) Relative abundance of sulfated monosaccharides (top row) of HSPGs in *hs6st* and *sulf1* mutants compared to controls. (B) Model of HSPG Glypican (left) and Syndecan (right). Adapted from Kleinshmit et al. 2013, Deijma et al. 2013 and Johnson et al. 2006.

antibodies to determine overlap of particular sulfation states with Wg/Gbb signal abundance (van Kuppevelt et al., 1998).

Interestingly, we observe differential effects on Dlp and Sdc HSPGs in *sulf1* and *hs6st* mutants. While there is a bi-directional effect on synaptic Dlp levels, which is elevated in *sulf1* and decreased in *hs6st*, Sdc is elevated in both mutant conditions (Fig. 11, Chapter 2). There are at least three differences in the architecture of these HSPGs that may account for this difference. First, Dlp is a glypican that is GPI-anchored to the membrane, while Sdc is a trans-membrane proteins (Bar-Shavit et al., 1996; Chen et al., 2009b) . Secondly, the HS glycosaminoglycan chain is attached relatively close to the membrane in the Dlp glypican, while transmembrane Sdc has HS chains farther from the cell surface (Filmus and Selleck, 2001; Couchman, 2003). Finally, Sdc also bears an additional chondroitin sulfate glycosaminoglycan, and there is potential for antagonistic/synergistic effects of the ligands bound by each of these sulfated glycosaminoglycans (Fig. 34) (Johnson et al., 2006).

Screen-derived target validation using pairs of glycogenes

Drosophila RNAi screens have successfully identified novel gene mechanisms in multiple cellular contexts (Mummery-Widmer et al., 2009; Neely et al., 2010; Pospisilik et al., 2010; Schnorrer et al., 2010). However, unique to my screening approach was the subsequent targeted investigation of gene pairs operating in the same pathway. For the work described in Chapter 3, I focused on one gene pair (*hs6st* and *sulf1*) that catalyzes the transfer and removal of a

single HSPG sulfate group. As a result, I uncover an 'exchange factor mechanism' regulating the availability of *trans*-synaptic Wg signals. Similarly for the work described in Chapter 4, I focused on a second gene pair (*pgant3* and *pgant35A*) that catalyzes the transfer of O-linked GalNAc sugars, and uncover a suppressive mechanism that regulates integrin signaling to neurotransmission strength and plasticity. Neither mechanism would have been identified without these gene pairs being studied in conjunction. Alternative interpretations, testable hypotheses and conclusions for these two mechanisms are outlined in the following sections.

Exchange factor mechanism regulates synaptic WNT signaling

Low-affinity interactions between signaling ligands and glycosaminoglycans have long been known to regulate intercellular signaling (Kjellén and Lindahl, 1991). A classic example is HS glycans that oligomerize Fibroblast Growth Factors (FGF) and also dictate FGF receptor dimerization, activation and cell proliferation (Spivak-Kroizman et al., 1994). Seminal studies in the developing *Drosophila* wing disc similarly show WNT signals are modulated by HSPG Dally and Dlp by virtue of its GAG modification (Lin and Perrimon 1999). This interaction strongly shapes the extracellular WNT morphogen gradient and signaling essential for normal development (Yan and Lin, 2009). It is known that the Dally:Dlp ratio affects the gradient, with Dlp both sequestering and presenting WNT ligands to the cognate dFz2 receptor (Han Lin 2005). Consistent with this HSPG 'exchange factor model' proposed in the developing wing disc, sulfation state regulation by *hs6st*/*sulf1* controls relative Dlp co-

receptor and dFz2 receptor abundance to dictate the corresponding Wg downstream signaling at the NMJ (Figure 35). Through this mechanism, *sulf1* and *hs6st* have opposite effects on dFz2 import, followed by C-terminus cleavage of the receptor for import into the nucleus and subsequent association with mRNP granules (Speese et al., 2012).

Interestingly, working with Sam Friedman, we found that the Dlp co-receptor mechanism also interfaces with the Fragile X mental retardation protein (FMRP) translational regulator (Friedman et al., 2013). Loss of FMRP causes Fragile X Syndrome (FXS), the most common monogenic form

of inherited intellectual disability and autism spectrum disorders (Gatto and Broadie, 2011). The *Drosophila* FXS disease model recapitulates neurological symptoms in the human condition, including both synaptic and behavioral defects (Tessier and Broadie, 2008; Gatto and Broadie, 2011; Kanellopoulos et al., 2012) . In loss of function mutant alleles of *dfmr1* HSPG co-receptor expression at the NMJ is grossly elevated (Dlp, ~90%; Sdc ~50%) (Friedman et al., 2013). Correspondingly, Wg levels are also elevated along with a decrease in intracellular dFz2C levels, consistent with the above 'exchange factor model' model (Fig 36). Importantly, genetic correction of the Dlp levels, in the *dfmr1* mutant background restores all synaptic structural phenotypes. Functional phenotypes include an elevation in neurotransmission strength the *dfmr1* null alleles, is also restored upon genetic correction of the elevated levels of both HSPG co-receptors (Dlp and Sdc) (Figure 32). Independent studies have also identified HSPG transcripts to be FMRP-bound targets via high throughput

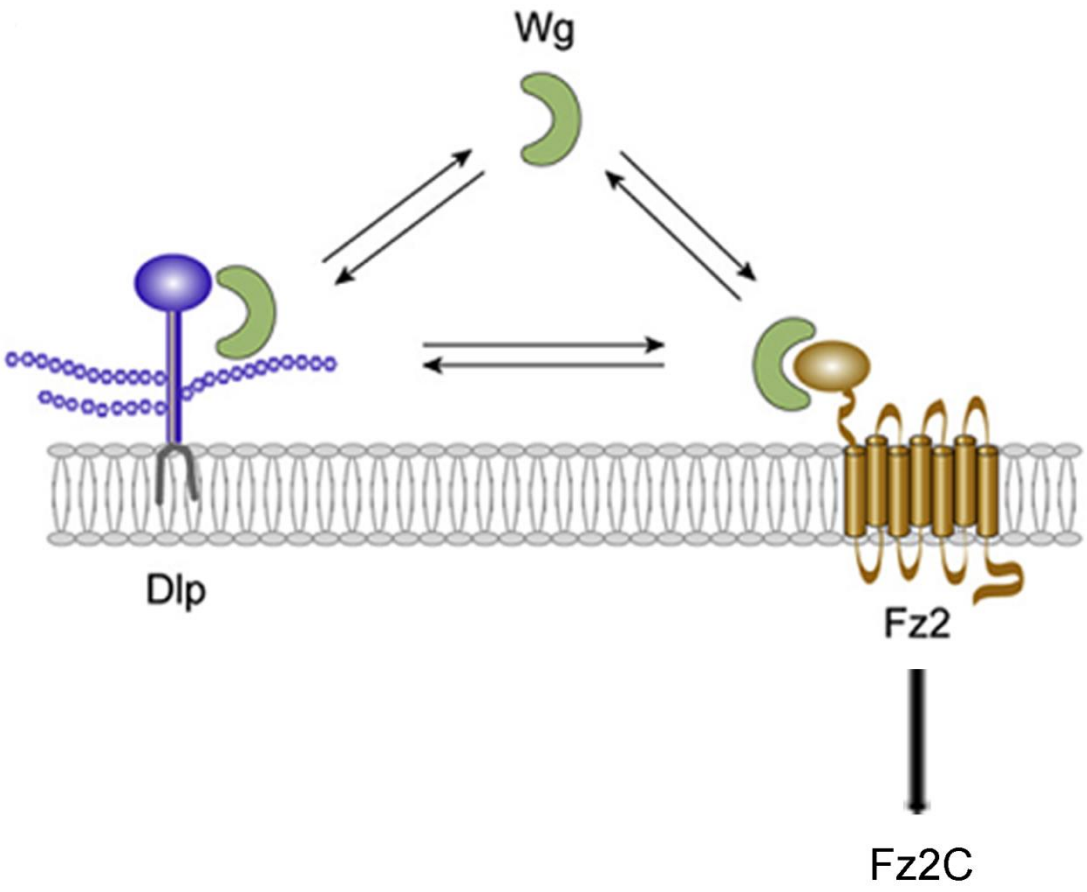

Control	Wg	Dlp	dFz2	Wg signaling (dFz2C)
Sulf1	Wg	Dlp	dFz2	Wg signaling (dFz2C)
Hs6st	Wg	Dlp	dFz2	Wg signaling (dFz2C)

Figure 35. Exchange Factor Model. (A) Exchange Factor Model depicts interaction between heparan sulfate proteoglycan (HSPG) Dally like protein (Dlp), trans-synaptic signal WNT (Wg), cognate receptor Frizzled2 (Fz2) and downstream Frizzled 2 C-terminus (Fz2C). **(B)** Ratio between Dlp and dFz2 dictates level of downstream Wg signaling (dFz2C) levels. Green arrows indicate level of each of the described components while lack of arrows indicate no difference as compared to control.

sequencing of mRNA isolated via crosslinking immunopreciptation (HITS-CLIP) (Darnell et al., 2011). Based on the combination of these results, we propose that HSPG-mediated co-receptor abundance and consequent co-receptor activity can be regulated by HS GAG sulfation and translational mechanisms to regulate synapse structure and function (Friedman et al., 2013).

Non-exchange factor model regulates synaptic BMP signaling

The elevation in the *trans*-synaptic BMP signal Glass bottom boat (Gbb) may not be regulated by the HSPG co-receptor mechanism. Neither Dlp nor Sdc are known to interact with this signaling ligand. Further, unlike the reciprocal regulation of WNT downstream signaling, *hs6st* and *sulf1* mutants exhibit elevated Gbb downstream signaling through phosphorylated Mothers against decapentaplegic (p-MAD) activation (Chapter 3). Altered Gbb signaling has been shown to affect NMJ synaptic morphology (McCabe et al., 2003), and we observe that the morphology parameters of bouton number, branch number and NMJ area are all elevated in both mutant conditions. It is therefore possible that synaptic morphology may be primarily regulated by BMP signaling in non-exchange factor mechanism. Further support for this hypothesis arises from p-MAD dependent downstream regulation of Trio, which has Rho-guanyl nucleotide exchange factor activity (Newsome et al., 2000). Importantly, Trio is known to activate Rac GTPase, which leads to changes in the cytoskeleton and modulation of NMJ growth (Ball et al., 2010). Thus, one model is that increased p-MAD leads to increased transcription of Trio, which in turn positively regulate actin polymerization and NMJ growth. This idea suggests that *sulf1/hs6*st

regulation of Wg and Gbb affect neurotransmission and growth respectively. Alternatively, my data also show elevated and depressed neurotransmission strength in *sulf1* and *hs6st* mutants, while Wg and Gbb levels remain elevated in both. Intriguingly, only when Wg and Gbb are simultaneously reduced in both *sulf1/hs6*st mutants is neurotransmission restored to wildtype levels. This suggests that there may also be a level of cross-talk between the Wg and Gbb signaling pathways. This forms a strong foundation for further investigation of glycan-regulated effects on coordinated WNT/BMP *trans*-synaptic signaling.

Suppressive regulation of O-glycosylation, neurotransmission and plasticity

In the second phase of this work (Chapter 4), I investigate synaptic O-linked glycosylation catalyzed by the family of protein-N-acetylgalactosaminyl transferases (pgants). Embarking on the investigation of two screen-identified genes, *pgant3* and *pgant35A,* I uncovered a unique suppressive interaction regulating NMJ functional properties (Figure 36). This suppressive interaction is defined by the observed result that the double mutants do not show any of the single mutant phenotypes and are essentially unchanged from control. This type of interaction is rare, but has been described previously, particularly in yeast studies. For example, mutations in the yeast homolog of cytoskeletal fimbrin (Sac6p) dominantly and reciprocally suppress phenotypes of the temperature-sensitive yeast actin mutation (act1-1), such that double mutants are essentially indistinguishable from controls (Adams and Botstein, 1989). In this case, the two proteins physically interact (Honts, 1994). Whether or not pgants physically interact is unknown, but multiple pgants are known to be co-distributed within the

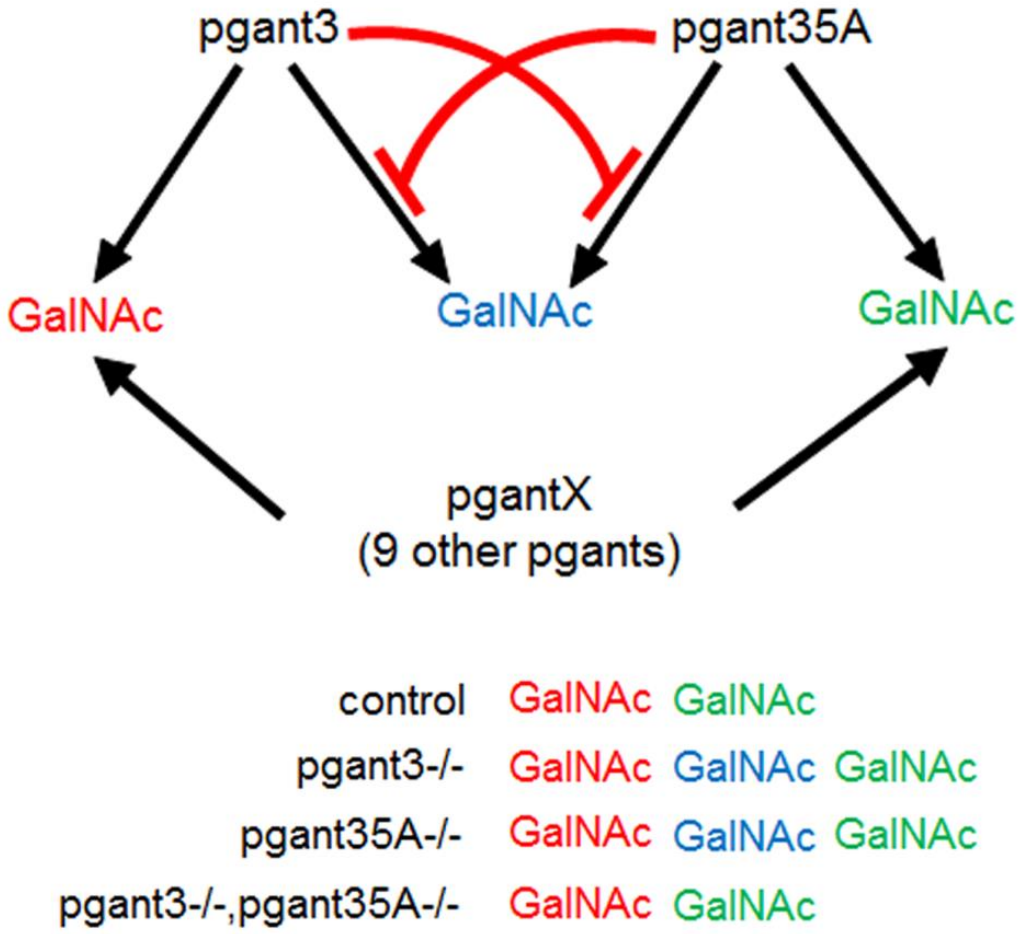

Figure 36. Pgant3 and Pgant35A suppressively regulate O-glycosylation. Pgant3 and Pgant35A suppressively regulate expression of GalNAc (blue), but independently regulate GalNAc (red) and GalNAc (green). Total GalNAc levels indicated in each mutant condition of single mutants *pgant3* (*pgant3*-/-), *pgant35A* (*pgant35A*-/-) and double mutant (*pgant3*-/-,*pgant*35A-/-).

cis and medial-Golgi compartments (Stanley, 2011). They function in a hierarchical manner such that early addition of O-GalNAc modifications can influence subsequent O-GalNAc additions as the protein is trafficked through the Golgi (Tian and Ten Hagen, 2009). Given that our studies of *pgant3* and *pgant35A* single mutants shown identical loss of function phenotypes for synaptic O-GalNAc glycosylation, it is possible that these proteins are localized in the same Golgi compartment, function at the same tier of glycosylation and may also physically interact. Efforts directed towards testing these hypotheses will further mechanistic insight into O-GalNAc synaptic glycosylation.

While this suppressive mechanism explains the observation that O-GalNAc levels remain unchanged in the double mutant condition, and is elevated only in the *pgant3* and *pgant35A* single mutant conditions, it does not account for how single mutants would elevate levels of O-GalNAc modification. At least three possibilities can be tested in this regard. First, it is known that pgants catalyze the transfer of monosaccharide GalNAc to naked serine/threonine residues to form the Tn antigen, which can be modified by addition of galactose to form the T antigen, and further modified by sialic acid to form SiaT antigens (Tian and Ten Hagen, 2009) . Given that glycosyltransferases that catalyze these reactions are sensitive to substrate concentrations and donor sugars that provide the monosaccharide, and in the presence of limited GalNAc in the single mutant conditions of either *pgant3* and *pgant35A* the critical levels of substrates may not be available for further modification (Bowles et al., 2006). Hence, Tn antigen GalNAcs may remain unmodified and available for further detection by the two

GalNAc recognizing lectin tools used in this study. This possibility could be tested by comparing relative levels of galactose and sialic acid, to determine if they are reciprocally reduced in the single mutant conditions and elevated in the control and double mutants.

A second possibility arises from the organization of the pgants within the Golgi, which is known to be sensitive to the activation of Src signaling (Gill et al., 2010). Activation of this pathway leads to the re-arrangement of the pgants from the cis/medial Golgi to the ER, leading to excessive O-GalNAc modifications added onto protein substrates, consequently elevating the level of glycosylation on the cell surface (Gill et al., 2010). Src is known to be activated downstream of integrin signaling. Critically, I have identified that an integrin receptor and Tenascin ligand combination, along with downstream Talin signaling, is suppressively regulated by both pgants (Chapter 4). It would therefore be of great interest to test the status of Src signaling in these contexts (Arias-Salgado et al., 2003). A third possibility arises from the fact that pgants are part of a family of genes with at least 12 members in *Drosophila* (Tian and Ten Hagen, 2009). Loss of either *pgant3* or *pgant35A* may potentially lead to an imbalance in the function of the other pgants or overcompensation by the other family members. While these changes may manifest at the gene expression level, it is known that pgants can modify both naked and pre-glycosylated substrates, and earlier disruption in O-GalNAc modifications (in the *pgant3* or *pgant35A* mutants) may affect subsequent glycosylation by the other family members, potentially leading to the observed elevation of synaptic O-GalNAc (Ten Hagen and Tran, 2002) .

Targets of the suppressive regulation: the integrin signaling pathway

I have identified integrin signaling to be regulated by the pgant dependent suppressive regulation (Chapter 4). This result is supported by studies in the *Drosophila* wing disc, where *pgant* mutations modulate the secretion of the integrin ligand Tiggrin, to regulate intercellular adhesion between the two wing disc cell layers (Zhang et al., 2008). However, there is no significant difference in Tiggrin levels at the NMJ in either of *pgant3* and *pgant35A* mutant conditions. This suggests that pgants show cell-specific regulation of integrin signaling, which is supported by the wing disc studies in which *pgant35A* mutants alone do not have any effects on wing disc integrin signaling and *pgant3* mutant effects cannot be rescued by pgant35A (Zhang et al., 2008). At the NMJ, the pgant-dependent neural effects suppressively regulates the integrin ligand/receptor pair Ten-m and αPS2, which are expressed pre-and postsynaptically and known to be potent regulators of the synaptic development and function (Beumer et al., 1999; Mosca et al., 2012). While Ten-m is known to form *trans*-synaptic adhesions with its synaptic partner Ten-a (Mosca et al., 2012), I show that Ten-m/αPS2 signaling occurs at intercellular adhesions at the neuromuscular synapse.

Both αPS2 and Ten-m contain strings of consecutive serine/threonine residues predicted to be recognized and modified by the pgant gene family. Importantly, Ten-m has been shown to be a predominant target of both *pgant3* and *pgant35A* in glycosyltransferase activity measurements *in vitro* (Zhang et al., 2008). Thus, Ten-m may plausibly be a direct target of O-GalNAc modification at the neuromuscular synapse. However, in both *pgant3* or *pgant35A* mutant

conditions, αPS2 and Ten-m levels are down-regulated, while O-GalNAc levels are elevated. The straight-forward interpretation is that *pgant* dysregulation decreases abundance of the integrin ligand/receptor pair. Alternatively increased O-linked glycosylation may perturb epitope recognition by antibodies against ligand/receptor. Another possibility is that increases in O-linked glycosylation, lead to greater interaction between the ligand and receptor to cause conformation changes that decrease epitope availability for subsequent detection by Ten-m and αPS2 antibodies. These options could be tested by use of appropriate de-glycosylating enzymes and lectin-pull down experiments, as well as the generation of direct epitope-tagged Ten-m and αPS2 transgenes.

Using cell-specific rescue experiments, I identify pre- and postsynaptic requirements for *pgant3* and *pgant35A* (Chapter 4). Both Ten-m ligand and αPS2 receptor are found pre and postsynaptically, with relatively greater expression of both targets in the postsynaptic membrane (Beumer et al., 1999; Mosca et al., 2012). Importantly, postsynaptic Ten-m has been shown to form a *trans*-synaptic pair with presynaptic Ten-a, with unknown roles for presynaptic Ten-m (Mosca et al., 2012). As only presynaptic rescue of *pgant3* and *pgant35A* can rescue the downregulated Ten-m levels in corresponding loss of function mutant backgrounds, *pgant* dependent suppressive mechanism in the presynaptic neuron may specifically regulate the Ten-m/αPS2 signaling. I identify both pre- and postsynaptic subcellular defects in *pgant3* and *pgant35A* mutants. Of particular interest is the regulation of the postsynaptic pocket (PSP) space, which is found apposing presynaptic active zones (Fig. 24, Chapter 4). The PSP is

significantly larger in *pgant3* and *pgant35A* single mutant conditions, but double mutants return to the control condition. The PSP compartment was first described by Estes et al. 1996 in *shibire* endocytosis mutants. Packard et al. 2002 later reported PSP enlargement in WNT signaling mutants. Enlarged PSPs have subsequently been reported in BMP Gbb mutants (Nahm et al., 2010), *sfl* mutants regulating HSPGs in the extracellular space (Ren et al., 2009), and Perlecan secreted HSPG mutants (Kamimura et al., 2013). Hence, PSPs are sensitive to defective glycosylation and *trans*-synaptic signaling.

Consistently, we find defective signaling at the Ten-m/αPS2 signaling axis. Ten-m/αPS2 integrin signaling drives cell adhesion (Graner et al., 1998) and pgants also promote adhesion and matrix secretion (Zhang and Ten Hagen, 2010). Both *pgant* mutants down-regulate synaptic Ten-m/αPS2 levels at the NMJ synapse, with no differences in *pgant* double mutants. Based on this extensive literature, we interpreted enlarged PSPs to be a consequence of impaired synaptic adhesion. Indeed, normally apposed pre- and postsynaptic membranes occur with *pgant* enlarged PSPs. This is not surprising as αPS2/Ten-m are both transmembrane, and integrin signaling is well known to bridge to the cytoskeleton. Thus, an adhesion defect can manifest on either side of the postsynaptic membrane due to impaired integrin signaling. Further investigation of the cytoskeletal differences associated with these using markers for presynaptic microtubules, and postsynaptic alpha-spectrin would further support this idea. Of further interest would be an ultrastructural analysis with gold-labeled antibodies against postsynaptic scaffold proteins and glutamate receptors given

the expansion of PSP in the *pgant* mutants and the single and double mutants under activity-dependent conditions (Chapter 4). Thus, I identify *pgant* dependent suppressive mechanism to control synaptic function, subcellular distribution and synaptic integrin signaling.

Integrins are also known to potently regulate synaptic plasticity. Earlier work shows significant depression of facilitation and augmentation phases in integrin mutants (Rohrbough et al., 2000). Consistent with identified dysregulation of integrin signaling in *pgant* mutants, I have found differences in the facilitation and augmentation phases during high frequency stimulation. I find that suppressive mechanisms controlling neurotransmission strength during high frequency are time-dependent, as single and double mutants largely behave similarly during this phase, but there is a restoration of suppressive effects of neurotransmission in the post-tetanic phases (Chapter 4). Using optogenetic strategies, I show that these differences in phasic properties can be explained by suppressive and non-suppressive regulation of integrin dependent downstream signaling. In response to tetanic stimulation, I find pFAK levels in the single/double mutants behave similarly, while in the post-tetanic phase, Talin levels are depressed in single mutants while double mutants are similar to controls (Fig. 30, Chapter 4). Further insight into these dynamics could be determined by also visualizing total FAK levels with FAK antibodies to determine if there are suppressive interactions on the FAK levels or if they are reciprocally regulated as compared to the pFAK levels.

I also show activity-dependent expansion of the PSP is controls and double mutants, which is largely absent in the single mutants (Fig. 31, Chapter 4). This change may arise from the altered dynamics of the Talin/pFAK activation. The interaction between Talin and pFAK remains an area of intense research where Talin is considered to be an obligate pFAK interactor. However, recent reports have shown that pFAK may in turn regulate Talin levels (Lawson et al., 2012). In these studies, pFAK and Talin are co-regulated in stable points of intercellular adhesion, while they are differentially regulated in adhesions at actively spreading 'environmental probing' extensions of the cell. Given that the PSP expansion is also a result of dynamic membrane changes, elicited by only 60 seconds of nerve stimulation, the observed expansion of the PSP compartment could arise from uncoupled pFAK and Talin dynamics. This question remains unresolved, but would be of significant interest to cell biologists and neurobiologists given the common interests in inter-cellular and cell-matrix adhesion. In summary, I was fortunate to discover novel synaptic glycan-mediated mechanisms, mediated by coupled gene pairs that are part of the same glycan pathway. I would strongly advocate using this paradigm for investigation of other complementary and inhibitory pairs of genes.

REFERENCES

Abbott KL, Troupe K, Lee I, Pierce M (2006) Integrin-dependent neuroblastoma cell adhesion and migration on laminin is regulated by expression levels of two enzymes in the O-mannosyl-linked glycosylation pathway, PomGnT1 and GnT-Vb. Exp Cell Res 312:2837–2850.

Aberle H, Haghighi AP, Fetter RD, McCabe BD, Magalhaes TR, Goodman CS (2002) wishful thinking encodes a BMP type II receptor that regulates synaptic growth in Drosophila. Neuron 33:545–558.

Adams AE, Botstein D (1989) Dominant suppressors of yeast actin mutations that are reciprocally suppressed. Genetics 121:675–683.

Afonso-Oramas D, Cruz-Muros I, Alvarez de la Rosa D, Abreu P, Giráldez T, Castro-Hernández J, Salas-Hernández J, Lanciego JL, Rodríguez M, González-Hernández T (2009) Dopamine transporter glycosylation correlates with the vulnerability of midbrain dopaminergic cells in Parkinson's disease. Neurobiol Dis 36:494–508.

Ai XB, Do AT, Lozynska O, Kusche-Gullberg M, Lindahl U, Emerson CP (2003) QSulf1 remodels the 6-O sulfation states of cell surface heparan sulfate proteoglycans to promote Wnt signaling. J Cell Biol 162:341–351.

Aikawa J, Esko JD (1999) Molecular cloning and expression of a third member of the heparan sulfate/heparin GlcNAc N-deacetylase/N-sulfotransferase family. J Biol Chem 274:2690–2695.

Akins MR, Biederer T (2006) Cell-cell interactions in synaptogenesis. Curr Opin Neurobiol 16:83–89.

Altmann F, Fabini G, Ahorn H, Wilson IBH (2001) Genetic model organisms in the study of N-glycans. Biochimie 83:703–712.

Ang LH, Kim J, Stepensky V, Hing H (2003) Dock and Pak regulate olfactory axon pathfinding in Drosophila. Development 130:1307–1316.

Aono S, Keino H, Ono T, Yasuda Y, Tokita Y, Matsui F, Taniguchi M, Sonta S, Oohira A (2000) Genomic organization and expression pattern of mouse neuroglycan C in the cerebellar development. J Biol Chem 275:337–342.

Arias-Salgado EG, Lizano S, Sarkar S, Brugge JS, Ginsberg MH, Shattil SJ (2003) Src kinase activation by direct interaction with the integrin beta cytoplasmic domain. Proc Natl Acad Sci U S A 100:13298–13302.

Arikawa-Hirasawa E, Rossi SG, Rotundo RL, Yamada Y (2002) Absence of acetylcholinesterase at the neuromuscular junctions of perlecan-null mice. Nat Neurosci 5:119–123.

Arnold CS, Johnson G V, Cole RN, Dong DL, Lee M, Hart GW (1996) The microtubule-associated protein tau is extensively modified with O-linked N-acetylglucosamine. J Biol Chem 271:28741–28744.

Ataman B, Ashley J, Gorczyca D, Gorczyca M, Mathew D, Wichmann C, Sigrist SJ, Budnik V (2006a) Nuclear trafficking of Drosophila Frizzled-2 during synapse development requires the PDZ protein dGRIP. Proc Natl Acad Sci U S A 103:7841–7846.

Ataman B, Ashley J, Gorczyca M, Ramachandran P, Fouquet W, Sigrist SJ, Budnik V (2008) Rapid activity-dependent modifications in synaptic structure and function require bidirectional Wnt signaling. Neuron 57:705–718.

Ataman B, Budnik V, Thomas U (2006b) Scaffolding proteins at the Drosophila neuromuscular junction. Fly Neuromuscul Junction Struct Funct Second Ed 75:181–216.

Augsburger A, Schuchardt A, Hoskins S, Dodd J, Butler S (1999) BMPs as mediators of roof plate repulsion of commissural neurons. Neuron 24:127–141.

Augustin H, Grosjean Y, Chen KY, Sheng Q, Featherstone DE (2007) Nonvesicular release of glutamate by glial xCT transporters suppresses glutamate receptor clustering in vivo. J Neurosci 27:111–123.

Baeg GH, Lin XH, Khare N, Baumgartner S, Perrimon N (2001) Heparan sulfate proteoglycans are critical for the organization of the extracellular distribution of Wingless. Development 128:87–94.

Baeg GH, Perrimon N (2000) Functional binding of secreted molecules to heparan sulfate proteoglycans in Drosophila. Curr Opin Cell Biol 12:575–580.

Bahr BA, Staubli U, Xiao P, Chun D, Ji ZX, Esteban ET, Lynch G (1997) Arg-Gly-Asp-Ser-selective adhesion and the stabilization of long-term potentiation: pharmacological studies and the characterization of a candidate matrix receptor. J Neurosci 17:1320–1329.

Ball RW, Warren-Paquin M, Tsurudome K, Liao EH, Elazzouzi F, Cavanagh C, An B-S, Wang T-T, White JH, Haghighi AP (2010) Retrograde BMP signaling controls synaptic growth at the NMJ by regulating trio expression in motor neurons. Neuron 66:536–549.

Barros CS, Franco SJ, Müller U, Mueller U (2011) Extracellular Matrix: Functions in the Nervous System. Cold Spring Harb Perspect Biol 3:a005108.

Bar-Shavit R, Maoz M, Ginzburg Y, Vlodavsky I (1996) Specific involvement of glypican in thrombin adhesive properties. J Cell Biochem 61:278–291.

Bastiani MJ, Harrelson AL, Snow PM, Goodman CS (1987) Expression of fasciclin-I and fasciclin-II glycoproteins on subsets of axon pathways during neurona development in the grasshopper. Cell 48:745–755.

Bazigou E, Apitz H, Johansson J, Loren CE, Hirst EMA, Chen PL, Palmer RH, Salecker I (2007) Anterograde jelly belly and Alk receptor tyrosine kinase signaling mediates retinal axon targeting in Drosophila. Cell 128:961–975.

Bellaiche Y, The I, Perrimon N (1998) Tout-velu is a Drosophila homologue of the putative tumour suppressor EXT-1 and is needed for Hh diffusion. Nature 394:85–88.

Belmonte MK, Allen G, Beckel-Mitchener A, Boulanger LM, Carper RA, Webb SJ (2004) Autism and abnormal development of brain connectivity. J Neurosci 24:9228–9231.

Bernfield M, Gotte M, Park PW, Reizes O, Fitzgerald ML, Lincecum J, Zako M (1999) Functions of cell surface heparan sulfate proteoglycans. Annu Rev Biochem 68:729–777.

Beumer K, Matthies HJG, Bradshaw A, Broadie K (2002) Integrins regulate DLG/FAS2 via a CaM kinase II-dependent pathway to mediate synapse elaboration and stabilization during postembryonic development. Development 129:3381–3391.

Beumer KJ, Rohrbough J, Prokop A, Broadie K (1999) A role for PS integrins in morphological growth and synaptic function at the postembryonic neuromuscular junction of Drosophila. Development 126:5833–5846.

Bewick GS, Young C, Slater CR (1996) Spatial relationships of utrophin, dystrophin, beta-dystroglycan and beta-spectrin to acetylcholine receptor clusters during postnatal maturation of the rat neuromuscular junction. J Neurocytol 25:367–379.

Bezakova G, Ruegg MA (2003) New insights into the roles of agrin. Nat Rev Mol Cell Biol 4:295–308.

Bieber AJ, Snow PM, Hortsch M, Patel NH, Jacobs JR, Traquina ZR, Schilling J, Goodman CS (1989) Drosophila neuroglian - a member of the

immunoglobulin superfamily with extensive homology to the vertebrate neural adhesion molecule L1. Cell 59:447–460.

Biederer T (2006) Bioinformatic characterization of the SynCAM family of immunoglobulin-like domain-containing adhesion molecules. Genomics 87:139–150.

Bishop JR, Schuksz M, Esko JD (2007) Heparan sulphate proteoglycans fine-tune mammalian physiology. Nature 446:1030–1037.

Blakely RD, De Felice LJ, Hartzell HC (1994) Molecular physiology of norepinephrine and serotonin transporters. J Exp Biol 196:263–281.

Bogdanik L, Framery B, Froelich A, Franco B, Mornet D, Bockaert J, Sigrist SJ, Grau Y, Parmentier ML (2008) Muscle Dystroglycan Organizes the Postsynapse and Regulates Presynaptic Neurotransmitter Release at the Drosophila Neuromuscular Junction. PLoS One 3:e2084.

Borchiellini C, Coulon J, LeParco Y (1996) The function of type IV collagen during Drosophila muscle development. Mech Dev 58:179–191.

Bowles D, Lim E-K, Poppenberger B, Vaistij FE (2006) Glycosyltransferases of lipophilic small molecules. Annu Rev Plant Biol 57:567–597.

Braccia A, Villani M, Immerdal L, Niels-Christiansen LL, Nystrom BT, Hansen GH, Danielsen EM (2003) Microvillar membrane Microdomains exist at physiological temperature - Role of galectin-4 as lipid raft stabilizer revealed by “superrafts.” J Biol Chem 278:15679–15684.

Brand AH, Perrimon N (1993) Targeted gene expression as a means of altering cell fates and generating dominant phenotypes. Development 118:401–415.

Brandon EP, Lin WC, D’Amour KA, Pizzo DP, Dominguez B, Sugiura Y, Thode S, Ko CP, Thal LJ, Gage FH, Lee KF (2003) Aberrant Patterning of neuromuscular synapses in choline acetyltransferase-deficient mice. J Neurosci 23:539–549.

Brewer CF, Miceli MC, Baum LG (2002) Clusters, bundles, arrays and lattices: novel mechanisms for lectin-saccharide-mediated cellular interactions. Curr Opin Struct Biol 12:616–623.

Broadie K, Bate M (1993a) Innervation directs receptor synthesis and localization in drosophila embryo synaptogenesis. Nature 361:350–353.

Broadie K, Bate M (1993b) Activity-dependent development of the neuromuscular synapse during embryogenesis. Neuron 11:607–619.

Broadie K, Baumgartner S, Prokop A (2011) Extracellular matrix and its receptors in Drosophila neural development. Dev Neurobiol 71:1102–1130.

Broadie KS, Bate M (1993c) Development of the embryonic neuromuscular synapse of drosophila-melanogaster. J Neurosci 13:144–166.

Brower DL, Wilcox M, Piovant M, Smith RJ, Reger LA (1984) Related cell-surface antigens expressed with positional specificity in Drosophila imaginal discs. Proc Natl Acad Sci 81:7485–7489.

Burkin DJ, Kim JE, Gu MJ, Kaufman SJ (2000) Laminin and alpha 7 beta 1 integrin regulate agrin-induced clustering of acetylcholine receptors. J Cell Sci 113:2877–2886.

Butler SJ, Dodd J (2003) A role for BMP heterodimers in roof plate-mediated repulsion of commissural axons. Neuron 38:389–401.

Carey DJ (1997) Syndecans: Multifunctional cell-surface co-receptors. Biochem J 327:1–16.

Castellani R, Smith MA, Richey PL, Perry G (1996) Glycoxidation and oxidative stress in Parkinson disease and diffuse Lewy body disease. Brain Res 737:195–200.

Ceccarelli B, Hurlbut WP, Mauro A (1972) Depletion of vesicles from frog neuromuscular junctions by prolonged tetanic stimulation. J Cell Biol 54:30–38.

Chan C-S, Weeber EJ, Kurup S, Sweatt JD, Davis RL (2003) Integrin requirement for hippocampal synaptic plasticity and spatial memory. J Neurosci 23:7107–7116.

Chan C-S, Weeber EJ, Zong L, Fuchs E, Sweatt JD, Davis RL (2006) Beta 1-integrins are required for hippocampal AMPA receptor-dependent synaptic transmission, synaptic plasticity, and working memory. J Neurosci 26:223–232.

Chandrasekaran S, Dean JW, Giniger MS, Tanzer ML (1991) Laminin carbohydrates are implicated in cell signaling. J Cell Biochem 46:115–124.

Chen CL, Huang SS, Huang JS (2006) Cellular heparan sulfate negatively modulates transforming growth factor-beta(1) (TGF-beta(1)) responsiveness in epithelial cells. J Biol Chem 281:11506–11514.

Chen KY, Augustin H, Featherstone D (2009a) Effect of ambient extracellular glutamate on Drosophila glutamate receptor trafficking and function. J Comp Physiol a-Neuroethology Sens Neural Behav Physiol 195:21–29.

Chen P, Abacherli LE, Nadler ST, Wang Y, Li Q, Parks WC (2009b) MMP7 shedding of syndecan-1 facilitates re-epithelialization by affecting alpha(2)beta(1) integrin activation. Vij N, ed. PLoS One 4:e6565.

Chen R, Jiang XN, Sun DG, Han GH, Wang FJ, Ye ML, Wang LM, Zou HF (2009c) Glycoproteomics Analysis of Human Liver Tissue by Combination of Multiple Enzyme Digestion and Hydrazide Chemistry. J Proteome Res 8:651–661.

Chen YW, Pedersen JW, Wandall HH, Levery SB, Pizette S, Clausen H, Cohen SM (2007) Glycosphingolipids with extended sugar chain have specialized functions in development and behavior of Drosophila. Dev Biol 306:736–749.

Chen Z-L, Indyk JA, Strickland S (2003) The hippocampal laminin matrix is dynamic and critical for neuronal survival. Mol Biol Cell 14:2665–2676.

Chia J, Tham KM, Gill DJ, Bard-Chapeau EA, Bard FA (2014) ERK8 is a negative regulator of O-GalNAc glycosylation and cell migration. Elife 3:e01828.

Chintapalli VR, Wang J, Dow JAT (2007) Using FlyAtlas to identify better Drosophila melanogaster models of human disease. Nat Genet 39:715–720.

Chiu AY, Ugozolli M, Meiri K, Ko J (1992) Purification and lectin-binding properties of s-laiminin, a synaptic isoform of the laminin-B1 chain. J Neurochem 59:10–17.

Chung CD, Patel VP, Moran M, Lewis LA, Miceli MC (2000) Galectin-1 induces partial TCR zeta-chain phosphorylation and antagonizes processive TCR signal transduction. J Immunol 165:3722–3729.

Collins CA, DiAntonio A (2007) Synaptic development: insights from Drosophila. Curr Opin Neurobiol 17:35–42.

Comoletti D, Flynn R, Jennings LL, Chubykin A, Matsumura T, Hasegawa H, Südhof TC, Taylor P (2003) Characterization of the interaction of a recombinant soluble neuroligin-1 with neurexin-1beta. J Biol Chem 278:50497–50505.

Couchman JR (2003) Syndecans: proteoglycan regulators of cell-surface microdomains? Nat Rev Mol Cell Biol 4:926–937.

Crnefinderle N, Sketelj J (1993) Congruity of acetylcholine-receptor, acetylcholinesterase, and Dolichos-bifluorus lectin binding glycoprotein in postsynaptic-like sarcolemmal specializations in noninnervated regenerating rat muscles. J Neurosci Res 34:67–78.

Dam TK, Brewer FC (2010) Maintenance of cell surface glycan density by lectin-glycan interactions: A homeostatic and innate immune regulatory mechanism. Glycobiology 20:1061–1064.

Damico P, Jacobs JR (1995) Lectin histochemistry of the drosophila embryo. Tissue Cell 27:23–30.

Dani N, Broadie K (2012) Glycosylated synaptomatrix regulation of trans-synaptic signaling. Dev Neurobiol 72:2–21.

Dani N, Nahm M, Lee S, Broadie K (2012) A targeted glycan-related gene screen reveals heparan sulfate proteoglycan sulfation regulates WNT and BMP trans-synaptic signaling. PLoS Genet 8:e1003031.

Darnell JC, Van Driesche SJ, Zhang C, Hung KYS, Mele A, Fraser CE, Stone EF, Chen C, Fak JJ, Chi SW, Licatalosi DD, Richter JD, Darnell RB (2011) FMRP stalls ribosomal translocation on mRNAs linked to synaptic function and autism. Cell 146:247–261.

Davis GW, Schuster CM, Goodman CS (1996) Genetic dissection of structural and functional components of synaptic plasticity .3. CREB is necessary for presynaptic functional plasticity. Neuron 17:669–679.

De Bernabe DB V, Currier S, Steinbrecher A, Celli J, van Beusekom E, van der Zwaag B, Kayserili H, Merlini L, Chitayat D, Dobyns WB, Cormand B, Lehesjoki AE, Cruces J, Voit T, Walsh CA, van Bokhoven H, Brunner HG (2002) Mutations in the O-mannosyltransferase gene POMT1 give rise to the severe neuronal migration disorder Walker-Warburg syndrome. Am J Hum Genet 71:1033–1043.

De Graaff E, Maat P, Hulsenboom E, van den Berg R, van den Bent M, Demmers J, Lugtenburg PJ, Hoogenraad CC, Sillevis Smitt P (2012) Identification of delta/notch-like epidermal growth factor-related receptor as the Tr antigen in paraneoplastic cerebellar degeneration. Ann Neurol 71:815–824.

Dejima K, Kanai MI, Akiyama T, Levings DC, Nakato H (2011) Novel Contact-dependent Bone Morphogenetic Protein (BMP) Signaling Mediated by Heparan Sulfate Proteoglycans. J Biol Chem 286:17103–17111.

Delon I, Brown NH (2007) Integrins and the actin cytoskeleton. Curr Opin Cell Biol 19:43–50.

Dennis JW, Nabi IR, Demetriou M (2009) Metabolism, Cell Surface Organization, and Disease. Cell 139:1229–1241.

Desai CJ, Popova E, Zinn K (1994) A Drosophila receptor tyrosine phosphatase expressed in the embryonic CNS and larval optic lobes is a member of the set of proteins bearing the “HRP” carbohydrate epitope. J Neurosci 14:7272–7283.

Devenport D, Bunch TA, Bloor JW, Brower DL, Brown NH (2007) Mutations in the Drosophila αPS2 integrin subunit uncover new features of adhesion site assembly. Dev Biol 308:294–308.

Dhoot GK, Gustafsson MK, Ai XB, Sun WT, Standiford DM, Emerson CP (2001) Regulation of Wnt signaling and embryo patterning by an extracellular sulfatase. Science 293:1663–1666.

Dias WB, Cheung WD, Wang Z, Hart GW (2009) Regulation of calcium/calmodulin-dependent kinase IV by O-GlcNAc modification. J Biol Chem 284:21327–21337.

Dick A, Hild M, Bauer H, Imai Y, Maifeld H, Schier AF, Talbot WS, Bouwmeester T, Hammerschmidt M (2000) Essential role of Bmp7 (snailhouse) and its prodomain in dorsoventral patterning of the zebrafish embryo. Development 127:343–354.

Dietzl G, Chen D, Schnorrer F, Su KC, Barinova Y, Fellner M, Gasser B, Kinsey K, Oppel S, Scheiblauer S, Couto A, Marra V, Keleman K, Dickson BJ (2007) A genome-wide transgenic RNAi library for conditional gene inactivation in Drosophila. Nature 448:151–156.

Dityatev A, Schachner M (2003) Extracellular matrix molecules and synaptic plasticity. Nat Rev Neurosci 4:456–468.

Dityatev A, Schachner M (2006) The extracellular matrix and synapses. Cell Tissue Res 326:647–654.

Dityatev A, Schachner M, Sonderegger P (2010a) The dual role of the extracellular matrix in synaptic plasticity and homeostasis. Nat Rev Neurosci 11:735–746.

Dityatev A, Seidenbecher CI, Schachner M (2010b) Compartmentalization from the outside: the extracellular matrix and functional microdomains in the brain. Trends Neurosci 33:503–512.

Dityatev A, Seidenbecher CI, Schachner M (2010c) Compartmentalization from the outside: the extracellular matrix and functional microdomains in the brain. Trends Neurosci 33:503–512.

Dreyfuss JL, Regatieri C V, Jarrouge TR, Cavalheiro RP, Sampaio LO, Nader HB (2009) Heparan sulfate proteoglycans: structure, protein interactions and cell signaling. An Acad Bras Cienc 81:409–429.

Drickamer K, Taylor ME (1993) Biology of animal lectins. Annu Rev Cell Biol 9:237–264.

Eaton BA, Davis GW (2005) LIM Kinase1 controls synaptic stability downstream of the type II BMP receptor. Neuron 47:695–708.

Edelman GM (1984) Modulation of cell adhesion during induction, histogenesis, and perinatal development of the nervous system. Annu Rev Neurosci 7:339–377.

Edri-Brami M, Rosental B, Hayoun D, Welt M, Rosen H, Wirguin I, Nefussy B, Drory VE, Porgador A, Lichtenstein RG (2012) Glycans in sera of amyotrophic lateral sclerosis patients and their role in killing neuronal cells. PLoS One 7:e35772.

Elkins T, Hortsch M, Bieber AJ, Snow PM, Goodman CS (1990) Drosophila fasciclin-I is a novel homophilic adhesion molecule that along with fasciclin-III can mediate cell sorting. J Cell Biol 110:1825–1832.

Endo M, Ohashi K, Sasaki Y, Goshima Y, Niwa R, Uemura T, Mizuno K (2003) Control of growth cone motility and morphology by LIM kinase and slingshot via phosphorylation and dephosphorylation of cofilin. J Neurosci 23:2527–2537.

Endo T (1999) O-mannosyl glycans in mammals. Biochim Biophys Acta-General Subj 1473:237–246.

Englund C, Loren CE, Grabbe C, Varshney GK, Deleuil F, Hallberg B, Palmer RH (2003) Jeb signals through the Alk receptor tyrosine kinase to drive visceral muscle fusion. Nature 425:512–516.

Featherstone DE, Rushton E, Broadie K (2002) Developmental regulation of glutamate receptor field size by nonvesicular glutamate release. Nat Neurosci 5:141–146.

Featherstone DE, Rushton E, Rohrbough J, Liebl F, Karr J, Sheng Q, Rodesch CK, Broadie K (2005) An essential Drosophila glutamate receptor subunit

that functions in both central neuropil and neuromuscular junction. J Neurosci 25:3199–3208.

Featherstone DE, Rushton EM, Hilderbrand-Chae M, Phillips AM, Jackson FR, Broadie K (2000) Presynaptic glutamic acid decarboxylase is required for induction of the postsynaptic receptor field at a glutamatergic synapse. Neuron 27:71–84.

Fenno L, Yizhar O, Deisseroth K (2011) The development and application of optogenetics. Annu Rev Neurosci 34:389–412.

Filmus J, Selleck SB (2001) Glypicans: proteoglycans with a surprise. J Clin Invest 108:497–501.

Fogel AI, Li Y, Giza J, Wang Q, Lam TT, Modis Y, Biederer T (2010) N-glycosylation at the SynCAM (synaptic cell adhesion molecule) immunoglobulin interface modulates synaptic adhesion. J Biol Chem 285:34864–34874.

Fogerty FJ, Fessler LI, Bunch TA, Yaron Y, Parker CG, Nelson RE, Brower DL, Gullberg D, Fessler JH (1994) Tiggrin, a novel Drosophila extracellular matrix protein that functions as a ligand for Drosophila alpha PS2 beta PS integrins. Development 120:1747–1758.

Fong SW, McLennan IS, McIntyre A, Reid J, Shennan KIJ, Bewick GS (2010) TGF-beta 2 alters the characteristics of the neuromuscular junction by regulating presynaptic quantal size. Proc Natl Acad Sci U S A 107:13515–13519.

Fox MA, Ho MSP, Smyth N, Sanes JR (2008) A synaptic nidogen: Developmental regulation and role of nidogen-2 at the neuromuscular junction. Neural Dev 3:24.

Fox MA, Sanes JR, Borza DB, Eswarakumar VP, Fassler R, Hudson BG, John SWM, Ninomiya Y, Pedchenko V, Pfaff SL, Rheault MN, Sado Y, Segal Y, Werle MJ, Umemori H (2007) Distinct target-derived signals organize formation, maturation, and maintenance of motor nerve terminals. Cell 129:179–193.

Franciscovich AL, Mortimer AA V, Freeman AA, Gu J, Sanyal S (2008) Overexpression Screen in Drosophila Identifies Neuronal Roles of GSK-3 beta/shaggy as a Regulator of AP-1-Dependent Developmental Plasticity. Genetics 180:2057–2071.

Franco B, Bogdanik L, Bobinnec Y, Debec A, Bockaert JRL, Parmentier ML, Grau Y (2004) Shaggy, the homolog of glycogen synthase kinase 3, controls neuromuscular junction growth in Drosophila. J Neurosci 24:6573–6577.

Frank CA (2014) How voltage-gated calcium channels gate forms of homeostatic synaptic plasticity. Front Cell Neurosci 8:40.

Fredieu JR, Mahowald AP (1994) Glycoconjugate expression during drosophila embryogenesis. Acta Anat (Basel) 149:89–99.

Freeze HH (2006) Genetic defects in the human glycome. Nat Rev Genet 7:537–551.

Freeze HH, Chong JX, Bamshad MJ, Ng BG (2014) Solving glycosylation disorders: fundamental approaches reveal complicated pathways. Am J Hum Genet 94:161–175.

Friedman SH, Dani N, Rushton E, Broadie K (2013) Fragile X mental retardation protein regulates trans-synaptic signaling in Drosophila. Dis Model Mech 6:1400–1413.

Friedrich M V, Schneider M, Timpl R, Baumgartner S (2000) Perlecan domain V of Drosophila melanogaster. Sequence, recombinant analysis and tissue expression. Eur J Biochem 267:3149–3159.

Gagneux P, Varki A (1999) Evolutionary considerations in relating oligosaccharide diversity to biological function. Glycobiology 9:747–755.

Gahring L, Carlson NG, Meyer EL, Rogers SW (2001) Granzyme B proteolysis of a neuronal glutamate receptor generates an autoantigen and is modulated by glycosylation. J Immunol 166:1433–1438.

Gaj T, Gersbach CA, Barbas CF (2013) ZFN, TALEN, and CRISPR/Cas-based methods for genome engineering. Trends Biotechnol 31:397–405.

Gao J, Chen T, Hu G, Gong Y, Qiang B, Yuan J, Peng X (2008) Nectin-like molecule 1 is a glycoprotein with a single N-glycosylation site at N290KS which influences its adhesion activity. Biochim Biophys Acta 1778:1429–1435.

Garlick RL, Mazer JS, Chylack LT, Tung WH, Bunn HF (1984) Nonenzymatic glycation of human lens crystallin. Effect of aging and diabetes mellitus. J Clin Invest 74:1742–1749.

Gascón S, García-Gallo M, Renart J, Díaz-Guerra M (2007) Endoplasmic reticulum-associated degradation of the NR1 but not the NR2 subunits of the

N-methyl-D-aspartate receptor induced by inhibition of the N-glycosylation in cortical neurons. J Neurosci Res 85:1713–1723.

Gatto CL, Broadie K (2008) Temporal requirements of the fragile X mental retardation protein in the regulation of synaptic structure. Development 135:2637–2648.

Gatto CL, Broadie K (2011) Drosophila modeling of heritable neurodevelopmental disorders. Curr Opin Neurobiol 6:834–841.

Gill DJ, Chia J, Senewiratne J, Bard F (2010) Regulation of O-glycosylation through Golgi-to-ER relocation of initiation enzymes. J Cell Biol 189:843–858.

Godula K, Bertozzi CR (2012) Density variant glycan microarray for evaluating cross-linking of mucin-like glycoconjugates by lectins. J Am Chem Soc 134:15732–15742.

Goode S, Melnick M, Chou TB, Perrimon N (1996) The neurogenic genes egghead and brainiac define a novel signalling pathway essential for epithelial morphogenesis during Drosophila oogenesis. Development 122:3863–3879.

Gorczyca D, Ashley J, Speese S, Gherbesi N, Thomas U, Gundelfinger E, Gramates LS, Budnik V (2007) Postsynaptic membrane addition depends on the discs-large-interacting t-SNARE gtaxin. J Neurosci 27:1033–1044.

Gorsi B, Stringer SE (2007) Tinkering with heparan sulfate sulfation to steer development. Trends Cell Biol 17:173–177.

Graham A, Franciswest P, Brickell P, Lumsden A (1994) The signaling molecule BMP4 mediates apoptosis in the rhombencephalic neural crest. Nature 372:684–686.

Gramates LS, Budnik V (1999) Assembly and maturation of the Drosophila larval neuromuscular junction. Neuromuscul Junctions Drosoph 43:93–+.

Graner MW, Bunch TA, Baumgartner S, Kerschen A, Brower DL (1998) Splice variants of the Drosophila PS2 integrins differentially interact with RGD-containing fragments of the extracellular proteins tiggrin, ten-m, and D-laminin 2. J Biol Chem 273:18235–18241.

Grow WA, Ferns M, Gordon H (1999) Agrin-independent activation of the agrin signal transduction pathway. J Neurobiol 40:356–365.

Grow WA, Gordon H (2000) Sialic acid inhibits agrin signaling in C2 myotubes. Cell Tissue Res 299:273–279.

Gruntman E, Turner GC (2013) Integration of the olfactory code across dendritic claws of single mushroom body neurons. Nat Neurosci 16:1821–1829.

Gurnett CA, De Waard M, Campbell KP (1996) Dual function of the voltage-dependent Ca2+ channel alpha 2 delta subunit in current stimulation and subunit interaction. Neuron 16:431–440.

Habuchi H, Tanaka M, Habuchi O, Yoshida K, Suzuki H, Ban K, Kimata K (2000) The occurrence of three isoforms of heparan sulfate 6-O-sulfotransferase having different specificities for hexuronic acid adjacent to the targeted N-sulfoglucosamine. J Biol Chem 275:2859–2868.

Hacker U, Nybakken K, Perrimon N (2005) Heparan sulphate proteoglycans: The sweet side of development. Nat Rev Mol Cell Biol 6:530–541.

Hagen KGT, Zhang LP, Tian E, Zhang Y (2009) Glycobiology on the fly: Developmental and mechanistic insights from Drosophila. Glycobiology 19:102–111.

Haghighi AP, McCabe BD, Fetter RD, Palmer JE, Hom S, Goodman CS (2003) Retrograde control of synaptic transmission by postsynaptic CaMKII at Drosophila neuromuscular. Neuron 39:255–267.

Haines N, Seabrooke S, Stewart BA (2007) Dystroglycan and protein O-mannosyltransferases 1 and 2 are required to maintain integrity of Drosophila larval muscles. Mol Biol Cell 18:4721–4730.

Haines N, Stewart BA (2007) Functional roles for beta 1,4-N-acetlygalactosaminyltransferase-A in Drosophila larval neurons and muscles. Genetics 175:671–679.

Hall AC, Lucas FR, Salinas PC (2000) Axonal remodeling and synaptic differentiation in the cerebellum is regulated by WNT-7a signaling. Cell 100:525–535.

Hall H, Deutzmann R, Timpl R, Vaughan L, Schmitz B, Schachner M (1997) HNK-1 carbohydrate-mediated cell adhesion to laminin-1 is different from heparin-mediated and sulfatide-mediated cell adhesion. Eur J Biochem 246:233–242.

Hall MK, Cartwright TA, Fleming CM, Schwalbe RA (2011) Importance of glycosylation on function of a potassium channel in neuroblastoma cells. PLoS One 6:e19317.

Hall ZW, Sanes JR (1993) Synaptic structure and development - the neuromuscular junction. Cell 72:99–121.

Halpern ME, Chiba A, Johansen J, Keshishian H (1991) Growth cone behavior underlying the development of stereotypic synaptic connections in drosophila embryos. J Neurosci 11:3227–3238.

Haltiwanger RS, Lowe JB (2004) Role of glycosylation in development. Annu Rev Biochem 73:491–537.

Han C, Yan D, Belenkaya TY, Lin XJ (2005) Drosophila glypicans Dally and Dally-like shape the extracellular Wingless morphogen gradient in the wing disc. Development 132:667–679.

Han W, Rhee J-S, Maximov A, Lao Y, Mashimo T, Rosenmund C, Südhof TC (2004) N-glycosylation is essential for vesicular targeting of synaptotagmin 1. Neuron 41:85–99.

Harrelson AL, Goodman CS (1988) Growth cone guidance in insects: fasciclin-II is a member of the immunoglobulin superfamily. Science 242:700–708.

Henion TR, Raitcheva D, Grosholz R, Biellmann F, Skarnes WC, Hennet T, Schwarting GA (2005) Beta1,3-N-acetylglucosaminyltransferase 1 glycosylation is required for axon pathfinding by olfactory sensory neurons. J Neurosci 25:1894–1903.

Henriquez JP, Webb A, Bence M, Bildsoe H, Sahores M, Hughes SM, Salinas PC (2008) Wnt signaling promotes AChR aggregation at the neuromuscular synapse in collaboration with agrin. Proc Natl Acad Sci U S A 105:18812–18817.

Henry MD, Satz JS, Brakebusch C, Costell M, Gustafsson E, Fässler R, Campbell KP (2001) Distinct roles for dystroglycan, beta1 integrin and perlecan in cell surface laminin organization. J Cell Sci 114:1137–1144.

Heuser JE, Reese TS (1981) Structural changes after transmitter release at the frog neuromuscular junction. J Cell Biol 88:564–580.

Hewitt JE (2009) Abnormal glycosylation of dystroglycan in human genetic disease. Biochim Biophys Acta-Molecular Basis Dis 1792:853–861.

Higashi-Kovtun ME, Mosca TJ, Dickman DK, Meinertzhagen IA, Schwarz TL (2010) Importin-beta 11 Regulates Synaptic Phosphorylated Mothers Against Decapentaplegic, and Thereby Influences Synaptic Development and Function at the Drosophila Neuromuscular Junction. J Neurosci 30:5253–5268.

Hirabayashi J, Hashidate T, Arata Y, Nishi N, Nakamura T, Hirashima M, Urashima T, Oka T, Futai M, Muller WEG, Yagi F, Kasai K (2002) Oligosaccharide specificity of galectins: a search by frontal affinity chromatography. Biochim Biophys Acta-General Subj 1572:232–254.

Hoffmann R, Valencia A (2004) A gene network for navigating the literature. Nat Genet 36:664.

Holt CE, Dickson BJ (2005) Sugar codes for axons? Neuron 46:169–172.

Honts JE (1994) Actin mutations that show suppression with fimbrin mutations identify a likely fimbrin-binding site on actin. J Cell Biol 126:413–422.

Hoyte K, Kang C, Martin PT (2002) Definition of pre- and postsynaptic forms of the CT carbohydrate antigen at the neuromuscular junction: ubiquitous expression of the CT antigens and the CT GalNAc transferase in mouse tissues. Mol Brain Res 109:146–160.

Hynes RO (2009) The Extracellular Matrix: Not Just Pretty Fibrils. Science 326:1216–1219.

Idoyaga-Vargas V, Carminatti H (1982) Postnatal changes in dolichol-pathway enzyme activities in cerebral cortex neurons. Biochem J 202:87–95.

Iglesias M, Ribera J, Esquerda JE (1992) Treatment with digestive agents reveals several glycoconjugates specifically associated with rat neuromuscular-junction. Histochemistry 97:125–131.

Inaki M, Yoshikawa S, Thomas JB, Aburatani H, Nose A (2007) Wnt4 is a local repulsive cue that determines synaptic target specificity. Curr Biol 17:1574–1579.

Inlow JK, Restifo LL (2004) Molecular and comparative genetics of mental retardation. Genetics 166:835–881.

Inoue Y, Hayashi S (2007) Tissue-specific laminin expression facilitates integrin-dependent association of the embryonic wing disc with the trachea in Drosophila. Dev Biol 304:90–101.

Iozzo R V (1998) Matrix proteoglycans: From molecular design to cellular function. Annu Rev Biochem 67:609–652.

Jaeken J, Matthijs G (2007) Congenital disorders of glycosylation: A rapidly expanding disease family. Annu Rev Genomics Hum Genet 8:261–278.

Jaeken J, Matthijs G, Schachter H, Freeze HH (2009) Glycosylation diseases: Quo vadis? Biochim Biophys Acta - Mol Basis Dis 1792:925–930.

Jan LY, Jan YN (1976) L-glutamate as an excitatory transmitter at Drosophila larval neuromuscular junction. J Physiol 262:215–236.

Jan LY, Jan YN (1982) Antibodies to horseradish-peroxidase as specific neuronal markers in drosophila and in grasshopper embryos. Proc Natl Acad Sci United States Am Sci 79:2700–2704.

Jenniskens GJ, Oosterhof A, Brandwijk R, Veerkamp JH, van Kuppevelt TH (2000) Heparan sulfate heterogeneity in skeletal muscle basal lamina: Demonstration by phage display-derived antibodies. J Neurosci 20:4099–4111.

Jing L, Chu X-P, Jiang Y-Q, Collier DM, Wang B, Jiang Q, Snyder PM, Zha X-M (2012) N-glycosylation of acid-sensing ion channel 1a regulates its trafficking and acidosis-induced spine remodeling. J Neurosci 32:4080–4091.

Johnson D, Montpetit ML, Stocker PJ, Bennett ES (2004) The sialic acid component of the beta1 subunit modulates voltage-gated sodium channel function. J Biol Chem 279:44303–44310.

Johnson KG, Tenney AP, Ghose A, Duckworth AM, Higashi ME, Parfitt K, Marcu O, Heslip TR, Marsh JL, Schwarz TL, Flanagan JG, Van Vactor D (2006) The HSPGs syndecan and dallylike bind the receptor phosphatase LAR and exert distinct effects on synaptic development. Neuron 49:517–531.

Juo P, Kaplan JM (2004) The anaphase-promoting the abundance of GLR-1 complex regulates glutamate receptors in the ventral nerve cord of C-elegans. Curr Biol 14:2057–2062.

Kainulainen V, Wang HM, Schick C, Bernfield M (1998) Syndecans, heparan sulfate proteoglycans, maintain the proteolytic balance of acute wound fluids. J Biol Chem 273:11563–11569.

Kalluri R (2003) Basement membranes: Structure, assembly and role in tumour angiogenesis. Nat Rev Cancer 3:422–433.

Kamimura K, Fujise M, Villa F, Izumi S, Habuchi H, Kimata K, Nakato H (2001) Drosophila heparan sulfate 6-O-sulfotransferase (dHS6ST) gene - Structure, expression, and function in the formation of the tracheal system. J Biol Chem 276:17014–17021.

Kamimura K, Koyama T, Habuchi H, Ueda R, Masu M, Kimata K, Nakato H (2006) Specific and flexible roles of heparan sulfate modifications in Drosophila FGF signaling. J Cell Biol 174:773–778.

Kamimura K, Ueno K, Nakagawa J, Hamada R, Saitoe M, Maeda N (2013) Perlecan regulates bidirectional Wnt signaling at the Drosophila neuromuscular junction. J Cell Biol 200:219–233.

Kanehisa M, Goto S (2000) KEGG: Kyoto Encyclopedia of Genes and Genomes. Nucleic Acids Res 28:27–30.

Kanellopoulos AK, Semelidou O, Kotini AG, Anezaki M, Skoulakis EMC (2012) Learning and memory deficits consequent to reduction of the fragile X mental retardation protein result from metabotropic glutamate receptor-mediated inhibition of cAMP signaling in Drosophila. J Neurosci 32:13111–13124.

Kanno E, Fukuda M (2008) Increased plasma membrane localization of O-glycosylation-deficient mutant of synaptotagmin I in PC12 cells. J Neurosci Res 86:1036–1043.

Kato S, Horiuchi S, Liu J, Cleveland DW, Shibata N, Nakashima K, Nagai R, Hirano A, Takikawa M, Kato M, Nakano I, Ohama E (2000) Advanced glycation endproduct-modified superoxide dismutase-1 (SOD1)-positive inclusions are common to familial amyotrophic lateral sclerosis patients with SOD1 gene mutations and transgenic mice expressing human SOD1 with a G85R mutation. Acta Neuropathol 100:490–505.

Kawasaki F, Felling R, Ordway RW (2000) A temperature-sensitive paralytic mutant defines a primary synaptic calcium channel in Drosophila. J Neurosci 20:4885–4889.

Kerrisk ME, Greer CA, Koleske AJ (2013) Integrin α3 is required for late postnatal stability of dendrite arbors, dendritic spines and synapses, and mouse behavior. J Neurosci 33:6742–6752.

Keshishian H, Broadie K, Chiba A, Bate M (1996) The drosophila neuromuscular junction: a model system for studying synaptic development and function. Annu Rev Neurosci 19:545–575.

Keshishian H, Kim YS (2004) Orchestrating development and function: retrograde BMP signaling in the Drosophila nervous system. Trends Neurosci 27:143–147.

Kim G. N. M (2010) Identification of downstream targets of the Bone Morphogenetic Protein pathway in the Drosophila nervous system. Dev Dyn 239:2413–2425.

Kim K, Lawrence SM, Park J, Pitts L, Vann WF, Betenbaugh MJ, Palter KB (2002) Expression of a functional Drosophila melanogaster N-acetylneuraminic acid (Neu5Ac) phosphate synthase gene: evidence for endogenous sialic acid biosynthetic ability in insects. Glycobiology 12:73–83.

Kimura T, Ikeda K, Takamatsu J, Miyata T, Sobue G, Miyakawa T, Horiuchi S (1996) Identification of advanced glycation end products of the Maillard reaction in Pick's disease. Neurosci Lett 219:95–98.

Kishimoto Y, Lee KH, Zon L, Hammerschmidt M, Schulte-Merker S (1997) The molecular nature of zebrafish swirl: BMP2 function is essential during early dorsoventral patterning. Development 124:4457–4466.

Kiss JZ, Rougon G (1997) Cell biology of polysialic acid. Curr Opin Neurobiol 7:640–646.

Kittel RJ, Hallermann S, Thomsen S, Wichmann C, Sigrist SJ, Heckmann M (2006) Active zone assembly and synaptic release. Biochem Soc Trans 34:939–941.

Kjellén L, Lindahl U (1991) Proteoglycans: structures and interactions. Annu Rev Biochem 60:443–475.

Kleene R, Schachner M (2004) Glycans and neural cell interactions. Nat Rev Neurosci 5:195–208.

Kleinschmit A, Koyama T, Dejima K, Hayashi Y, Kamimura K, Nakato H (2010) Drosophila heparan sulfate 6-O endosulfatase regualtes Wingless morphogen gradient formation. Dev Biol 345:204–214.

Koles K, Irvine KD, Panin VM (2004) Functional characterization of Drosophila sialyltransferase. J Biol Chem 279:4346–4357.

Koles K, Lim JM, Aoki K, Porterfield M, Tiemeyer M, Wells L, Panin V (2007) Identification of n-glycosylated proteins from the central nervous system of Drosophila melanogaster. Glycobiology 17:1388–1403.

Korkut C, Ataman B, Ramachandran P, Ashley J, Barria R, Gherbesi N, Budnik V (2009) Trans-Synaptic Transmission of Vesicular Wnt Signals through Evi/Wntless. Cell 139:393–404.

Korkut C, Budnik V (2009) WNTs tune up the neuromuscular junction. Nat Rev Neurosci 10:627–634.

Kose H, Rose D, Zhu XM, Chiba A (1997) Homophilic synaptic target recognition mediated by immunoglobulin-like cell adhesion molecule Fasciclin III. Development 124:4143–4152.

Kramer KL (2010) Specific sides to multifaceted glycosaminoglycans are observed in embryonic development. Semin Cell Dev Biol 21:631–637.

Kruse J, Mailhammer R, Wernecke H, Faissner A, Sommer I, Goridis C, Schachner M (1984) Neural cell-adhesion molecules and myelin-associated glycoprotein share a common carbohydrate moiety recognized by monoclonal antibody-L2 and antibody-HNK-1. Nature 311:153–155.

Kuberan B, Lech M, Zhang LJ, Wu ZLL, Beeler DL, Rosenberg RD (2002) Analysis of heparan sulfate oligosaccharides with ion pair-reverse phase capillary high performance liquid chromatography-microelectrospray ionization time-of-flight mass spectrometry. J Am Chem Soc 124:8707–8718.

Kummer TT, Misgeld T, Sanes JR (2006) Assembly of the postsynaptic membrane at the neuromuscular junction: paradigm lost. Curr Opin Neurobiol 16:74–82.

Kwon SE, Chapman ER (2012) Glycosylation is dispensable for sorting of synaptotagmin 1 but is critical for targeting of SV2 and synaptophysin to recycling synaptic vesicles. J Biol Chem 287:35658–35668.

Lai J-P, Sandhu DS, Yu C, Han T, Moser CD, Jackson KK, Guerrero RB, Aderca I, Isomoto H, Garrity-Park MM, Zou H, Shire AM, Nagorney DM, Sanderson SO, Adjei AA, Lee J-S, Thorgeirsson SS, Roberts LR (2008) Sulfatase 2 up-regulates glypican 3, promotes fibroblast growth factor signaling, and decreases survival in hepatocellular carcinoma. Hepatology 47:1211–1222.

Lamanna WC, Kalus I, Padva M, Baldwin RJ, Merry CLR, Dierks T (2007) The heparanome - The enigma of encoding and decoding heparan sulfate sulfation. J Biotechnol 129:290–307.

Latvanlehto A, Fox MA, Sormunen R, Tu HM, Oikarainen T, Koski A, Naumenko N, Shakirzyanova A, Kallio M, Ilves M, Giniatullin R, Sanes JR, Pihlajaniemi T (2010) Muscle-Derived Collagen XIII Regulates Maturation of the Skeletal Neuromuscular Junction. J Neurosci 30:12230–12241.

Laughlin ST, Baskin JM, Amacher SL, Bertozzi CR (2008) In vivo imaging of membrane-associated glycans in developing zebrafish. Science 320:664–667.

Lawson C, Lim S-T, Uryu S, Chen XL, Calderwood DA, Schlaepfer DD (2012) FAK promotes recruitment of talin to nascent adhesions to control cell motility. J Cell Biol 196:223–232.

Ledesma MD, Bonay P, Colaço C, Avila J (1994) Analysis of microtubule-associated protein tau glycation in paired helical filaments. J Biol Chem 269:21614–21619.

Lee HH, Norris A, Weiss JB, Frasch M (2003) Jelly belly protein activates the receptor tyrosine kinase Alk to specify visceral muscle pioneers. Nature 425:507–512.

Lee I, Guo H-B, Kamar M, Abbott K, Troupe K, Lee J-K, Alvarez-Manilla G, Pierce M (2006) N-acetylglucosaminyltranferase VB expression enhances beta1 integrin- dependent PC12 neurite outgrowth on laminin and collagen. J Neurochem 97:947–956.

Lee JS, Chien CB (2004) When sugars guide axons: Insights from heparan sulphate proteoglycan mutants. Nat Rev Genet 5:923–935.

Lefrancois L, Bevan MJ (1985) Functional modifications of cyto-toxic T-lymphocyte T200 glycoprotein recognized by monoclonal antibodies. Nature 314:449–452.

Levine A, Bashan-Ahrend A, Budai-Hadrian O, Gartenberg D, Menasherow S, Wides R (1994) Odd Oz: a novel Drosophila pair rule gene. Cell 77:587–598.

Li L-B, Chen N, Ramamoorthy S, Chi L, Cui X-N, Wang LC, Reith MEA (2004) The role of N-glycosylation in function and surface trafficking of the human dopamine transporter. J Biol Chem 279:21012–21020.

Li X, Molina H, Huang H, Zhang Y-Y, Liu M, Qian S-W, Slawson C, Dias WB, Pandey A, Hart GW, Lane MD, Tang Q-Q (2009) O-linked N-acetylglucosamine modification on CCAAT enhancer-binding protein beta: role during adipocyte differentiation. J Biol Chem 284:19248–19254.

Lin DM, Goodman CS (1994a) Ectopic and increased expression of fasciclin II alters motoneuron growth cone guidance. Neuron 13:507–523.

Lin DM, Goodman CS (1994b) Ectopic and increased expression of Fasciclin II alters motoneuron growth cone guidance. Neuron 13:507–523.

Lin XH, Perrimon N (2000) Role of heparan sulfate proteoglycans in cell-cell signaling in Drosophila. Matrix Biol 19:303–307.

Lind T, Lindahl U, Lidholt K (1993) Biosynthesis of heparin heparan-sulfate - identification of a 70-kDa protein catalyzing both the D-glucuronosyltransferase and the N-acetyl-D-glucosaminyl transferase reactions. J Biol Chem 268:20705–20708.

Lis H, Sharon N (1986) Lectins as molecules and as tools. Annu Rev Biochem 55:35–67.

Liu Y, Eckstein-Ludwig U, Fei J, Schwarz W (1998) Effect of mutation of glycosylation sites on the Na+ dependence of steady-state and transient currents generated by the neuronal GABA transporter. Biochim Biophys Acta 1415:246–254.

Long AA, Kim E, Leung H-T, Woodruff E, An L, Doerge RW, Pak WL, Broadie K (2008) Presynaptic calcium channel localization and calcium-dependent synaptic vesicle exocytosis regulated by the Fuseless protein. J Neurosci 28:3668–3682.

Loren CE, Scully A, Grabbe C, Edeen PT, Thomas J, McKeown M, Hunter T, Palmer RH (2001) Identification and characterization of DAlk: a novel Drosophila melanogaster RTK which drives ERK activation in vivo. Genes to Cells 6:531–544.

Lucas FR, Salinas PC (1997) WNT-7a induces axonal remodeling and increases synapsin I levels in cerebellar neurons. Dev Biol 192:31–44.

Lüdemann N, Clement A, Hans VH, Leschik J, Behl C, Brandt R (2005) O-glycosylation of the tail domain of neurofilament protein M in human neurons and in spinal cord tissue of a rat model of amyotrophic lateral sclerosis (ALS). J Biol Chem 280:31648–31658.

Lüthi T, Haltiwanger RS, Greengard P, Bähler M (1991) Synapsins contain O-linked N-acetylglucosamine. J Neurochem 56:1493–1498.

Lyles JM, Linnemann D, Bock E (1984) Biosynthesis of the D2-cell adhesion molecule: post-translational modifications, intracellular transport, and developmental changes. J Cell Biol 99:2082–2091.

Maccarana M, Sakura Y, Tawada A, Yoshida K, Lindahl U (1996) Domain structure of heparan sulfates from bovine organs. J Biol Chem 271:17804–17810.

Marazzi G, Wang YQ, Sassoon D (1997) Msx2 is a transcriptional regulator in the BMP4-mediated programmed cell death pathway. Dev Biol 186:127–138.

Margeta MA, Shen K (2010) Molecular mechanisms of synaptic specificity. Mol Cell Neurosci 43:261–267.

Marie B, Pym E, Bergquist S, Davis GW (2010) Synaptic Homeostasis Is Consolidated by the Cell Fate Gene gooseberry, a Drosophila pax3/7 Homolog. J Neurosci 30:8071–8082.

Marques G (2005) Morphogens and synaptogenesis in Drosophila. J Neurobiol 64:417–434.

Marques G, Bao H, Haerry TE, Shimell MJ, Duchek P, Zhang B, O'Connor MB (2002) The Drosophila BMP type II receptor wishful thinking regulates neuromuscular synapse morphology and function. Neuron 33:529–543.

Marth JD, Grewal PK (2008) Mammalian glycosylation in immunity. Nat Rev Immunol 8:874–887.

Martin D, Zusman S, Li X, Williams EL, Khare N, DaRocha S, Chiquet-Ehrismann R, Baumgartner S (1999a) wing blister, a new Drosophila laminin alpha chain required for cell adhesion and migration during embryonic and imaginal development. J Cell Biol 145:191–201.

Martin PT (2002) Glycobiology of the synapse. Glycobiology 12:1R–7R.

Martin PT (2003a) Dystroglycan glycosylation and its role in matrix binding in skeletal muscle. Glycobiology 13:55R–66R.

Martin PT (2003b) Glycobiology of the neuromuscular junction. J Neurocytol 32:915.

Martin PT (2007) Congenital muscular dystrophies involving the O-mannose pathway. Curr Mol Med 7:417–425.

Martin PT, Kaufman SJ, Kramer RH, Sanes JR (1996) Synaptic integrins in developing, adult, and mutant muscle: Selective association of alpha 1, alpha 7A, and alpha 7B integrins with the neuromuscular junction. Dev Biol 174:125–139.

Martin PT, Sanes JR (1995) Role for a synapse-specific carbohydrate in agrin-induced clustering of acetylcholine-receptors. Neuron 14:743–754.

Martin PT, Scott LJ, Porter BE, Sanes JR (1999b) Distinct structures and functions of related pre- and postsynaptic carbohydrates at the mammalian neuromuscular junction. Mol Cell Neurosci 13:105–118.

Martínez-Maza R, Poyatos I, López-Corcuera B, N úñez E, Giménez C, Zafra F, Aragón C (2001) The role of N-glycosylation in transport to the plasma membrane and sorting of the neuronal glycine transporter GLYT2. J Biol Chem 276:2168–2173.

Maruo K, Nagata T, Yamamoto S, Nagai K, Yajima Y, Maruo S, Nishizaki T (2003) Tunicamycin inhibits NMDA and AMPA receptor responses independently of N-glycosylation. Brain Res 977:294–297.

Maruo K, Yamamoto S, Kanno T, Yaguchi T, Maruo S, Yashiya S, Nishizaki T (2006) Tunicamycin decreases the probability of single-channel openings for N-methyl-D-aspartate and alpha-amino-3-hydroxy-5-methyl-4-isoxazole propionic acid receptors. Neuroreport 17:313–317.

Maselli RA, Ng JJ, Anderson JA, Cagney O, Arredondo J, Williams C, Wessel HB, Abdel-Hamid H, Wollmann RL (2009) Mutations in LAMB2 causing a severe form of synaptic congenital myasthenic syndrome. J Med Genet 46:203–208.

Matani P, Sharrow M, Tiemeyer M (2007) Ligand, modulatory, and co-receptor functions of neural glycans. Front Biosci 12:3852–3879.

Mathew D, Ataman B, Chen JY, Zhang YL, Cumberledge S, Budnik V (2005) Wingless signaling at synapses is through cleavage and nuclear import of receptor DFrizzled2. Science 310:1344–1347.

McCabe BD, Hom S, Aberle H, Fetter RD, Marques G, Haerry TE, Wan H, O'Connor MB, Goodman CS, Haghighi AP (2004) Highwire regulates presynaptic BMP signaling essential for synaptic growth. Neuron 41:891–905.

McCabe BD, Marques G, Haghighi AP, Fetter RD, Crotty ML, Haerry TE, Goodman CS, O'Connor MB (2003) The BMP homolog Gbb provides a retrograde signal that regulates synaptic growth at the Drosophila neuromuscular junction. Neuron 39:241–254.

McDonnell KMW, Grow WA (2004) Reduced glycosaminoglycan sulfation diminishes the agrin signal transduction pathway. Dev Neurosci 26:1–10.

Meng YH, Zhang Y, Tregoubov V, Janus C, Cruz L, Jackson M, Lu WY, MacDonald JF, Wang JY, Falls DL, Jial ZP (2002) Abnormal spine

morphology and enhanced LTP in LIMK-1 knockout mice. Neuron 35:121–133.

Misgeld T, Burgess RW, Lewis RM, Cunningham JM, Lichtman JW, Sanes JR (2002) Roles of neurotransmitter in synapse formation: Development of neuromuscular junctions lacking choline acetyltransferase. Neuron 36:635–648.

Misgeld T, Kummer TT, Lichtman JW, Sanes JR (2005) Agrin promotes synaptic differentiation by counteracting an inhibitory effect of neurotransmitter. Proc Natl Acad Sci U S A 102:11088–11093.

Mitra SK, Schlaepfer DD (2006) Integrin-regulated FAK-Src signaling in normal and cancer cells. Curr Opin Cell Biol 18:516–523.

Mohammadi M, Olsen SK, Goetz R (2005) A protein canyon in the FGF-FGF receptor dimer selects from an a la carte menu of heparan sulfate motifs. Curr Opin Struct Biol 15:506–516.

Monnier VM, Cerami A (1981) Nonenzymatic browning in vivo: possible process for aging of long-lived proteins. Science 211:491–493.

Montell DJ, Goodman CS (1989) Drosophila laminin - sequence of B2 subunit and expression of all three subunits during embryogenesis. J Cell Biol 109:2441–2453.

Morin P, Sagne C, Gasnier B (2004) Functional characterization of wild-type and mutant human sialin. Embo J 23:4560–4570.

Morin X, Daneman R, Zavortink M, Chia W (2001) A protein trap strategy to detect GFP-tagged proteins expressed from their endogenous loci in Drosophila. Proc Natl Acad Sci U S A 98:15050–15055.

Mosca TJ, Hong W, Dani VS, Favaloro V, Luo L (2012) Trans-synaptic Teneurin signalling in neuromuscular synapse organization and target choice. Nature 484:237–241.

Mosca TJ, Schwarz TL (2010) The nuclear import of Frizzled2-C by Importins-beta 11 and alpha 2 promotes postsynaptic development. Nat Neurosci 13:935–U50.

Muhlenhoff M, Oltmann-Norden I, Weinhold B, Hildebrandt H, Gerardy-Schahn R (2009) Brain development needs sugar: the role of polysialic acid in controlling NCAM functions. Biol Chem 390:567–574.

Mummery-Widmer JL, Yamazaki M, Stoeger T, Novatchkova M, Bhalerao S, Chen D, Dietzl G, Dickson BJ, Knoblich JA (2009) Genome-wide analysis of Notch signalling in Drosophila by transgenic RNAi. Nature 458:987–992.

Muntoni F, Torelli S, Brockington M (2008) Muscular dystrophies due to glycosylation defects. Neurotherapeutics 5:627–632.

Nahm M, Long AA, Paik SK, Kim S, Bae YC, Broadie K, Lee S (2010) The Cdc42-selective GAP Rich regulates postsynaptic development and retrograde BMP transsynaptic signaling. J Cell Biol 191:661–675.

Nakamura N, Stalnaker SH, Lyalin D, Lavrova O, Wells L, Panin VM (2010) Drosophila Dystroglycan is a target of O-mannosyltransferase activity of two protein O-mannosyltransferases, Rotated Abdomen and Twisted. Glycobiology 20:381–394.

Nakato H, Kimata K (2002) Heparan sulfate fine structure and specificity of proteoglycan functions. Biochim Biophys Acta-General Subj 1573:312–318.

Neely GG et al. (2010) A Genome-wide Drosophila Screen for Heat Nociception Identifies alpha 2 delta 3 as an Evolutionarily Conserved Pain Gene. Cell 143:628–638.

Nelson CM, Bissell MJ (2006) Of extracellular matrix, scaffolds, and signaling: Tissue architecture regulates development, homeostasis, and cancer. Annu Rev Cell Dev Biol 22:287–309.

Newsome TP, Schmidt S, Dietzl G, Keleman K, Asling B, Debant A, Dickson BJ (2000) Trio combines with dock to regulate Pak activity during photoreceptor axon pathfinding in Drosophila. Cell 101:283–294.

Nguyen VH, Trout J, Connors SA, Andermann P, Weinberg E, Mullins MC (2000) Dorsal and intermediate neuronal cell types of the spinal cord are established by a BMP signaling pathway. Development 127:1209–1220.

Nishimune H, Sanes JR, Carlson SS (2004) A synaptic laminin-calcium channel interaction organizes active zones in motor nerve terminals. Nature 432:580–587.

Noakes PG, Gautam M, Mudd J, Sanes JR, Merlie JP (1995) Aberrant differentiation of neuromuscular-junctions in mice lacking s-laminin β2. Nature 374:258–262.

Noma K, Kimura K, Minatohara K, Nakashima H, Nagao Y, Mizoguchi A, Fujiyoshi Y (2009) Triple N-glycosylation in the long S5-P loop regulates the

activation and trafficking of the Kv12.2 potassium channel. J Biol Chem 284:33139–33150.

Ohtsubo K, Marth JD (2006) Glycosylation in cellular mechanisms of health and disease. Cell 126:855–867.

Oohira A, Shuo T, Tokita Y, Nakanishi K, Aono S (2004) Neuroglycan C, a brain-specific part-time proteoglycan, with a particular multidomain structure. Glycoconj J 21:53–57.

Orestes P, Osuru HP, McIntire WE, Jacus MO, Salajegheh R, Jagodic MM, Choe W, Lee J, Lee S-S, Rose KE, Poiro N, Digruccio MR, Krishnan K, Covey DF, Lee J-H, Barrett PQ, Jevtovic-Todorovic V, Todorovic SM (2013) Reversal of neuropathic pain in diabetes by targeting glycosylation of Ca(V)3.2 T-type calcium channels. Diabetes 62:3828–3838.

Otsuki S, Hanson SR, Miyaki S, Grogan SP, Kinoshita M, Asahara H, Wong C-H, Lotz MK (2010) Extracellular sulfatases support cartilage homeostasis by regulating BMP and FGF signaling pathways. Proc Natl Acad Sci U S A 107:10202–10207.

Packard M, Koo ES, Gorczyca M, Sharpe J, Cumberledge S, Budnik V (2002) The Drosophila Wnt, wingless, provides an essential signal for pre- and postsynaptic differentiation. Cell 111:319–330.

Packard M, Mathew D, Budnik V (2003) Wnts and TGF beta in synaptogenesis: Old friends signalling at new places. Nat Rev Neurosci 4:113–120.

Palmer RH, Vernersson E, Grabbe C, Hallberg B (2009) Anaplastic lymphoma kinase: signalling in development and disease. Biochem J 420:345–361.

Parkhomovskiy N, Kammesheidt A, Martin PT (2000) N-acetyllactosamine and the CT carbohydrate antigen mediate agrin-dependent activation of MuSK and acetylcholine receptor clustering in skeletal muscle. Mol Cell Neurosci 15:380–397.

Parkhomovskiy N, Martin PT (2000) alpha-galactosidase stimulates acetylcholine receptor aggregation in skeletal muscle cells via PNA-binding carbohydrates. Biochem Biophys Res Commun 270:899–902.

Parkinson W, Dear ML, Rushton E, Broadie K (2013) N-glycosylation requirements in neuromuscular synaptogenesis. Development 140:4970–4981.

Parnas D, Haghighi AP, Fetter RD, Kim SW, Goodman CS (2001) Regulation of postsynaptic structure and protein localization by the Rho-type guanine nucleotide exchange factor dPix. Neuron 32:415–424.

Patel NH, Snow PM, Goodman CS (1987) Characterization and cloning of fasciclin-III - a glycoprotein expressed on a subset of neurons and axon pathways in drosophila. Cell 48:975–988.

Patnaik SK, Potvin B, Carlsson S, Sturm D, Leffler H, Stanley P (2006) Complex N-glycans are the major ligands for galectin-1, -3, and -8 on Chinese hamster ovary cells. Glycobiology 16:305–317.

Patton BL (2003) Basal lamina and the organization of neuromuscular synapses. J Neurocytol 32:883–903.

Patton BL, Cunningham JM, Thyboll J, Kortesmaa J, Westerblad H, Edstrom L, Tryggvason K, Sanes JR (2001) Properly formed but improperly localized synaptic specializations in the absence of laminin alpha 4. Nat Neurosci 4:597–604.

Peng HB, Ali AA, Daggett DF, Rauvala H, Hassell JR, Smalheiser NR (1998) The relationship between perlecan and dystroglycan and its implication in the formation of the neuromuscular junction. Cell Adhes Commun 5:475–489.

Peppa M, Uribarri J, Vlassara H (2003) Glucose, Advanced Glycation End Products, and Diabetes Complications: What Is New and What Works. Clin Diabetes 21:186–187.

Perillo NL, Pace KE, Seilhamer JJ, Baum LG (1995) Apoptosis of T-cells mediated by galectin-1. Nature 378:736–739.

Persson U, Izumi H, Souchelnytskyi S, Itoh S, Grimsby S, Engstrom U, Heldin CH, Funa K, ten Dijke P (1998) The L45 loop in type I receptors for TGF-beta family members is a critical determinant in specifying Smad isoform activation. Febs Lett 434:83–87.

Pertusa M, Madrid R, Morenilla-Palao C, Belmonte C, Viana F (2012) N-glycosylation of TRPM8 ion channels modulates temperature sensitivity of cold thermoreceptor neurons. J Biol Chem 287:18218–18229.

Pfeiffer S, Ricardo S, Manneville JB, Alexandre C, Vincent JP (2002) Producing cells retain and recycle wingless in Drosophila embryos. Curr Biol 12:957–962.

Pilgram GSK, Potikanond S, Baines RA, Fradkin LG, Noordermeer JN (2010) The Roles of the Dystrophin-Associated Glycoprotein Complex at the Synapse. Mol Neurobiol 41:1–21.

Pospisilik JA et al. (2010) Drosophila Genome-wide Obesity Screen Reveals Hedgehog as a Determinant of Brown versus White Adipose Cell Fate. Cell 140:148–160.

Pozo K, Cingolani LA, Bassani S, Laurent F, Passafaro M, Goda Y (2012) β3 integrin interacts directly with GluA2 AMPA receptor subunit and regulates AMPA receptor expression in hippocampal neurons. Proc Natl Acad Sci U S A 109:1323–1328.

Prokop A (1999) Integrating bits and pieces: synapse structure and formation in Drosophila embryos. Cell Tissue Res 297:169–186.

Prokop A (2006) Organization of the efferent system and structure of neuromuscular junctions in Drosophila. Fly Neuromuscul Junction Struct Funct Second Ed 75:71–90.

Prokop A, Martin-Bermudo MD, Bate M, Brown NH (1998) Absence of PS integrins or laminin A affects extracellular adhesion, but not intracellular assembly, of hemiadherens and neuromuscular junctions in Drosophila embryos. Dev Biol 196:58–76.

Prokopenko SN, He YC, Lu Y, Bellen HJ (2000) Mutations affecting the development of the peripheral nervous system in drosophila: A molecular screen for novel proteins. Genetics 156:1691–1715.

Rasmussen TN, Plenge P, Bay T, Egebjerg J, Gether U (2009) A single nucleotide polymorphism in the human serotonin transporter introduces a new site for N-linked glycosylation. Neuropharmacology 57:287–294.

Rawson JM, Lee M, Kennedy EL, Selleck SB (2003) Drosophila neuromuscular synapse assembly and function require the TGF-beta type I receptor saxophone and the transcription factor mad. J Neurobiol 55:134–150.

Reichling C, Meyerhof W, Behrens M (2008) Functions of human bitter taste receptors depend on N-glycosylation. J Neurochem 106:1138–1148.

Reichsman F, Smith L, Cumberledge S (1996) Glycosaminoglycans can modulate extracellular localization of the wingless protein and promote signal transduction. J Cell Biol 135:819–827.

Reiner DJ, Ailion M, Thomas JH, Meyer BJ (2008) C-elegans anaplastic lymphoma kinase ortholog SCD-2 controls dauer formation by modulating TGF-beta signaling. Curr Biol 18:1101–1109.

Ren Y, Kirkpatrick CA, Rawson JM, Sun M, Selleck SB (2009) Cell Type-Specific Requirements for Heparan Sulfate Biosynthesis at the Drosophila Neuromuscular Junction: Effects on Synapse Function, Membrane Trafficking, and Mitochondrial Localization. J Neurosci 29:8539–8550.

Rendic D, Sharrow M, Katoh T, Overcarsh B, Nguyen K, Kapurch J, Aoki K, Wilson IBH, Tiemeyer M (2010) Neural-specific alpha 3-fucosylation of N-linked glycans in the Drosophila embryo requires Fucosyltransferase A and influences developmental signaling associated with O-glycosylation. Glycobiology 20:1353–1365.

Rengifo J, Gibson CJ, Winkler E, Collin T, Ehrlich BE (2007) Regulation of the inositol 1,4,5-trisphosphate receptor type I by O-GlcNAc glycosylation. J Neurosci 27:13813–13821.

Repnikova E, Koles K, Nakamura M, Pitts J, Li HW, Ambavane A, Zoran MJ, Panin VM (2010) Sialyltransferase Regulates Nervous System Function in Drosophila. J Neurosci 30:6466–6476.

Rexach JE, Clark PM, Mason DE, Neve RL, Peters EC, Hsieh-Wilson LC (2012) Dynamic O-GlcNAc modification regulates CREB-mediated gene expression and memory formation. Nat Chem Biol 8:253–261.

Ribera J, Esquerda JE, Comella JX (1987) Phylogenetic polymorphism on lectin binding to junctional and nonjunctional basal lamina at the vertebrate neuromuscular-junction. Histochemistry 87:301–307.

Rider CC (2006) Heparin/heparan sulphate binding in the TGF-beta cytokine superfamily. Biochem Soc Trans 34:458–460.

Rohrbough K. J. B, Rohrbough J, Broadie K (2010) Anterograde jelly belly ligand to Alk receptor signaling at developing synapses is regulated by mind the gap. Development 137:3523–3533.

Rohrbough J, Grotewiel MS, Davis RL, Broadie K (2000) Integrin-mediated regulation of synaptic morphology, transmission, and plasticity. J Neurosci 20:6868–6878.

Rohrbough J, Rushton E, Woodruff E, Fergestad T, Vigneswaran K, Broadie K (2007) Presynaptic establishment of the synaptic cleft extracellular matrix is required for post-synaptic differentiation. Genes Dev 21:2607–2628.

Rosenberg RD, Shworak NW, Liu J, Schwartz JJ, Zhang LJ (1997) Heparan sulfate proteoglycans of the cardiovascular system - Specific structures emerge but how is synthesis regulated? J Clin Invest 100:S67–S75.

Roth J, Kempf A, Reuter G, Schauer R, Gehring WJ (1992) Occurence of sialic acids in drosophila melanogaster. Science 256:673–675.

Roy S, Huang H, Liu S, Kornberg TB (2014) Cytoneme-mediated contact-dependent transport of the Drosophila decapentaplegic signaling protein. Science 343:1244624.

Ruiz-Canada C, Budnik V (2006) Introduction on the use of the Drosophila embryonic/larval neuromuscular junction as a model system to study synapse development and function, and a brief summary of pathfinding and target recognition. Fly Neuromuscul Junction Struct Funct Second Ed 75:1–31.

Rupp F, Payan DG, Magillsolc C, Cowan DM, Scheller RH (1991) Structure and expression of rat agrin. Neuron 6:811–823.

Rushton E, Rohrbough J, Broadie K (2009) Presynaptic secretion of mind-the-gap organizes the synaptic extracellular matrix-integrin interface and postsynaptic environments. Dev Dyn 238:554–571.

Rushton E, Rohrbough J, Deutsch K, Broadie K (2012) Structure-function analysis of endogenous lectin mind-the-gap in synaptogenesis. Dev Neurobiol.

Russo MA, Paolillo M, Sanchez-Hernandez Y, Curti D, Ciusani E, Serra M, Colombo L, Schinelli S (2013) A small-molecule RGD-integrin antagonist inhibits cell adhesion, cell migration and induces anoikis in glioblastoma cells. Int J Oncol 42:83–92.

Rutishauser U (1998) Polysialic acid at the cell surface: biophysics in service of cell interactions and tissue plasticity. J Cell Biochem 70:304–312.

Rutishauser U (2008) Polysialic acid in the plasticity of the developing and adult vertebrate nervous system. Nat Rev Neurosci 9:26–35.

Sadat MA et al. (2014) Glycosylation, hypogammaglobulinemia, and resistance to viral infections. N Engl J Med 370:1615–1625.

Sadoul R, Hirn M, Deagostinibazin H, Rougon G, Goridis C (1983) Adult and embryonic mouse neural cell-adhesion molecules have different binding properties. Nature 304:347–349.

Salinas PC (2003) Synaptogenesis: Wnt and TGF-beta take centre stage. Curr Biol 13:R60–R62.

Salinas PC (2005) Retrograde signalling at the synapse: a role for Wnt proteins. Biochem Soc Trans 33:1295–1298.

Sanes JR, Lichtman JW (2001) Induction, assembly, maturation and maintenance of a postsynaptic apparatus. Nat Rev Neurosci 2:791–805.

Sato C, Yamakawa N, Kitajima K (2010) Measurement of glycan based interactions by frontal affinity chromatography and surface plasmon resonance. Methods Enzymol Vol 478 Glycomics 478:219–232.

Schachter H (2009) Paucimannose N-glycans in Caenorhabditis elegans and Drosophila melanogaster. Carbohydr Res 344:1391–1396.

Schegg B, Hulsmeier AJ, Rutschmann C, Maag C, Hennet T (2009) Core Glycosylation of Collagen Is Initiated by Two beta(1-O)Galactosyltransferases. Mol Cell Biol 29:943–952.

Schlessinger J, Plotnikov AN, Ibrahimi OA, Eliseenkova A V, Yeh BK, Yayon A, Linhardt RJ, Mohammadi M (2000) Crystal structure of a ternary FGF-FGFR-heparin complex reveals a dual role for heparin in FGFR binding and dimerization. Mol Cell 6:743–750.

Schnorrer F, Schönbauer C, Langer CCH, Dietzl G, Novatchkova M, Schernhuber K, Fellner M, Azaryan A, Radolf M, Stark A, Keleman K, Dickson BJ (2010) Systematic genetic analysis of muscle morphogenesis and function in Drosophila. Nature 464:287–291.

Schuster CM, Davis GW, Fetter RD, Goodman CS (1996) Genetic dissection of structural and functional components of synaptic plasticity .1. Fasciclin II controls synaptic stabilization and growth. Neuron 17:641–654.

Schwander M, Shirasaki R, Pfaff SL, Muller U (2004) beta 1 integrins in muscle, but not in motor neurons, are required for skeletal muscle innervation. J Neurosci 24:8181–8191.

Schwientek T, Bennett EP, Flores C, Thacker J, Hollmann M, Reis CA, Behrens J, Mandel U, Keck B, Schäfer MA, Haselmann K, Zubarev R, Roepstorff P, Burchell JM, Taylor-Papadimitriou J, Hollingsworth MA, Clausen H (2002) Functional conservation of subfamilies of putative UDP-N-acetylgalactosamine:polypeptide N-acetylgalactosaminyltransferases in Drosophila, Caenorhabditis elegans, and mammals. One subfamily composed of l(2)35Aa is essential in Drosophila. J Biol Chem 277:22623–22638.

Scott H, Panin VM (2014) The role of protein N-glycosylation in neural transmission. Glycobiology 24:407–417.

Scott LJC, Bacou F, Sanes JR (1988) A synapse-specific carbohydrate at the neuromuscular junction: association with both acetylecholinesterase and a glycolipid. J Neurosci 8:932–944.

Seet B, Dikic I, Zhou M, Pawson T (2006) Reading protein modifications with int... [Nat Rev Mol Cell Biol. 2006] - PubMed - NCBI. Nat Rev Mol Cell Biol:473–483 Available at: http://www.ncbi.nlm.nih.gov/pubmed/16829979 [Accessed August 27, 2014].

Sela-Donenfeld D, Kalcheim C (2000) Inhibition of noggin expression in the dorsal neural tube by somitogenesis: a mechanism for coordinating the timing of neural crest emigration. Development 127:4845–4854.

Sen A, Yokokura T, Kankel MW, Dimlich DN, Manent J, Sanyal S, Artavanis-Tsakonas S (2011) Modeling spinal muscular atrophy in Drosophila links Smn to FGF signaling. J Cell Biol 192:481–495.

Sepp KJ, Schulte J, Auld VJ (2001) Peripheral glia direct axon guidance across the CNS/PNS transition zone. Dev Biol 238:47–63.

Shah NM, Groves AK, Anderson DJ (1996) Alternative neural crest cell fates are instructively promoted by TGF beta superfamily members. Cell 85:331–343.

Shcherbata HR, Yatsenko AS, Patterson L, Sood VD, Nudel U, Yaffe D, Baker D, Ruohola-Baker H (2007) Dissecting muscle and neuronal disorders in a Drosophila model of muscular dystrophy. Embo J 26:481–493.

Shen K, Cowan CW (2010) Guidance Molecules in Synapse Formation and Plasticity. Cold Spring Harb Perspect Biol 2:a001842.

Shimokawa K, Kimura-Yoshida C, Nagai N, Mukai K, Matsubara K, Watanabe H, Matsuda Y, Mochida K, Matsuo I (2011) Cell Surface Heparan Sulfate Chains Regulate Local Reception of FGF Signaling in the Mouse Embryo. Dev Cell 21:257–272.

Shirinian M, Varshney G, Loren CE, Grabbe C, Palmer RH (2007) Drosophila Anaplastic Lymphoma Kinase regulates Dpp signalling in the developing embryonic gut. Differentiation 75:418–426.

Shishido E, Ono N, Kojima T, Saigo K (1997) Requirements of DFR1/heartless, a mesoderm-specific Drosophila FGF-receptor, for the formation of heart, visceral and somatic muscles, and ensheathing of longitudinal axon tracts in CNS. Development 124:2119–2128.

Simionescu M, Simionescu N, Palade GE (1982) Differentiated microdomains on the luminal surface of capillary endothelium: distribution of lectin receptors. J Cell Biol 94:406–413.

Skorobogatko Y, Landicho A, Chalkley RJ, Kossenkov A V, Gallo G, Vosseller K (2014) O-linked β-N-acetylglucosamine (O-GlcNAc) site thr-87 regulates synapsin I localization to synapses and size of the reserve pool of synaptic vesicles. J Biol Chem 289:3602–3612.

Smalheiser NR, Kim E (1995) Purification of cranin, a laminin-binding membrane protein: identity with dystroglycan and reassessment of its carbohydrate moieties. J Biol Chem 270:15425–15433.

Smet-Nocca C, Broncel M, Wieruszeski J-M, Tokarski C, Hanoulle X, Leroy A, Landrieu I, Rolando C, Lippens G, Hackenberger CPR (2011) Identification of O-GlcNAc sites within peptides of the Tau protein and their impact on phosphorylation. Mol Biosyst 7:1420–1429.

Smith MA, Richey PL, Taneda S, Kutty RK, Sayre LM, Monnier VM, Perry G (1994) Advanced Maillard reaction end products, free radicals, and protein oxidation in Alzheimer's disease. Ann N Y Acad Sci 738:447–454.

Snow PM, Patel NH, Harrelson AL, Goodman CS (1987) Neural-specific carbohydrate moiety shared by many surface glycoproteins in drosophila and grasshopper embryos. J Neurosci 7:4137–4144.

Soleman S, Filippov MA, Dityatev A, Fawcett JW (2013) Targeting the neural extracellular matrix in neurological disorders. Neuroscience 253:194–213.

Sorokin L (2010) The impact of the extracellular matrix on inflammation. Nat Rev Immunol 10:712–723.

Speese SD, Ashley J, Jokhi V, Nunnari J, Barria R, Li Y, Ataman B, Koon A, Chang Y-T, Li Q, Moore MJ, Budnik V (2012) Nuclear envelope budding enables large ribonucleoprotein particle export during synaptic Wnt signaling. Cell 149:832–846.

Spivak-Kroizman T, Lemmon MA, Dikic I, Ladbury JE, Pinchasi D, Huang J, Jaye M, Crumley G, Schlessinger J, Lax I (1994) Heparin-induced oligomerization of FGF molecules is responsible for FGF receptor dimerization, activation, and cell proliferation. Cell 79:1015–1024.

Spring J, Painesaunders SE, Hynes RO, Bernfield M (1994) Drosophila Syndecan - conservation of a cell-surface heparan-sulfate proteoglycan. Proc Natl Acad Sci U S A 91:3334–3338.

Springer BA, Pantoliano MW, Barbera FA, Gunyuzlu PL, Thompson LD, Herblin WF, Rosenfeld SA, Book GW (1994) Identification and concerted function of 2 receptor-binding surfaces on basic fibroblast growth-factor required for mitogenesis. J Biol Chem 269:26879–26884.

Stanley P (2011) Golgi glycosylation. Cold Spring Harb Perspect Biol 3:a005199–.

Staubli U, Chun D, Lynch G (1998) Time-Dependent Reversal of Long-Term Potentiation by an Integrin Antagonist. J Neurosci 18:3460–3469.

Storey GP, Opitz-Araya X, Barria A (2011) Molecular determinants controlling NMDA receptor synaptic incorporation. J Neurosci 31:6311–6316.

Subramanian A, Wayburn B, Bunch T, Volk T (2007) Thrombospondin-mediated adhesion is essential for the formation of the myotendinous junction in Drosophila. Development 134:1269–1278.

Sugita S, Saito F, Tang J, Satz J, Campbell K, Sudhof TC (2001) A stoichiometric complex of neurexins and dystroglycan in brain. J Cell Biol 154:435–445.

Sugiyama J, Bowen DC, Hall ZW (1994) Dystroglycan binds nerve and muscle agrin. Neuron 13:103–115.

Sutachan JJ, Watanabe I, Zhu J, Gottschalk A, Recio-Pinto E, Thornhill WB (2005) Effects of Kv1.1 channel glycosylation on C-type inactivation and simulated action potentials. Brain Res 1058:30–43.

Talts JF, Andac Z, Gohring W, Brancaccio A, Timpl R (1999) Binding of the G domains of laminin alpha 1 and alpha 2 chains and perlecan to heparin, sulfatides, alpha-dystroglycan and several extracellular matrix proteins. Embo J 18:863–870.

Taylor EW, Wang K, Nelson AR, Bredemann TM, Fraser KB, Clinton SM, Puckett R, Marchase RB, Chatham JC, McMahon LL (2014) O-GlcNAcylation of AMPA receptor GluA2 is associated with a novel form of long-term depression at hippocampal synapses. J Neurosci 34:10–21.

Ten Hagen KG, Fritz TA, Tabak LA (2003a) All in the family: the UDP-GalNAc:polypeptide N-acetylgalactosaminyltransferases. Glycobiology 13:1R–16R.

Ten Hagen KG, Tran DT (2002) A UDP-GalNAc:polypeptide N-acetylgalactosaminyltransferase is essential for viability in Drosophila melanogaster. J Biol Chem 277:22616–22622.

Ten Hagen KG, Tran DT, Gerken TA, Stein DS, Zhang Z (2003b) Functional characterization and expression analysis of members of the UDP-GalNAc:polypeptide N-acetylgalactosaminyltransferase family from Drosophila melanogaster. J Biol Chem 278:35039–35048.

Tessier CR, Broadie K (2008) Drosophila fragile X mental retardation protein developmentally regulates activity-dependent axon pruning. Development 135:1547–1557.

Thoenen H (1995) Neurotrophins and neuronal plasticity. Science 270:593–598.

Thomas U, Ebitsch S, Gorczyca M, Koh YH, Hough CD, Woods D, Gundelfinger ED, Budnik V (2000) Synaptic targeting and localization of Discs-large is a stepwise process controlled by different domains of the protein. Curr Biol 10:1108–1117.

Tian E, Ten Hagen KG (2006) Expression of the UDP-GalNAc: polypeptide N-acetylgalactosaminyltransferase family is spatially and temporally regulated during Drosophila development. Glycobiology 16:83–95.

Tian E, Ten Hagen KG (2007) A UDP-GalNAc : polypeptide N-acetylgalactosaminyltransferase is required for epithelial tube formation. J Biol Chem 282:606–614.

Tian E, Ten Hagen KG (2009) Recent insights into the biological roles of mucin-type O-glycosylation. Glycoconj J 26:325–334.

Tran DT, Ten Hagen KG (2013) Mucin-type O-glycosylation during development. J Biol Chem 288:6921–6929.

Tsai P-I, Wang M, Kao H-H, Cheng Y-J, Lin Y-J, Chen R-H, Chien C-T (2012a) Activity-dependent retrograde laminin A signaling regulates synapse growth at Drosophila neuromuscular junctions. Proc Natl Acad Sci U S A 109:17699–17704.

Tsai P-I, Wang M, Kao H-H, Cheng Y-J, Walker JA, Chen R-H, Chien C-T (2012b) Neurofibromin mediates FAK signaling in confining synapse growth at Drosophila neuromuscular junctions. J Neurosci 32:16971–16981.

Tsen G, Halfter W, Kroger S, Cole GJ (1995) Agrin is a heparan-sulfate proteoglycan. J Biol Chem 270:3392–3399.

Tsim KWK, Ruegg MA, Escher G, Kroger S, McMahan UJ (1992) cDNA that encodes active agrin. Neuron 8:677–689.

Tweedie S, Ashburner M, Falls K, Leyland P, McQuilton P, Marygold S, Millburn G, Osumi-Sutherland D, Schroeder A, Seal R, Zhang H (2009) FlyBase: enhancing Drosophila Gene Ontology annotations. Nucleic Acids Res 37:D555–D559.

Umemori H, Linhoff MW, Ornitz DM, Sanes JR (2004) FGF22 and its close relatives are presynaptic organizing molecules in the mammalian brain. Cell 118:257–270.

Van Kuppevelt TH, Dennissen MA, van Venrooij WJ, Hoet RM, Veerkamp JH (1998) Generation and application of type-specific anti-heparan sulfate antibodies using phage display technology. Further evidence for heparan sulfate heterogeneity in the kidney. J Biol Chem 273:12960–12966.

Van Reeuwijk J, Janssen M, van den Elzen C, de Bernabe DB V, Sabatelli P, Merlini L, Boon M, Scheffer H, Brockington M, Muntoni F, Huynen MA, Verrips A, Walsh CA, Barth PG, Brunner HG, van Bokhoven H (2005) POMT2 mutations cause alpha-dystroglycan hypoglycosylation and Walker-Warburg syndrome. J Med Genet 42:907–912.

Van Vactor D, Wall DP, Johnson KG (2006) Heparan sulfate proteoglycans and the emergence of neuronal connectivity. Curr Opin Neurobiol 16:40–51.

Vandenborre G, Van Damme EJM, Ghesquiere B, Menschaert G, Hamshou M, Rao RN, Gevaert K, Smagghe G (2010) Glycosylation Signatures in Drosophila: Fishing with Lectins. J Proteome Res 9:3235–3242.

Varki A (2011) Evolutionary Forces Shaping the Golgi Glycosylation Machinery: Why Cell Surface Glycans Are Universal to Living Cells. Cold Spring Harb Perspect Biol 3:a005462.

Varki A, Cummings RD, Esko JD, Freeze HH, Stanley P, Bertozzi CR, Hart GW, Etzler ME (1999) Essentials of glycobiology. Essentials Glycobiol:xvii+653p.

Varki NM, Varki A (2007) Diversity in cell surface sialic acid presentations: implications for biology and disease. Lab Investig 87:851–857.

Vautrin J (2010) The synaptomatrix: A solid though dynamic contact disconnecting transmissions from exocytotic events. Neurochem Int 57:85–96.

Veldhuis NA, Lew MJ, Abogadie FC, Poole DP, Jennings EA, Ivanusic JJ, Eilers H, Bunnett NW, McIntyre P (2012) N-glycosylation determines ionic permeability and desensitization of the TRPV1 capsaicin receptor. J Biol Chem 287:21765–21772.

Verheijen FW, Verbeek E, Aula N, Beerens C, Havelaar AC, Joosse M, Peltonen L, Aula P, Galjaard H, van der Spek PJ, Mancini GMS (1999) A new gene, encoding an anion transporter, is mutated in sialic acid storage diseases. Nat Genet 23:462–465.

Viswanathan K, Tomiya N, Park J, Singh S, Lee YC, Palter K, Betenbaugh MJ (2006) Expression of a functional Drosophila melanogaster CMP-sialic acid synthetase - Differential localization of the drosophila and human enzymes. J Biol Chem 281:15929–15940.

Viviano BL, Paine-Saunders S, Gasiunas N, Gallagher J, Saunders S (2004) Domain-specific modification of heparan sulfate by Qsulf1 modulates the binding of the bone morphogenetic protein antagonist noggin. J Biol Chem 279:5604–5611.

Vlassara H, Brownlee M, Cerami A (1983) Excessive nonenzymatic glycosylation of peripheral and central nervous system myelin components in diabetic rats. Diabetes 32:670–674.

Voigt A, Pflanz R, Schafer U, Jackle H (2002) Perlecan participates in proliferation activation of quiescent Drosophila neuroblasts. Dev Dyn 224:403–412.

Wagh DA, Rasse TM, Asan E, Hofbauer A, Schwenkert I, Dürrbeck H, Buchner S, Dabauvalle M-C, Schmidt M, Qin G, Wichmann C, Kittel R, Sigrist SJ, Buchner E (2006) Bruchpilot, a protein with homology to ELKS/CAST, is required for structural integrity and function of synaptic active zones in Drosophila. Neuron 49:833–844.

Wairkar YP, Fradkin LG, Noordermeer JN, DiAntonio A (2008) Synaptic defects in a Drosophila model of congenital muscular dystrophy. J Neurosci 28:3781–3789.

Walker A, Turnbull JE, Gallagher JT (1994) Specific heparan-sulfate saccharides mediate the activity of basic activity of basic fibroblast growth-factor. J Biol Chem 269:931–935.

Wallace BG (1990) Inhibition of agrin-induced acetylcholine-receptor aggregation by heparin, heparan sulfate, and other polyanions. J Neurosci 10:3576–3582.

Wang JZ, Grundke-Iqbal I, Iqbal K (1996) Glycosylation of microtubule-associated protein tau: an abnormal posttranslational modification in Alzheimer's disease. Nat Med 2:871–875.

Wang K, Liu Y, Li Y, Guo Y, Song P, Zhang X, Zeng S, Wang Z (2011) Precise spatiotemporal control of optogenetic activation using an acousto-optic device. Samuel A, ed. PLoS One 6:e28468.

Watanabe S, Liu Q, Davis MW, Hollopeter G, Thomas N, Jorgensen NB, Jorgensen EM (2013a) Ultrafast endocytosis at Caenorhabditis elegans neuromuscular junctions. Elife 2:e00723.

Watanabe S, Rost BR, Camacho-Pérez M, Davis MW, Söhl-Kielczynski B, Rosenmund C, Jorgensen EM (2013b) Ultrafast endocytosis at mouse hippocampal synapses. Nature 504:242–247.

Watson FL, Porcionatto MA, Bhattacharyya A, Stiles CD, Segal RA (1999) TrkA glycosylation regulates receptor localization and activity. J Neurobiol 39:323–336.

Weinhold B, Seidenfaden R, Röckle I, Mühlenhoff M, Schertzinger F, Conzelmann S, Marth JD, Gerardy-Schahn R, Hildebrandt H (2005) Genetic ablation of polysialic acid causes severe neurodevelopmental defects rescued by deletion of the neural cell adhesion molecule. J Biol Chem 280:42971–42977.

Wharton KA, Cook JM, Torres-Schumann S, de Castro K, Borod E, Phillips DA (1999) Genetic analysis of the bone morphogenetic protein-related gene, gbb, identifies multiple requirements during Drosophila development. Genetics 152:629–640.

Wodarz A, Hinz U, Engelbert M, Knust E (1995) Expression of crumbs confers apical character on plasma membrane domains of ectodermal epithelia of Drosophila. Cell 82:67–76.

Woodworth A, Fiete D, Baenziger JU (2002) Spatial and temporal regulation of tenascin-R glycosylation in the cerebellum. J Biol Chem 277:50941–50947.

Wopereis S, Lefeber DJ, Morava E, Wevers RA (2006) Mechanisms in protein O-glycan biosynthesis and clinical and molecular aspects of protein O-glycan biosynthesis defects: A review. Clin Chem 52:574–600.

Wreden CC, Wlizla M, Reimer RJ (2005) Varied mechanisms underlie the free sialic acid storage disorders. J Biol Chem 280:1408–1416.

Wu HT, Xiong WC, Mei L (2010) To build a synapse: signaling pathways in neuromuscular junction assembly. Development 137:1017–1033.

Wu ZLL, Zhang LJ, Yabe T, Kuberan B, Beeler DL, Love A, Rosenberg RD (2003) The involvement of heparan sulfate (HS) in FGF1/HS/FGFR1 signaling complex. J Biol Chem 278:17121–17129.

Xiang Y-Y, Dong H, Yang BB, Macdonald JF, Lu W-Y (2014) Interaction of Acetylcholinesterase with Neurexin-1β regulates Glutamatergic Synaptic stability in Hippocampal neurons. Mol Brain 7:15.

Xing B, Long AA, Harrison DA, Cooper RL (2005) Developmental consequences of neuromuscular junctions with reduced presynaptic calcium channel function. Synapse 57:132–147.

Yamaguchi Y (2001) Heparan sulfate proteoglycans in the nervous system: their diverse roles in neurogenesis, axon guidance, and synaptogenesis. Semin Cell Dev Biol 12:99–106.

Yamaguchi Y (2002) Glycobiology of the synapse: the role of glycans in the formation, maturation, and modulation of synapses. Biochim Biophys Acta 1573:369–376.

Yan D, Lin X (2009) Shaping Morphogen Gradients by Proteoglycans. Cold Spring Harb Perspect Biol 1:a002493.

Yan D, Wu Y, Feng Y, Lin S-C, Lin X (2009) The Core Protein of Glypican Daily-Like Determines Its Biphasic Activity in Wingless Morphogen Signaling. Dev Cell 17:470–481.

Yang X, Ongusaha PP, Miles PD, Havstad JC, Zhang F, So WV, Kudlow JE, Michell RH, Olefsky JM, Field SJ, Evans RM (2008) Phosphoinositide signalling links O-GlcNAc transferase to insulin resistance. Nature 451:964–969.

Yano H, Yamamoto-Hino M, Goto S (2009) Spatial and temporal regulation of glycosylation during Drosophila eye development. Cell Tissue Res 336:137–147.

Ye Z-Y, Li D-P, Byun HS, Li L, Pan H-L (2012) NKCC1 upregulation disrupts chloride homeostasis in the hypothalamus and increases neuronal activity-sympathetic drive in hypertension. J Neurosci 32:8560–8568.

Yee GH, Hynes RO (1993) A novel, tissue-specific integrin subunit, beta nu, expressed in the midgut of Drosophila melanogaster. Development 118:845–858.

Yoshida A, Kobayashi K, Manya H, Taniguchi K, Kano H, Mizuno M, Inazu T, Mitsuhashi H, Takahashi S, Takeuchi M, Herrmann R, Straub V, Talim B,

Voit T, Tapaloglu H, Toda T, Endo T (2001) Muscular dystrophy and neuronal migration disorder caused by mutations in a glycosyltransferase, POMGnT1. Dev Cell 1:717–724.

Yoshida H, Fuwa TJ, Arima M, Hamamoto H, Sasaki N, Ichimiya T, Osawa K-II, Ueda R, Nishihara S (2008) Identification of the Drosophila core 1 beta 1,3-galactosyltransferase gene that synthesizes T antigen in the embryonic central nervous system and hemocytes. Glycobiology 18:1094–1104.

You J, Belenkaya T, Lin X (2011) Sulfated Is a Negative Feedback Regulator of Wingless in Drosophila. Dev Dyn 240:640–648.

Zeidan Q, Hart GW (2010) The intersections between O-GlcNAcylation and phosphorylation: implications for multiple signaling pathways. J Cell Sci 123:13–22.

Zhang L, Syed ZA, van Dijk Härd I, Lim J-M, Wells L, Ten Hagen KG (2014) O-glycosylation regulates polarized secretion by modulating Tango1 stability. Proc Natl Acad Sci U S A 111:7296–7301.

Zhang L, Ten Hagen KG (2010) Dissecting the biological role of mucin-type O-glycosylation using RNA interference in Drosophila cell culture. J Biol Chem 285:34477–34484.

Zhang L, Ten Hagen KG (2011) The cellular microenvironment and cell adhesion: a role for O-glycosylation. Biochem Soc Trans 39:378–382.

Zhang L, Tran DT, Ten Hagen KG (2010) An O-glycosyltransferase promotes cell adhesion during development by influencing secretion of an extracellular matrix integrin ligand. J Biol Chem 285:19491–19501.

Zhang L, Zhang Y, Hagen KG Ten (2008) A mucin-type O-glycosyltransferase modulates cell adhesion during Drosophila development. J Biol Chem 283:34076–34086.

Zhong Y, Shanley J (1995) Altered nerve-terminal arborization and synaptic transmission in Drosophila mutants of cell-adhesion molecule fasciclin-1. J Neurosci 15:6679–6687.